![Geoscience BC logo]

GEOSCIENCE BC
SUMMARY OF ACTIVITIES 2015

GEOSCIENCE BC
SUMMARY OF ACTIVITIES 2015

Geoscience BC Report 2016-1

Cover photo: J. Angen and J. Logan looking out from the top of the Capoose showing, TREK project area, central British Columbia
Photo credit: R. Kim, 2015

Acknowledgments

I would like to thank the government of British Columbia for its ongoing support of Geoscience BC and recognize the $5 million investment made in 2015, allowing for our continued delivery of projects that generate new Earth science information for everyone. I would also like to express appreciation for the leaders in British Columbia's mineral exploration, mining and energy sectors who support our organization through their guidance, use and recognition of the information that we collect and distribute.

Robin Archdekin
President & CEO
Geoscience BC
www.geosciencebc.com

Foreword

Geoscience BC is pleased to present results from several of our ongoing geoscience projects in our eighth edition of the *Geoscience BC Summary of Activities*. The volume is divided into three sections, 'Minerals', 'Energy' and 'Scholarship Recipients', and contains a total of 22 papers.

The 'Minerals' section contains five papers from Geoscience BC minerals geoscience projects throughout BC. Three of the projects are part of the TREK and Search major project initiatives, while two of the projects are multiyear studies. Angen et al. provide a second year update for the three-year integrated bedrock and geology mapping initiative. The paper presents an updated bedrock map, detailed descriptions of rock units and mineral occurrences within the map area, and analytical results from rock samples. Jackaman and Sacco conducted a helicopter-supported biogeochemical survey within a relatively inaccessible part of the TREK project area. Samples were collected from the tops of spruce trees within a 1000 km^2 area centred to the south of the Blackwater gold-silver deposit. This paper presents the objectives of this project, as well as sampling and analytical methods. Results will be available in early 2016.

Bouzari et al. present the results of an ongoing project to assess potential geochemical and mineralogical targeting tools to identify metal-fertile plutons. The paper compares results for rock samples and select accessory minerals collected from both mineralized and unmineralized phases of three batholiths in south-central BC. Hoy reports partial results from a multiyear mapping program for the western part of the east Penticton map area of southern BC. The paper provides new geology maps for two 1:20 000 scale TRIM map areas within the Kettle River area, and describes the component rock units, structures and mineralization.

Madu introduces the Search project: Geoscience BC's newest multiyear mineral geoscience initiative in west-central BC. Preliminary plans for four phases of work to be completed over three years are outlined, and details of the recently completed phase I airborne magnetic survey are provided. Results will be available in early 2016.

The 'Energy' section contains seven papers from Geoscience BC's oil and gas and geothermal projects throughout BC. Two papers, by Brown et al. and Hayes et al., discuss key projects that contribute to groundwater mapping of an area of northeastern BC, as part of the multiyear, collaborative Peace project. Brown et al. present the method and preliminary results of the recently completed SkyTEM airborne electromagnetic survey. Hayes et al. describes the method for interpretation of Quaternary sediments and depth to bedrock, using surficial geology maps and downhole data from petroleum boreholes. The results of this work will be used to calibrate airborne survey data, for subsequent processing and modelling of groundwater resources within the Peace project area.

Two papers, by Bustin and Bustin, and Letham and Bustin, highlight continuing work quantifying the gas- and liquid-in-place and flow capacity of important shales in northeastern BC. Bustin and Bustin present the compiled results of publicly available data and new laboratory results as a series of maps of thermal maturity trends and of the oil window for prospective horizons. Preliminary maps show the distribution of produced gas within the Montney Formation. Letham and Bustin report significant progress on better methods to quantify flow characteristics within fine-grained shale rocks. The paper discusses the impact of gas slippage on permeability and, ultimately, on production predictions.

Two papers, by Mahani et al. and Quinton et al., are from projects that address potential impacts of fluctuating water supply within the subsurface and surface of northeastern BC. Mahani et al. present an evaluation of the performance of a regional seismic network that is jointly funded and managed by Geoscience BC together with other members of the British Columbia Seismic Research Consortium. Quinton et al. highlight knowledge gaps in the current understanding of permafrost thaw, in Geoscience BC's new collaborative project with the Consortium for Permafrost Ecosystems in Transition. The paper introduces the scope and methods of this project, as well as results to date.

Hickson et al. introduce a new energy project that will determine the resource and development potential for direct-use geothermal energy in BC communities. The paper presents an example decision matrix, which will uniquely include both technical and community factors, to build a 'Road Map' as a resource to support communities with geothermal resource–related decisions.

The 'Scholarship Recipients' section presents 10 papers from Geoscience BC's 2015 student scholarship winners. The scholarships are awarded annually to postgraduate students working on thesis topics relevant to mineral, oil and gas, or geothermal exploration and development in BC.

Abadzadesahraei et al. present research objectives, field methods and data collected to date for the quantification of the water budget for the Coles Lake watershed. This work will provide baseline information for a hydrological model that will help decision-makers to balance the water needs of industry, communities and ecological systems in this area of northeastern BC.

Gegolick et al. and Prenoslo et al. present research goals for developing predictive models for identification of quality reservoirs within the Montney Formation of northeastern BC. Gegolick and Prenoslo plan to unravel the complex depositional scenario of bioturbated intervals in two areas of this formation: near Fort St. John in northeastern BC (Gegolick et al.), and near Dawson Creek along the northeastern BC border with Alberta (Prenoslo et al.).

Kim et al. present year 2 results for a postgraduate study that is part of Geoscience BC's TREK geology project. The paper includes four mapped type sections with descriptions and lithogeochemical results for volcanic rocks of the Late Cretaceous Kasalka Group—the hostrock to the Blackwater gold-silver deposit. Geochronological results are pending. McGoldrick et al. present mapping results and detailed rock unit descriptions for two areas of the Nahlin ultramafic body, within the Cache Creek terrane of northwestern BC. Preliminary interpretations will be supported by biostratigraphic data and geochemical analyses of rock samples.

Bodnar and Winterburn, and Rich and Winterburn present study plans and preliminary mapping results aimed at providing an improved understanding of the processes controlling ion migration and associated geochemical patterns within the regolith cover of buried mineral deposits. Both research projects will integrate geochemical sample results, self-potential measurements and soil hydrocarbon results above known sulphide deposits: the Lara volcanogenic massive sulphide deposit on Vancouver Island (Bodnar and Winterburn) and the Deerhorn copper-gold porphyry deposit in central BC (Rich and Winterburn).

Granek and Haber present an example of mineral prospectivity mapping applied to Geoscience BC's QUEST dataset, using a support vector machine approach to general algorithms that preserves uncertainties within datasets. It was noted that some limitations to the approach, such as insensitivity to spatial patterns in the data, are an emerging area of research.

Harrichhausen et al. present a synthesis of preliminary field observations from detailed vein and structure mapping at the Brucejack gold deposit in northwestern BC. The structural relationships between the various observed structural elements, as well as vein infill of quartz, carbonate and electrum, are key to understanding the potential for colloidal deposition of gold. Rosset and Hart focus on the characterization and mapping of hydrothermal and alteration assemblages for the Kerr and Deep Kerr porphyry deposits on the KSM property. Next steps will be a review of analytical results from chip samples, to also characterize spatial and temporal distributions of alteration and mineralization.

Readers are encouraged to visit our website for additional information on all Geoscience BC–funded projects, including project descriptions, posters and presentations, previous *Summary of Activities* and *Geological Fieldwork* papers, and final datasets and reports. The website is launching an interactive web-mapping portal, which readers can use to explore all of Geoscience BC's public datasets, as well as select public geoscience databases. All papers in this and past volumes are available for download through Geoscience BC's website (www.geoscience bc.com). Limited print copies of past volumes are also available from the Geoscience BC office.

Geoscience BC Publications 2015

In addition to this *Summary of Activities* volume, Geoscience BC releases interim and final products from our projects as Geoscience BC reports. All Geoscience BC data and reports can be accessed through our website at www.geoscience bc.com/s/DataReleases.asp. Geoscience BC datasets and reports released in 2015 are:

- 21 technical papers in the *Geoscience BC Summary of Activities 2014* volume

- **Investigation of Tree Sap as a Sample Medium for Regional Geochemical Exploration in Glacial Sediment Covered Terrains: A Case History from the Endako Area, North-Central BC (NTS 093F/14, /15, 093K/02, /03)**, by D.R. Heberlein, C.E. Dunn and E. Hoffman (Geoscience BC Report 2015-02)

- **Characterization of Belloy and Debolt Water Disposal Zones in the Montney Play Fairway, Northeast BC**, by Petrel Robertson Consulting Ltd. (Geoscience BC Report 2015-03)

- **Catchment Analysis Applied to the Interpretation of New Stream Sediment Data, Northern Vancouver Island, Canada (NTS 102I, 092L)**, by D. Arne and O. Brown, CSA Global (Geoscience BC Report 2015-04)

- **Historical Exploration Data Capture Pilot Project, Northwestern British Columbia (NTS 093L)**, by C.E. Kilby, Cal Data Ltd. (Geoscience BC Report 2015-06)

- **A Geo-Exploration Atlas of the Endako Porphyry Molybdenum District (NTS 093K)**, by F.A.M. Devine, M. Pond, D.R. Heberlein, P. Kowalczyk and W. Kilby (Geoscience BC Report 2015-08)

- **Geochemical Reanalysis of Archived Till Samples, TREK Project, Interior Plateau, Central BC (Parts of NTS 093C, B, F, K)**, by W. Jackaman, D. Sacco and R.E. Lett (Geoscience BC Report 2015-09)

- **Preliminary Geological Map of the TREK Project Area, Central British Columbia (Parts of NTS 093B, C, F, G)**, by J.J. Angen, E. Westberg, C.J.R. Hart, R. Kim and M. Rahami (Geoscience BC Map 2015-10-01, also as Geoscience BC Report 2015-10)

- **Economic Viability of Selected Geothermal Resources in British Columbia**, by Kerr Wood Leidal Associates Ltd. and GeothermEx Inc. (Geoscience BC Report 2015-11)

- **Regional Geochemical and Mineralogical Data, TREK Project – Year 2, Interior Plateau, British Columbia (Parts of NTS 093B, C, F, G)**, by W. Jackaman, D.A. Sacco and R.E. Lett (Geoscience BC Report 2015-12)

- **The Structural Controls of the Kimberley Gold Trend, East Kootenay District, Southeast British Columbia (Parts of 082F, G)**, by M. Seabrook and T. Höy (Geoscience BC Report 2015-13)

- **Characterization of Belloy and Debolt Water Disposal Zones in the Montney Play Fairway, Northeast BC, Phase 2**, by Canadian Discovery Ltd. (Geoscience BC Report 2015-14)

- **Toward an Improved Basis for Beneath-Cover Mineral Exploration in the QUEST Area, Central British Columbia: New Structural Interpretation of Geophysical and Geological Datasets (NTS 093A, B, G, H, J, K, N)**, by M. Sánchez, T. Bissig and P. Kowalczyk (Geoscience BC Report 2015-15)

- **Tracing the Source of Anomalous Geochemical Patterns in Soil, Water and Seepage Gas Near the Nazko Volcanic Cone, BC (NTS 093B/13)**, by R. Lett and W. Jackaman (Geoscience BC Report 2015-16)

- **Use of a Field Portable Photometer for Rapid Geochemical Analysis of Stream and Spring Waters: A Case History from Poison Mountain, British Columbia (NTS 092O/02)**, by R. Yehia and D.R. Heberlein (Geoscience BC Report 2015-17)

All releases of Geoscience BC reports and data are announced through our website and e-mail list. If you are interested in receiving e-mail regarding these reports and other Geoscience BC news, please contact info@geosciencebc.com.

Acknowledgments

Contents

TREK Geological Mapping Project, Year 2: Update on Bedrock Geology and Mineralization in the TREK Project Area, Central British Columbia (parts of NTS 093B, C, F, G)

J.J. Angen, Mineral Deposit Research Unit, University of British Columbia, Vancouver, BC, jangen@eos.ubc.ca

J.M. Logan, Consulting Geologist, North Saanich, BC

C.J.R. Hart, Mineral Deposit Research Unit, University of British Columbia, Vancouver, BC

R. Kim, Mineral Deposit Research Unit, University of British Columbia, Vancouver, BC

Introduction

The Interior Plateau region of British Columbia is considered to have high exploration potential as it hosts a variety of deposit types including Late Cretaceous and Eocene epithermal Au and Ag deposits (e.g., Blackwater, Capoose and Wolf) and porphyry Cu and Mo deposits (e.g., Endako and Chu) ranging in age from Late Jurassic to Eocene. Exploration activity has historically been hindered by a limited understanding of the character and distribution of prospective units owing to the masking effects of overlying Eocene and Neogene basalt flows and extensive glacial till cover. The **T**argeting **R**esources through **E**xploration and **K**nowledge (TREK) project is a Geoscience BC initiative to integrate geophysical, geological and geochemical data in order to improve our geological understanding and, ultimately, reduce the risk associated with exploration in such a poorly understood region (Clifford and Hart, 2014).

As a component of the TREK project, a targeted regional mapping program was undertaken to provide new geological information to integrate with existing geochemical and geophysical datasets. Interpretation of available aeromagnetic and gravity data was utilized to plan traverses and aid in delineating geological features (Aeroquest Airborne Ltd., 2014; Buckingham, 2014). This was particularly useful for redefining the boundaries of Eocene and Neogene basalts (Angen et al., 2015b). During the regional mapping campaign (Figure 1), 87 samples were collected for geochemical assay. Some samples reflect new mineral occurrences and
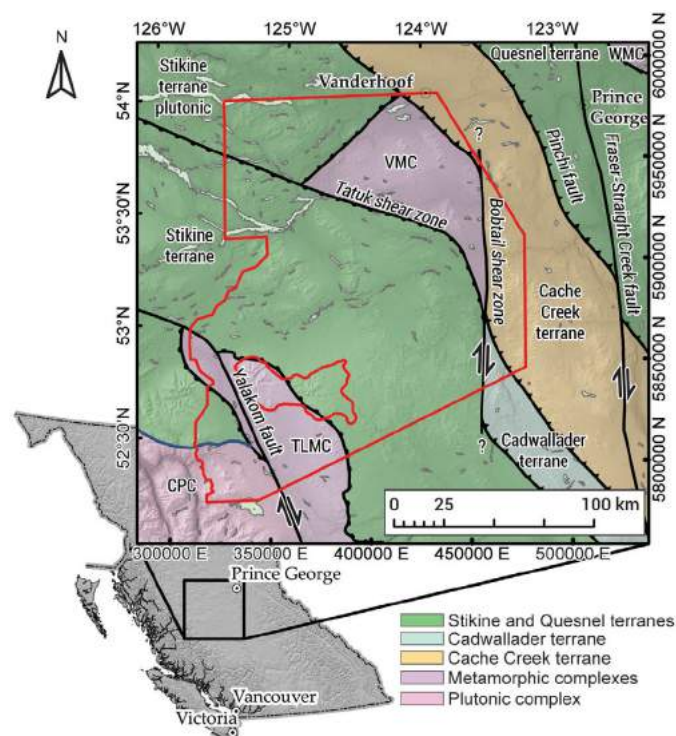
Figure 1. Location of the **T**argeting **R**esources through **E**xploration and **K**nowledge (TREK) study area in central BC. Outline of study area in red. Faults are interpreted from aeromagnetic and gravity data (Aeroquest Airborne Ltd., 2014; Buckingham, 2014). Tectonic domains are modified after Massey et al. (2005). Abbreviations: CPC, Coast Plutonic Complex; TLMC, Tatla Lake metamorphic complex; VMC, Vanderhoof metamorphic complex; WMC, Wolverine metamorphic complex.

even new styles of mineralization within the region. A discussion of selected samples provides value for interested explorers.

Geological Setting

The TREK study area is underlain predominantly by the Stikine island-arc terrane with minor exposure of oceanic

Cache Creek terrane in the east (Figure 1). Both terranes are extensively mantled by overlap assemblages. The southwestern part of the study area is underlain by intrusions and associated metamorphic rocks of the Coast Plutonic Complex. These three tectonic domains are separated by metamorphic complexes and major faults: the Tatla Lake metamorphic complex and Yalakom fault in the west, and the Vanderhoof metamorphic complex and Bobtail shear zone in the east. The TREK mapping project is focused on the geology and mineralization of the Stikine terrane and overlap assemblages. The oldest Stikine terrane rocks belong to the Paleozoic Stikine assemblage (Monger, 1977; Gunning et al., 2006) or the Asitka Group (Lord, 1948). Unconformably overlying the Asitka Group are the Upper Triassic marine sedimentary rocks of the Lewes River Group and submarine volcanic rocks of the Stuhini Group (Souther, 1977). These are in turn unconformably overlain by the predominantly subaerial volcanic and associated sedimentary rocks of the Early to Middle Jurassic Hazelton Group (Tipper and Richards, 1976; Marsden and Thorkelson, 1992; Gagnon et al., 2012). Middle Jurassic accretion is documented by obduction of Cache Creek blueschist onto Stikine terrane (Mihalynuk et al., 2004). Erosion of the uplifted Cache Creek terrane produced the chert-rich detritus preserved in the Middle Jurassic to Early Cretaceous Bowser Lake Group overlap assemblage (Evenchick and Thorkelson, 2005). Continued erosion and unroofing produced the muscovite-rich metamorphic detritus preserved along with continental-arc volcanic rocks in the Early to mid-Cretaceous Skeena Group (Bassett, 1995). Subsequent continental-arc magmatism is recorded by the Late Cretaceous Kasalka Group and associated Bulkley and Blackwater plutonic suites and the Eocene Ootsa Lake and Endako groups and associated Quanchus Plutonic Suite. Flood basalts of the Miocene to Pleistocene Chilcotin Group unconformably cover low-lying areas (Andrews and Russell, 2008), while isolated shield volcanoes and cinder cones of the Miocene to Pliocene Anahim Volcanics define a northeast-trending hotspot track (Kuehn et al., 2015).

Stratigraphy

The eight volcanic and sedimentary sequences covered by this study, from oldest to youngest, are: Early to Middle Jurassic Hazelton Group; Middle to Late Jurassic Bowser Lake Group; Early to Late Cretaceous Skeena Group; Late Cretaceous Kasalka Group; Eocene Ootsa Lake Group; Eocene Endako Group; Neogene Chilcotin Group; and Neogene Anahim Volcanics.

Hazelton Group

The Early and Middle Jurassic Hazelton Group of Tipper and Richards (1976) comprises three formations that from oldest to youngest include: Telkwa, Nilkitkwa and Smithers. Gagnon et al. (2012) subdivided the Hazelton Group into a lower interval of dominantly arc-related volcanic rocks of Hettangian-Sinemurian age and an upper interval of mainly clastic rocks of Pliensbachian to Callovian age that are separated from the lower interval by a regionally diachronous unconformity. In the Nechako River area, the Hazelton Group consists of a marine sequence of rhyolite to basalt fragmental rocks intercalated with sedimentary rocks that comprise the Middle Jurassic, Bajocian Entiako and Naglico formations (Tipper, 1963; Diakow et al., 1997).

Lower Hazelton Group

Telkwa Formation

The Lower Hazelton Group comprises volcanic rocks of Hettangian-Sinemurian age (Tipper and Richards, 1976; Gagnon et al., 2012) that are locally represented by the Telkwa Formation. It is composed of maroon and green andesitic lapilli tuff with abundant plagioclase (up to 40%) ±pyroxene±hornblende phenocrysts. Volcanic boulder conglomerate with a red tuffaceous matrix and well-rounded clasts occurs locally. Anderson et al. (1998) report planar crossbeds, flame structures, and cut-and-fill structures in rich bedded tuffs north of Knewstubb Lake, indicating shallow subaqueous deposition (Figure 2). One such tuff yielded corresponding zircon and titanite ages of 195.2 ±1.1 Ma and 195.9 ±0.7 Ma, respectively (Struik et al., 2007). Similar andesitic lapilli tuffs and reworked crystal tuffs are observed south of the Nechako Reservoir and northeast of the Capoose prospect (MINFILE 093F 040; BC Geological Survey, 2015).

Upper Hazelton Group

The Upper Hazelton Group comprises sedimentary and volcanic rocks of Pliensbachian through Callovian age (Tipper and Richards, 1976; Gagnon et al., 2012). Locally, thick sections of lava flows and volcaniclastic rocks are not well age-constrained either by fossils or isotopic means. Following Diakow et al. (1997), the Upper Hazelton Group is subdivided into the Entiako and Naglico formations in this region. Possible correlations are suggested.

Entiako Formation

The Entiako Formation consists of a lower marine tuffaceous sedimentary unit of Toarcian to Bajocian(?) age and an upper unit of intermediate to felsic volcanic and epiclastic members (Diakow and Levson, 1997; Diakow et al., 1997). Included with the undifferentiated Entiako Formation are thin-bedded variegated siltstone, fine lithic sandstone and ash tuff that correlate with the Quock Formation (Thomson et al., 1986; Gagnon et al., 2012). These are well exposed in a roadcut at the turnoff for the Blackwater mine access road where it departs from the Kluskus-Ootsa Forest Service road (Figure 2). Here, thinly bedded (0.25–5.0 cm), grey, cream, black and pyritic cherty siltstone, argillite and fine ash tuff beds are folded and faulted into a

south-southwest-verging thrust panel. The unit shows soft sediment deformation and normal fault displacements.

Liesegang Basalt: This unit is characterized by abundant flattened amygdules, and hematitic Liesegang rings (Figure 3a). Coherent flow units (2.5–4 m thick), commonly with brecciated flow-tops or bases are locally separated by intraflow fragmental lapilli tuffs, and block breccias occur rarely. The flows are aphyric, sparsely plagioclase-phyric to crowded (1–2 mm, 20–35%) to trachytic with variably hematized and chloritized pyroxene and/or hornblende phenocrysts (2 mm, 2–5%).

The upper and lower contacts of the unit are not exposed but it is stratigraphically above rocks tentatively assigned to the Telkwa Formation south of the Nechako Reservoir in a shallow west-dipping sequence. The Liesegang basalt unit is again observed adjacent to the Telkwa Formation in the eastern Tatuk Hills. It also occurs stratigraphically below quartz-feldspar lapilli tuff of the Entiako Formation in two localities where it is close to the brick-red ash-lapilli lithic tuff and flow-banded rhyolite-dacite units described below: ~1 km south of the turnoff for the Blackwater access road, and south of the Key stock along the Blue Forest Service road (Figure 2).

Red Tuff: Nonwelded, brick-red lithic lapilli tuff and ash tuff is best exposed south of the Key stock along the Blue Forest Service road (Figure 2). Fine-grained bedded ash horizons are defined by abundance and crystal size of white feldspar. Lapilli up to 10 cm are predominantly of purple plagioclase-phyric andesite with lesser red dacite and beige rhyolite (Figure 3b). This unit may correspond to the Toarcian Eagle Peak Formation defined in the Skeena-Nass area (MacIntyre et al., 1994), formerly the Red Tuff Member of the Nilkitkwa Formation (Tipper and Richards, 1976).

Red Dacite: White, grey, purple and red flow-banded dacite and spherulitic rhyolite is traced around the southern margin of the Key stock. Some occurrences were previously mapped as Ootsa Lake Group and Entiako Formation. Flow bands are contorted and locally exhibit quartz-filled vugs (Figure 3c). A similar maroon flow-banded dacite occurs below Entiako Formation quartz-feldspar lapilli tuff along the Kluskus-Ootsa Forest Service road, ~1 km south of the Blackwater access road and on the western flank of Fawnie Dome.

Entiako Lapilli Tuff: A white-weathering quartz-feldspar crystal-lithic lapilli tuff—conspicuous by the presence of lithic clasts of maroon/red tuff, and flow-laminated and quartz eye–bearing rhyolite clasts—crops out south of the Key stock, on the western flank of Fawnie Dome, and at the Entiako Formation type section (5 km marker on the Kluskus-Malaput Forest Service road; Diakow et al., 1997). Red tuff clasts indicate that this distinctive lapilli

tuff postdates the brick-red ash tuff described above (Figure 3d). Purple- to pink-weathering plagioclase and quartz crystal lithic tuff extends from the developed 3TS prospect (MINFILE 093F 055, 093F 068) toward the northwest where it is truncated by the Laidman batholith (this study; Diakow and Levson, 1997; Figure 2). Here the tuff is lithic dominated, rhyolitic and monomict. Rounded to broken plagioclase, K-feldspar and quartz phenocrysts average 2–5 mm, and comprise 20–25% each within a siliceous salmon-pink matrix that lacks foreign maroon lithic clasts.

Naglico Formation

Overlying the Entiako felsic tuffaceous units, apparently unconformably (Diakow et al., 1997), are pyroxene-phyric coherent basalt, breccia, conglomerate and pyroxene-rich sandstone and epiclastic deposits. Age constraints include a probable early Bajocian fossiliferous limestone (south of the Capoose pluton) and latest early Bajocian, or early late Bajocian, bivalves and ammonites from siltstone, sandstone and conglomerate southeast of the 3TS prospect (MINFILE 093F 055, 093F 068).

Interlayered and graded coarse plagioclase- and pyroxene-crystal sandstone, lithic conglomerate and plagioclase-pyroxene–phyric basalt overly parallel-laminated, variegated beds of cherty siltstone and sandstone at the Entiako Formation type section (Diakow et al., 1997). On Fawnie Dome, pink K-feldspar–phyric dacite of the Entiako Formation is overlain by massive, amygdaloidal pyroxene-plagioclase–phyric coherent basalt. The basalt is characterized by stubby white plagioclase laths (1–3 mm, 30%) and sparse equant pyroxene phenocrysts (2–4 mm, 10–12%) within a fine-grained matrix of plagioclase, pyroxene and disseminated magnetite. Chlorite and spotty epidote alteration is ubiquitous.

Bowser Lake Group

Ashman Formation

Middle Jurassic clastic rocks of the Ashman Formation in the TREK study area comprise a deep-water facies of fine-grained mudstone and siltstone with limy lenses and an overlying eastward-thickening wedge of conglomerate, sandstone and siltstone (Diakow et al., 1997).

Black shale interbedded with fine sandstone and fossiliferous greywacke is exposed at the Buck showing (MINFILE 093F 050), on the Blackwater mine access road (kilometre 0.5 to 2.5) and west of Chedakuz Creek (Diakow and Levson, 1997). At the Buck showing, black mudstone, parallel-laminated argillite and siltstone comprise an upward-facing sedimentary panel ~50 m thick that grades upward into pyroxene-porphyry basalt and volcaniclastic rocks of the Nechako Formation. The same stratigraphic relationships also occur along the Blackwater mine access road.

Figure 2: Bedrock geology of the **T**argeting **R**esources through **E**xploration and **K**nowledge (TREK) study area. Abbreviations: FSR, Forest Service road; G, G-pluton. Modified after Angen et al., 2015a. Legend continued on the following page.

VOLCANIC AND SEDIMENTARY ROCKS

Miocene to Holocene
Anahim Volcanics
Basanites to basaltic trachyandesites and trachytes

Miocene to Pliocene
Chilcotin Group
Olivine basalt lava flows

Eocene to Oligocene
Endako Group
Basaltic andesite and andesitic lava flows

Eocene
Ootsa Lake Group
Rhyolite to andesite flows and volcaniclastic rocks

Upper Cretaceous
Kasalka Group
Hornblende andesite
Crystal-lithic tuff
Vitric tuff
Flow-laminated rhyolite
Undifferentiated andesite to rhyolite flows and volcaniclastic rocks

Lower Cretaceous
Skeena Group
Chert- and quartz-rich sandstone and conglomerate

Upper Jurassic
Nechako Formation
Pyroxene- and hornblende-phyric basalt

Middle and Upper Jurassic
Bowser Lake Group
Chert pebble conglomerate, sandstone, siltstone and mudstone

Stikine terrane

Lower and Middle Jurassic
Hazelton Group
Naglico Formation
Pyroxene-phyric basalt, lapilli tuff and sedimentary rocks
Entiako Formation
Crystal-lithic tuff
Red tuff
Red dacite
Liesegang basalt
Undifferentiated sedimentary and bimodal volcanic sequence
Telkwa Formation
Rhyolite to basalt flows and volcaniclastic rocks
Undifferentiated
Rhyolite to basalt flows and associated volcaniclastic rocks

Triassic
Limestone

Cache Creek terrane
Permian – Triassic
Metasedimentary rocks and basalt
Serpentinite

PLUTONIC ROCKS

Eocene
Quanchus Plutonic Suite
Biotite-hornblende granodiorite to tonalite
Assumed Eocene mafic intrusions inferred from aeromagnetic data

Late Cretaceous
Blackwater Plutonic Suite
Biotite-hornblende quartz monzonite to monzogranite
Plagioclase-phyric diorite

Jurassic to Paleogene
Coast Plutonic Complex
Diorite to granodiorite related volcanic rocks

Late Jurassic to Early Cretaceous
Francois Lake Plutonic Suite
Biotite monzogranite to hornblende-biotite granodiorite

Early and Middle Jurassic
Stag Lake Plutonic Suite
Quartz monzonite to tonalite

Triassic to Jurassic
Brooks Diorite Complex
Variably foliated gabbro to monzonite

METAMORPHIC ROCKS

Jurassic to Cretaceous
Tatla Lake metamorphic complex
Mylonite and migmatitic gneiss

Triassic to Jurassic
Vanderhoof metamorphic complex
Orthogneiss and schist

OTHER FEATURES

- City
- Road
- River
- Lake

Mineral Occurrences
- Porphyry Cu-Au: vein, breccia
- Porphyry Mo (Low F- type)
- Epithermal Au-Ag-Cu: high sulphidation
- Epithermal Au-Ag: low sulphidation
- Subvolcanic Cu-Ag-Au (As-Sb)
- Polymetallic veins Ag-Pb-Zn+/-Au
- Carbonate-hosted disseminated Au-Ag
- Cu skarn
- Fe skarn
- Ultramafic-hosted asbestos
- Lignite
- Volcanic redbed Cu

An isolated outcrop of white-weathering chert pebble–granule conglomerate and lithic sandstone, crops out north of Fawnie Dome (Diakow and Levson, 1997). The conglomerate is well sorted, massive or thickly bedded and clast-supported. It is composed of white, grey, black and pale green subangular to well-rounded chert pebbles (4–15 mm). The conglomerate has been silicified, probably due to the pyroxene diorite intrusion that forms the hilltop 300 m to the south. Ashman Formation conglomerate is well exposed in the Nechako Range (Diakow et al., 1997).

Nechako Formation

Coarse pyroxene-phyric basalt breccia, pyroxene-phyric clast-dominated polymict conglomerate and rare fine-grained bedded epiclastic units underlie the area north of Top Lake, south of the Capoose prospect (Fawnie Nose), and the western flank of the Nechako Range (Diakow and Levson, 1997). North of Top Lake, the fault-bounded unit includes a dominantly effusive lower member of coarse pyroxene-phyric basalt with stubby to equant euhedral black pyroxene phenocrysts (0.5 by 1 mm, up to 10 mm, 15–20%) and white tabular, subhedral plagioclase phenocrysts (2–3 mm, 20%) within a black, green or red hematitic fine-grained matrix. This is overlain by an upper member of pyroxene-dominated polymict fragmental and epiclastic rocks that fines upward into well-bedded fossiliferous siltstone, sandstone and wacke. Contacts are not exposed but sedimentary facing directions suggest the sedimentary units overlie the pyroxene basalt. The volcanic rocks are intruded by coarse crowded pyroxene-plagioclase sills (2–4 m thick) and fine-grained equigranular pyroxene diorite dikes (1–2 m wide). The dikes display vesicular margins.

Thickly bedded, chaotic matrix-supported polymict volcanic boulder conglomerate, with rare well-bedded normal-graded sandstone and siltstone intervals, dominate the upper member. These units are exposed along the Kluskus-Ootsa Forest Service road, south of Fawnie Dome (Figure 2), and in drilling northwest of the Black Bear prospect (MINFILE 093F 075; Webster, 2013). Lithic clasts include intermediate to felsic volcanic rocks that are black, green and maroon; aphyric to plagioclase–, plagioclase+ hornblende– and plagioclase+pyroxene–phyric; and weather white. Matrix to the conglomerate is a pyroxene-crystal–rich litharenite derived primarily from volcanic sources. Upsection, the volcanic stratigraphy fines and is replaced by thinly bedded, interlayered sandstone and siltstone, calcareous fossiliferous wacke and argillaceous mudstone. Calcareous centimetre-thick beds of quartz, plagioclase and chert/rhyolite lithic wacke weather yellow and contain abundant belemnoids, bivalves and coaly plant fragments. Early Callovian ammonites and numerous other less diagnostic fossils were reported from similar sedimentary rocks located 800 m southeast (Collection GSC C-143395, as discussed in Diakow et al. 1997).

Figure 3: Characteristic features of newly identified members of the Entiako Formation: **a)** hematitic Liesegang rings developed in basalt at the new Liesegang volcanic redbed-copper showing; **b)** lithic lapilli tuff characteristic of the Red tuff unit; **c)** flow-banded rhyodacite of the Red dacite unit with quartz-filled vugs along flow bands; **d)** crystal-lithic lapilli tuff with distinct red to purple lapilli derived from the underlying Red tuff unit.

Skeena Group

Sedimentary rocks with late Albian to early Cenomanian palynomorphs are reported from the area along the Entiako River where it enters the Nechako Reservoir (Diakow et al., 1997). These rocks are age correlative with the Skeena Group which is characterized elsewhere in the Interior Plateau by polylithic chert-rich conglomerate, mudstone and muscovite-bearing sandstone (Bassett and Kleinspehn, 1997). Age equivalent chert pebble conglomerate, chert-rich sandstone and siltstone of the Nazko and Redstone belts are also included with the Skeena Group (Riddell, 2011).

Kasalka Group

The stratigraphy of the Kasalka Group is described in detail by Kim et al. (2016). It is composed of a basal conglomerate, felsic to intermediate volcaniclastic rocks, flow-banded rhyolite, and locally columnar-jointed andesite flows. It is well exposed in the vicinity of the Blackwater

mine, including a prominent ridge that follows the eastern faulted(?) contact with the Laidman batholith, and southeast of Cabin Lake (Figure 2). Observations from drillcore at the Blackwater mine indicate that the Kasalka Group was deposited unconformably on the Ashman Formation (Looby, 2015). This is in contrast with observations along the Blackwater access road where the Ashman Formation is overlain by Nechako Formation basalt, suggesting that the Kasalka Group was deposited onto a significant erosional surface.

Ootsa Lake Group

The Ootsa Lake Group covers the majority of the southeast quadrant of the map area and a significant portion of the region west of Knewstubb Lake (Figure 2). It is composed of predominantly felsic flows and associated volcaniclastic rocks. A basal conglomerate locally contains plutonic clasts (Andrew, 1988). This is overlain by acicular hornblende-bearing dacite, biotite-phyric ash flows, and perlitic vitreous black dacite locally with up to 1% pyroxene

phenocrysts (Mihalynuk et al., 2008; Bordet, 2014). White, pink and grey, locally flow-banded rhyolite and rhyolitic lapilli tuff with up to 5% quartz, 7% plagioclase and 2% biotite phenocrysts locally dominates the Ootsa Lake Group (Diakow et al., 1997; Bordet, 2014). The U-Pb and Ar-Ar constraints indicate that Ootsa Lake Group volcanism persisted from 54.6 to 46.6 Ma (Bordet et al., 2014). Based on new correlations, the extent of Ootsa Lake Group rocks in the vicinity of the Blackwater mine has been significantly reduced (Figure 2; Kim et al., 2016).

Endako Group

The Endako Group consists of metre-thick, commonly vesicular flows with pumiceous margins or flow-brecciated tops and bottoms, with rare entablature columnar-jointed sections in the vicinity of Kenney Dam. Basalt textures include the following: coarsely vesicular to pumiceous aphyric flows; fine-grained green- and brown-mottled matrix containing glomeroporphyritic plagioclase and sparse ophitic pyroxene crystals; and medium-grained felted matrix of vitreous plagioclase laths (0.5–0.8 mm, 75%), sparse equant pyroxene phenocrysts (1.0 mm, 5–7%), and very fine grained disseminated magnetite (Angen et al., 2015b).

Chilcotin Group

Chilcotin basalts underlie a substantial area south of Batnuni Lake. The basalt is orange to deep red weathering, vesicular to pumiceous and generally subhorizontal. In cross-section it shows fluidal lamination with entrained angular blocks and lapilli and locally, in plan view, good polygonal jointing is preserved in the thicker units. The basalt is coarsely porphyritic with 2.5–5.0 mm phenocrysts of olivine and pyroxene comprising 5–7% within a commonly aphyric matrix. Thicker flows are characterized by a felted matrix of translucent plagioclase laths (1.0 mm, 30%) and pyroxene and olivine phenocrysts (1–2.5 mm, 7–10%). The Cheslatta Lake suite, herein included with the Chilcotin Group, contains distinct xenoliths of dunite to lherzolite (Anderson et al., 2001; Angen et al., 2015b).

Anahim Volcanics

The Anahim volcanic rocks form a series of small, 1–3 km diameter, volcanic cones composed of dark grey and red unconsolidated scoriaceous breccia as well as trachyandesite, trachyte, phonolite, and lesser alkali basalt and basanite flows and dikes (Kuehn, 2014; Kuehn et al., 2015). These volcanic rocks are interpreted as the product of a hotspot currently located near Nazko (Figure 2; Souther, 1977; Kuehn, 2014; Kuehn et al., 2015).

Plutonic Suites

Brooks Diorite Complex

The Brooks Diorite Complex is composed of unfoliated to gneissic, fine- to coarse-grained mafic intrusions including hornblende±biotite diorite, monzodiorite, monzonite, and gabbro (Wetherup, 1997). It is exposed southeast of the Kenney Dam road (Figure 2). Crosscutting relationships with more foliated phases cutting less foliated ones indicate that the complex is synkinematic with respect to steeply dipping, northwest-striking foliation. It has not yet been dated but may correlate with the Late Triassic foliated Stern Creek Plutonic Suite of the Endako batholith defined by Villeneuve et al. (2001).

Stag Lake Plutonic Suite

The Stag Lake suite is compositionally heterogeneous, but in general more mafic than younger suites. It comprises gabbro, diorite, quartz monzodiorite, quartz monzonite and monzogranite. A megacrystic monzogranite, with concentrically zoned pale pink K-feldspar crystals up to 5 cm long, was observed southeast of Francois Lake (Figure 2); it is interpreted to correspond to the Caledonia phase, described by Struik et al. (1997), immediately to the north in which the K-feldspar megacrysts are pale pink to beige. The Stag Lake suite ranges in age from 180 to 161 Ma (Villeneuve et al., 2001).

Francois Lake Plutonic Suite

The Francois Lake Plutonic Suite includes fine- to coarse-grained biotite monzogranite and hornblende-biotite granodiorite (Villeneuve et al., 2001). Intrusions belonging to this suite are exposed in the north-central portion of the map area where they host Mo porphyry mineralization at Nithi Mountain (MINFILE 093F 012) and in the vicinity of Laidman Lake where they comprise the Laidman batholith (Figure 2). The recently closed Endako mine is also hosted in Francois Lake suite granodiorite immediately north of Francois Lake (Figure 2). The presence of pink or orange K-feldspar is ubiquitous. It was emplaced between 157 and 145 Ma (Villeneuve et al., 2001).

Laidman Batholith

The Laidman batholith is a coarse-grained biotite-hornblende quartz monzonite to granodiorite that underlies approximately 200 km^2 including parts of both the Kluskus-Malaput and Kluskus-Ootsa Forest Service roads. Internal heterogeneities in the reduced-to-pole total magnetic intensity (Aeroquest Airborne Ltd., 2014) across the batholith suggest it includes at least two separate phases. A sample was collected for U-Pb zircon geochronology, to test whether an internal annular high reflects an intrusion of the same age or younger.

The majority of the Laidman batholith is composed of pale grey to pink, generally coarse-grained quartz monzonite containing numerous (centimetre–metre sized) fine-grained hornblende diorite xenoliths. Tabular, twinned pink to salmon-red K-feldspar and white to grey plagioclase laths, typically 5–10 mm, comprise 75–80% of the rock with vitreous subangular quartz grains up to 8%. Mafic minerals include black stubby prisms and crystal aggregates of hornblende (2–4 mm, 7–10%); black, euhedral fresh biotite (2 mm, 2–4%); and trace amounts of sphene and magnetite as discrete grains and crystal aggregates. North of the Kluskus-Ootsa Forest Service road are outcrops of pink weakly altered, coarse-grained hornblende-biotite leucogranite. Stubby to euhedral twinned crystals of K-feldspar (3–15 mm, 40%) and vitreous, anhedral to rounded quartz (2–12 mm, 35–40%) comprise the majority of the granite. Intergrown with the K-feldspar are stubby crystal aggregates of plagioclase (20%), biotite (2 mm, 1–3%) and traces of shredded hornblende and magnetite.

A K-Ar biotite cooling age of 141 ±4 Ma and U-Pb titanite crystallization age of 148.1 ±0.6 Ma (Diakow and Levson, 1997), as well as three U-Pb zircon ages of 148.3 ±0.3, 148.8 ±0.5 and 147.2 ±0.3 Ma (Poznikoff et al., 2000) establish a Late Jurassic age for the northwestern portion of the Laidman batholith.

Blackwater Plutonic Suite

The Blackwater suite is a series of granodiorite to quartz monzonite intrusions of latest Late Cretaceous age. It is distinguished from the early Late Cretaceous Bulkley suite that crops out further west by its younger age. It includes the Capoose pluton, G-pluton, Blackwater pluton, Key stock, and several small unnamed bodies.

Capoose Pluton

The Capoose pluton is a northwest-trending body that underlies approximately 145 km^2 centred on Capoose Lake. Historically it had been grouped with exposures of similar hornblende-biotite quartz monzonite and granodiorite that extend as far south as Laidman and Moose lakes and referred to as the Capoose batholith (Diakow and Levson, 1997). However, on the Total Magnetic Intensity (TMI) reduced-to-pole map the Capoose pluton is surrounded by an annular magnetic anomaly (Aeroquest Airborne Ltd., 2014). Exposures of the southern part of the pluton are deeply weathered and overlain by up to 5 m of coarsely granulated material. The intrusion is pale grey and pink and comprises medium- to coarse-grained equigranular hornblende-biotite granite, potassium feldspar megacrystic hornblende-biotite quartz monzonite and granodiorite. In hand specimen zoned, tabular pinkish crystals of K-feldspar are typically 4–6 mm; but exceed 1.5 cm in the megacrystic variety and generally comprise 25 to 30% of the rock. White, subhedral, stubby plagioclase laths of about the same size are intergrown with K-feldspar. Quartz grains are generally less than 2 mm and comprise 20–25% of the rock. Mafic minerals include; tabular hornblende (3–6 mm, 5%), euhedral biotite books (2–3 mm, 7%) and accessory amounts of titanite (3–4 mm) and magnetite which occur interstitial or as inclusions in feldspar. Published age determinations on the pluton includes a K-Ar biotite age of 67.1 ±4.6 Ma (Andrew, 1988) and two U-Pb zircon ages of 64.1 +5.4/–7.7 Ma and 69.6 ±0.4 Ma (Friedman et al., 2001).

G-pluton

The G-pluton is an equigranular to quartz-phyric hornblende-biotite granite that crops out on the Blackwater mine access road at kilometre 3. In outcrop it is massive to weakly jointed, unaltered and locally contains miarolitic cavities. Marginal phases are fine grained and quartz± plagioclase–phyric, while the interior of the pluton is typically medium grained and equigranular. Pink potassium feldspar (30%) forms tabular crystals typically 2–5 mm long, occasionally up to 10 mm, or occurs as irregularly distributed matrix intergrown with white euhedral 2–3 mm plagioclase laths (20–25%). Grey, vitreous quartz grains are generally subrounded to euhedral (3–5 mm, 20–25%). Interstitial to feldspar and quartz are weak chlorite-altered, 1–3 mm hornblende crystals and vitreous euhedral 2–4 mm biotite books that comprise approximately 5–7% of the rock. Disseminated magnetite and pyrite are accessory minerals.

A Late Cretaceous U-Pb zircon crystallization age for the G-pluton, which is older than previously suspected, and new intrusive relationships that further constrain the age of the rhyolite country rock in the area (i.e., to be older than the pluton) was reported by R. Whiteaker (pers. comm., 2015). The porphyritic variety closely resembles the quartz-feldspar crystal-lithic lapilli tuff that caps the ridge 5 km southeast.

Blackwater Pluton

The Blackwater pluton is an equigranular, medium-grained biotite±hornblende granodiorite to monzogranite. Its margins are particularly well defined in the total magnetic intensity reduced-to-pole aeromagnetic data. The U-Pb zircon ages from granodiorite of the Blackwater pluton and monzogranite of the Key stock indicate crystallization ages of 69.5 Ma and 68.5 Ma, respectively (Whiteaker, 2015). The Re-Os age of mineralization, as determined from molybdenite hosted in the Blackwater pluton at Blackwater South and molybdenum mineralization at the Key occurrence, returned ages of 66.7 Ma and 68.4 Ma, respectively (Whiteaker, 2015).

Quanchus Plutonic Suite

The Quanchus Plutonic Suite is locally represented by the CH pluton, the Frank Lake pluton and the Grizzly pluton. They are composed of white and black equigranular biotite±hornblende granodiorite containing conspicuous titanite (1–3 mm), magnetite (1–2 mm) and rare tourmaline.

In the CH pluton, the equigranular granodiorite is cut by dikes of fine-grained quartz-phyric granite and sheeted dikes of aplite with coarse pegmatite segregations that are thought to be coeval and comagmatic with the main intrusion. These late stage siliceous phases are thought to be associated with the molybdenite mineralization reported to occur at the Chu developed prospect (Allnorth Consulting Limited, 2007; MINFILE 093F 001). In addition, the pluton is intruded by metre-wide hornblende-porphyry diorite dikes with chilled flow-banded margins that likely postdate crystallization of the main phase granodiorite. Diakow et al. (1995) reported K-Ar hornblende and biotite ages for the CH pluton of 51.8 ±1.8 Ma and 48.8 ±1.3 Ma, respectively. A similar age of 51.8 ±1Ma was determined from U-Pb dating on zircon separates from the same location (Diakow and Levson, 1997). A U-Pb zircon sample from the Frank Lake pluton yielded an age of 55 Ma (no reported errors, Struik et al., 2007).

Mineral Occurrences

The identification of the Blackwater South porphyry Cu-Mo mineralization and confirmation of the Key porphyry Cu-Mo mineralization during the summer of 2014 highlights the continued prospectivity of this region, not only for epithermal style, but also for deeper larger porphyry targets (Whiteaker, 2015). During the TREK mapping campaign, a total of 87 rock samples were collected from both known MINFILE occurrences and newly identified showings. Samples were submitted to Acme Laboratories Ltd. (Bureau Veritas) in Vancouver, BC. A 15 g split from each sample underwent aqua-regia digestion and was analyzed for 37 elements via inductively coupled plasma–mass spectrometry. Samples representing new mineralization, as well as a selection of MINFILE occurrences are discussed below. Rock sample descriptions and geochemical results for selected samples are presented in Table 1.

Holy Cross (MINFILE 093F 029)

Two samples of brecciated flow-banded rhyolite with vuggy quartz infill and 1–2% finely disseminated pyrite were collected from the Holy Cross showing. Sample 14EW105A returned 5.62 g/t Ag and 0.349 g/t Au, and sample 14EW108A returned 4.86 g/t Ag, 0.0342 g/t Au and 1075 ppm As (Table 1). The flow-banded rhyolite, hosting the mineralization, forms a series of resistant knobs trending northwest that were interpreted to be intrusive domes (Barber, 1989). The same brecciated flow-banded

rhyolite is found at low topography between the knobs and is flanked to the northeast and southwest by weakly foliated Hazelton Group volcanic rocks; these exhibit variable silicification and potassic alteration that is magnetite destructive. The flow-banded rhyolite and associated mineralization at Holy Cross was assigned to the Eocene Ootsa Lake Group based on similarity to other Eocene low-sulphidation epithermal deposits (Lane and Schroeter, 1997). The authors suggest that the rhyolite and mineralization may be Late Cretaceous in age because the associated alteration does not appear to affect the plagioclase- and hornblende-phyric andesite flows, which were dated by Friedman et al. (2001) as 65.7 ±5.4 Ma (K-Ar hornblende). A sample of flow-banded rhyolite collected in 2014 for U-Pb geochronology failed to yield zircons.

Sample 14JA111A was collected from an exceptionally gossanous outcrop of Skeena Group conglomerate that exhibits pahoehoe like flow-top textures interpreted to reflect deposition as a subaerial debris flow (Figure 4a). It returned 3.06 g/t Ag and 100.2 ppm Cu. This is in agreement with a previous report indicating up to 5% disseminated pyrite from silicified conglomerate in the vicinity of the Holy Cross prospect (Barber, 1989).

Key West (MINFILE 092F 613)

The Key West showing consists of poorly exposed, highly quartz-sericite–altered andesitic volcanic rocks, with up to 10% finely disseminated pyrite. In 2010, a grab sample from this showing returned 4.57 g/t Au, 15.1 g/t Ag and 1685 ppm Cu (Torgerson, 2010). An approximately 300 m diameter exposure of hornblende-phyric quartz monzonite is located immediately northeast of the pyritized and silicified andesite. It was assigned to the Late Jurassic Laidman batholith by Diakow et al. (1995) but is tentatively assigned to the Late Cretaceous Blackwater suite, a proposal that will be tested by U-Pb zircon geochronology. Sample 15JL128A was collected from the eastern part of the Key West zone from maroon lapilli breccia with epidote alteration and malachite staining. It returned 0.11 g/t Au, 35.6 g/t Ag, and 0.52% Cu.

Havana (New)

At this locality, magnetite pyrite veinlets with pink K-feldspar alteration haloes were observed rarely in outcrop, but as high density sheeted veinlets in float (Figure 4b). The veinlets cut hornblende-phyric quartz monzonite indistinguishable from the one exposed at Key West approximately 2.5 km to the north. Furthermore, the till immediately west of this locality is extremely gossanous and predominantly composed of quartz-sericite-pyrite–altered andesite similar to the outcrop exposures at Key West (Figure 4c). Sample 15JA109A was collected from the float boulder with sheeted magnetite pyrite veinlets. It returned only 0.18 g/t Ag and 100 ppm Cu.

Table 1. Assay results for selected elements and samples collected during the Targeting Resources through Exploration and Knowledge (TREK) mapping project.

Station	Easting[1]	Northing[1]	Comments
14EW062A	363571	5973670	Quartz/sericite(?) altered rhyolite with minor sulphides localized along fracture planes.
14EW066A	348486	5979685	Plagioclase-phyric andesite cut by fault breccia with quartz infill. Sample of 5% disseminated pyrite adjacent to breccia zone.
14EW081A	381865	5924177	Fault breccia with quartz infill contains limonite, hematite and 1% pyrite. Pyrite is entirely within quartz vugs.
14EW105A	369874	5961626	Silica infill around breccia cutting flow-banded rhyolite; 1% disseminated pyrite.
14EW108A	368669	5962936	Silica infill around breccia cutting flow-banded rhyolite; 1–2% pyrite disseminated and on fracture surfaces.
14EW164A	394426	5908901	2% pyrite and <1% molybdenite in rusty weathering tonalite.
14JA111A	369999	5960657	Gossanous polylithic conglomerate with iron-oxide–rich matrix. Common quartz and unidentified aphanitic black veinlets. Pyritohedron vugs observed locally.
14RK144A	354409	5928735	Epidote- and chlorite-altered andesitic lapilli tuff with 1% disseminated pyrite. Very rusty weathered surfaces.
15JA001A	358924	5896673	Veinlets of po, py and black sulphosalts(?) surrounded by silica alteration halo with finely disseminated po (locally up to 10%).
15JA056A	349184	5878682	Up to 10% patchy and disseminated py and po in biotite hornfelsed andesite.
15JA065A	368922	5885929	5% finely disseminated sulphides with py>po in intensely silicified andesite.
15JA067A	369519	5885807	10% finely disseminated and poddy sulphides with py>po>>cpy in intensely quartz sericite–altered andesite.
15JA070A	370233	5885792	1% disseminated pyrite in exceptionally rusty silicified andesite.
15JA074A	369435	5886398	5% finely disseminated and blebby pyrite in quartz sericite altered andesite.
15JA079A	348408	5882051	5% disseminated pyrite in sandstone with quartz sericite alteration overprinting chlorite epidote alteration.
15JA092A	375125	5885739	Up to 10% disseminated sulphides (py>po>sp>>cpy) in felsic lapilli tuff. Sphalerite occurs as dull brown concentric bands around fragments and rarely as up to 1 cm clusters of brown crystals.
15JA093A	375113	5885796	2% py and po and trace cpy in epiclastic coarse-grained biotite–altered sandstone interbedded with lithic lapilli tuff.
15JA109A	369829	5883100	Float sample of sheeted magnetite veinlets with pyrite cores and potassic alteration haloes in quartz monzodiorite.
15JA113A	362091	5916397	Fault breccia with quartz, calcite, adularia infill with 3% finely disseminated py.
15JA125A	356288	5915365	Float sample but veins of same gangue material abundant in outcrop; 3% native Cu and trace malachite in epidote, quartz, calcite vein.
15JA189A	349579	5897824	Up to 2 cm wide magnetite vein with garnet alteration halo.
15JL128A	371457	5885635	Epidote alteration and malachite stain on maroon lapilli breccia.
15RK191A	449302	5921000	Subhorizontal quartz chrysocolla vein 5 cm wide cutting pyroxene-plagioclase–phyric andesite.

[1] UTM Zone 10 (NAD 83)

Abbreviations: cpy, chalcopyrite; po, pyrrhotite; py, pyrite; sp, sphalerite

Table 1 (continued)

Station	Au (ppb)	Ag (ppb)	Mo (ppm)	Cu (ppm)	Pb (ppm)	Zn (ppm)	Ni (ppm)	Co (ppm)	Mn (ppm)	Fe (%)	As (ppm)	Sb (ppm)	Bi (ppm)	Ba (ppm)	S (%)	Hg (ppb)	Te (ppm)
Detection limit	0.2	2	0.01	0.01	0.01	0.1	0.1	0.1	1	0.01	0.1	0.02	0.02	0.5	0.02	5	0.02
14EW062A	60.7	1368	9.39	5.31	80.72	107.6	0.7	0.7	3343	1.25	119.8	2.69	0.52	75.8	<0.02	12	0.04
14EW066A	88.2	6111	49.13	124.68	116.2	141.8	3	48.4	1935	5.09	77.8	1.9	20.14	169.3	0.08	14	0.81
14EW081A	350	435	2.32	10.49	1.54	4.6	3	1.5	130	1.31	219.5	5.52	<0.02	25.8	0.22	24	<0.02
14EW105A	349	5619	119.6	65.74	30.8	5.7	0.7	0.6	34	0.9	19.8	16.94	4.8	201.8	0.39	112	1.77
14EW108A	34.2	4859	36.47	7.65	68.34	29.2	0.7	1.4	35	1.96	1074.5	36.49	0.37	75.2	1.08	215	0.36
14EW164A	32.3	3534	49.25	349.36	11.03	83.4	7.1	13.9	235	3.29	1564.7	3.48	4.15	100.2	1.44	<5	1.36
14JA111A	15.6	3056	74.88	100.17	19.59	115.7	9.6	4.2	164	12.2	15.1	3.74	0.08	37	0.05	9	0.47
14RK144A	4.8	939	3.2	5.3	47.46	91.6	2	7.9	751	3.72	44.5	0.58	0.05	72.7	0.9	5	0.7
15JA001A	1	687	0.1	418.45	19.57	43.7	144.8	104.4	782	6.51	16.4	0.28	0.64	25.6	3.16	13	0.36
15JA056A	13.1	844	1.42	71.81	110.8	85.8	4.4	24.8	324	4.12	13.4	0.57	0.07	114.8	1.31	15	<0.02
15JA065A	1.1	124	0.56	51.39	8.67	69.9	20.8	23.2	607	6.18	0.4	0.12	0.05	19.5	4.71	13	0.9
15JA067A	0.3	164	0.86	73.78	19.38	87.6	7.5	19.8	1195	5.12	1.5	0.17	0.04	35.4	2.07	18	0.04
15JA070A	1.2	242	4.4	46.32	49.03	32.7	0.9	1.2	140	1.56	25.1	0.3	0.11	113.6	0.33	13	<0.02
15JA074A	<0.2	118	1.78	26.39	13.65	66.6	3.4	10	622	3.45	6	0.22	0.04	66.8	2.43	15	<0.02
15JA079A	<0.2	348	0.49	100.78	25.78	73	36.1	30.6	802	4.35	24.1	1.86	0.05	66.3	1.02	10	<0.02
15JA092A	19.5	506	0.87	82.87	12.02	3868.4	58.5	23.9	241	3.75	162.7	1.1	10.65	87.7	2.37	<5	0.37
15JA093A	1.8	282	0.48	86.38	16.66	88.1	62.8	21.2	227	2.49	110.5	1.39	0.51	162.5	1.03	9	0.12
15JA109A	0.6	178	1.36	100.54	5.72	86.4	4.1	7.1	1172	4.56	2.3	0.1	0.15	76.7	0.11	6	0.02
15JA113A	0.4	786	0.12	2.85	14.59	102.4	0.8	10.3	1808	4.49	1.9	0.26	0.07	287.9	0.51	<5	<0.02
15JA125A	2.9	7047	0.2	>10000.00	2.54	8.1	1	1.7	435	1.22	26.9	0.05	<0.02	5.9	<0.02	1263	<0.02
15JA189A	103	643	0.17	6.09	41.95	827	1.2	3.4	2636	5.28	35.1	2.33	0.24	39.3	<0.02	<5	0.2
15JL128A	115	35619	0.42	5223.62	5.78	147.5	18.7	34.2	1424	3.43	6.6	0.47	0.16	239.9	0.04	47	0.03
15RK191A	9.8	144	7.47	>10000.00	5.37	12.7	13.7	13.8	470	3.94	9.1	0.82	0.21	18.3	<0.02	362	0.3

Figure 4: a) Gossanous Skeena Group conglomerate with apparent flow-top texture in bottom left corner. Sample collection site for 14JA111A; **b)** sheeted magnetite-pyrite veinlets with K-feldspar alteration haloes at the Havana showing; **c)** gossanous till composed predominantly of quartz-sericite-pyrite–altered andesite at the Havana showing, rock hammer for scale highlighted in red; **d)** native Cu in epidote-calcite-quartz vein float at the Liesegang showing.

Liesegang (New)

Irregular, 1–3 cm wide, epidote veins with minor calcite and quartz are hosted in basalt with pronounced hematitic Liesegang rings at this newly identified mineral occurrence south of the Nechako Reservoir (Figure 2). An angular boulder of the same epidote-dominated vein material was observed to host approximately 4% native Cu with trace malachite (Figure 4d). Sample 15JA125A yielded >1% Cu (over limit) and 7.05 g/t Ag, but only 2.9 ppb Au and 8.1 ppm Zn (Table 1). Given the well-developed Liesegang rings observed in the basalt hosting these veins, this mineralization is interpreted as a volcanic redbed-copper–type mineral showing. This is further supported by the association of the host basalt with brick red tuffs, the gangue mineralogy of the veins, and the association of Cu with Ag, but not Au or Zn, all common features of these deposits (Lefebure and Church, 1996). Volcanic-hosted redbed-copper mineralization is observed elsewhere in BC, most notably at the Sustut Copper deposit, which contains a com-bined resource of 7.047 million tonnes grading 1.67% Cu and 5.50 g/t Ag at a 0.6% Cu cutoff (Gray, 2003).

Pickle (New)

Another probable volcanic redbed-copper showing occurs at the Pickle showing, where a 5 cm wide, horizontal quartz-chrysocolla vein occurs within locally Liesegang-bearing basalt and andesite. A grab sample from this vein (Table 1, 15RK191A) returned >1% Cu with low Zn and Au, similar to sample 15JA125A. However, at the Pickle showing mineralization contains only 144 ppb Ag. The hostrocks are tentatively assigned to the Entiako Formation Liesegang basalt sequence and the occurrence is likely a volcanic redbed-copper–style of mineralization.

Conclusion

The TREK project is intended to reduce exploration risk in the northern Interior Plateau of British Columbia. Targeted regional mapping has refined our understanding of the geo-

logical framework of this region and identified several new stratigraphic units, including the Liesegang basalt, Red tuff and Red dacite units of the Entiako Formation. It has also identified new mineral occurrences including the Havana, Liesegang and Pickle showings. Samples collected during the regional mapping campaign have yielded new assay results that warrant further investigation.

The Late Cretaceous mineralizing event is of utmost importance for companies exploring in this region. The potential extension of this event to include the Havana prospect may lead to future discoveries. Observations at the Holy Cross prospect suggest that it may also be a Late Cretaceous feature, elevating the prospectivity of an already actively explored property.

The ubiquitous development of Liesegang rings in basalt of the Entiako Formation, but not observed in younger basalt of the Naglico and Nechako formations, suggests that a significant hydrothermal system was active prior to emplacement of the Naglico Formation. The high-grade Cu mineralization identified at the Liesegang and Pickle showings indicates that this older basalt is a prospective target for volcanic redbed-copper deposits: a style of mineralization not previously documented in the region.

Acknowledgments

References

Aeroquest Airborne Ltd. (2014): Report on a fixed wing and magnetic geophysical survey, TREK Project, Interior Plateau/Nechako Region, British Columbia, Canada; Geoscience BC, Report 2014-04, 40 p., URL <http://www.geosciencebc.com/s/Report2014-04.asp> [October 2015].

Allnorth Consulting Limited (2007): Geological and geochemical report CHU molybdenum property, Omineca Mining Division, British Columbia; BC Ministry of Energy and Mines, Assessment Report 29393, 671 p., URL <http://aris.empr.gov.bc.ca/ArisReports/29393.PDF> [November 2015].

Anderson, R.G., Resnick, J., Russell, J.K., Woodsworth, G.J., Villeneuve, M.E. and Grainger, N.C. (2001): The Cheslatta Lake suite: Miocene mafic, alkaline magmatism in central British Columbia; Canadian Journal of Earth Sciences, v. 38, p. 697–717, URL <http://www.nrcresearchpress.com/doi/pdf/10.1139/e00-121> [November 2015].

Anderson, R.G., Snyder, L.D., Resnick, J. and Barnes, E. (1998): Geology of the Big Bend Creek map area, central British Columbia; in Current Research 1998-A, Geological Survey of Canada, p. 145–154, URL <http://ftp2.cits.rncan.gc.ca/pub/geott/ess_pubs/209/209427/cr_1998_ab.pdf> [November 2015].

Andrews, G.D.M. and Russell, J.K. (2008): Cover thickness across the southern Interior Plateau, British Columbia (NTS 092O, P; 093A, B, C, F): constraints from water-well records; in Geoscience BC Summary of Activities 2007, Geoscience BC, Report 2008-1, p. 11–20, URL <http://www.geosciencebc.com/i/pdf/SummaryofActivities2007/SoA2007-Andrews_original.pdf> [November 2014].

Andrew, K.P.E. (1988): Geology and genesis of the Wolf precious metal epithermal prospect and the Capoose base and precious metal porphyry-style prospect, Capoose Lake area, central British Columbia; M.Sc. thesis, University of British Columbia, 334 p., URL <https://circle.ubc.ca/bitstream/handle/2429/27791/UBC_1988_A6_7%20A52.pdf?sequence=1> [November 2015].

Angen, J.J., Westberg, E., Hart, C.J.R., Kim, R. and Rahimi, M. (2015a): Preliminary geological map of the TREK project area, central British Columbia; Geoscience BC Map 2015-10-01, scale 1:250 000, URL <http://www.geosciencebc.com/i/project_data/GBCReport2015-10/TREK_Geology_PrelimMap_2015-10-1.pdf> [November 2015].

Angen, J.J., Westberg, E., Hart, C.J.R., Kim, R. and Raley, C. (2015b): TREK geology project: recognizing Endako Group and Chilcotin Group basalts from airborne magnetic data in the Interior Plateau region, south-central British Columbia (NTS 093B, C, F, G); in Geoscience BC Summary of Activities 2014, Geoscience BC, Report 2015-1, p. 21–32., URL <http://www.geosciencebc.com/i/pdf/SummaryofActivities2014/SoA2014_Angen.pdf> [November 2015].

Barber, R. (1989): Geological and geochemical report on the Holy Cross Property (HC 1, 4, 5, HCM 1-3 mineral claims), Omineca Mining Division, British Columbia; BC Ministry of Energy and Mines, Assessment Report 19627, 79 p., URL <http://aris.empr.gov.bc.ca/ArisReports/19627.PDF> [October 2015].

Bassett, K.N. (1995): A basin analysis of the Lower to mid-Cretaceous Skeena Group, west-central British Columbia: implications for regional tectonics and terrane accretion; Ph.D. thesis, University of Minnesota, 411 p.

Bassett, K.N. and Kleinspehn, K.L. (1997): Early to middle Cretaceous paleogeography of north-central British Columbia: stratigraphy and basin analysis of the Skeena Group; Canadian Journal of Earth Sciences, v. 34, p. 1644–1669, URL <http://www.nrcresearchpress.com/doi/pdf/10.1139/e17-132> [November 2015].

BC Geological Survey (2015): MINFILE BC mineral deposits database; BC Ministry of Energy and Mines, BC Geological Survey, URL <http://minfile.ca/> [November 2015].

Bordet, E. (2014): Eocene volcanic response to the tectonic evolution of the Canadian Cordillera; Ph.D. thesis, University of British Columbia, 220 p., URL <https://circle.ubc.ca/bitstream/handle/2429/46271/ubc_2014_spring_bordet_esther.pdf?sequence=1> [November 2015].

Bordet, E., Mihalynuk, M.G., Hart, C.J.R., Mortensen, J.K., Friedman, R.M. and Gabites, J. (2014): Chronostratigraphy of Eocene volcanism, central British Columbia; Canadian

Journal of Earth Sciences, v. 51, p. 56–103, URL <http://www.nrcresearchpress.com/doi/pdf/10.1139/cjes-2013-0073> [November 2015].

Buckingham, A. (2014): Enhancement filtering and structure detection, magnetic data, MDRU TREK project; unpublished report, Fathom Geophysics, August 2014, 22 p.

Clifford, A. and Hart, C.J.R. (2014): Targeting Resources through Exploration and Knowledge (TREK): Geoscience BC's newest minerals project, Interior Plateau region, south-central British Columbia (NTS 093B, C, F, G); in Geoscience BC Summary of Activities 2013, Geoscience BC, Report 2014-1, p. 13–18, URL <http://www.geosciencebc.com/i/pdf/SummaryofActivities2013/SoA2013_Clifford Hart.pdf> [November 2015].

Diakow, L.J. and Levson, V.M. (1997): Bedrock and surficial geology of the southern Nechako plateau, central British Columbia; BC Ministry of Energy and Mines, BC Geological Survey, Geoscience Map 1997-2, scale 1:100 000, URL <http://www.empr.gov.bc.ca/Mining/Geoscience/PublicationsCatalogue/Maps/GeoscienceMaps/Documents/GM1997-02.pdf> [November 2015].

Diakow, L.J., Webster, I.C.L., Richards, T.A. and Tipper, H.W. (1997): Geology of the Fawnie and Nechako ranges, southern Nechako Plateau, central British Columbia (93F/2, 3, 6, 7); in Interior Plateau Geoscience Project: Summary of Geological, Geochemical and Geophysical Studies, L.J. Diakow, J.M. Newell and P. Metcalfe (ed.), BC Ministry of Energy and Mines, BC Geological Survey, Open File 1997-2 and Geological Survey of Canada, Open File 3448, p. 7–30, URL <http://www.empr.gov.bc.ca/mining/geoscience/publicationscatalogue/papers/documents/p1997-02_02.pdf> [November 2015].

Diakow, L.J., Webster, I.C.L., Whittles, J.A. and Richards, T.A. (1995): Stratigraphic highlights of bedrock mapping in the southern Nechako Plateau, northern Interior Plateau region; in Geological Fieldwork 1994, BC Ministry of Energy and Mines, BC Geological Survey, Paper 1995-l, p. 171–176, URL <http://www.empr.gov.bc.ca/Mining/Geoscience/PublicationsCatalogue/Fieldwork/Documents/1994/171-176-diakow.pdf> [November 2015].

Evenchick, C.A. and Thorkelson, D.J. (2005): Geology of the Spatsizi River map area, north-central British Columbia; Geological Survey of Canada, Bulletin 577, 276 p., URL <http://geoscan.nrcan.gc.ca/starweb/geoscan/servlet.starweb?path=geoscan/downloade.web&search1=R=215877> [November 2015].

Friedman, R.M., Diakow, L.J., Lane, R.A. and Mortensen, J.K. (2001): New U–Pb age constraints on latest Cretaceous magmatism and associated mineralization in the Fawnie Range, Nechako Plateau, central British Columbia; Canadian Journal of Earth Sciences, v. 38, p. 619–637, URL <http://www.nrcresearchpress.com.ezproxy.library.ubc.ca/doi/pdf/10.1139/e00-122> [November 2015].

Gagnon, J.F., Barresi, T., Waldron, J.F., Nelson, J.L., Poulton, T.P. and Cordey, F. (2012): Stratigraphy of the Upper Hazelton Group and the Jurassic evolution of the Stikine terrane, British Columbia; Canadian Journal of Earth Sciences, v. 49, p. 1027–1052, URL <http://cjes.geoscienceworld.org/content/49/9/1027.full.pdf+html> [November 2015].

Gray, P.D. (2003): Diamond drilling assessment report Sustut 1-2 and NT 1-3 claims, mining lease #315076 Sustut copper property, Omineca Mining Division, British Columbia; BC Ministry of Energy and Mines, Assessment Report 27141, 137 p., URL <http://aris.empr.gov.bc.ca/ArisReports/27141.PDF> [November 2015].

Gunning, M.H., Hodder, R.W. and Nelson, J.L. (2006): Contrasting volcanic styles and their tectonic implications for the Paleozoic Stikine assemblage, western Stikine terrane, northwestern British Columbia; in Paleozoic Evolution of Pericratonic Terranes at the Ancient Pacific Margin of North America, Canadian and Alaskan Cordillera, M. Colpron and J. Nelson (ed.), Geological Association of Canada, Special Paper 45, p. 201–228.

Kim, R.S., Hart, C.J.R., Angen, J.J. and Logan, J.M. (2015): Stratigraphic and lithological constraints of Late Cretaceous volcanic rocks in the TREK project area, central British Columbia (NTS 093E); in Geoscience BC Summary of Activities 2015, Geoscience BC, Report 2016-1, p.139–148.

Kuehn, C. (2014): A second North American hot-spot: Pleistocene volcanism in the Anahim volcanic belt, west-central British Columbia; Ph.D. thesis, University of Calgary, 343 p., URL <http://theses.ucalgary.ca/bitstream/11023/1936/4/ucalgary_2014_kuehn_christian.pdf> [November 2015].

Kuehn, C., Guest, B., Russell, J.K. and Benowitz, J.A. (2015): The Satah Mountain and Baldface Mountain volcanic fields: Pleistocene hot spot volcanism in the Anahim volcanic belt, west-central British Columbia, Canada; Bulletin of Volcanology, v. 77, p. 1–27, URL <http://link.springer.com.ezproxy.library.ubc.ca/content/pdf/10.1007%2Fs00445-015-0907-1.pdf> [November 2015].

Lane, R.A. and Schroeter, T.G. (1997): A review of metallic mineralization in the Interior Plateau, central British Columbia (parts of 93/B, C, F); in Interior Plateau Geoscience Project: Summary of Geological, Geochemical and Geophysical Studies, L.J. Diakow, J.M. Newell and P. Metcalfe (ed.), BC Ministry of Energy and Mines, BC Geological Survey, Open File 1997-2 and Geological Survey of Canada, Open File 3448, p. 237–256, URL <http://www.empr.gov.bc.ca/Mining/Geoscience/PublicationsCatalogue/Papers/Documents/P1997-02_13.pdf> [November 2015].

Lefebure, D.V. and Church, B.N. (1996): Volcanic Redbed Cu; in Selected British Columbia Mineral Deposit Profiles, Volume 1 - Metallic Deposits, D.V. Lefebure and T. Höy (ed.), BC Ministry of Energy and Mines, Open File 1996-13, p. 5–7, URL <http://www.empr.gov.bc.ca/Mining/Geoscience/MineralDepositProfiles/ListbyDepositGroup/Pages/DContinentalSedimentsVocanics.aspx#D03> [November 2015].

Looby, E.L. (2015): The Timing and Genesis of the Blackwater Gold-Silver Deposit, Central British Columbia: Constraints from Geology, Geochronology and Stable Isotopes; M.Sc. thesis, University of British Columbia, 184 p., URL <https://open.library.ubc.ca/media/download/pdf/24/1.0135681/2> [November 2015].

Lord, C.S. (1948): McConnell Creek map-area, Cassiar District, British Columbia; Geological Survey of Canada, Memoir 251, 72 p.

MacIntyre, D.G., Ash, C.H. and Britton, J.M (1994): Geological compilation, Skeena-Nass area, west-central British Columbia (NTS 93 E, L, M; 94D; 103 G, H, I, J, O, P; 104 A, B); BC Ministry of Energy and Mines, Open File 1994-14, 1:250 000, URL <http://www.empr.gov.bc.ca/Mining/Geoscience/PublicationsCatalogue/OpenFiles/1994/Pages/1994-14.aspx> [November 2015].

Marsden, H. and Thorkelson, D.J. (1992): Geology of the Hazelton volcanic belt in British Columbia: implications for

Early to Middle Jurassic evolution of Stikinia; Tectonics, v. 11, p. 1266–1287, URL <http://onlinelibrary.wiley.com/doi/10.1029/92TC00276/epdf> [November 2015].

Massey, N.W.D., MacIntyre, D.G., Desjardins, P.J., and Cooney, R.T. (2005): Geology of British Columbia, BC Ministry of Energy, Mines and Petroleum Resources, Geoscience Map 2005-3, (3 sheets), scale 1:1 000 000, URL <http://www.empr.gov.bc.ca/Mining/Geoscience/PublicationsCatalogue/Maps/GeoscienceMaps/Pages/2005-3.aspx> [November 2015].

Mihalynuk, M.G., Erdmer, P., Ghent, E.D., Cordey, F., Archibald, D.A., Friedman, R.M. and Johannson, G.G. (2004): Coherent French Range blueschist: subduction to exhumation in <2.5 m.y.?; Geological Society of America Bulletin, v. 116, p. 910–922, URL <http://gsabulletin.gsapubs.org/content/116/7-8/910.full.pdf+html> [November 2015].

Mihalynuk, M.G., Peat, C.R., Terhune, K. and Orovan, E.A. (2008): Regional geology and resource potential of the Chezacut map area, central British Columbia (NTS 093C/08); in Geological Fieldwork 2007, BC Ministry of Energy and Mines, BC Geological Survey, Paper 2008-1 and Geoscience BC, Report 2008-1, p. 117–134, URL <http://www.empr.gov.bc.ca/Mining/Geoscience/PublicationsCatalogue/Fieldwork/Documents/2007/13-Mihalynuk-Chezacut34526.pdf> [November 2015].

Monger, J.W.H. (1977): Upper Paleozoic rocks of the Western Canadian Cordillera and their bearing on Cordilleran evolution; Canadian Journal of Earth Sciences, v. 14, p. 1832–1859, URL <http://www.nrcresearchpress.com/doi/pdf/10.1139/e77-156> [November 2015].

Poznikoff, L.N., Mortensen, J.K., Friedman, R.M. and Gabites, J.E. (2000): Geochronological and lead isotopic constraints on the age and origin of the Laidman gold prospect, central British Columbia; in Geological Fieldwork 1999, BC Ministry of Energy and Mines, BC Geological Survey, Paper 2000-1, p. 173–184, URL <http://www.empr.gov.bc.ca/Mining/Geoscience/PublicationsCatalogue/Fieldwork/Documents/1999/GF11_Mortensen_173-183.pdf> [November 2015].

Riddell, J.M. (2011): Lithostratigraphic and tectonic framework of Jurassic and Cretaceous intermontane sedimentary basins of south-central British Columbia; Canadian Journal of Earth Sciences, v. 48, p. 870–896, URL <http://www.nrcresearchpress.com/doi/pdf/10.1139/e11-034> [November 2015].

Souther, J.G. (1977): Volcanism and tectonic environments in the Canadian cordillera – a second look; in Volcanic Regimes of Canada, Geological Association of Canada, Special Paper 16, p. 1–24.

Struik, L.C., MacIntyre, D.G. and Williams, S.P. (2007): Nechako NATMAP Project: a digital suite of geoscience information for central British Columbia; Geological Survey of Canada,

Open File 5623 and BC Ministry of Energy and Mines, Open File 2007-10, URL <http://ftp2.cits.rncan.gc.ca/pub/geott/ess_pubs/224/224578/of_5623.zip> [November 2015].

Struik, L.C., Whalen, J.B., Letwin, J.M. and L'Heureux, R.L. (1997): General geology of southeast Fort Fraser map area, central British Columbia; in Current Research 1997-A/B, Geological Survey of Canada, p. 65–75, URL <http://www.empr.gov.bc.ca/Mining/Geoscience/PublicationsCatalogue/OpenFiles/2007/2007-10/Papers/CurrentResearch/Pages/sl972.aspx> [November 2015].

Thomson, R.C., Smith, P.L. and Tipper, H.W. (1986): Lower to Middle Jurassic (Pliensbachian to Bajocian) stratigraphy of the northern Spatsizi area, north-central British Columbia; Canadian Journal of Earth Sciences, v. 23, no. 12, p. 1963–1973, URL <http://www.nrcresearchpress.com/doi/pdf/10.1139/e86-182> [October, 2015].

Tipper, H.W. (1963): Nechako River map area, British Columbia; Geological Survey of Canada, Memoir 324, 59 p.

Tipper, H.W. and Richards, T.A. (1976): Jurassic stratigraphy and history of north-central British Columbia; Geological Survey of Canada, Bulletin 270, 73 p., URL <http://ftp2.cits.rncan.gc.ca/pub/geott/ess_pubs/103/103065/bu_270.zip> [November 2014].

Torgerson, D.K. (2010): 2010 assessment report for the KEY property, Nechako Plateau, Omineca Mining Division, British Columbia; BC Ministry of Energy and Mines, Assessment Report 31702, 53 p., URL <http://aris.empr.gov.bc.ca/ArisReports/31702.PDF> [October 2015].

Villeneuve, M., Whalen, J.B., Anderson, R.G. and Struik, L.C. (2001): The Endako Batholith: episodic plutonism culminating in formation of the Endako porphyry molybdenite deposit, north-central British Columbia; Economic Geology, v. 96, p. 171–196, URL <http://econgeol.geoscienceworld.org/content/96/1/171.full.pdf+html> [November 2015].

Webster, I.C.L. (2013): Assessment report the Big Bear property, Omineca Mining Division, British Columbia; BC Ministry of Energy and Mines, Assessment Report 34134, 678 p., URL <https://aris.empr.gov.bc.ca/ArisReports/34134.PDF> [November 2015].

Wetherup, S. (1997): Geology of the Nulki Hills and surrounding area (NTS 93F/9 and F/16), central British Columbia; in Geological Survey of Canada Current Research 1997-A, p. 125–132, URL <http://ftp2.cits.rncan.gc.ca/pub/geott/ess_pubs/208/208594/cr_1997_ab.pdf> [November 2015].

Whiteaker, R. (2015): Blackwater project exploration update, Nechako Plateau, British Columbia, Canada; 2015 Kamloops Exploration Group Annual Conference, Kamloops, BC, April 14, 2015, presentation, URL <http://www.newgold.com/files/doc_presentations/2015/BW_2015-BLACKWATER_KEG_Prestn_v-FINAL2.pdf> [November 2015].

Mineralogical and Geochemical Characteristics of Porphyry-Fertile Plutons: Guichon Creek, Takomkane and Granite Mountain Batholiths, South-Central British Columbia

F. Bouzari, Mineral Deposit Research Unit, University of British Columbia, Vancouver, BC, fbouzari@eos.ubc.ca

C.J.R. Hart, Mineral Deposit Research Unit, University of British Columbia, Vancouver, BC

T. Bissig, Mineral Deposit Research Unit, University of British Columbia, Vancouver, BC

G. Lesage, Mineral Deposit Research Unit, University of British Columbia, Vancouver, BC

Introduction

The fundamental relationship of porphyry Cu (Au, Mo) deposits with bodies of intrusive rocks is well established (e.g., Sillitoe, 1973), but distinguishing metal-fertile from barren plutons remains a significant challenge for exploration. Information that contributes such *a priori* knowledge provides guidance early in the exploration process to make decisions more effectively and efficiently on focusing exploration resources on more prospective targets. This research project, therefore, provides tools and strategies that emphasize porphyry fertility in the British Columbia context (see Figure 1 for project location).

The most fundamental process in the formation of porphyry copper deposits is the exsolution of metal-rich magmatic hydrothermal fluids from large crystallizing batholiths and their transport to the site of the deposit (e.g., Dilles and Einaudi, 1992). These buoyant fluids are focused in cupolas above the batholiths to form perched porphyry copper deposits, but in many districts large deposits are hosted within or adjacent to the large plutons that form part of the mineralizing system. In all cases, these plutons will host evidence that records porphyry fertility characteristics. The relationship between magmatic processes and ore deposits has long been the focus of ore deposit research, but past studies have generally concentrated on the deposit scale. This project looks at the district to batholith scale, which will provide a level of assessment not previously documented in BC.

The characterization of fertility features is of particular importance for BC porphyry exploration. In BC, many porphyry systems occur within or around the edges of large batholiths, or have been tilted such that the deeper plutonic parts of the system are exposed. This paper summarizes 2015 summer fieldwork and provides preliminary results on a subset of samples.

Field and Laboratory Works

Field and laboratory work is focused on characterization of accessory minerals in various intrusive bodies of three well-documented and mapped batholiths, the Guichon Creek, Takomkane and the Granite Mountain batholiths, located in southern and central BC (Figure 1). In total, 113 samples were collected during the 2015 summer season: 52 from Guichon Creek, 35 from Takomkane and 26 from the Granite Mountain batholith. Samples were collected from various intrusive phases of each batholith. Samples were disaggregated using the electric pulse disaggregator (EPD) at Overburden Drilling Management (Nepean, Ontario), to break the rock along mineral grain boundaries, providing a larger number of unbroken mineral grains. Subsequently, mineral separation was performed at the Mineral Deposit Research Unit (MDRU) using Frantz® magnetic separation and heavy liquids. Grains are selected by hand-picking to be mounted and polished in preparation for electron microprobe and trace-element laser analyses. Rock samples were analyzed for whole-rock major- and trace-element analysis at Acme Analytical Laboratories Ltd. (Vancouver) to characterize the geochemical signature of each intrusive unit and to compare the mineral chemistry with whole-rock chemistry. Polished thin sections were prepared from representative samples for petrography. This paper summarizes preliminary results from 6 samples based on 133 spot electron microprobe analyses on apatite grains.
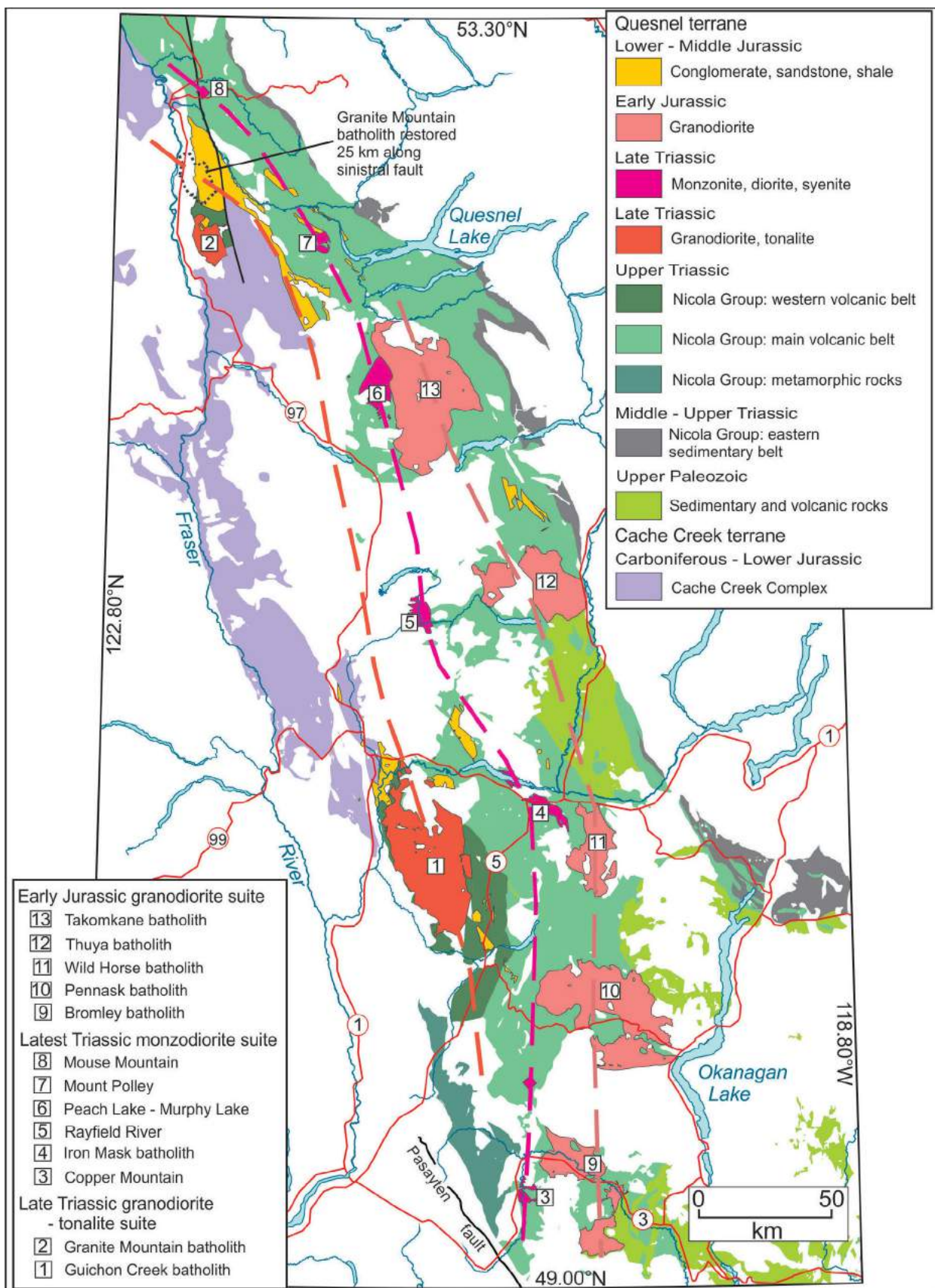
Guichon Creek Batholith

The Late Triassic Guichon Creek batholith is north trending, approximately 65 km long by 30 km wide. The batholith is composite and ranges from diorite and quartz diorite

Figure 1. Simplified geology map of south-central British Columbia showing location of major plutonic bodies. Dashed lines illustrate parallel belts of calcalkaline or alkaline plutons that show a progressive younging from west to east (from Schiarizza, 2014).

compositions at the border, to younger granodiorite in the centre (Casselman et al., 1995; Byrne et al., 2013). These phases from the margins inward, are named: the Border phase, the Highland Valley phases (consisting of Guichon and Chataway subphases); the Bethlehem phases (consisting of Bethlehem and Skeena subphases); and the Bethsaida phase. Bethlehem, Skeena and Bethsaida phases host most of the Highland Valley porphyry Cu-Mo deposits (Valley, Lornex, Highmont, Alwin, Bethlehem and JA).

Takomkane Batholith

The Takomkane batholith is a large (40 by 50 km) Late Triassic–Early Jurassic composite intrusive body that hosts several mineralized centres including the Woodjam porphyry camp (Megabuck, Takom, Southeast and Deerhorn). The Takomkane batholith records a magmatic evolution lasting 11 m.y., with three separate mineralizing events at Woodjam (del Real, 2015). Moreover, the presence of Cu-Au and Cu-Mo deposits together with the regional northwest tilting of geological units provides an insight into different levels of exposure and potentially subtle geochemical variations within the intrusive bodies.

Granite Mountain Batholith

The Granite Mountain batholith (18 by 10 km) occurs near McLeese Lake in south-central BC and hosts the Gibraltar porphyry Cu-Mo mine. The Late Triassic Granite Mountain batholith is subdivided into three main units, namely from southwest to northeast: Border phase diorite to quartz diorite; Mine phase tonalite; and Granite Mountain phase leucocratic tonalite. The Burgess Creek stock (Panteleyev, 1978), occurring at the northeast of the Granite Mountain batholith, comprises a heterogeneous assemblage of tonal-

ite, quartz diorite, and diorite that intrudes the Nicola Group. Panteleyev (1978) considered the stock to be younger than the Granite Mountain batholith, but Ash et al. (1999) concluded that the assemblage represents part of the batholith, and referred to them as border phase quartz diorite.

It was originally thought that the Granite Mountain batholith intruded the Cache Creek terrane (Bysouth et al., 1995). But recent mapping by Schiarizza (2014) recognized Nicola Group strata occurring on the northeastern margin of the batholith and suggested that it is more likely a part of the Quesnel terrane. This is also supported by recent interpretation of aeromagnetic data that assign the Granite Mountain area to the Quesnel terrane (Sánchez et al., 2015). Thus, the Granite Mountain batholith is correlative with the Late Triassic, calcalkaline Guichon Creek batholith, host to the Highland Valley porphyry Cu-Mo deposits, 250 km to the southsoutheast.

Geochemical Characteristics

Samples were analyzed for whole-rock major and trace elements at Acme Analytical Laboratories Ltd. (Vancouver). Results of 19 samples from the Guichon Creek batholith and 15 samples from the Granite Mountain batholith were obtained so far. Total alkali-silica (TAS) diagram (Figure 2) shows that samples from both batholiths are calcalkaline arc rocks ranging from granodiorite to diorite. Within the batholiths, border phases are more mafic than central portions. Trace-element data were normalized to the compositions of C1 carbonaceous chondrite meteorites using the normalization values of Sun and McDonough (1989). Normalized rare-earth element (REE) diagrams show that all Guichon Creek samples display patterns typical of subduc-
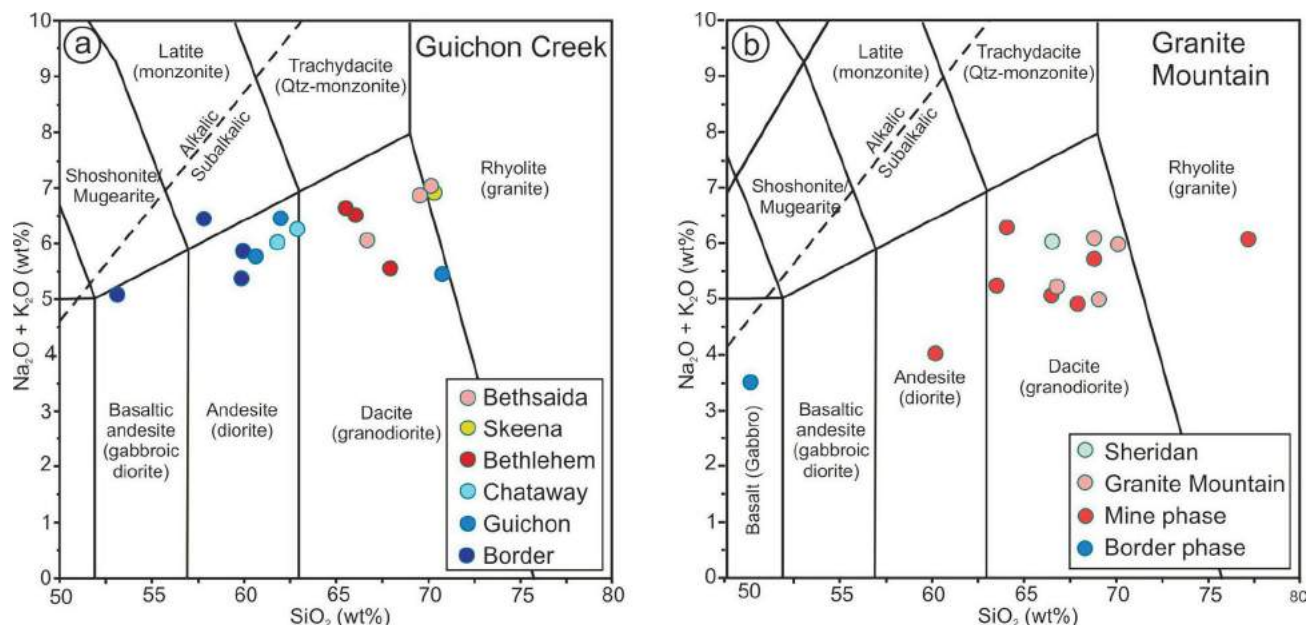

Figure 2. Total-alkali diagram showing the composition of intrusive units.

tion-related magmas, characterized by enrichments in large-ion lithophile elements (Figure 3a) relative to heavy rare-earth elements (HREE). All rock samples from Guichon Creek lack Eu anomalies. Late central more felsic phases have listric-shaped patterns with depleted middle rare-earth elements (MREE) and HREE suggesting hornblende and garnet fractionation. These features are characteristics of typical porphyry-fertile suites and indicate high magmatic water content and high oxidation state (Lang and Titley, 1998; Richards, 2012; Loucks, 2014). Rare-earth element signatures of the Granite Mountain and Mine phases of the Granite Mountain batholith differ from those at Guichon Creek by having less depleted HREE, possibly due to lack of significant garnet fractionation (Figure 3b). More importantly, samples from Granite Mountain show an Eu anomaly that ranges from minimal to negative. This indicates variable degrees of plagioclase fractionation which incorporates Eu^{2+}. A possible explanation for the observed REE patterns could be fluctuation in magmatic water content and/or oxidation state. Two samples from the Burgess Creek and Border phases display distinctly flat REE patterns typical of more primitive magmas. Further detailed petrographic work is required to better interpret the observed variations at Granite Mountain.

Mineralogical Characteristics

Preliminary results of electron microprobe analysis on apatite of six samples from the three batholiths are presented. Apatite petrography was studied using a cathodoluminescence (CL) microscope. Apatite grains display brown, pale brown, brownish-green and yellow luminescence (Figure 4). The brown luminescence colour is more common in rocks from the Granite Mountain and Takomkane batholiths and mafic phases of the Guichon Creek batholith, whereas yellow luminescence is common in the felsic Bethsaida phase of the Guichon Creek batholith. Apatite grains with yellow luminescence from the Bethsaida phase

have higher (>0.2%) MnO concentrations and are chemically similar to the apatite occurring in felsic (>70% SiO_2) I-type granite at Lachlan Fold Belt, Australia (Sha and Chappell, 1999; Bouzari et al., 2011). Apatite grains with brown luminescence have lower Mn concentration (<0.2% MnO). Apatite texture varies from uniform to zoned. The zoned apatite grains commonly have a more brownish CL core surrounded by a less brownish to yellow-green CL rim, and locally multiple zones occur (Figure 4b, c).

Chemical analysis of apatite grains by electron microprobe analysis shows distinct variations between mineralized and barren phases of the batholiths (Figure 5). At the Guichon Creek batholith, the Bethsaida phase, main host to the Highland Valley porphyry deposits, has less Cl and S relative to the Chataway phase. The Cl concentration of apatite in both phases is significantly less than Cl concentrations in the Border phase apatite, but the Border phase apatite has very low S concentration (Figure 5a). Similarly, the mineralized Woodjam Creek unit of the Takomkane batholith and the Mine phase of the Granite Mountain batholith have lower Cl and S concentrations than the unmineralized phases of the batholiths (Figure 5b, c). The zoned apatite grains show a similar trend for Cl and S. The core of apatite with the more brownish CL colour has higher concentrations of Cl and S relative to the less brownish luminescence at the rim (Figures 4b, 6).

These preliminary observations suggest that in each batholith, the intrusive bodies evolved to phases with less Cl and S, and even the mineralized intrusive body became progressively depleted in Cl and S. Sulphur in magma can form sulphide phases or be incorporated into minerals such as anhydrite. Chlorine is the main constituent for forming copper complexes in hydrothermal fluids. The depletion in sulphur is attributed to the evolution of early magma that is oxidizing and sulphate-rich to a melt that is sulphate-poor as a result of crystallization of anhydrite (Streck and Dilles,
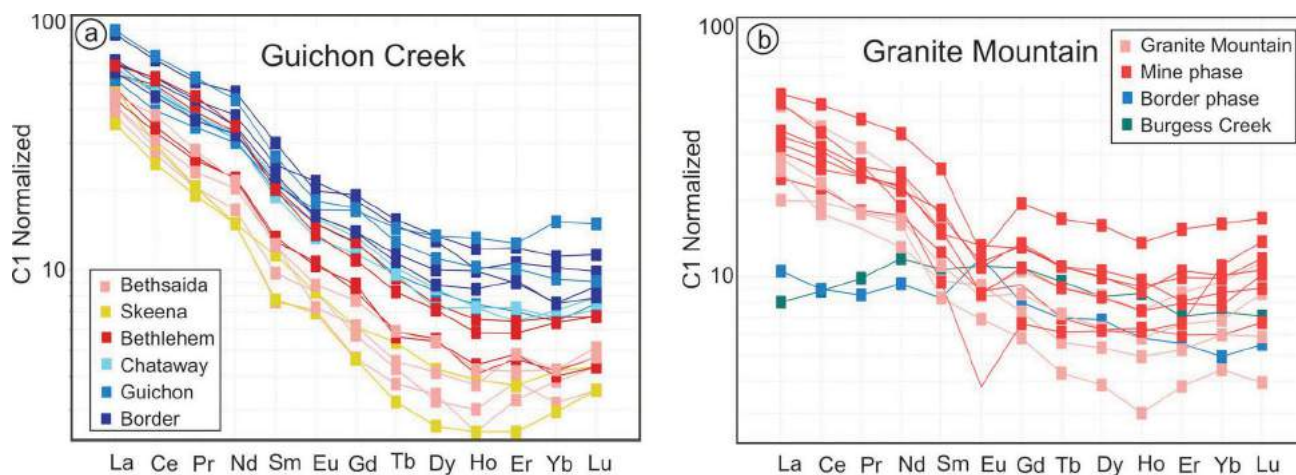
Figure 3. Chondrite-normalized rare-earth element (REE) spider diagrams: **a)** Guichon Creek batholith; **b)** Granite Mountain batholith (normalization values of Sun and McDonough, 1989).

1998; Liaghat and Tosdal, 2008). The depletion of chlorine suggests that both Cl and S were depleted because of exsolution of sulphur-bearing hydrothermal fluids, which eventually generated porphyry copper deposits.
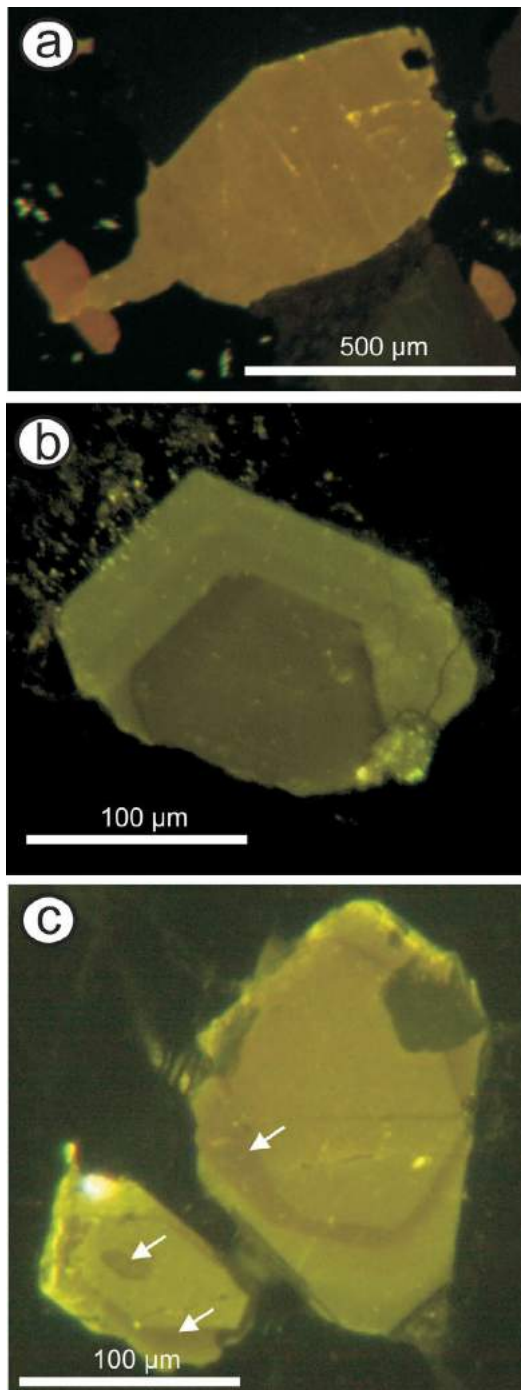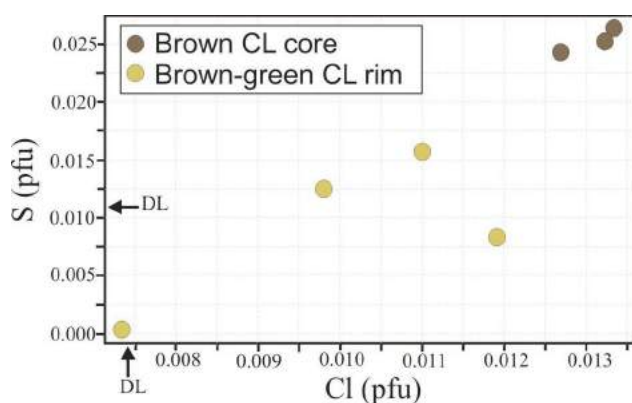

Figure 4. Cathodoluminescence image of apatite grains: **a)** large apatite grains from the Woodjam Creek unit of the Takomkane batholith with pale brown luminescence; **b)** zoned apatite grain from the Bethsaida phase with brown luminescence at the core and pale brown-green luminescence at the rim; **c)** apatite grains in Bethlehem granodiorite with a light brown core, a distinct dark brown zone and a more green-brown cathodoluminescence (CL) at the rim.

Conclusion and Further Work

These preliminary results suggest that both geochemical and mineralogical characteristics of plutons can be used to distinguish fertile phases. Porphyry-fertile plutons commonly display depleted HREE without significant negative Eu anomalies, consistent with hornblende and garnet fractionation, which is favoured by high magmatic water content and oxidation state. Moreover, porphyry-fertile plutons host apatite, which become progressively depleted in Cl and S. Chlorine and sulphur were probably consumed during the orthomagmatic processes which could potentially generate hydrothermal fluids rich in chlorine, sulphur
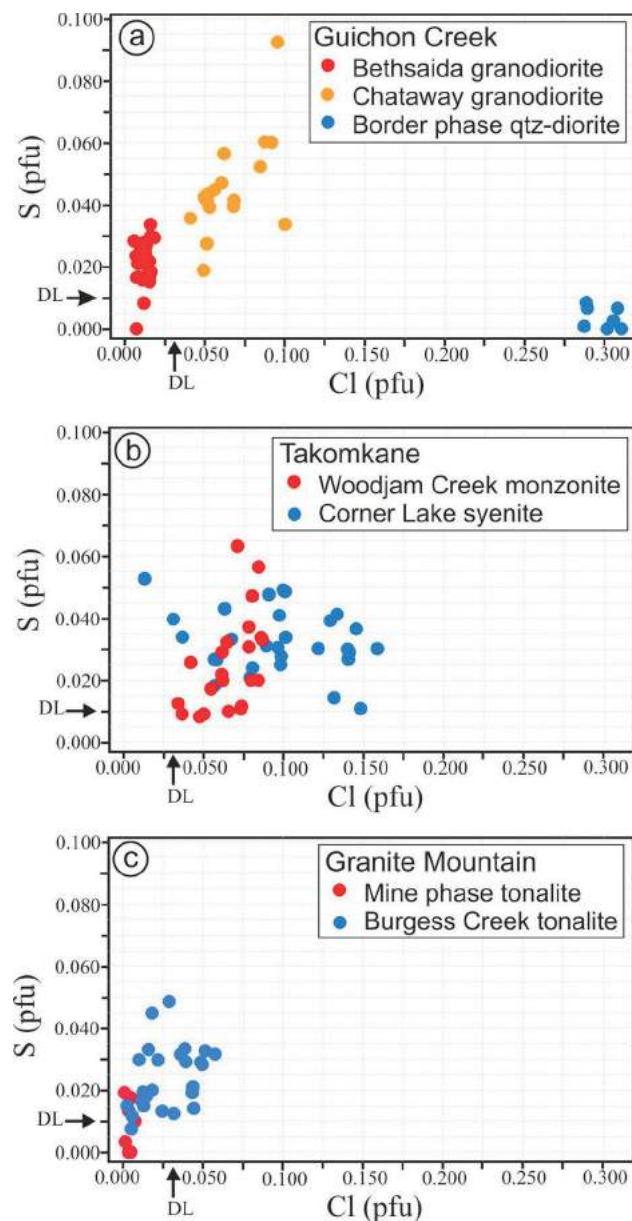
Figure 5. Binary diagram showing correlation of the apatite composition with various pluton phases; Cl and S values are calculated per formula units (pfu). Abbreviations: DL, detection limit; qtz, quartz.

Figure 6. Binary diagram showing correlation of apatite luminescence in a single zoned apatite grain (see Figure 4b) with Cl and S concentrations. Abbreviations: CL, cathodoluminescence; pfu, per formula units.

and copper, capable of producing porphyry copper ores. Further geochemical and mineralogical studies on a complete suite of samples from each batholith is underway. A suite of indicator minerals including apatite, titanite, zircon and hornblende will be studied.

Acknowledgments

References

Ash, C.H., Rydman, M.O., Payne, C.W. and Panteleyev, A. (1999): Geological setting of the Gibraltar mine, south-central British Columbia (93B/8, 9); *in* Exploration and Mining in British Columbia 1998, BC Ministry of Energy and Mines, BC Geological Survey, p. A1–A15.

Bouzari, F., Hart, C.J.R., Barker, S. and Bissig, T. (2011): Porphyry indicator minerals (PIMs): exploration for concealed deposits in central British Columbia; Geoscience BC, Report 2011-17, 31 p., URL <http://www.geosciencebc.com/i/project_data/GBC_Report2011-17/GBCReport2011-17_report.pdf> [November 2015].

Byrne, K., Stock, E., Ryan, J., Johnson, C., Nisenson, J., Alva Jimenez, T., Lapointe, M., Stewart, H., Grubisa, G. and Sykora, S. (2013): Porphyry Cu-(Mo) deposits in the Highland Valley district, south central British Columbia; *in* Porphyry Systems of Central and Southern BC, Tour of Central BC Porphyry Deposits from Prince George to Princeton, J. Logan. and T. Schroeter (ed.), Society of Economic Geologists, Field Guidebook Series, v 44, p. 99–116.

Bysouth, G.D., Campbell, K.V., Barker, G.E. and Gagnier, G.K. (1995): Tonalite trondhjemite fractionation of peraluminous magma and the formation of syntectonic porphyry copper mineralization, Gibraltar mine, central British Columbia; *in* Porphyry Deposits of the Northwestern Cordillera of North America, T.G. Schroeter (ed.), Canadian Institute of Mining, Metallurgy and Petroleum, Special Volume 46, p. 201–213.

Casselman, M.J., McMillan, W.J. and Newman, K.M. (1995): Highland Valley porphyry copper deposits near Kamloops, British Columbia: a review and update with emphasis on the Valley deposit; *in* Porphyry Deposits of the Northwestern Cordillera of North America, T.G. Schroeter (ed.), Canadian Institute of Mining and Metallurgy, Special Volume 46, p. 161–191.

del Real, I. (2015): Geology, alteration, mineralization and magmatic evolution of the Southeast Zone (Cu-Mo) and Deerhorn (Cu-Au) porphyry deposits, Woodjam, central British Columbia, Canada; M.Sc. thesis, University of British Columbia, 315 p.

Dilles, J.H. and Einaudi, M.T. (1992): Wall-rock alteration and hydrothermal flow paths about the Ann-Mason porphyry copper deposit, Nevada: a 6-km vertical reconstruction; Economic Geology, v. 87, p. 1963–2001.

Lang, J.R. and Titley, S.R. (1998): Isotopic and geochemical characteristics of Laramide magmatic systems in Arizona and implications for the genesis of porphyry copper deposits; Economic Geology, v. 93, p. 138–170.

Liaghat, S. and Tosdal, R. (2008): Apatite chemical composition and textures as a probe into magmatic conditions at Galore Creek porphyry copper-gold deposit, British Columbia (abstract): 18th Annual V.M. Goldschmidt Conference; Geochimica et Cosmochimica Acta, v. 72, no. 12, p. A550.

Loucks, R.R. (2014): Distinctive composition of copper-ore-forming arc magmas; Australian Journal of Earth Sciences, v. 61, no. 1, p. 5–16.

Panteleyev, A. (1978): Granite Mountain project (93B/8); *in* Geological Fieldwork 1977, BC Ministry of Energy and Mines, BC Geological Survey, Paper 1977-1, p. 39–42.

Richards, J. (2012): High Sr/Y magmas reflect arc maturity, high magmatic water content, and porphyry $Cu \pm Mo \pm Au$ potential: examples from the Tethyan arcs of central and eastern Iran and western Pakistan; Economic Geology, v. 107, p. 295–332.

Sánchez, M.G., Bissig, T. and Kowalcyzk, P. (2015): Toward an improved basis for beneath-cover mineral exploration in the QUEST area, central British Columbia: new structural interpretation of geophysical and geological datasets (NTS 093A, B, G, H, J, K, N); Geoscience BC Report 2015-15.

Schiarizza, P. (2014): Geological setting of the Granite Mountain batholith, host to the Gibraltar porphyry Cu-Mo deposit, south-central British Columbia; *in* Geological Fieldwork 2013, BC Ministry of Energy and Mines, BC Geological Survey Paper 2014-1, p. 95–110.

Sha, L.K. and Chappell, B.W. (1999): Apatite chemical composition determined by electron microprobe and laser-ablation inductively coupled plasma mass spectrometry, as a probe into granite petrogenesis; Geochimica et Cosmochimica Acta, v. 63, p. 3861–3881.

Sillitoe, R.H. (1973): The tops and bottoms of porphyry copper deposits; Economic Geology, v. 68, p. 799-815.

Streck, M.J. and Dilles, J.H. (1998): Sulfur evolution of oxidized arc magmas as recorded in apatite from a porphyry copper batholith; Geology, v. 26, p. 523–526.

Sun, S.-s. and McDonough, W.F. (1989): Chemical and isotopic systematics of oceanic basalts: implications for mantle composition and processes; *in* Magmatism in the Ocean Basins, A.D. Saunders and M.J. Norry (ed.), Geological Society of London, p. 313–345.

Geology of the Kettle River Area, Almond Mountain Project, Southern British Columbia (NTS 082E/07)

T. Höy, Consultant, Sooke, BC, thoy@shaw.ca

Introduction

The Almond Mountain project, funded by Geoscience BC, includes geological mapping and compilation of a large part of the 1:50 000 scale Almond Mountain map area (NTS 082/07), located in the Monashee Mountains of southern British Columbia (BC). The project is an extension to the west of mapping, compilation and mineral-potential evaluation of the east half of the 1:250 000 scale Penticton map area (NTS 082E), which included the Grand Forks (NTS 082E/01), Deer Park (NTS 082E/08) and Burrell Creek (NTS 082E/09) map areas (Figure 1; Höy and Jackaman, 2005, 2010, 2013). This project, and the continuation to the north in the Christian Valley map area (NTS 082E/10) in 2016, focuses mainly on the structural, stratigraphic and magmatic controls of base- and precious-metal mineralization in areas dominated by Tertiary[1] extensional tectonics.

The Almond Mountain project involved mainly geological mapping at a scale of 1:20 000 in the western part of the study area (Figure 2), which is dominated by Tertiary faulting that produced a complex north-trending graben filled with Eocene volcanic and sedimentary rocks. These unconformably overlie Paleozoic basement rocks, and Mesozoic and Eocene intrusive rocks. The graben hosts a variety of mineral occurrences, most notably base- and precious-metal veins that have similarities to deposits in the Beaverdell mining camp to the west and the Greenwood camp to the southeast.

Geological and Exploration History

The results of geological mapping in the vicinity of the Almond Mountain map area (NTS 082E/07) are shown in Figure 2. The area appears on the Kettle River map sheet (east half), mapped at a scale of 1:253 440 (1 inch to 4 miles) by Little (1957), and is included in the Penticton map area (NTS 082E), mapped and compiled at a scale of 1:250 000 by Tempelman-Kluit (1989). The geology of areas immediately to the east mapped at a scale of 1:50 000 has been published by Höy and Jackaman (2005, 2010 and 2013), based on new mapping and on compilation of previous studies, most notably those of Drysdale (1915), Preto (1970), Acton et al. (2002) and Laberge and Pattison (2007), and in the northern part of the area, extending into the Beaverdell camp, by Reinecke (1915).

Geological mapping in the Almond Mountain map area in 2014 and 2015 was focused along the western side of the area shown on 1:20 000 scale TRIM map areas 082E/036 and 082E/046. This work is based on approximately 40 days of fieldwork as well as compilation of mapping by Reinecke (1915), Greig and Flasha (2005), and Massey and Duffy (2008a, b). Further work will include compilation in digital format of all regional geological, geophysical and geochemical data collected under the National Geochemical Reconnaissance and the BC Regional Geochemical Survey programs. This will be combined with mineral occurrence and geology databases to produce 1:20 000 and 1:50 000 scale maps, suitable for directing and focusing mineral exploration.
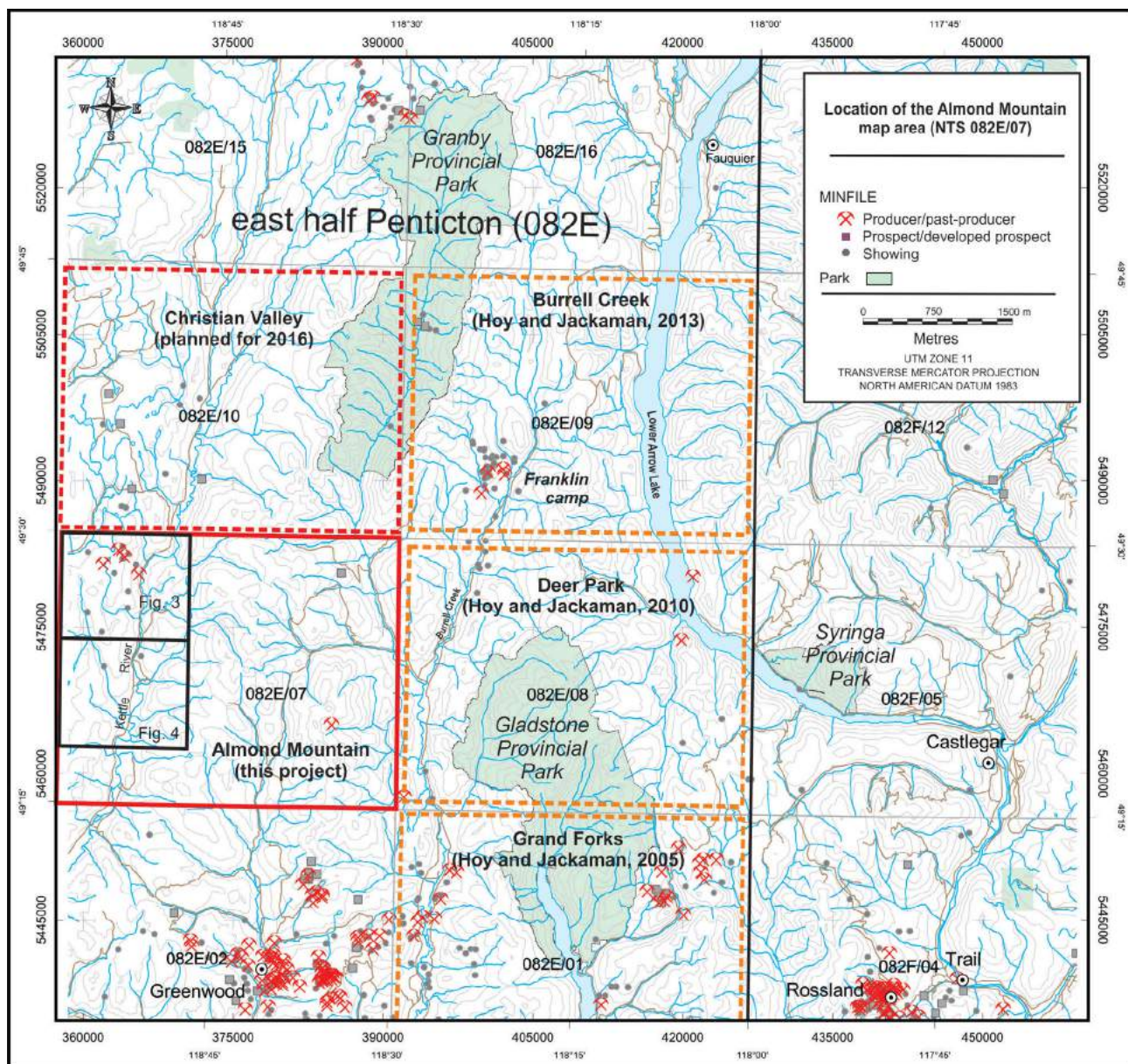
Exploration in the Almond Mountain map area was initially based on the successful discovery and exploitation of the base- and precious-metal deposits in the Beaverdell and Greenwood camps, and more recently of gold deposits in the Republic District of northern Washington. Mining in the Beaverdell camp, located approximately 5 km west of the map area (Figure 2), operated from 1913 to 1991 and, based on MINFILE information (BC Geological Survey, 2015), produced approximately 99.2 million g Ag (35 million oz.) and 481 941 g Au (17 000 oz.) from narrow, high-grade lead-zinc veins. Deposits in the Phoenix mine area in the Greenwood camp, 30 km to the southeast (Figure 2), produced more than 2.5 million g Au (910 000 oz.) and 116.7 million g Ag (5.9 million oz.) until its closure in 1978, and several other deposits in the camp continue to be actively explored (e.g., Dufresne and Schoeman, 2014). Exploration elsewhere continues to be active, particularly

---

Figure 1. Location of the 1:50 000 scale Almond Mountain map area (NTS 082E/07) in southern British Columbia; modified from BC MapPlace (BC Geological Survey, 2015).

with the recent discovery of new zones of epithermal-gold mineralization in a similar geological setting at the Brett property, approximately 30 km west of Vernon (Caron, 2014).

Exploration in the immediate area is summarized mainly from MINFILE data and from provincial government assessment reports. This exploration resulted in the discovery of a number of base- and precious-metal veins and breccia zones largely restricted to the graben in the western part of the map area. Work on these has included considerable geological mapping, soil sampling, ground geophysical surveys and limited drilling (summarized in Greig and Flasha, 2005).

Regional Geology

The Almond Mountain area is underlain by Quesnel terrane rocks intruded by a variety of igneous rocks ranging in age from Jurassic to Eocene. Paleozoic metasedimentary and metavolcanic rocks within the Quesnel terrane form a subterrane that can be subdivided into two distinct successions, the oceanic Okanagan subterrane, which includes the Knob Hill Group and Anarchist Schist, and the arc-related Harper Ranch subterrane (Wheeler et al., 1991). Overlying arc-volcanic rocks include the Triassic Nicola Group, exposed in the Greenwood area to the south and throughout the Thompson Plateau area to the west (Preto, 1979), and the Early Jurassic Rossland Group along the southeastern
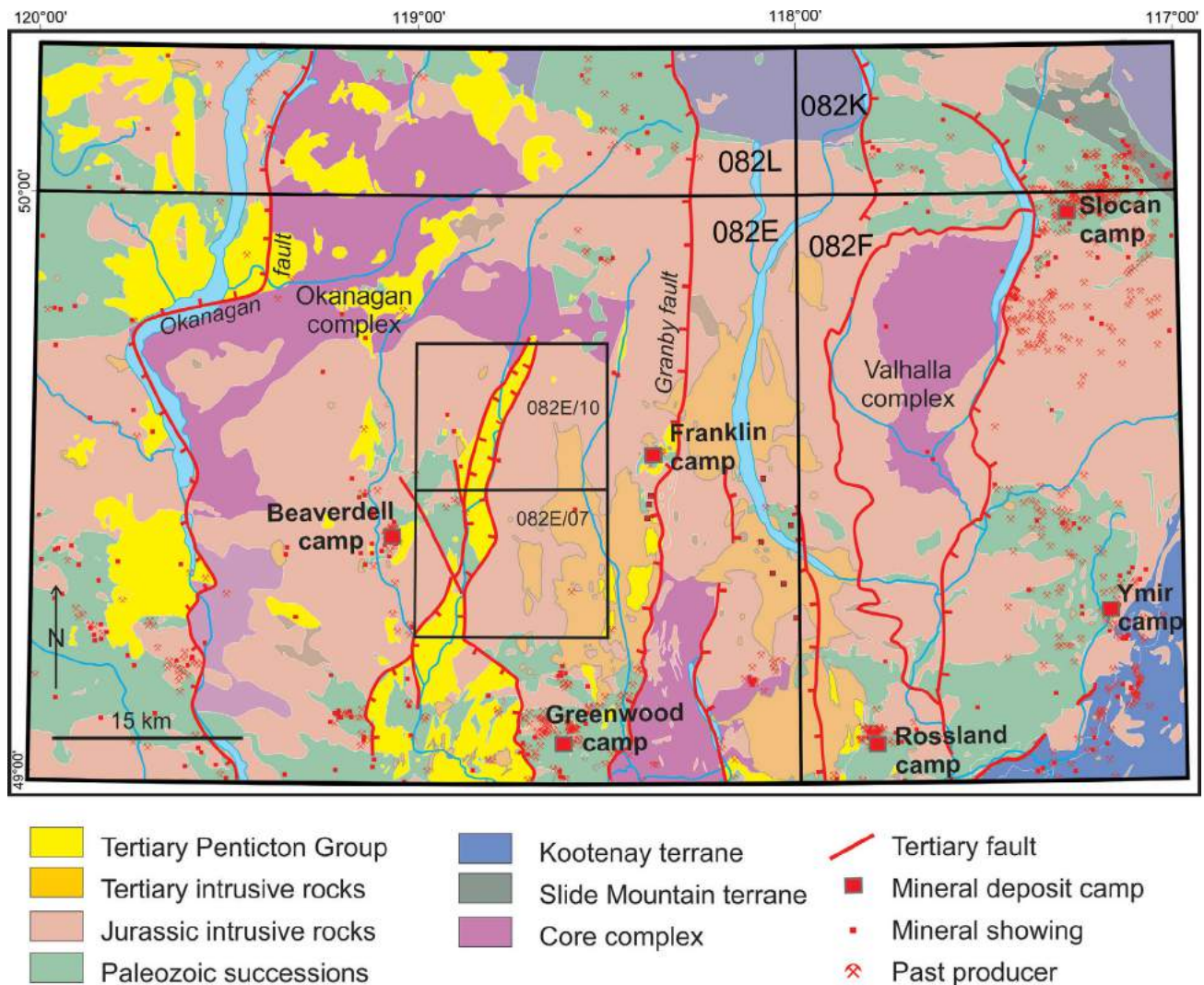
Figure 2. Geology of part of the Penticton area, showing the location of the Almond Mountain (NTS 082E/07) and Christian Valley (NTS 082E/10) map areas in southern British Columbia (modified from Tempelman-Kluit, 1989).

margin of the Quesnel terrane (Höy and Dunne, 2001). Jurassic granodiorite of the Nelson plutonic suite, and Jurassic and Eocene (?) granite and granodiorite of the Okanagan batholith underlie a large part of the Penticton map area (Tempelman-Kluit, 1989).

Regional extension during the Tertiary had a profound effect on the physiography and metallogeny of south-central BC, with low-angle detachment faults exhuming Proterozoic and Paleozoic gneissic and platform rocks that formed the metamorphic-core complexes of the southern Monashee Mountains, including the Grand Forks complex (Preto, 1970). Extension in the hangingwall terrane, between the Granby fault at the western margin of the Grand Forks complex and the Okanagan detachment fault to the west (Figure 2), resulted in the intrusion of alkalic plutons of the Eocene Coryell intrusive suite; the formation of north-trending grabens filled with Eocene and younger coarse sediments and alkalic volcanic rocks; and the localization of both

base- and precious-metal deposits. These include the veins in the Beaverdell camp immediately west of the Almond Mountain area and numerous structurally controlled mineral occurrences throughout the Kettle River area.

Geology of the Kettle River Area

The Kettle River area lies along the western margin of the Almond Mountain map area ((NTS 082E/07; Figure 1). It is underlain by a complex north-trending graben that exposes Paleozoic metasedimentary and metavolcanic rocks intruded by Jurassic diorite and granodiorite. These are overlain unconformably by an Eocene sedimentary and volcanic succession that constitutes the graben fill. Eocene stocks, including alkalic rocks of the Coryell suite and megacrystic granite, are locally exposed within the graben, as is a suite of generally north-trending dikes. A number of base- and precious-mineral veins, related to Eocene extension, are found within the graben.

Wallace Group

The Wallace group was initially defined by Reinecke (1915) to include Paleozoic metasedimentary and metavolcanic rocks that lie in the northwestern part of the area (Figure 3), extending west toward the town of Beaverdell. These rocks have been assumed to be part of the Anarchist Schist, but because of considerable lithological differences, Massey and Duffy (2008a) preferred to retain the term 'Wallace group', a usage that is adopted in this paper.

The Wallace group in the Kettle River area is described by Massey and Duffy (2008a). They noted that a considerable part of the area that is underlain by Wallace group rocks in original mapping (Reinecke, 1915) includes younger Jurassic and/or Tertiary rocks. Other workers in the area, notably Greig and Flasha (2005), also realized the difficulty in distinguishing between Paleozoic metavolcanic rocks and recrystallized or finer grained, younger intrusions. The distribution of the Wallace group, as shown in Figures 3 and 4, is based, in part, on mapping undertaken during this study and on attempts to reconcile previous work.

A large part of the Wallace group comprises interbedded, laminated argillite and siltstone (unit Pw). These are commonly hornfelsed and recrystallized, masking original sedimentary structures. Siltstone beds are tan to grey, whereas argillite beds are dark grey to black. Some sections of laminated 'siltstone' are light green and may represent thin, mafic tuffaceous layers. Disseminated pyrite and quartz-carbonate veins, with minor pyrite, are common and, in areas of interbedded plagioclase-phyric 'flows', the presence of malachite staining and chalcopyrite was noted.

Massey and Duffy (2008a, b) differentiated a limestone and a greenstone member in the Wallace. The informally named 'Larse Creek limestone member' (unit Pl; Massey and Duffy, op. cit.) occurs in the northern part of 1:20 000 scale TRIM map area 082E/046, immediately south of Beaverdell Creek (Figure 3). This distinctive, light grey-weathering limestone, with numerous calcite-quartz veins and pods, ranges from massive to well bedded, to locally intensely folded (Figure 5).

The limestone is overlain by massive mafic flows of the informally named 'Crouse Creek member' (unit Pv; Massey and Duffy, op. cit.). The flows locally include vague amygdules and feldspar or pyroxene phenocrysts. Interbeds of siltstone or laminated mafic tuffaceous rocks are common. Massive mafic flows are also mapped as a separate unit on the eastern side of the Kettle River (Figures 3 and 4) and are referred to as part of the Crouse Creek member, although direct correlation is not known. As well, the large section of undifferentiated Wallace group in the central part of both map areas (unit Pw) contains considerable mafic volcanic rocks, but it is possible that it includes sections of younger undifferentiated, fine-grained intrusive diorite.

Minor- and trace-element analyses of volcanic rocks of the Crouse Creek member and within the siltstone/volcanic-rock section suggest that these Paleozoic rocks are a calc-alkaline volcanic-arc succession (Massey, 2010). They differ considerably from the tholeiitic rocks of the Knob Hill Group or the Anarchist Schist (Massey, op. cit.) and may be part of the arc-related Harper Ranch subterrane.

Triassic–Jurassic Intrusive Rocks

Middle Jurassic and Triassic granodiorite and diorite underlie a considerable part of the Almond Mountain map area. In the Kettle River area (Figures 3 and 4), Jurassic(?) diorite occurs as two isolated stocks between the Crouse Creek and Christian Valley faults in the northern part of the map area. Isolated bodies of granodiorite in the northwestern part of the map area (unit Jgd in Figure 3) are part of the Westkettle batholith (Reinecke, 1915), which hosts many of the veins in the Beaverdell camp as well as some veins in the central part of the Kettle River area. These intrusive rocks have been correlated with the Jurassic Nelson plutonic suite, as defined by Tempelman-Kluit (1989) and Little (1961). However, U-Pb zircon analysis of the Westkettle batholith, from a sample located just west of 1:20 000 scale map area 082E/049, returned a date of 213.5 Ma (Massey et al., 2010), similar to a Triassic age obtained from an intrusion in the Christina Lake area, informally named the 'Josh Creek diorite' (Acton et al., 2002). Additional samples of these units, as well as from other intrusions in the Kettle River area, are being submitted to the geochronology laboratory of the University of British Columbia for testing by the $^{40}Ar/^{39}Ar$ method of age determination.

Unit Jgd comprises dominantly light grey to medium grey, medium- to coarse-grained granodiorite and lesser quartz diorite (Figure 6). Quartz content ranges up to 20% and the mafic minerals, hornblende and biotite, from typically 10 to 30%. These rocks are locally altered to pale green, and veined with quartz, chlorite and epidote.

Diorite (unit Jd) is exposed in two irregular stocks in the central part of the northern 1:20 000 map area (082E/046). The southwestern stock includes medium-grained to locally porphyritic diorite and lesser granodiorite composed mainly of plagioclase, hornblende and up to 20% quartz. It is fractured and chlorite altered adjacent to the Crouse Creek fault. Porphyritic granodiorite contains euhedral to subhedral phenocrysts of white feldspar up to several centimetres in size in a granular feldspar-hornblende-quartz matrix. The northeastern stock is similar, but includes a distinctive unit, termed a "hornblende crowded feldspar diorite" by Greig and Flasha (2005). The diorite is host to many of the base- and precious-metal veins in the Triple
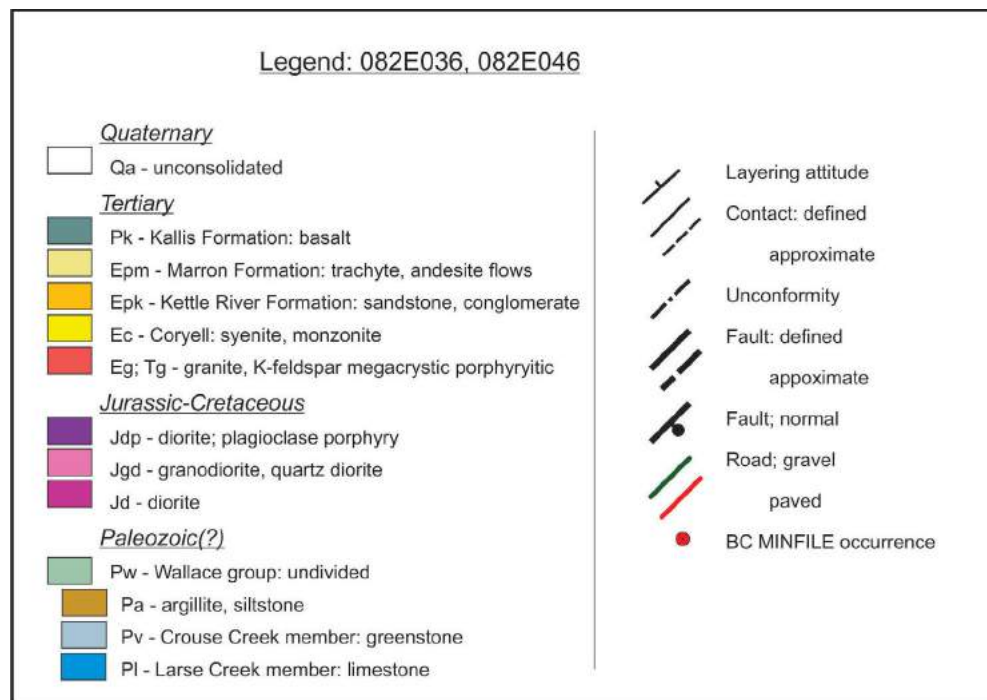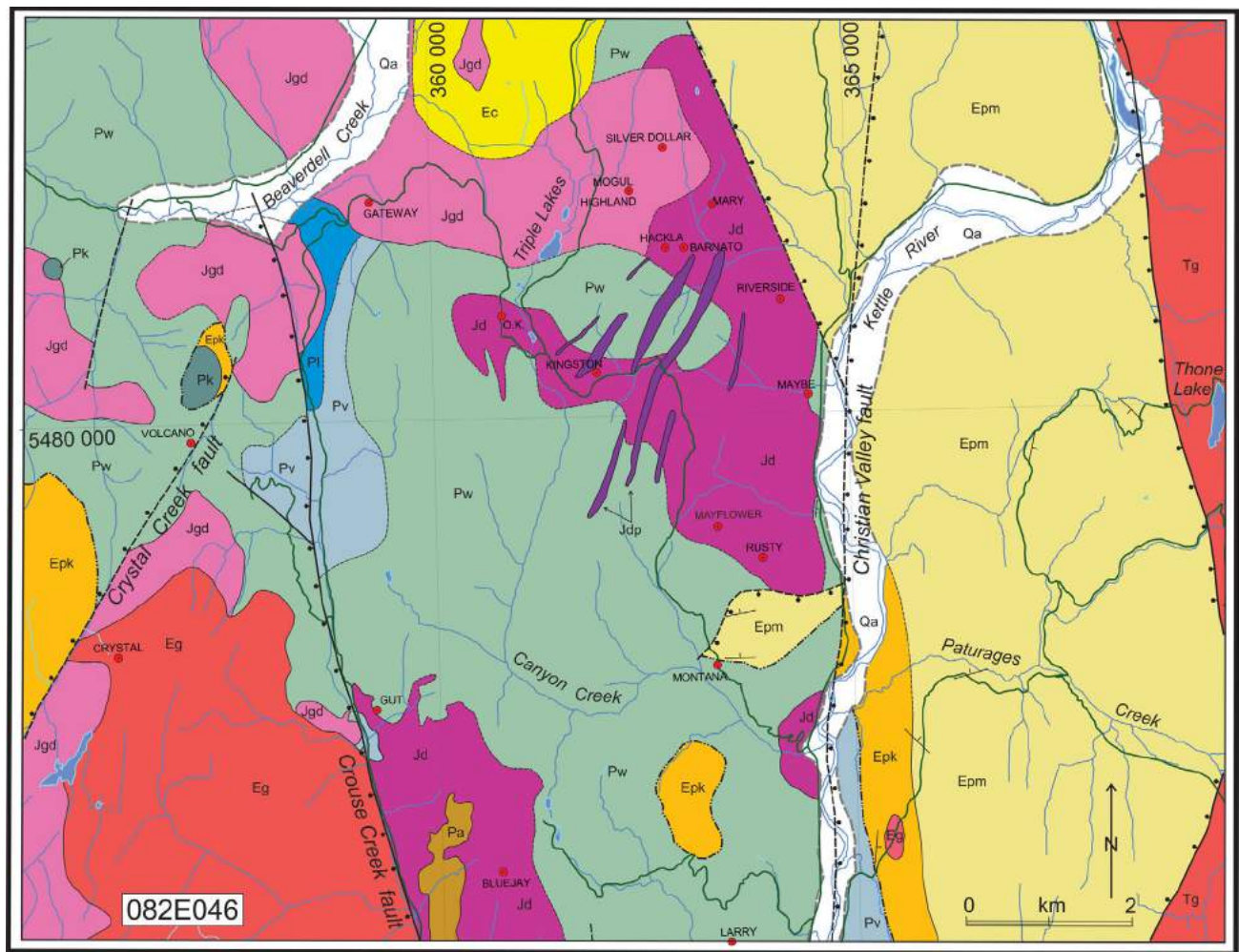
Figure 3. Geology of 1:20 000 TRIM map area 082F/046, showing location of selected mineral occurrences in the Kettle River area.
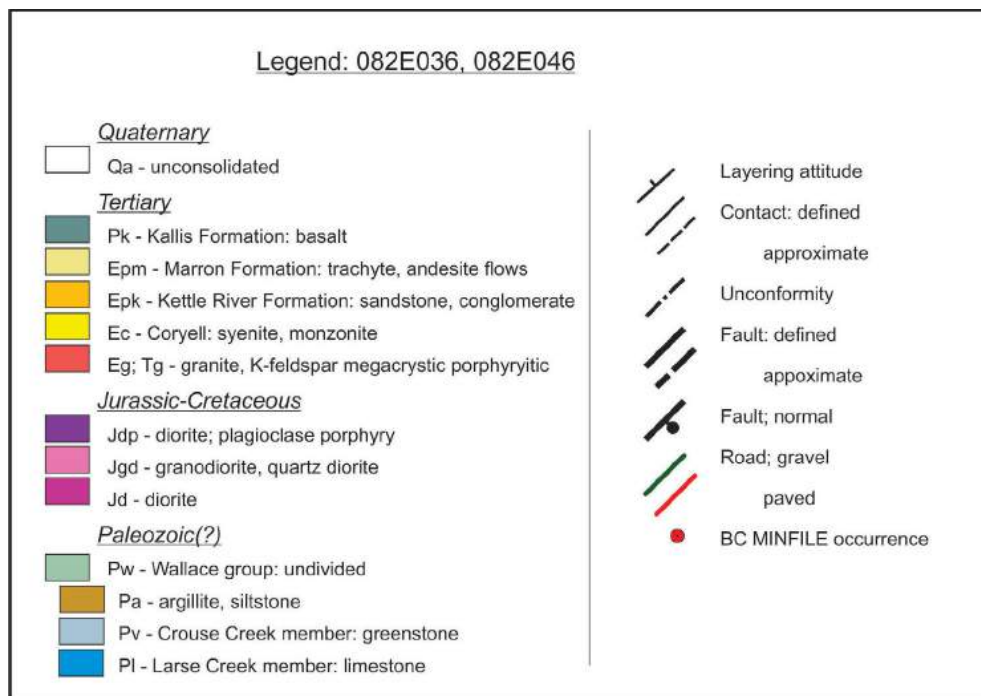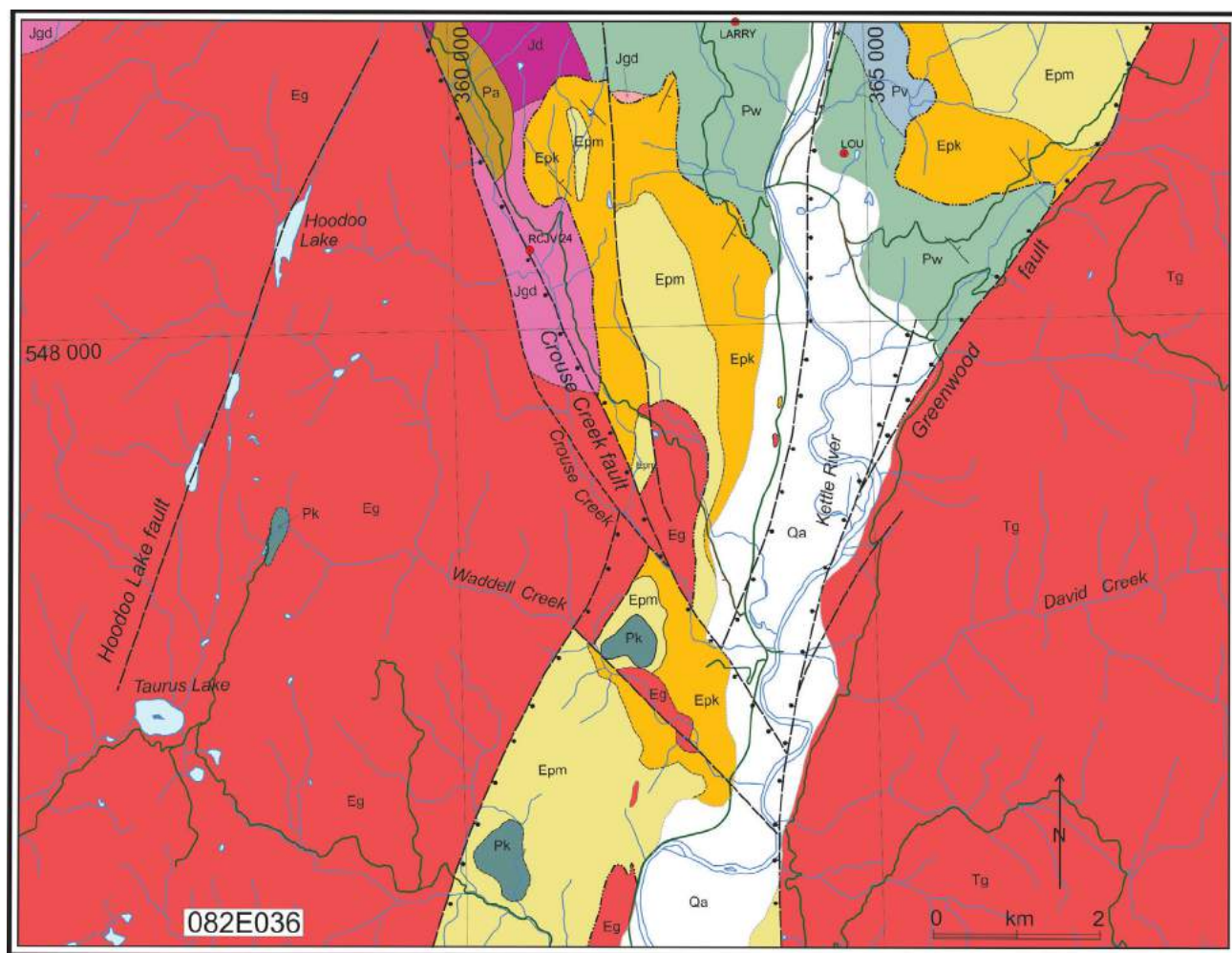
Figure 4. Geology of 1:20 000 TRIM map area 082F/036, showing location of selected mineral occurrences in the Kettle River area. Not all units and symbols shown on the legend, which accompanies Figures 3 and 4, appear on this figure.

Figure 5. Banded grey and white limestone of the Larse Creek member, Wallace group, Kettle River area.

Figure 6. Medium-grained, relatively fresh granodiorite of unit Jgd, from the Kettle River area.

Lakes area (Figure 3). Similar plagioclase porphyry is exposed near the mouth of Canyon Creek (Figure 3).

Numerous, generally north-northeast-trending dikes and small stocks (unit Jdp) cut the diorite stock and host Wallace group rocks in the Triple Lakes area. These include fine-grained to porphyritic diorite, lithologically similar to unit Jd, and plagioclase porphyry latite and hornblende-plagioclase porphyry dikes. The ages of these dikes are not known; some have a distinctive pink cast, suggesting the presence of fine-grained K-feldspar in the matrix, and may be part of the alkalic Eocene intrusive suite.

Porphyritic Granite (unit Eg)

Distinctive coarse-grained megacrystic granite occurs west of the Crouse Creek fault and in isolated exposures to the east and south. The granite is correlated with the 'Cretaceous' Valhalla complex intrusions of Little (1957) and, in subsequent papers, these intrusions are generally referred to as 'Jura-Cretaceous' (e.g., Tempelman-Kluit, 1989). In the Kettle River area, the megacrystic granite intrudes the Wallace group and Middle Jurassic granodiorite and is unconformably overlain by Eocene Penticton Group rocks. A K-Ar date of 49.4 ±1.9 Ma was obtained from a lithologically similar megacrystic granite south of Beaverdell (Church, 1996) and a U-Pb zircon date of 56.0 ±1.0 Ma (Parrish, 1992) as well as a hornblende ^{39}Ar/^{40}Ar date of 52.8 ±1.6 Ma (Höy, 2013) for a similar granite in the Burrell Creek area. Hence, pending further radiometric analysis, the Kettle River megacrystic granite is assigned an Eocene age, following the lead of Massey et al. (2010).

The granite is typically medium to coarse grained, with large, pink, euhedral K-feldspar phenocrysts set in a granular matrix of K-feldspar, plagioclase and up to 10% biotite and hornblende. It is generally fresh, although bleached and fractured beneath the sub-Tertiary unconformity, and

chlorite-altered, fractured and veined adjacent to the Crouse Creek fault.

Granite (unit Tg)

Granite and granodiorite of the 'Cretaceous and/or Jurassic' Okanagan batholith underlie a large part of the Almond Mountain map area, east of the Greenwood fault and west of the Kettle River area in the footwall of the Okanagan fault (Tempelman-Kluit, 1989). Based on lithological similarities to the porphyritic granite (unit Eg) and the Eocene 'Ladybird' granite in the Deer Park and Burrell Creek areas, unit Tg is assumed to be Eocene in age.

Exposures of the granite immediately east of the Greenwood fault (Figures 3 and 4) comprise mainly medium-grained, massive to porphyritic quartz-orthoclase-plagioclase granite, with minor biotite and hornblende. Porphyritic phases, similar to unit Eg, are common near David Creek in the southern part of the area.

Eocene Coryell (unit Ec)

The alkalic to subalkalic Coryell plutonic suite consists of Middle Eocene intrusions. They underlie a large part of the Almond Mountain map area, but within the Kettle River area are restricted to a small pluton in the northern part of 1:20 000 scale map area 082E/046, referred to as the 'Collier Lake stock' (Massey and Duffy, 2008a). The stock is a porphyritic syenite, with phenocrysts of pink K-feldspar. Its eastern contact is a chilled-margin phase of finer grained material, whereas the southern contact with unit Jgd is coarse grained, suggesting a faulted relationship.

Penticton Group

The Tertiary Penticton Group is described and defined by Church (1973) as comprising six formation members: basal Springbrook and coeval Kettle River formations, volcanic rocks of the Marron and 'McNamara' formations, and dom-

inantly sedimentary rocks of the White Lake and Skaha formations. In the Kettle River area, three units are recognized, a basal succession of conglomerate and sandstone of the Kettle River Formation, the Marron Formation and overlying basalt, referred to as the 'Kallis formation' by Massey and Duffy (2008b).

Kettle River Formation (unit Epk)

The Kettle River Formation and overlying Marron Formation occur within a well-defined, north-trending graben that extends from the Rock Creek area west of the Greenwood camp (Figure 2) through the western part of the Almond Mountain map area, and northward into the Christian Valley map area. In the Kettle River area, it also occurs in several isolated exposures immediately west of Kettle River.

The formation is well exposed on the eastern side of the Kettle River, near Paturages Creek (Figures 3, 4), where it unconformably overlies volcanic rocks of the Wallace group. It comprises a basal unit of coarse conglomerate, with large rounded boulders of dominantly granite and greenstone in a medium green grit-sandstone matrix. The basal part of the Kettle River Formation in the southern exposure on the western side of the Kettle River is also a coarse conglomerate, with dominantly granitic clasts in a fine- to medium-grained grit matrix (Figure 7). In the Canyon Creek area, 2 to 3 km to the north, the basal part of the Kettle River Formation is a thick (approximately 100 m) succession of immature conglomerate, with coarse angular clasts of dominantly greenstone and diorite typical of the underlying Wallace group and unit Jd.

Basal conglomerate grades upward into coarse-grained, tan-coloured grit, sandstone and siltstone that form the bulk of the Kettle River Formation (Figure 8), which is typically well bedded and light coloured, forming white cliffs visible from a distance (Figure 9). Thin shale or argillite beds occur locally, and plagioclase-phyric flows, typical of the Marron Formation, occasionally occur in the upper part of the Kettle River Formation. Elsewhere, coarse grit or sandstone directly overlies Jurassic granodiorite or, near the mouth of Crouse Creek (Figure 4), the megacrystic granite of unit Eg. Here, the grit is derived entirely from the granite and it is difficult to determine the exact location of the contact between the two units as the granite is very friable, weathered and bleached.

The Kettle River Formation is similar to basal successions of the Penticton Group described elsewhere, including the Springbrook Formation in the White Lake basin (Church, 1973) and the Kettle River in the Greenwood area, where it is described as a "discontinuous basal conglomerate, above which is white to buff, locally plant bearing arkosic sandstone, siltstone, and minor shale and conglomerate, all largely derived from acid volcanic and granitic rocks" (Little and Monger, 1966, p. 67).


Figure 7. Coarse conglomerate that forms the basal part of the Kettle River Formation, in southern British Columbia; note large angular to subrounded clasts of granodiorite, which is similar to that shown in Figure 6, and a medium-grained, chlorite-altered groundmass.

Figure 8. Interbedded conglomerate and grit layers in the base of the Kettle River Formation, in southern British Columbia. These grade up into bedded to massive grit and sandstone, more typical of the Kettle River Formation.
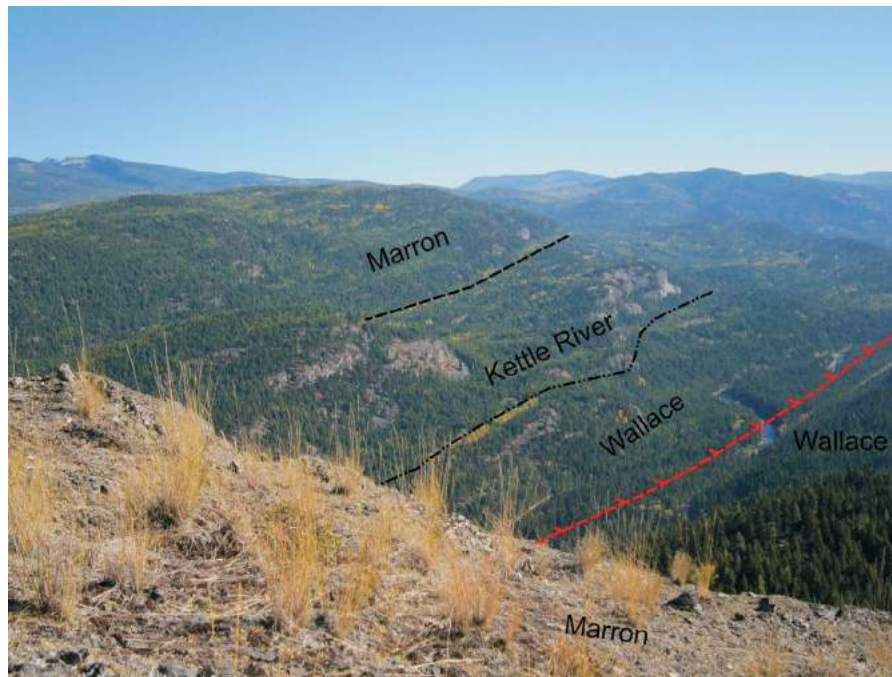
Figure 9. View to the southeast, looking across the Kettle River, in southern British Columbia. Note cliff forming exposures of the Kettle River Formation on the near slopes; these unconformably overlie volcanic rocks of the Wallace group and are in turn overlain by Marron Formation volcanic rocks approximately 5 km in the distance. An east-dipping Tertiary normal fault follows approximately the Kettle River valley.

Marron Formation (unit Epm)

The type section of the Marron Formation in the White Lake basin area is described by Church (1973) and is correlated with a similar section in the Greenwood area (Church, 1986). The Marron Formation directly overlies the Kettle River Formation or, locally, older pre-Tertiary 'basement' rocks. In the Burrell Creek area, the contact between the Kettle River and Marron is locally unconformable (Höy, 2013), and hence the absence of the basal part of the Kettle River Formation may record either nondeposition or erosion prior to volcanism of the Marron Formation.

The Marron Formation comprises a thick succession of volcanic rocks that varies in composition from alkalic basalt to trachyte, and ranges from lava flows to well-banded mafic tuffs and blocky tephra. In contrast with Wallace group flows, volcanic textures, including amygdules, vesicles, phenocrysts and clasts, are well preserved. A section of black to red shales a few tens of metres thick occurs in the central part of the Marron Formation, west of Thone Lake.

Kallis Formation (unit Pk)

The Kallis formation is preserved in isolated topographic highs throughout the area. It lies on the Marron Formation and represents the remnants of widespread Neogene plateau basalt. It consists typically of a black, fine-grained, aphyric or olivine-phyric basalt.

Structure

The structure of the Kettle River area is dominated by north-trending normal faults that record a period of Tertiary extension in south-central BC (Parrish et al., 1988). An earlier deformation, present only locally in the Paleozoic Wallace group, contrasts with penetrative deformation that has been recorded in Paleozoic rocks elsewhere, notably in the Knob Hill Group and Anarchist Schist to the south (e.g., Massey, 2006, 2007). In the Greenwood area, the Paleozoic Attwood Group, Knob Hill Group and Triassic Brooklyn Formation are locally tightly folded within a series of northward-dipping thrust sheets (Fyles, 1990).

The lack of prominent marker units and the abundance of intrusive rocks in most of the Wallace group precludes a detailed structural interpretation of these rocks. As well, hornfelsing and veining adjacent to intrusions further mask both their structures and primary sedimentary features. Tight minor folds were noted in the 'basal' Larse Creek limestone just south of Beaverdell Creek, but a large part of the Wallace group lacks structures or regional metamorphism that could be attributed to a regional deformational event. Thrust faults, similar to those described in the Greenwood area (Fyles, 1990), are also not recognized here; serpentinites that mark the thrust faults and folding characteristic of the thrust sheets at Greenwood appear to be also absent.

A complex north-trending graben, bounded by high-angle Tertiary normal faults, extends from near Rock Creek in the south, through the Kettle River area and into the Christian Valley map area (NTS 082E/10). The Paleozoic Wallace group forms a tectonic high in the Kettle River area, and Tertiary graben fill of the Kettle River and Marron formations onlap Wallace basement rocks and exposed Jurassic and Eocene intrusions.

A west-dipping, north-trending normal fault, the Greenwood fault, forms the eastern margin of the graben. It juxtaposes Tertiary granite on the eastern side against Marron and Kettle River formations and Wallace group rocks on the western side. Exposures of the fault surface were not seen, but observed granite and granodiorite on the eastern side of the fault were locally sheared, with shear zones dipping relatively steeply (40–50°) to the west. The western margin of the graben is marked by an east-dipping normal fault that follows the trend of the Kettle River south to the Crouse Creek area, and there it is offset to the west by the north to northwest-trending Crouse Creek fault.

The Crouse Creek fault (Figure 10) is a brittle structure marked by considerable shearing, brecciation and mainly chloritic alteration (Greig and Flasha, 2005). It trends north-northwest and generally dips at a high angle to the west. The amount of displacement on the fault is not known; it is assumed to be oblique with left-lateral and normal west-side–down movement, based mainly on the relative levels of the Penticton Group exposures at the southern end of the fault. A northwest-trending splay of the Crouse

Creek fault, south of Beaverdell Creek (Figure 3), contains a pronounced shear and mylonite zone along it; a prominent topographic linear feature that extends to the southeast, across the Crouse Lake fault and following a branch of Canyon Creek, may mark the extension of this fault.

The northeast-trending Crystal Creek fault has net normal west-side–down movement along it, with Kettle River Formation in its hangingwall juxtaposed with Jurassic and Eocene intrusive rocks to the east (Figure 3). Farther south, the Hoodoo Lake fault defines a pronounced northeast-trending linear feature within the granite. Several exposures immediately northwest of Hoodoo Lake indicate right lateral movement along a steep, west-dipping fault surface.

Numerous other faults and shears, generally too small to be shown on the maps, occur within the central part of the graben. These are marked by outcrop shear zones, brecciation, alteration and, commonly, sulphide mineralization.

Mineralization

An important focus of this study is to determine the relationships, on both a local and regional scale, between base- and precious-metal mineralization and structures, and magmatism. Previous work in the Deer Park and Burrell Creek areas to the east (Höy, 2010; 2013) underscored the importance of Jurassic and Eocene magmatism as well as Tertiary structures, in localizing mineralization. To the west, shear-hosted silver-rich veins in the Beaverdell camp appear to be Eocene in age, whereas the Carmi veins imme-
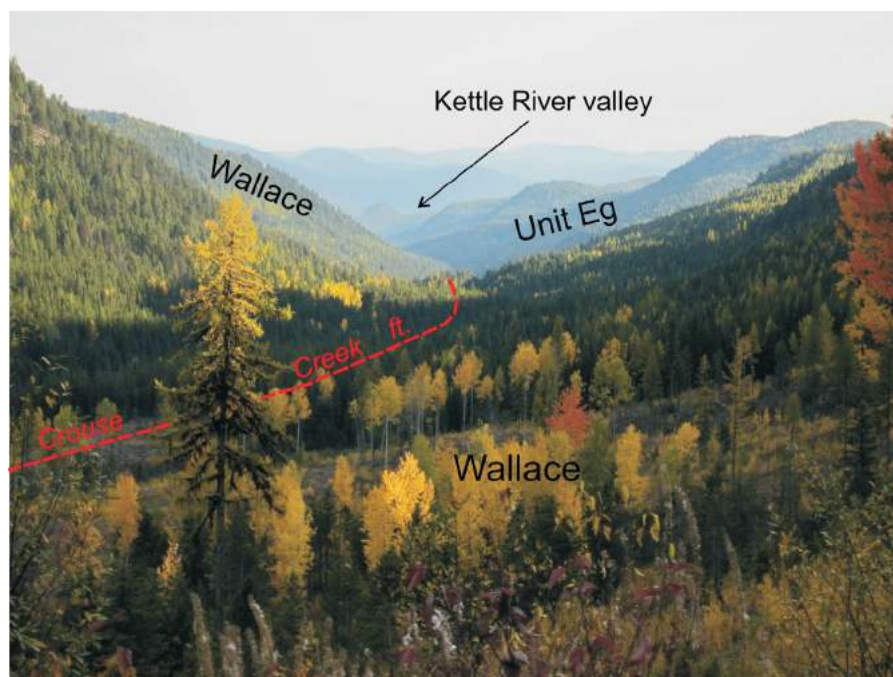
Figure 10. View to the south of the Crouse Creek valley, and location of the Crouse Creek fault in southern British Columbia; the Kettle River valley is approximately 8 km in the distance. Abbreviation: Eg, megacrystic porphyritic granite.

diately to the north have isotopic signatures that suggest they are Jurassic (Watson et al., 1982).

Mineralization within the Kettle River area has been described by Gale (2000), and Greig and Flasha (2005), based mainly on work done on the GK property, owned by Bitterroot Resources, and the Ward area respectively. The following summary is based largely on this work. Mineral occurrences from the BC MINFILE database are plotted on Figures 3 and 4.

Mineralization in the Kettle River area is similar to that in the Beaverdell camp: polymetallic or quartz-gold veins and breccia zones related to late structures that cut Wallace group metavolcanic and metasedimentary rocks, and Jurassic intrusions. The attitudes of host structures are variable, but commonly trend north to north-east, parallel with many of the Eocene extensional faults. Limited production from several of these occurrences, notably the Barnato (MINFILE 082ESE109) and Maybe (MINFILE 082ESE246) deposits, produced a total of 19 626 g Au and 21 398 g Ag from 744 milled tonnes. Further work on the controls of mineralization and dating of hostrocks, as well as an update of the BC MINFILE database, will continue in the 2016 field season.

Summary and Conclusions

The oldest rocks in the Kettle River area, those of the Wallace group, include minor limestone, fine-grained siliciclastic rocks and abundant mafic volcanic rocks. Their age is not known, but is assumed to be late Paleozoic, based mainly on the ages of the possibly correlative Anarchist Schist and Knob Hill Group to the south. However, Massey (2010) argued that the Wallace is part of a calcalkaline volcanic-arc succession, distinct from the dominantly tholeiitic rocks of the Knob Hill and Anarchist.

Two pulses of magmatism are recognized in the Early Eocene: alkalic Coryell syenite and possibly contemporaneous megacrystic porphyritic granite. Since these are not in contact, it is difficult to determine relative ages. Numerous, generally north to northeast-trending alkalic dikes cut older intrusions and the Wallace group in the Triple Lakes area.

The Penticton Group was deposited during Middle Eocene regional extension and faulting, with infill of a narrow, north-trending graben that follows the approximate trace of the Kettle River valley. The Kettle River Formation, a basal succession of dominantly conglomerate and sandstone, filled topographic lows developing in the graben and to the northwest along the approximate trace of Crouse Creek. A thick succession of dominantly mafic flows and tuffs of the Marron Formation continued filling the north-northeast-trending structural basin, locally depositing directly on Wallace group basement rocks or onlapping pre–Early Eocene tectonic highs. These are overlain by olivine-phyric mafic flows of the Kallis formation, now preserved on isolated topographic highs throughout the Kettle River area. Extension continued after deposition of the Kettle River and Marron formations, with continued movement along graben-bounding faults and along younger structures that cut these formations.

Mineralization in the area includes base- and precious-metal veins, breccia zones and disseminated sulphides in mainly Jurassic Wallace group diorite and granodiorite. As noted by Greig and Flasha (2005), mineralization is spatially and probably genetically related to north-northeast trending structures and dikes and, as it locally cuts some dikes that appear to be part of the alkalic Eocene suite, is probably Eocene in age, a model similar to that found in the Beaverdell camp to the west.

On a regional scale, virtually all known mineral occurrences are within a north-northwest trending tectonic high that crosses the north-trending Eocene graben. The topographic high formed prior to deposition of the Penticton Group, which onlaps exposures of the Wallace group and Jurassic–Eocene intrusions, and projects southeast to the highly mineralized Greenwood camp (Figure 2). A similar model for controls of mineralization has been noted in the Franklin camp area, with intrusion of the Jurassic Averill plutonic complex and associated mineralization localized along the intersection of the north-trending Granby fault and other northwest-trending structures (Höy, 2013). Further mapping and identification of these structures in the Penticton map area will help direct and focus future mineral exploration throughout the southern Monashee Mountains and Okanagan Highland of southern BC.

Acknowledgments

References

Acton, S.L., Simony, P.S. and Heaman, L.M. (2002): Nature of the basement to Quesnel Terrane near Christina Lake, southeastern British Columbia; Canadian Journal of Earth Sciences, v. 69, p. 65–78.

BC Geological Survey (2015): MapPlace GIS internet mapping system; BC Ministry of Energy and Mines, BC Geological Survey, MapPLace website, URL <http://www.MapPlace.ca> [January 2015].

BC Geological Survey (2015): MINFILE BC mineral deposits database: BC Ministry of Energy and Mines, BC Geological Survey, URL, <http://minfile.ca/> [January 2015].

Caron, L. (2014): Assessment report, ground geophysics on the Brett property, Whiteman Creek area; BC Ministry of Energy and Mines, BC Geological Survey, Assessment Report 35058, 16 p.

Church, B.N. (1973): Geology of the White Lake basin; BC Ministry of Energy and Mines, BC Geological Survey, Bulletin 61, 120 p.

Church, B.N. (1986): Geological setting and mineralization in the Mount Attwood–Phoenix area of the Greenwood camp; BC Ministry of Energy and Mines, BC Geological Survey, Paper 1986-2, 65 p.

Church, B.N. (1996):Several new industrial mineral and ornamental stone occurrences in the Okanagan-Boundary district (82E, 82L); in Exploration in British Columbia 1995, BC Ministry of Energy and Mines, p. 123–130.

Drysdale, C.W. (1915): Geology of the Franklin mining camp, southern British Columbia; Geological Survey of Canada, Memoir 15, 246 p.

Dufresne, M and Schoeman, P. (2014): Assessment report for 2014 exploration, Greenwood property, southern British Columbia; BC Ministry of Energy and Mines, Assessment Report 35018, 52 p.

Fyles, J.T. (1990): Geology of the Greenwood–Grand Forks area, British Columbia, NTS 82E/1,2; BC Ministry of Energy and Mines, BC Geological Survey, Open File 1990-25.

Gale, R.E. (2000): Geological, geochemical, VLF-EM survey and trenching report, Ward Group, Greenwood Mining Division, British Columbia; BC Ministry of Energy and Mines, BC Geological Survey, Assessment Report 26369, 15 p.

Greig, C.G. and Flasha, S.T. (2005): 2004-2005 exploration program on the GK property; BC Ministry of Energy and Mines, BC Geological Survey, Assessment Report 28179, 122 p.

Höy, T. (2010): Geology of the Deer Park map area, southeastern British Columbia (NTS 082E/08); in Geoscience BC Summary of Activities 2009, Geoscience BC Report 2010, p. 137–140.

Höy, T. (2013): Burrell Creek map area: setting of the Franklin mining camp, southeastern British Columbia; in Geoscience BC Summary of Activities 2012, Geoscience BC, Report 2013-1, p. 91–101.

Höy, T. and Dunne, K.P.E. (2001): Metallogeny and mineral deposits of the Nelson-Rossland area, Part II: The early Jurassic Rossland Group, southeastern British Columbia; BC Ministry of Energy and Mines, BC Geological Survey, Bulletin 109, 195 p.

Hoy, T. and Jackaman, W. (2005): Geology of the Grand Forks map sheet, British Columbia (NTS 082E/01); BC Ministry of Energy and Mines, BC Geological Survey, Geoscience Map 2005-2, scale 1:50 000.

Höy, T. and Jackaman, W. (2010): Geology of the Deer Park map sheet (NTS 82E/08); Geoscience BC, Map 2010-7-1, scale 1:50 000.

Höy, T. and Jackaman, W. (2013): Geology of the Burrell Creek map sheet (NTS 82E/09); Geoscience BC, Map 2013-07-1, scale 1:50 000.

Laberge, J.R. and Pattison, D.R.M. (2007): Geology of the western margin of the Grand Forks Complex: high grade Cretaceous metamorphism followed by early Tertiary extension on the Granby fault; Canadian Journal of Earth Sciences, v. 44, p. 199–208.

Little, H.W. (1957): Kettle River (East half); Geological Survey of Canada, Map 6-1957, scale 1:253 440

Little, H.W. (1961): Kettle River (West half); Geological Survey of Canada, Map 15-1961, scale 1:253 440.

Little, H.W. and Monger, J.W.H. (1966): Greenwood map area (west half); Geological Survey of Canada, Report of Activities 1965, Paper 66-1, p. 67–71.

Massey, N.W.D. (2006): Boundary project: reassessment of Paleozoic rock units of the Greenwood area, southern BC; in Geological Fieldwork 2005, BC Ministry of Energy and Mines, BC Geological Survey, Paper 2006-1, p. 99–107.

Massey, N.W.D. (2007): Boundary project: Rock Creek area (082/02W, 3E), southern British Columbia; in Geological Fieldwork 2006, BC Ministry of Energy and Mines, BC Geological Survey, Paper 2007-1 and Geoscience BC, Report 2007-1, p. 117–128.

Massey, N.W.D. (2010): Boundary project: geochemistry of volcanic rocks of the Wallace Formation, Beaverdell area, south-central BC; in Geological Fieldwork 2008, BC Ministry of Energy and Mines, BC Geological Survey, Paper 2009-1, p. 143–152.

Massey, N.W.D. and Duffy, A. (2008a): Boundary project: McKinney Creek and Beaverdell areas, south-central BC; in Geological Fieldwork 2007, BC Ministry of Energy and Mines, BC Geological Survey, Paper 2008-1, p. 87–102.

Massey, N.W.D. and Duffy, A. (2008b): Geology and mineral deposits of the area east of Beaverdell, British Columbia; BC Ministry of Energy and Mines, BC Geological Survey, Open File 2008-9, scale 1:25 000.

Massey, N.W.D., Gabites, J.E., Mortensen, J.K. and Ullrich, T.D. (2010): Boundary project: geochronology and geochemistry of Jurassic and Eocene intrusions, southern British Columbia (NTS 082E); in Geological Fieldwork 2009, BC Ministry of Energy and Mines, BC Geological Survey, Paper 2010-1, p. 127–142.

Parrish, R.R. (1992): Miscellaneous U-Pb zircon dates from southeast British Columbia; in Radiogenic Age and Isotopic Studies, Geological Survey of Canada, Report 5, Paper 91-2, p. 143–153.

Parrish, R.R., Carr, S.D. and Parkinson, D.L. (1988): Eocene extensional tectonics and geochronology of the southern Omineca belt, British Columbia and Washington; Tectonics, v. 72, p. 181–212.

Preto, V.A. (1970): Structure and petrology of the Grand Forks Group, BC; Geological Survey of Canada, Paper 69-22.

Preto, V.A. (1979): Geology of the Nicola Group between Merritt and Princeton; BC Ministry of Energy and Mines, BC Geological Survey, Bulletin 69, 90 p.

Reinecke, L (1915): Ore deposits of the Beaverdell map area; Geological Survey of Canada, Memoir 79, 172 p.

Tempelman-Kluit, D. J. (1989): Geology, Penticton, British Columbia; Geological Survey of Canada, Map 1736A, scale 1:250 000.

Watson, P.H., Godwin, C.I. and Christopher, P.A. (1982): General geology and genesis of silver and gold veins in the Beaverdell area, south-central British Columbia; Canadian Journal of Earth Sciences, v. 19, p. 1264–1274.

Wheeler, J.O. and McFeely, P. (1991): Tectonic assemblage map of the Canadian Cordillera and adjacent parts of the United States of America; Geological Survey of Canada, Map 1712A, scale 1:2 000 000.

Reconnaissance Biogeochemical Survey using Spruce Tops in the West Road (Blackwater) River Area, Fraser Plateau, Central British Columbia (parts of NTS 093C/14, /15, 093F/02, /03)

W. Jackaman, **Noble Exploration Services Ltd., Jordan River, BC, wjackaman@shaw.ca**

D.A. Sacco, **Palmer Environmental Consulting Group Inc., Vancouver, BC**

Introduction

The fundamental objective of the TREK project is to promote mineral exploration in underexplored parts of the Interior Plateau, British Columbia. This is accomplished through the production of high-quality integrated geoscience data that can be used to advance the understanding of the economic geology in a region with potential to host porphyry copper, porphyry molybdenum and epithermal gold deposits. Historically, exploration activities within the region have been hindered by Neogene Chilcotin Group basalt flows and extensive glacial drift that obscure the underlying, and potentially prospective, bedrock units. To address these difficulties, the TREK project combines information from ground geochemical, airborne geophysical, and geological initiatives to provide a foundation for more advanced resource development in this important region (Clifford and Hart, 2014).

The surficial geochemistry component of the TREK project began in 2013 and includes a collection of 1233 subglacial till samples and 281 lake sediment samples. In addition, 1711 archived till samples have been reanalyzed and geochemical data from previous geochemical surveys have been compiled. This has resulted in one of the highest quality and most comprehensive geochemical datasets available (Jackaman et al., 2015a; Sacco and Jackaman, 2015). Although a total of more than 4500 geochemical samples for geochemical analysis have been collected from lake- and stream-sediment, water, till and biological media in the region since the 1990s, several key tracts of prospective ground still have limited or no geochemical coverage. This lack of data is largely due to thick vegetation cover, few lakes and limited road networks (Figure 1), which significantly limits the types of survey techniques that can be applied. To address this problem, a helicopter-supported,

Figure 1. Biogeochemical survey area, Fraser Plateau, British Columbia.

spruce-top twig-and-needle survey was conducted in a selected area to generate geochemical information to assist in locating hidden mineralization.

Biogeochemical Survey Area

The 2015 biogeochemical survey area is located 40 km north of Anahim Lake within the Fraser Plateau and extends north from the Itcha and Ilgachuz mountain ranges to the West Road (Blackwater) River Basin (Figure 2). This area is characterized by gentle north-facing slopes that are blanketed with glacial drift and dissected by streams that flow into the flat-floored valley. Interspersed throughout the 1000 km² survey area are stands of lodgepole pine (*Pinus contorta*), white spruce (*Picea glauca*) and Engelmann spruce (*Picea engelmannii*). A hybrid species of white and Engelmann spruce (known as Interior spruce) is also common in the central Interior. Fortunately, these spruce species have very similar chemical characteristics (C. Dunn, pers. comm., 2015). Wetland features and sedge grass meadows are common. Evidence of beetle-killed pine, recent forest fires and regeneration from previous forest fires was also observed. Access roads do not currently extend into the survey area, but forest service roads are located immediately to the east and north.

The survey area is underlain by Hazelton Group and Ootsa Lake Group rocks, and Chilcotin Group volcanic rocks.
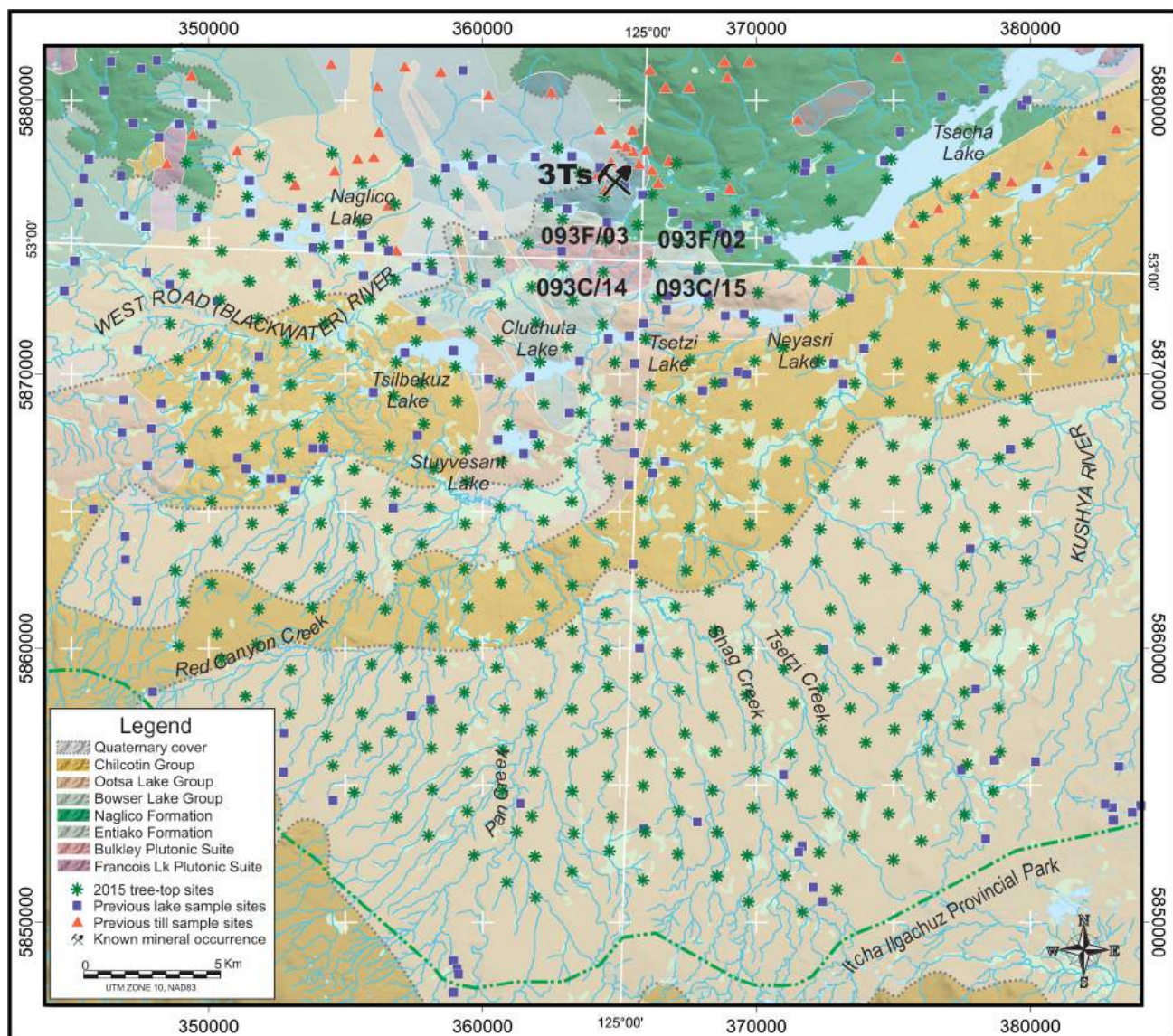
Figure 2. Generalized bedrock geology (after Angen et al., 2015), generalized Quaternary cover (after Massey et al., 2005), 3Ts mineral occurrence (MINFILE 093F 068; BC Geological Survey, 2015), archived lake-sample sites (Cook and Jackaman, 1994; Jackaman, 2006) and archived till-sample sites (Levson et al., 1994; Jackaman et al., 2015b). Digital elevation model from Canadian digital elevation data (GeoBase®, 2015).

Several developed prospects that contain Au, Ag, Zn, Pb and Cu mineralization are located in the region. The Black-water-Davidson intermediate sulphidation epithermal Au-Ag deposit (NTS 093F/02; MINFILE 093F 037; BC Geological Survey, 2015) is located 15 km north of the survey area, and the 3Ts polymetallic Ag–Pb–Zn±Au deposit (NTS 093F/03; MINFILE 093F 068) is situated on the northern survey boundary. No recorded mineral occurrences exist within the survey area south of the West Road (Blackwater) River.

Historical Geochemical Data

Previous vegetation sampling has not been attempted in the 2015 biogeochemical survey area; however, several re-

gional biogeochemical surveys and research programs have been conducted in other parts of the TREK project area. To the north of the current study, ground-based regional surveys were completed using lodgepole-pine bark (Dunn and Hastings, 1998, 1999, 2000), and to the south, a helicopter-supported reconnaissance survey was conducted over the Fish Lake property (NTS 092O/05E; MINFILE 092O 041) using lodgepole-pine tops (Dunn et al., 1994). In addition, several research programs have investigated the application of biogeochemical techniques in areas of thick glacial sedimentary rocks and Neogene Chilcotin Group basalt flows (Dunn, 1995; Dunn and Levson, 2010; Heberlein et al., 2013).

2015 Spruce-Top Biogeochemical Survey

Field Methods

Field survey methods and sample preparation and analysis protocols in the 2015 biogeochemical survey were based on previous field surveys, orientation investigations and detailed research (Dunn, 1995, 2007). During a six-day period in June 2015, a 1000 km^2 area was surveyed using predetermined flight-lines along an offset grid with 1500 m spacing. A total of 421 side-branch samples, comprising 1 kg of twigs, needles and cones, were systematically collected near the tops of 401 healthy spruce trees (Figure 3). Location co-ordinates were carefully recorded at each site.

The target spruce trees were healthy, 80–100 years old, 20–25 m tall and commonly extended 2–3 m above a lower canopy of lodgepole pine, which typically showed effects of the mountain pine beetle infestation. A recent forest fire in the northern part of the survey area and several immature patches of forest regeneration limited the availability of spruce for a small number of the predetermined sites.

Sample Preparation and Analysis

After collection, each 1 kg sample was systematically processed in the field prior to shipment to the commercial laboratory. Cones were removed and the branches were trimmed to include only 5–7 years of growth. Each of the field-processed samples weighed approximately 500 g and was delivered to the Bureau Veritas Commodities laboratory (Vancouver, BC). After the samples were oven dried at 60°C, the needles and twigs were separated. The twigs were macerated to 1 mm and analyzed for 53 elements by inductively coupled plasma–mass spectrometry (ICP-MS) following aqua-regia digestion. Needles were reduced to ash at 475°C and 0.5 g of ash material was analyzed for 53 elements plus rare-earth elements by ICP-MS following aqua-regia digestion.

Quality Control

In addition to the in-house quality-control procedures of the commercial lab, quality control for analytical determinations included the use of field duplicates, analytical duplicates and control reference standards. Duplicate samples determine sampling and analytical variability, and reference standards measure the accuracy and precision of the analytical methods. For each batch of 20 sequential samples, one field duplicate (taken at a randomly selected sample site), one analytical duplicate (a sample split during the lab preparation process) and one reference standard are included in the geochemical analyses. Certified reference standards for plant materials are not readily available; however, ash and spruce twig control samples with known element concentrations were included to monitor the precision of the analytical results (C. Dunn, pers. comm., 2015).

Figure 3. Helicopter-supported spruce-top collecting of distal side-branch samples consisting of twigs, needles and cones.

Summary

Generating a comprehensive collection of high-quality, regional geochemical analytical data and field information is a primary objective of the geochemical component of the TREK project. Maximizing geochemical coverage for the entire TREK project area has required innovative approaches to access and collect data in challenging locations. Ongoing research supports the effectiveness of biogeochemistry, and combined with advances in analytical methods, establishes biogeochemical surveys as a valid exploration option for generating valuable geochemical information. The TREK biogeochemical survey helps complete the coverage of surface geochemical data in the TREK project area, and generates geochemical results that are complementary to existing geoscience datasets, providing a comprehensive collection of information that supports the search for potential mineral deposits in the Interior Plateau, British Columbia.

References

Angen, J.J., Westberg, E., Hart, C.J.R, Kim, R. and Rahimi, M. (2015): Preliminary geological map of the TREK Project area, Central British Columbia; Geoscience BC, Report 2015-10, URL <http://www.geosciencebc.com/s/Report2015-10.asp> [October 2015].

BC Geological Survey (2015): MINFILE BC mineral deposits database; BC Ministry of Energy and Mines, BC Geological Survey, URL <http://minfile.ca/> [October 2015].

Clifford, A. and Hart, C.J.R. (2014): Targeting resources through exploration and knowledge (TREK): Geoscience BC's newest minerals project, Interior Plateau Region, central British Columbia (NTS 093B, C, F, G); *in* Geoscience BC Summary

of Activities 2013, Geoscience BC, Report 2014-1, p. 13–18, URL <http://www.geosciencebc.com/s/SummaryofActivities.asp?ReportID=619756> [October 2015].

Cook, S.J. and Jackaman, W. (1994): Regional lake sediment and water geochemistry of part of the Nechako River map area (93F/2, 3; parts of 93F/6, 11, 12, 13, 14); BC Ministry of Energy and Mines, Open File 1994-19, 31 p., URL <http://www.empr.gov.bc.ca/Mining/Geoscience/PublicationsCatalogue/OpenFiles/1994/Pages/1994-19.aspx> [October 2015].

Dunn, C.E. (1995): Biogeochemical prospecting in drift-covered terrain of British Columbia; *in* Drift Exploration in the Canadian Cordillera, P.T. Bobrowsky, S.J. Sibbick, J.M. Newell and P.F. Matysek (ed.), BC Ministry of Energy and Mines, Paper 1995-2, p. 229–238, URL <http://www.empr.gov.bc.ca/Mining/Geoscience/PublicationsCatalogue/Papers/Pages/1995-2.aspx> [October 2015].

Dunn, C.E. (2007): Biogeochemistry in mineral exploration; Handbook of Exploration and Environmental Geochemistry, v. 9, M. Hale (ser. ed.), Elsevier, Amsterdam, 462 p.

Dunn, C.E. and Hastings, N.L. (1998): Biogeochemical survey of the Ootsa-François lakes area using outer bark of lodgepole pine (NTS 93F/13, 14, and part of 12), north central British Columbia; Geological Survey of Canada, Open File 3587, 1 diskette, URL <http://geochem.nrcan.gc.ca/cdogs/content/pub/pub01533_e.htm> [October 2015].

Dunn, C.E. and Hastings, N.L. (1999): Biogeochemical survey of the Fraser Lake area using outer bark of lodgepole pine (NTS 93K02/03), central British Columbia; Geological Survey of Canada, Open File 3696, 1 diskette, URL <http://geochem.nrcan.gc.ca/cdogs/content/pub/pub01535_e.htm> [October 2015].

Dunn, C.E. and Hastings, N.L. (2000): Biogeochemical survey of Nechako River area using outer bark of lodgepole pine (NTS 93 F 15/16 and parts of 93 F 9/10), central British Columbia; Geological Survey of Canada, Open File 3594, 1 diskette, URL <http://geochem.nrcan.gc.ca/cdogs/content/pub/pub01534_e.htm> [October 2015].

Dunn, C.E. and Levson, V.M. (2010): Biogeochemical orientation survey data from NTS 93F/2 and 7 (Davidson-Blackwater): outer bark of lodgepole pine, central British Columbia; BC Ministry of Energy and Mines, Open File 2010-05, 14 p., URL <http://www.empr.gov.bc.ca/Mining/Geoscience/PublicationsCatalogue/OpenFiles/2010/Pages/2010-5.aspx> [October 2015].

Dunn, C.E., Balma, R.G. and Spirito, W.A. (1994): Reconnaissance biogeochemical survey using lodgepole pine tops: Fish Lake area (NTS 92O), west-central British Columbia; Geological Survey of Canada, Open File 2839, 152 p., URL <http://geochem.nrcan.gc.ca/cdogs/content/pub/pub00238_e.htm> [October 2015].

GeoBase® (2015): Canadian digital elevation data; Natural Resources Canada, URL <http://geogratis.gc.ca/api/en/nrcan-rncan/ess-sst/3A537B2D-7058-FCED-8D0B-76452EC9D01F.html> [October 2015].

Heberlein, D.R., Dunn, C.E. and MacFarlane, W. (2013): Use of organic media in the geochemical detection of blind porphyry copper-gold mineralization in the Woodjam property area, south-central British Columbia; *in* Geoscience BC Summary of Activities 2012, Geoscience BC, Report 2013-1, p. 47–62, URL <http://www.geosciencebc.com/s/SummaryofActivities.asp?ReportID=566724> [October 2015].

Jackaman, W. (2006): Regional drainage sediment and water geochemistry of part of the Nechako River and Anahim Lake map areas (NTS 93C and 93F); Geoscience BC, Report 2006-4, 463 p., URL <http://www.geosciencebc.com/s/Report2006-04.asp> [October 2015].

Jackaman, W., Sacco, D. and Lett, R.E. (2015a): Geochemical reanalysis of archived till samples, TREK Project, Interior Plateau, central BC (parts of NTS 093C, 093B, 093F & 093K); Geoscience BC, Report 2015-09, 5 p., URL <http://www.geosciencebc.com/s/Report2015-09.asp> [October 2015].

Jackaman, W., Sacco, D.A. and Lett, R.E. (2015b): Regional geochemical and mineralogical data, TREK Project – Year 2, Interior Plateau, British Columbia; Geoscience BC, Report 2015-12, 13 p., URL <http://www.geosciencebc.com/s/Report2015-12.asp> [October 2015].

Levson, V.M., Giles, T.R., Cook, S.J. and Jackaman, W. (1994): Till geochemistry of the Fawnie Creek area (93F/03); BC Ministry of Energy and Mines, Open File 1994-18, 34 p., URL <http://www.empr.gov.bc.ca/Mining/Geoscience/PublicationsCatalogue/OpenFiles/1994/Pages/1994-18.aspx> [October 2015].

Massey, N.W.D., MacIntyre, D.G., Desjardins, P.J. and Cooney, R.T. (2005): Digital geology map of British Columbia: whole province; BC Ministry of Energy and Mines, BC Geological Survey, GeoFile 2005-1, scale 1:250 000, URL <http://www.empr.gov.bc.ca/Mining/Geoscience/PublicationsCatalogue/GeoFiles/Pages/2005-1.aspx> [October 2013].

Sacco, D.A. and Jackaman, W. (2015): Targeted geochemical and mineralogical surveys in the TREK project area, central British Columbia (parts of NTS 093B, C, F, G): year two; *in* Geoscience BC Summary of Activities 2014, Geoscience BC, Report 2015-1, p. 1–12, URL <http://www.geosciencebc.com/s/SummaryofActivities.asp?ReportID=691235> [October 2015].

Search: Geoscience BC's New Minerals Project in West-Central British Columbia (Phases I and II, covering NTS 093E, F, G, K, L, M, N, 103I)

B.E. Madu, Geoscience BC, Vancouver, BC, madu@geosciencebc.com

Introduction

The Search project was conceived by the Geoscience BC's Minerals Technical Advisory Committee to generate high quality regional magnetic data and complementary geoscience for key mineral areas of the province. Geoscience BC has previously conducted similar projects that included regional magnetic surveys, including the TREK, Northern Vancouver Island, QUEST-Northwest and Jennings River projects. The minerals industry will be able to use this new information to focus their exploration efforts in under-explored areas of the province. Communities and First Nations will also benefit from new geoscience information to assist with resource management decisions and realizing economic opportunities.

The project will include up to three years of work, to be accomplished in four phases (Figure 1). Phases I and II of the Search project are based on the successful QUEST-West project of 2008 to 2010. In June 2015, the planning process for Phase I of the Search project was announced and $2.415 million allocated to the project. This budget will permit the completion of Phase I and fund initial Phase II activities.

The project name 'Search' was attractive since it contains the word 'arch' and is a reference to the early phases of the program focusing on the Skeena arch: a paleotopographic high that was eroded into the Bowser and Nechako basins (Tipper and Richards, 1976) and today bridges the span between the Stikine and Quesnel geological terranes. Several active and closed mines, such as Huckleberry, Endako, Bell-Granisle and Equity Silver, are located within the Skeena arch. Proximity to infrastructure, modest topography and skilled labour are a few of the advantages that make developing projects in this region attractive.

Geophysical Program

The QUEST-West project completed airborne time-domain electromagnetic (TDEM) and gravity surveys at a line spacing of 4 and 2 km respectively in this region (Kowalczyk, 2009). Detailed aerial surveys were flown over six known deposits: Morrison, Bell-Granisle, Equity Silver, Endako and Huckleberry (MINFILE 093M 007, 093M 001, 093L 146, 093L 001, 093K 006 and 093E 037; BC Geological Survey, 2015).

Like these recent surveys, an airborne magnetic survey with a line spacing of 250 m creates an opportunity for new geological interpretations at a property-scale for explorers. The regional-scale coverage supports the development of a refined tectonic framework in areas of poor access or low rock outcrop as seen in the TREK project.

Phase I field activities for the Search project began in August 2015 and were officially launched in September, with a media event in Terrace. The planning process identified two blocks to be flown in 2015 and a contract was awarded to Vancouver-based Precision GeoSurveys Inc., who flew both blocks as one (Figure 2), using a stinger-mounted helicopter flying a fixed height drape over the land surface. The survey plan consisted of east-west trending flight lines, with north-south tie lines specified at 2500 m intervals. The total flight line distance, including tie lines, was estimated at 30 000 km. Owing to significant topographic relief and coastal weather conditions, it was expected to be a challenging program to complete. Data acquisition was substantially complete at the time of writing and results are expected to be ready for release at the Mineral Exploration Roundup 2016 conference. Quality assurance and quality control services for the program were provided by PK Geophysics Inc. In addition, Hemmera provided an ungulate management plan to minimize the impact of the program on caribou and goats in the area. Survey pilots and crew tracked ungulate interactions and were empowered to deviate flight patterns to lessen negative effects on animals.

Planning for 2016 Phase II activities is expected to commence in late fall 2015 and continue into 2016.
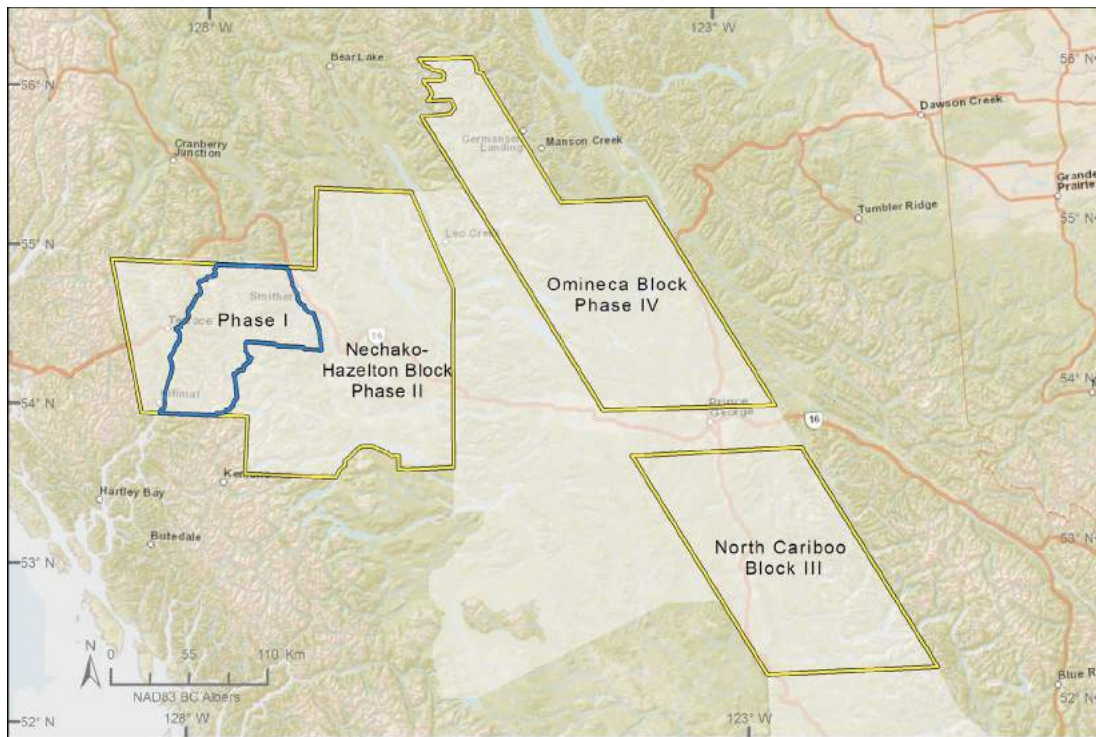
Geochemical Program

The Search project area has excellent geochemical coverage owing to re-analyses and infill sampling under previous Geoscience BC projects, such as QUEST-West

Figure 1. Conceptual location of the four proposed blocks in the Search project and their phased completion. Planning and consultation processes for all phases is expected to alter ultimate activity areas. Blue outline, Search Phase I survey area; yellow outlines, coverage of proposed phases of the Search project; transparent mask, coverage of previous airborne geophysical surveys conducted by Geoscience BC. Background data from GeoBC, 2015a–d.
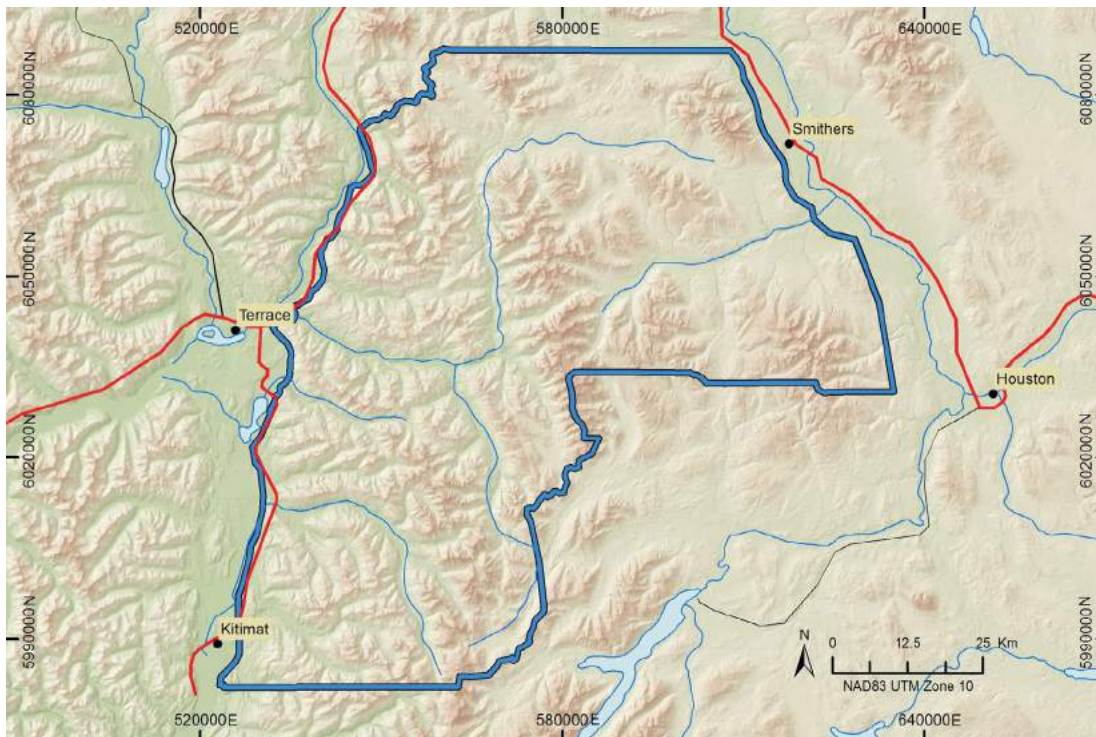
Figure 2. Phase I planning identified a 6700 km^2 target area (outlined in blue) to be flown in 2015. The planned survey will generate approximately 30 000 line-kilometres of new magnetic data. Background data from GeoBC, 2015a–d.

(Jackaman et al., 2009). Phase I of this program did not include funding for new geochemical sample collection; however, it is anticipated that value-added or innovative geochemical proposals will be considered in the future. Additional funds have been allocated for geochemistry work, as a part of Phase II of the Search project. Specific funding allocations for geochemistry would be made available as suitable projects were identified and/or further budget allocations occurred.

Integration Program

A desired outcome when generating large multiparameter datasets is to integrate them into new products with increased value that promote new understanding about the mineral potential of an area. The Search project is expected to stimulate renewed interest since it adds new fundamental information in an already data-rich region. Recent geological mapping by the BC Geological Survey in the Terrace–Kitimat area by Nelson (2009) will benefit from new high quality geophysical information and conversely provide better interpretation of the survey data itself. East of the Terrace area, the Nechako Project of the Geological Survey of Canada's National Geoscience Mapping Program (NATMAP) produced a comprehensive data library of digital geoscience information (Struik et al., 2007*).* Financial support is planned for integration proposals as the Search project continues.

Summary

The Search project is a multiyear major project for Geoscience BC that is focused on generating new high quality regional magnetic survey data and complementary geoscience for key mineral areas of the province. In 2015, the program was launched with an airborne survey covering 6700 km^2. Data from the survey will be made available through both Geoscience BC's website and its web mapping application—the Earth Science Viewer.

References

BC Geological Survey (2015): MINFILE BC mineral deposit database; BC Ministry of Energy and Mines, BC Geological Survey, URL <http://www.minfile.ca> [October 2015].

GeoBC (2015a): BC 1:250 000 digital elevation model; BC Ministry of Forests, Lands and Natural Resource Operations, URL <http://catalogue.data.gov.bc.ca/dataset/bc-1-250-000-digital-elevation-model> [December 2015].

GeoBC (2015b): BC major cities points 1:2 000 000 (digital baseline mapping); BC Ministry of Forests, Lands and Natural Resource Operations, URL <http://catalogue.data.gov.bc.ca/dataset/bc-major-cities-points-1-2-000-000-digital-baseline-mapping> [December 2015].

GeoBC (2015c): BC river, lake and wetland polygons 1:2 000 000 (digital baseline mapping); BC Ministry of Forests, Lands and Natural Resource Operations, URL <http://catalogue.data.gov.bc.ca/dataset/bc-river-lake-and-wetland-polygons-1-2-000-000-digital-baseline-mapping> [December 2015].

GeoBC (2015d): BC transport lines 1:2 000 000 (digital baseline mapping); BC Ministry of Forests, Lands and Natural Resource Operations, URL <http://catalogue.data.gov.bc.ca/dataset/bc-transport-lines-1-2-000-000-digital-baseline-mapping> [December 2015].

Jackaman, W., Balfour, J.S. and Reichheld, S.A. (2009): QUEST-West project geochemistry: field survey and data reanalysis (parts of NTS 093E, F, J, K, L, M, N), central British Columbia; *in* Geoscience BC Summary of Activities 2008, Geoscience BC, Report 2009-1, p. 7–14.

Kowalczyk, P.K (2009): QUEST-West geophysics in central British Columbia (NTS 093E, F, G, K, L, M, N, 103I): new regional gravity and helicopter time-domain electromagnetic data; *in* Geoscience BC Summary of Activities 2008, Geoscience BC, Report 2009-1, p. 1–6.

Nelson, J.L. (2009): Terrace regional mapping project, year 4: extension of Paleozoic volcanic belt and indicators of volcanogenic massive sulphide-style mineralization near Kitimat, British Columbia (NTS 103I/02, 07); *in* Geological Fieldwork 2008, BC Ministry of Energy and Mines, BC Geological Survey, Paper 2009-01, p. 7–20.

Struik, L.C., MacIntyre, D.G. and Williams, S.P. (2007): Nechako NATMAP project: a digital suite of geoscience information for central British Columbia (NTS map sheets 093N, 093K, 093F, 093G/W, 093L/9,16, & 093M/1,2,7,8); BC Ministry of Energy and Mines, BC Geological Survey, Open File 2007-10.

Tipper, H.W. and Richards, T.A. (1976): Jurassic stratigraphy and history of north-central British Columbia; Geological Survey of Canada, Bulletin 270, 73 p.

SkyTEM Airborne Electromagnetic Systems for Hydrogeological Mapping in Northeastern British Columbia

B. Brown, SkyTEM Canada Inc., Ayr, ON, bb@skytem.com

P. Gisselø, SkyTEM Surveys ApS, Aarhus, Denmark

M. Best, Bemex Consulting International, Victoria, BC

Introduction

Information presented in this report is the result of the Peace Project, a Geoscience BC–funded project focused on mapping and assessing groundwater in the Peace Region of British Columbia. This report presents data from a SkyTEM airborne electromagnetic (AEM) geophysical survey that was employed to map the hydrogeology in the Peace Project area.

The Montney gas play in the Peace Region of BC contains significant volumes of gas. The region is also an important agricultural area. Water in the region supports communities, First Nations' activities and various industrial sectors. For the first time in over 100 years, BC has a Water Sustainability Act, which protects and regulates the use of groundwater. To make appropriate policies, make regulations, aid in the regulator's permit decisions and support public discussion on issues related to water, it is necessary to obtain detailed information on the location, depth, extent and recharge of aquifers.

Several studies have been carried out by various agencies and companies to increase understanding of surface water and groundwater resources within the Fort St. John region. These projects have included the acquisition of data from ground time-domain electromagnetic (TDEM) and shallow 3-D seismic investigations, as well as recalibrated gamma-ray log data from wells in the area. These initiatives provide useful information on groundwater aquifers; however, data collection points are widely dispersed across the region, with most being in the vicinity of producing gas fields. There are currently no large-scale surveys that tie the hydrogeology of the entire Peace Region together. To address this gap, the Peace Project was planned to deliver regional hydrogeological data through an integration of pre-existing data from shallow wells and 3-D seismic surveys with the

results of an airborne geophysical survey. Airborne geophysics was considered an essential tool to provide more cost-effective and time-efficient coverage of a large area, than ground-based geophysical methods. The AEM system employed for the project was SkyTEM312[FAST], a helicopter-borne TDEM system. The 8000 km^2 area was covered in 43 days.

Project Summary

The Peace Project is a collaborative effort involving Geoscience BC, BC Ministry of Forests, Lands and Natural Resource Operations, BC Ministry of Environment, BC Oil and Gas Commission, BC Ministry of Natural Gas Development, Northern Development Initiative Trust, BC Oil and Gas Research and Innovation Society, Progress Energy Canada Ltd. and ConocoPhillips Canada, with additional support from the Peace River Regional District and the Canadian Association of Petroleum Producers.

Historically, to increase understanding of the surface water and groundwater resources within the greater Peace Region, several geophysical techniques have been, and continue to be, applied. The BC government completed a combined ground TDEM and shallow seismic investigation within the Groundbirch paleovalley designed to map the bedrock topography and locate potential aquifers within the Quaternary sediments. Monitoring wells, lined with PVC casing, were installed and gamma-ray and resistivity logs were run. In an attempt to use as much of the pre-existing geophysical data as possible, the current Peace Project will correct gamma-ray logs within the shallow cased-hole sections of petroleum wells for attenuation effects and use these corrected logs to map the Quaternary sediments and provide depth-to-bedrock maps of the region (Hayes et al., 2016). The gamma-ray log study will partially fill this gap; however, the well spacing is concentrated around producing fields with limited coverage between them.

In order to cost-effectively acquire the data needed to identify potential Quaternary and bedrock aquifers within the large study area and obtain information on the bedrock topography, AEM was chosen. Geoscience BC tested the ap-

plicability of AEM in 2011 during the Horn River Basin Aquifer Project (SkyTEM Canada Inc., 2014) and the method showed its ability to map deep paleochannels as well as near-surface aquifers and recharge areas. It was therefore decided to use AEM for the Peace Project as it was expected to provide similar results.

The objective of the AEM survey was to collect resistivity data from near surface to depths up to 300 m and combine this new information with prior data to 1) interpret potential Quaternary and bedrock aquifers within the area; 2) provide a map of the Quaternary–bedrock interface and thus Quaternary sediment thickness; and 3) generate a magnetic structure map of the basement. In general, it is expected that a joint interpretation of all geophysical data will help to determine optimal places for accessing and/or protecting the groundwater and finding nonpotable sources of water for energy sector use.
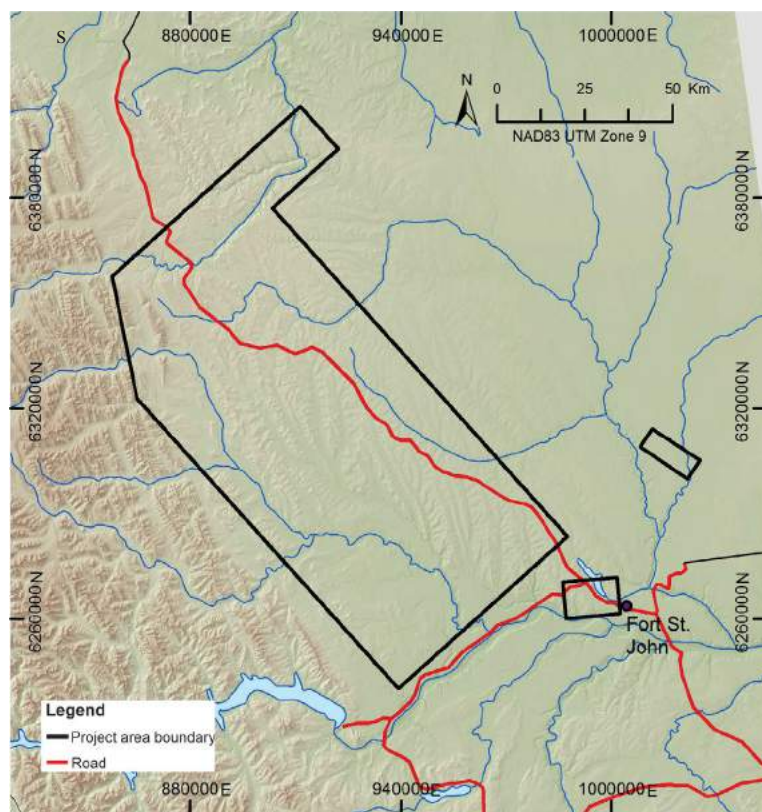
The AEM survey involved collecting over 21 000 line-km of data, covering an area of about 8000 km^2 as shown in Figure 1. The depth of interest in the study area was from surface to a 300 m depth. Flight lines were flown with 600 m spacing and tie lines used for levelling the magnetic data flown at a line spacing of 2400 m. The electromagnetic loop was towed at an average height of 58.4 m above terrain and its depths of investigation ranged from <10 m to ap-

proximately 300 m. The airborne system used, SkyTEM312[Fast], collected TDEM and magnetic data with an average speed of 118.8 km/h over the entire survey area. Preliminary data was delivered for quality assurance–quality control purposes every 48 to 72 hours to a third-party consulting firm. At the time of writing this paper, the final data and inversion results were still in the processing stage.

An important component of the airborne survey was communication and outreach with Treaty 8 First Nations and communities within the survey area. Flights were planned and co-ordinated daily to avoid disturbance of First Nation cultural events, farmers and ranchers in the area. Through discussions with the Blueberry River, Doig River and Halfway River First Nations, the original survey area was expanded to include areas of interest over sections of their traditional lands. Additionally, an area around Fort St. John was flown in response to a request from the Peace River Regional District.

Method

SkyTEM is a helicopter-borne TDEM geophysical system designed for hydrogeological, environmental and mineral investigations. The basic concepts of the SkyTEM system are described by Sørensen and Auken (2012). The system is shown in operation in Figure 2.

SkyTEM energizes the ground in dual-moment mode. This patented feature provides shallow imaging concurrently with penetration of the ground for deep imaging. The SkyTEM receiver is null-coupled to eliminate noise from the primary field improving discrimination between subtle changes in resistivity and maximizing depth of penetration. Ancillary data collected includes laser altitude, GPS elevation, and the attitude of both transmitter and EM receivers. All sensors are installed on the rigid carrier frame, which is flown as close as possible to the ground in order to obtain high data accuracy and highest possible resolution. This enables rigorous quantitative interpretation of the EM data and delivery of products within hours of acquisition. The system is lightweight, operator-less and easily configured to operate at a range of base frequencies and delay times to optimize for a range of geological mapping objectives. SkyTEM data is clean and robust enough to process soon after the helicopter lands and simple inversions can be produced within 24 hours of data collection. The SkyTEM312[Fast] system is carried as an external sling load that is independent of the helicopter. The transmitter, mounted on a lightweight aerodynamic frame, is a 12-turn, 341 m^2, eight-sided loop divided

Figure 1: Location of the 2015 airborne electromagnetic survey, Peace Project area, northeastern British Columbia (background data from GeoBC, 2015a–d).

Figure 2: The SkyTEM312^{Fast} system in operation.

into segments for transmitting a low moment (LM) in two turns and a high moment (HM) in 12 turns. The LM transmits approximately 5.9 amperes (A) with a turn-off time of about 18 µs; the HM transmits approximately 120 A and has a turn-off time of about 320 µs. This yields a maximum magnetic moment of approximately 490 000 A·m^2.

Two lasers, placed on the frame, measure the distance to terrain continuously and an inclinometer measures the tilt of the frame. Two differential GPS (DGPS) units are used for positioning and time stamping of the collected data. Power is supplied by a generator placed between the helicopter and the frame. The magnetic sensor is situated in the front boom and records the Earth's magnetic field during the off-times of the electromagnetic HM pulses.

The z-component receiver coil is placed approximately 2 m above the frame in what is practically a null-coupled position relative to the transmitter loop. Measurements are carried out continuously while flying. Every single transient is stored in a binary format, and prestacked. The stack size for LM is 140 transients for a stacklength of 0.333 s and the stack size for HM is 60 transients for a stacklength of 1.0 s. The transients are recorded in time windows. The 19 LM time windows have gate centre times from 4.7 to 1396 µs. The 26 HM windows have gate centre times from 385 to 11 400 µs. The overlap in gate centre times between the LM and HM windows provides continuous information from the very early times of 4.7 µs to the late times of 11 400 µs.

SkyTEM312^{Fast} is aerodynamically engineered to remain straight and level at speeds approaching 150 km/h. This allows a marked increase in heliborne data acquisition rates.

At this speed, over 21 000 line-km of data were collected for the Peace Project in 43 days. This efficiency is due in part to the aerodynamically engineered composite carrier frame, which consists of composite elements with an enhanced material strength. This design improves manoeuvrability of the system and also permits a larger frame area, allowing for increased magnetic moments and depth of investigation (DOI).

Results and Discussion

The collected electromagnetic and magnetic data are presented in Figure 3. The two supplemental areas shown in Figure 1 (in the southeast) have not been included in Figures 3 and 4. The acquisition of laser altimeter data and DGPS data has provided the digital elevation model. The magnetic data has been processed to provide a total magnetic intensity for the entire block. The raw EM data presented below show the different structures revealed by the early LM and late HM gate centre times. The nearly identical signal pattern from the overlapping late LM gate centre times and the early HM gate centre times verifies the unbroken data collection obtained by the SkyTEM dual-moment system.

Based on the raw data presented above, data-inversion was carried out using the laterally constrained inversion (LCI) method developed at Aarhus University, Denmark (Auken et al., 2005). The LCI technique is a relatively new inversion methodology whereby field data are filtered then modelled against a subsurface layer structure that is constrained laterally on a number of chosen model parameters (including layer conductivity and layer thickness). The results of
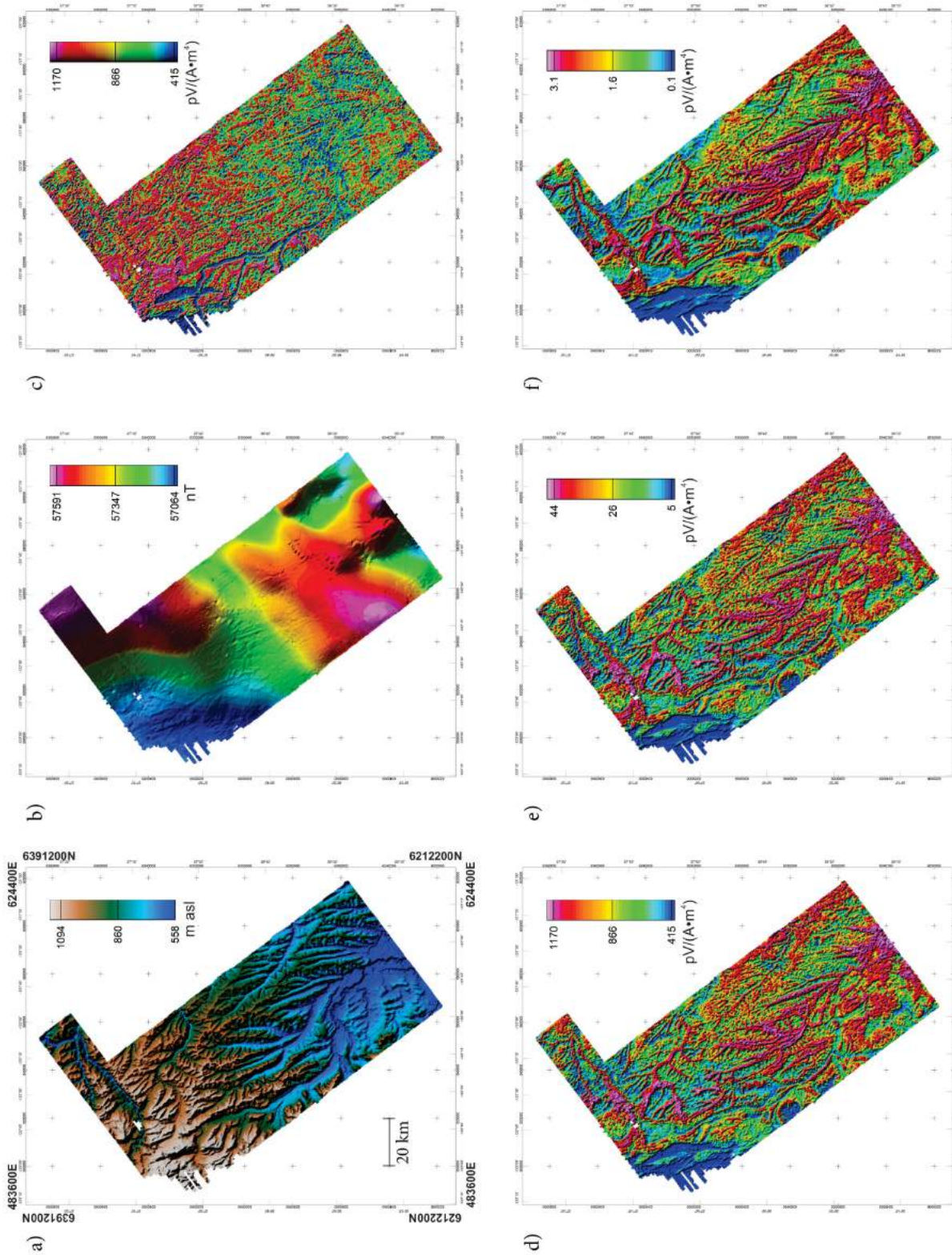
Figure 3: Presentation of gridded survey results from the Peace Project area: **a)** digital elevation model; **b)** total magnetic intensity; **c)** early low-moment raw electromagnetic data; **d)** late low-moment raw electromagnetic data; **e)** early high-moment raw electromagnetic data; and **f)** late high-moment electromagnetic data. Abbreviations: A, ampere; n, nano; p, pico; T, tesla; V, volt.
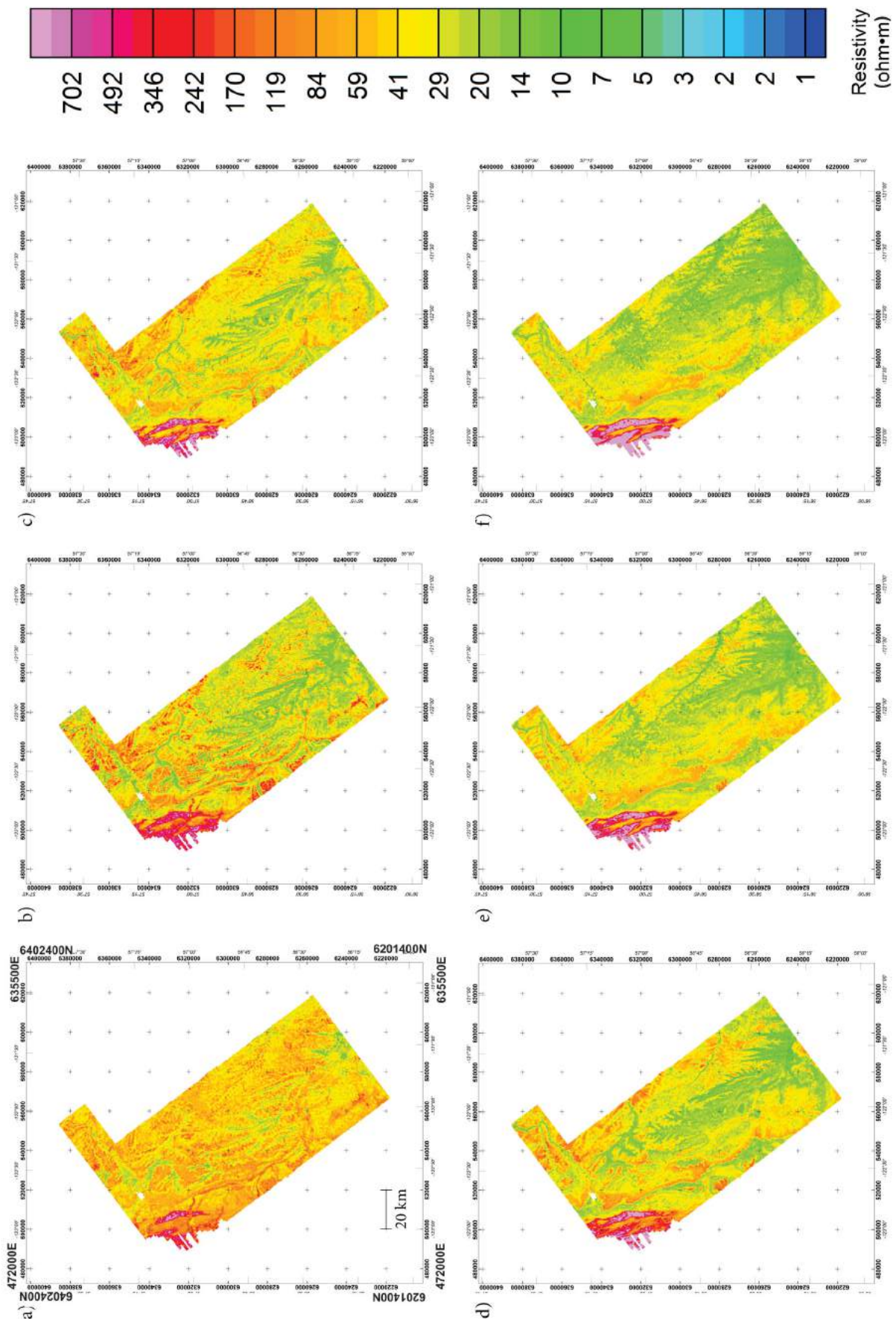
Figure 4: Laterally constrained inversions of survey results from the Peace Project area. Each image, from upper left to lower right, show survey responses at progressively deeper intervals below surface: **a)** 9.7–12.9 m; **b)** 25.4–30.6 m; **c)** 50.7–59.2 m; **d)** 91.8–105.6 m; **e)** 138.6–158.4 m; and **f)** 180.7–205.9 m.

the LCI for the Peace Project area are presented in Figure 4 for six different depth intervals. These depth intervals represent the changes in the resistivity model with depth for the Peace Project area.

The inversion results show very detailed structures in both the near-surface and deeper layers. Higher resistivities in the northwestern corner at all depths correlate with the presence of bedrock. High values of resistivity present in the shallower levels, indicate the presence of coarser material, such as sand, gravel and till, near the surface. The deeper levels are dominated by lower resistivities, which indicate the presence of more clay-rich material, till, water-saturated sediments and/or bedrock shale and siltstone.

Acknowledgments

References

Auken, E., Christiansen, A.V., Jacobsen, B.H., Foged, N. and Sørensen, K.I. (2005): Piecewise 1D laterally constrained inversion of resistivity data; Geophysical Prospecting, v. 53, p. 497–506.

GeoBC (2015a): BC 1:250 000 digital elevation model; BC Ministry of Forests, Lands and Natural Resource Operations, URL <http://catalogue.data.gov.bc.ca/dataset/bc-1-250-000-digital-elevation-model> [December 2015].

GeoBC (2015b): BC major cities points 1:2 000 000 (digital baseline mapping); BC Ministry of Forests, Lands and Natural Resource Operations, URL <http://catalogue.data.gov.bc.ca/dataset/bc-major-cities-points-1-2-000-000-digital-baseline-mapping> [December 2015].

GeoBC (2015c): BC river, lake and wetland polygons 1:2 000 000 (digital baseline mapping); BC Ministry of Forests, Lands and Natural Resource Operations, URL <http://catalogue.data.gov.bc.ca/dataset/bc-river-lake-and-wetland-polygons-1-2-000-000-digital-baseline-mapping> [December 2015].

GeoBC (2015d): BC transport lines 1:2 000 000 (digital baseline mapping); BC Ministry of Forests, Lands and Natural Resource Operations, URL <http://catalogue.data.gov.bc.ca/dataset/bc-transport-lines-1-2-000-000-digital-baseline-mapping> [December 2015].

Hayes, B.J.R., Levson, V., Carey, J. and Mykula, Y. (2016): Interpretation of Quaternary sediments and depth to bedrock, Peace Project area, northeastern British Columbia: project update; in Geoscience BC Summary of Activities 2015, Geoscience BC, Report 2016-1, p. 61–68.

SkyTEM Canada Inc. (2014): Results from a pilot airborne electromagnetic survey, Horn River Basin, British Columbia; Geoscience BC, Geoscience BC Report 2012-4, URL <http://www.geosciencebc.com/s/Report2012-04.asp> [November 2015].

Sørensen, K.I. and Auken, E. (2004): SkyTEM - a new high-resolution helicopter transient electromagnetic system; Exploration Geophysics, v. 35, p. 191–199.

Potential for Natural-Gas Liquid from Western Canadian Shales: Regional Variation in Thermal Maturity and Gas Composition, Northeastern British Columbia

R.M. Bustin, Department of Earth and Ocean Sciences, University of British Columbia, Vancouver, BC, bustin@mail.ubc.ca

A.M.M. Bustin, Department of Earth and Ocean Sciences, University of British Columbia, Vancouver, BC

Introduction

Over the last thirty years a large volume of data has been collected on petroleum source rocks in Western Canada by government laboratories, university researchers and industry. The retained (nonmigrated) hydrocarbons in petroleum source rocks are now being exploited by horizontal drilling and fracturing as unconventional petroleum reservoirs. Much of the data collected for petroleum source-rock evaluation has new relevance for predicting the distribution and producibility of retained hydrocarbons referred to as shale gas and shale oil. As part of this study on predicting the distribution and producibility of liquid-bearing, fine-grained unconventional rocks (shales) in northeastern British Columbia (BC), new, publicly available data on maturity, source-rock properties and production are being compiled, and integrated with EXbase[1] data to map and predict the liquids-production potential of source rocks. The gaps in the datasets are being filled by data from additional sampling and analyses. The maps and related data in turn will be used to achieve the overall research goal of constraining petroleum-system models.

The present study builds on many excellent, previous studies and data compilations on source rocks in the Western Canadian Sedimentary Basin (WCSB) that have been produced to date. It is beyond the scope of this progress report to review all previous work and this task is reserved for a lengthier future contribution; this report only references papers of particular relevance to northeastern BC.

The variation in organic maturation and other source-rock properties in the WCSB occurs at multiple levels of hierarchy. The degree of organic maturation that governs hydrocarbon generation has been shown to occur at three such levels at least, referred to as 1st, 2nd and 3rd order variations by Bustin (1991). First-order variations that encompass the northeastern (Interior Plains) to southwestern (disturbed belt) region show an increase in organic maturity for all strata. This is a reflection of the overall westward thickening of the sedimentary prism, and hence depth of current and paleoburial. Third-order variations are local highs and lows (bull's eyes on maturity maps) thought to be due to faulting (in the disturbed belt), thermal anomalies and, in some areas, likely a lack of control. The most important and well-established 2nd order variations in maturity occur in the Peace River Arch of northeastern BC and adjacent parts of Alberta. In this area, it was documented early on (Karst and White, 1980) that there is a reversal in thermal maturity (coal rank) from the southwesterly trends of increasing maturity (1st order variation in maturity) to one of southwesterly decreasing maturity in northeastern BC and adjacent parts of Alberta. The importance of the reversal to oil exploration is that part of the WCSB succession in the deformed belt of northeastern BC is within the oil window rather than being overmature with respect to the oil window, and thus is prospective for liquid-hydrocarbon exploration.

This progress report presents updated mapping of the regional variation in organic maturity in northeastern BC and adjacent parts of Alberta. The maps are used to establish the spatial distribution of the oil window for specific horizons and to provide some initial results on the distribution of produced gas in the Montney Formation.

Methods

Publicly available data together with new information from analyses of cuttings and core samples taken from 125 wells in northeastern BC and adjacent parts of Alberta are used in this study. These samples were tested for maturation and typical source analysis by a combination of organic petrology and Rock-Eval–type pyrolyses. Handpicked mud-rock

---

chips were microscopically selected from cuttings samples for Rock-Eval and total organic carbon analyses. To date, about 3000 samples have been analyzed by Rock-Eval–type instruments (Espitalié, 1986), of which about 30% were either too mature and/or had S2 analyzer results that were too low to reliably determine maturity data. Vitrinite reflectance of handpicked coal fragments from cuttings samples was performed using well-established techniques.

To assess the potential effects of drying on vitrinite reflectance and Rock-Eval–type analyses of the cuttings samples (which is done routinely at the government storage facility and wellsite), outcrop samples of low maturation were previously run through the sample dryer used at the BC Ministry of Natural Gas Development sample-storage facility at Charlie Lake. No measurable change in T_{max} or vitrinite reflectance was detected that could be attributed to having dried the samples.

High-quality vitrinite reflectance data is limited to the major coal-bearing intervals of the Albian (Gates and Spirit River formations), as well as the Portlandian and Neocomian (Minnes Group and Nikanassin Formation). Vitrinite reflectance was measured on carbonaceous Mesozoic strata throughout the study area, and although these data are used to support the maturity data derived from T_{max}, neither their quality nor their quantity are sufficient for them to be considered separately. The T_{max} data used for preparation of the maps and cross-sections are based on trends from a series of sample analyses from specific wells (rather than single samples), since there can be considerable variation from sample to sample. Such variability is considered to reflect the compounded problems caused by cavings (since mainly cuttings were used), possible organic contamination from drilling fluids, variable kerogen types and instrumental variance.

Regional Trends in Maturity

The maturation data of surface exposures (Figure 1) for all analyzed horizons is generally consistent with northeastward-dipping isomaturity surfaces from the Interior Plains to the edge of the deformed belt, which mimics the current regional structure. Within the southwestern part of the study area, in the deformed belt, the isomaturity surfaces reverse and dip to the southwest and, where adequate data are available to allow validation, reverse once again to dip to the northeast. Superimposed on these regional trends are local highs and lows in maturity that define more complex patterns. Example isomaturity maps are presented here for select horizons only: Portlandian and Neocomian strata and the Upper Jurassic Gordondale Member (formerly the informal Nordegg member) of the Fernie Formation.

The maturation trends of Albian (not shown) as well as Portlandian and Neocomian strata (Figure 2) are similar, with the exception that the older strata have somewhat
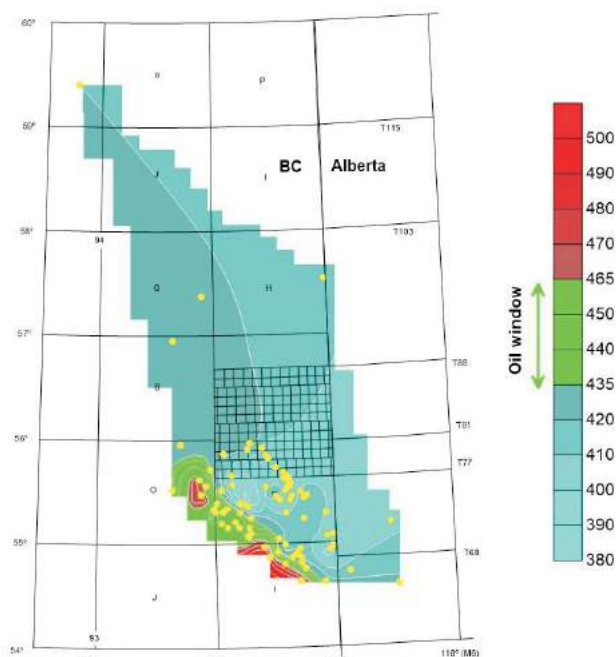

Figure 1. Isomaturity map of surface exposures, mainly in the northeastern British Columbia portion of the Western Canada Sedimentary Basin. Only the area up to the edge of the deformed belt is shown.

higher reflectance values (thermal maturity). Overall, on a regional scale, isoreflectance lines for both sequences parallel structural contours, which in turn parallel the northwest trend of the deformed belt. From northeast to southwest, maturation increases to maximum values at the eastern edge of the deformed belt, then decreases and, where adequate data exist to allow validation (for example in NTS 093P and 093O), increases once again. To the north-
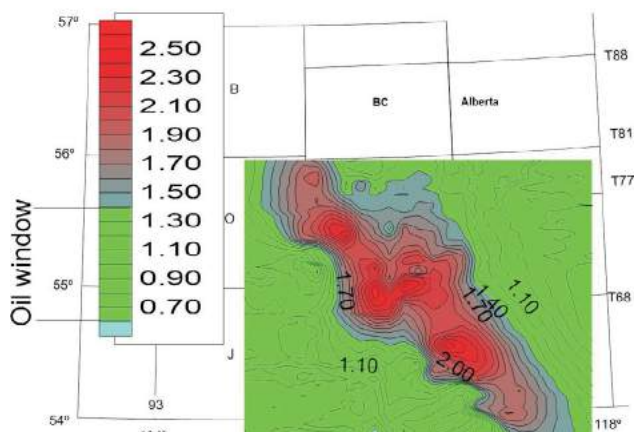
Figure 2. Isomaturity map for Portlandian and Neocomian strata in northeastern British Columbia. Contours are in % Ro_{max} from vitrinite reflectance.
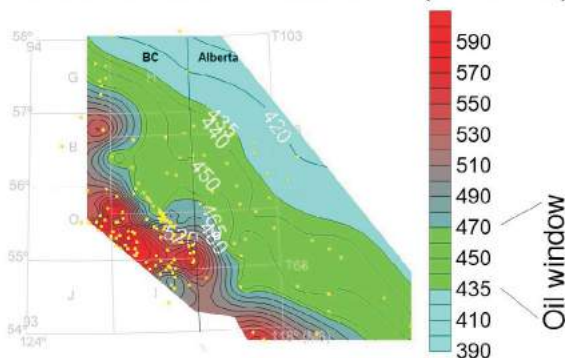
west, maturation also decreases but not as markedly as the trends noted in the southwest. Superimposed on these regional trends are low-maturation lows and highs that form 'bull's eyes' on the isomaturation maps.

Regional trends in maturation for the Lower Jurassic Gordondale Member of the Fernie Formation (Figure 3) and other intervals (not shown) were based on T_{max} values from Rock-Eval–type analyses and corroborated by reflectance data collected from adjacent carbonaceous strata. In general, the maturation trends for both the Gordondale Member and Shaftesbury Formation (not shown) mimic those of the Albian as well as the Portlandian and Neocomian strata: isomaturation lines parallel structural contours, as well as the edge of the deformed belt, and the maturity initially increases toward the southwest, then declines. The trend is similar for the Gordondale Member. However, where data are available to allow validation, a second increase in maturity is evident.

Spatial Distribution of the Oil Window

Based on the combination of vitrinite reflectance and T_{max} data, the depth to the top (Ro = 1.35%; T_{max} 465°C) and base (Ro = 0.65%; T_{max} 435°C) of the oil window, as well as the thickness of strata within the oil window, have been mapped throughout the study area (Figure 4a, b, c). The depth to both the top and base of the oil window decreases to the southwest from the Interior Plains, toward the eastern edge of the deformed belt, and then increases in the deformed belt. This trend mimics the patterns shown on isomaturation maps of selected horizons outlined above. In the southeastern and northwestern parts of the study area, the top of the oil window occurs at depths ranging up to 1400 m (subsea), whereas to the southwest, the top of the oil window is missing (projected to be greater than 2600 m above sea level). The base of the oil window occurs at depths ranging up to 3500 m (subsea) in the southeastern part of the study area, is eroded in the southwestern part of the study area (projected to depth, thus about 1500 m above

a) Depth to top of oil window (subsea)
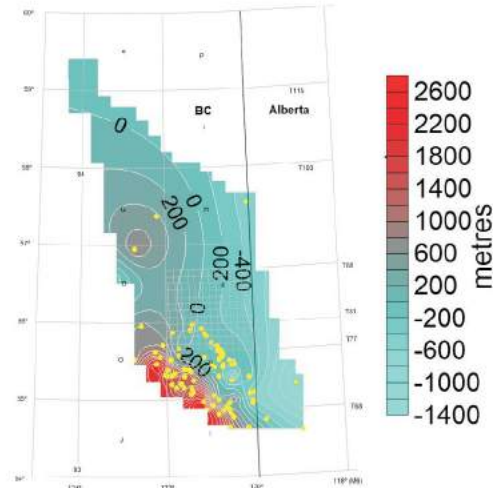
b) Depth to base of oil window (subsea)
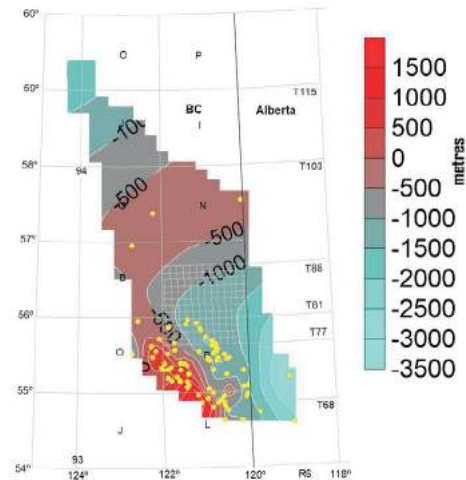
c) Thickness of strata in oil window

Figure 4. Regional maps, showing **a)** depth (subsea) to the top of the oil window; **b)** depth to the base of the oil window; **c)** thickness for strata within the oil window in northeastern British Columbia. These maps are based on the assumption that the oil window is invariant with kerogen type. Horizon-specific data needs to include consideration of kerogen type.


Gordondale Member Maturation (Tmax °C)

Figure 3. Isomaturity map for the Gordondale Member, in northeastern British Columbia, based on T_{max} °C data and corroborated by some vitrinite-reflectance data.
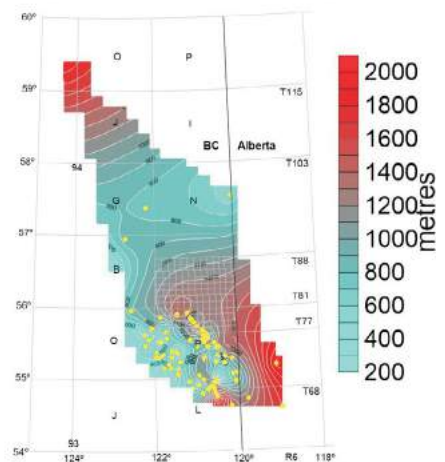
sea level), and initially decreases and then increases in depth toward the northwest. The thickness of strata within the oil window varies from 200 to >2000 m (Figure 4), with the thickest strata occurring in the southeastern and northwestern parts of the study area.

Montney Formation

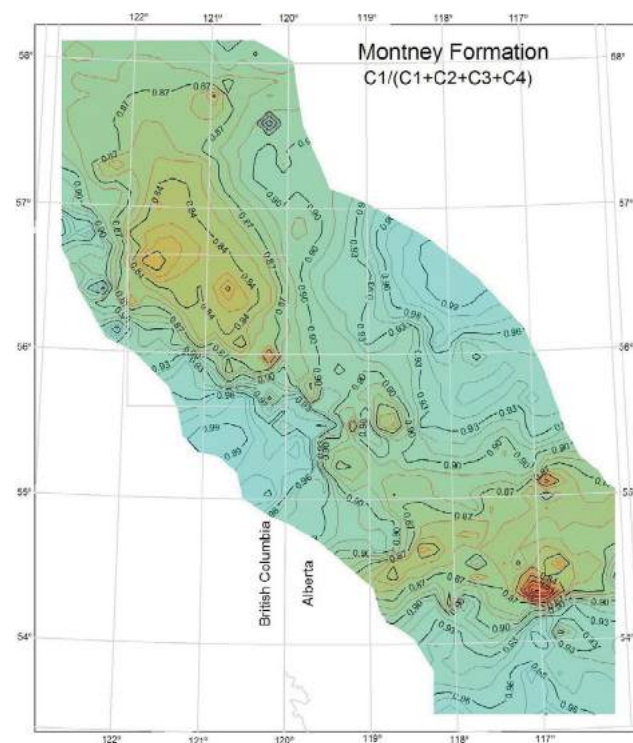As a result of the economic importance of the Montney Formation, a large number of wells cored in the formation have been tested over the last decade. Based on the integration of new data from this work, the thermal maturity of the Montney Formation is shown in Figure 5. Overall, maturity increases with depth of burial, but there is substantial variation that is at least partly attributable to varying paleogeothermal gradients, as determined from maturation gradients of individual wells (Bustin, 1991, 1999). The wetness of produced gas, as calculated from production tests (publicly available data), is mapped in Figure 6. On a regional scale, the degree of correlation between the variation in wetness and thermal maturity is as anticipated, with wetness initially increasing from northeast to southwest into the oil window and then decreasing at higher levels of maturity. The variation in hydrogen-sulphide content in produced Montney gas does not correlate with thermal maturity, depth of burial, or gas wetness and therefore requires further investigation.

Figure 6. Gas wetness calculated using C1/(C1+C2+C3+C4), applied to gas hydrocarbons C1 through C4 (C1, methane; C2, ethane; C3, propane; C4, butane). The values are from analyses of samples collected in producing or tested wells in northeastern British Columbia.

Figure 5. Regional thermal maturity of the Montney Formation, northeastern British Columbia, based on selective T_{max} values from Rock-Eval–type analyses. The lighter green corresponds to the early stage of the oil window and the darker green, to the last stage.
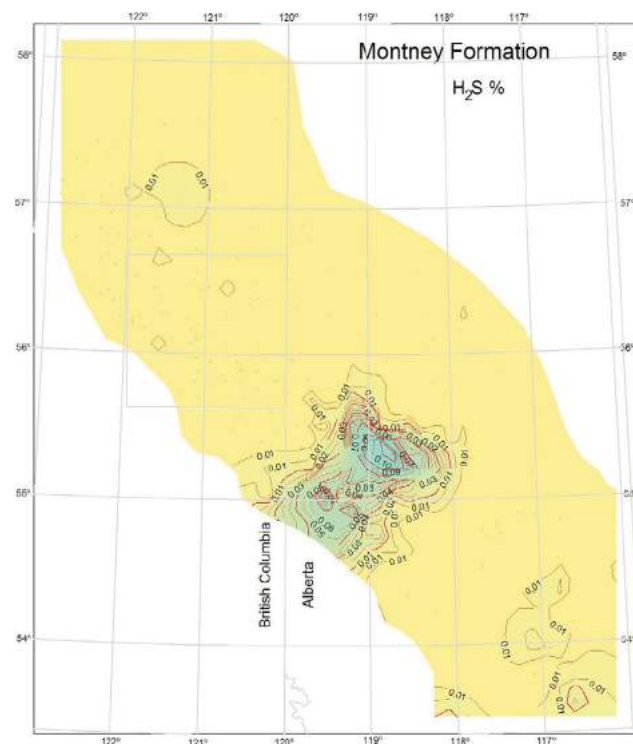
Figure 7. Distribution of hydrogen sulphide in Montney gas from produced or tested wells in northeastern British Columbia.

Summary and Conclusions

As part of this study on the resource potential for natural-gas liquid in northeastern BC, updated regional maps of thermal maturation, source-rock parameters and other relevant data are being produced. This mapping is based on the integration of a vast database of previous work by government, industry and researchers, and is augmented by new publicly available data and laboratory test results. The preliminary maps demonstrate at least three levels of hierarchy in thermal maturity and other parameters.

Acknowledgments

References

Bustin, R. M. (1991): Organic maturity in the western Canada sedimentary basin; International Journal of Coal Geology, v. 19, p. 319–358.

Bustin, R.M. (1999): Organic maturity in the Peace River Arch area of the Western Canada Sedimentary Basin, Northeastern British Columbia; *in* Digging Deeper: Finding a Better Bottom Line, B. Wrathall, G. Johnston, A. Arts, L. Rozs, J.-P. Zonneveld, D. Arcuri and S. McLellan (ed.), Canadian Society of Petroleum Geologists and Petroleum Society of the Canadian Institute of Mining and Metallurgy, 1999 Joint Annual Conference, June 1999, Calgary, Alberta, Canadian Society of Petroleum Geologists, Special Publication 99-12.

Esptialié, J. (1986): Use of Tmax as a maturation index for different types of organic matter. Comparison with vitrinite reflectance; *in* Thermal Modeling in Sedimentary Basins, Exploration Research Conference Proceeedings, Orléans France, Editions Technip, p. 475–496.

Karst, R. and White, G. (1980): Coal rank distribution within the Bluesky-Gething stratigraphic horizon of northeastern British Columbia; *in* Geological Fieldwork 1979, a summary of field activities: Province of British Columbia, Ministry of Energy, Mines and Petroleum Resources Paper 1980-1: p. 103–107.

Apparent Permeability Effective Stress Laws: Misleading Predictions Resulting from Gas Slippage, Northeastern British Columbia

E.A. Letham, University of British Columbia, Vancouver, BC, ealetham@gmail.com

R.M. Bustin, University of British Columbia, Vancouver, BC

Introduction

Northeastern British Columbia hosts a tremendous oil and gas resource trapped in fine-grained, unconventional reservoirs (shale oil and shale gas). To efficiently harness the potential economic benefit this resource represents, basin-scale inventories and distributions of gas and liquid hydrocarbons need to be determined. Equally important to inventories and distributions is petrophysical characterization of the host strata's storage and transport properties, which in large part govern production potential.

Thorough, accurate, petrophysical characterization of shale-oil and shale-gas reservoir rocks has been hampered by lack of suitable equipment and techniques for analyzing heterogeneous, low-permeability, nanoporous rocks. Development of new techniques and refinement of existing techniques, successfully applied to the analysis of conventional reservoir rocks, will yield the capacity to evaluate important petrophysical parameters of fine-grained rocks, and ultimately the ability to predict shale hydrocarbon production potential.

A multifaceted study supported by Geoscience BC and industry partners is underway at the University of British Columbia. The study seeks to better predict the areal distribution of natural gas-liquid–bearing shale in northeastern BC and its production potential. One component of the study is development of better methods for quantifying shale-oil– and shale-gas–matrix flow characteristics. This paper reports some of the progress to date for this particular component of the study. Specifically, the impact of gas slippage on experimentally derived permeability effective stress laws is investigated.

Gas Slippage in Shales

A defining characteristic of shale-oil and shale-gas reservoirs is their fine grain size and therefore smaller pores and pore throats in comparison to conventional hydrocarbon reservoir rocks. Inherent to rocks with smaller pores and pore throats is the increased significance of gas slippage (Klinkenberg, 1941). Gas slippage enhances transport efficiency relative to that predicted by Darcy's law when the mean free path of a gas (average distance a gas molecule travels before colliding with another molecule) approaches the size of the pores and pore throats through which it is flowing. Hence, gas slippage is more pronounced in shale-oil and shale-gas reservoir rocks with nanometre-scale pore systems than in conventional reservoir rocks with larger pores and pore throats.

Mean free path of a gas is controlled by temperature, pressure and the size of the individual gas molecules that comprise the gas. Mean free path is larger (and therefore gas slippage is more pronounced) at higher temperature and/or lower pressure and/or for a gas composed of smaller gas molecules. Typical reservoir pressures in conventional reservoir rocks are high enough and pore throats large enough that gas slippage is unlikely to be of practical significance for reservoir modelling; nowhere in a conventional reservoir is the mean free path of the gas being produced large enough that flow is in the slip-flow regime (Klinkenberg, 1941). Gas slippage, however, can be responsible for significant permeability variation in conventional reservoir rocks in the laboratory, where permeability measurements are often made at lower-than-reservoir pore fluid pressures (for instance a flow-through permeameter with atmospheric pressure on the downstream end of the core). In this case, laboratory measurements need to be 'corrected' for gas slippage (slip-corrected or Klinkenberg-corrected permeability) in order to be used in reservoir models.

Unlike in conventional reservoir rocks, gas slippage can significantly influence permeability in shale-gas reservoirs in situ (e.g., Clarkson et al., 2012). In the near-wellbore region during the later stages of production and pore fluid pressure (pore pressure herein) drawdown, the mean free path of the gas being produced can be large enough that flow takes place in the slip-flow regime. Gas slippage will be most significant in ultratight (nanodarcy permeability) dry gas reservoirs, which have the smallest gas molecules and, characteristically, the smallest pores.

Gas slippage can significantly influence matrix permeability when analyzing shale-oil and shale-gas reservoir rocks in the laboratory. Laboratory measurements of matrix permeability are often made at lower-than-reservoir pore pressure using gaseous probing fluids. Helium, an essentially inert gas, is commonly used as a probing fluid to avoid complications associated with adsorption when using a hydrocarbon gas (e.g., methane) as a probing fluid (Cui et al., 2009). However, helium gas molecules are smaller than any hydrocarbon gas molecules, and therefore will have a larger mean free path at any given temperature and pressure. A larger mean free path results in more gas slippage.

Although it has been recognized in the literature that gas slippage is far more pronounced in shale-oil and shale-gas reservoir rocks than in conventional reservoir rocks, the full extent to which gas slippage influences laboratory matrix permeability measurements has not yet been realized. This paper highlights the fact that gas slippage can have a significant effect on permeability effective stress laws for shale-oil and shale-gas reservoir rocks, even when permeability measurements are made at high pore pressures (>7 megapascals [MPa]), where gas slippage is assumed to be negligible by many researchers.

Impact of Gas Slippage on Experimentally Derived Permeability Effective Stress Laws

An effective stress law is used to predict a rock property that varies with confining pressure and pore pressure. Application of an effective stress law combines confining pressure and pore pressure into a single variable: effective stress. This variable can be used to predict the value of the measured rock property outside the ranges of confining pressures and pore pressures at which the property was measured at in the laboratory (Robin, 1973). For instance, permeability at high confining pressure and pore pressure could be predicted using measurements made at lower pressures.

In its most basic form, effective stress laws can simply be the difference between confining pressure and pore pressure:

$$\sigma'_{eff} = P_C - P_P \qquad (1)$$

where σ'_{eff} is effective stress, P_C is confining pressure and P_P is pore pressure. Slightly more complicated effective stress laws invoke an effective stress law coefficient, α:

$$\sigma'_{eff} = P_C - \alpha P_P \qquad (2)$$

Equations 1 and 2 are examples of linear effective stress laws. Effective stress laws can also be nonlinear, in which case their utility is severely limited, as permeability needs to be measured over the particular pressure range of interest in order to predict permeability within

that range (Robin, 1973). Schematic examples of linear and nonlinear effective stress laws are presented in Figure 1.

Development of an effective stress law assumes that the variation of the rock property being quantified is solely the result of changing pore structure that has resulted from changes in confining pressure and pore pressure. If another process is in part responsible for variation of the rock property, it will be captured quantitatively by the effective stress law, but not theoretically (i.e., the variation is assumed to be controlled by effective stress, some function of confining pressure and pore pressure). The result would be a misleading effective stress law.

Permeability varies with confining pressure and pore pressure because pore structures are not fixed and change in response to varying stress. Increasing confining pressure constricts pores and pore throats, thereby decreasing permeability. Increasing pore pressure has the opposite effect, as increased pressure applied to the pore walls from within the pores expands the pore structure. Permeability effective stress laws are meant to capture the variation in pore structure and therefore permeability resulting from changing confining pressure and pore pressure. If a gaseous probing fluid is used for permeability measurements and the magnitude of permeability variation due to gas slippage is significant in comparison to permeability variation due to stress changes alone, misleading permeability effective stress laws would result. In this case, it would not be possible to use the effective stress law to predict permeability to a liquid or another species of gas with either bigger or smaller gas molecules, or to extrapolate the effective stress law to pore pressure–confining pressure combinations other than
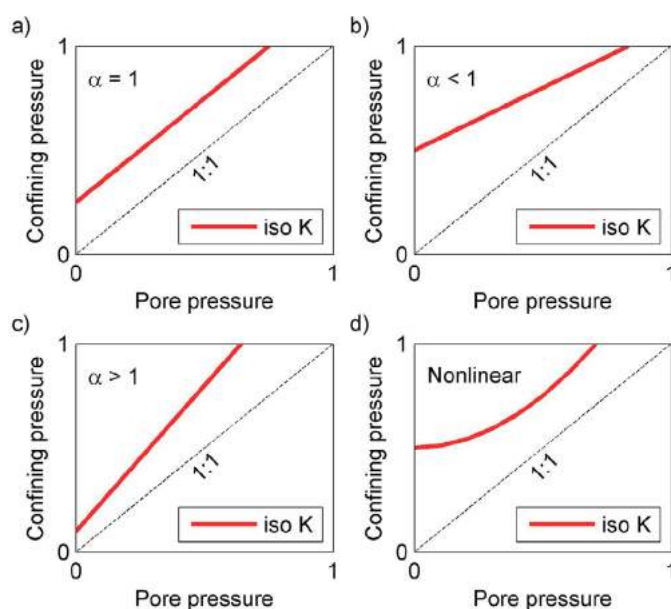
Figure 1. Schematic plots of **a–c)** linear and **d)** nonlinear permeability effective stress laws using permeability contours (iso-K lines) in confining pressure–pore pressure space (modified from E.A. Letham and R.M. Bustin, unpublished paper, 2015).

those measured during development of the effective stress law. Previous studies have been conscious of the misleading impacts gas slippage could have on experimentally derived permeability effective stress laws (Warpinski and Teufel, 1992; Li et al., 2009; Heller et al., 2014), but have assumed that gas slippage is negligible at pore pressures higher than ~7 MPa. To test the validity of this assumption, the permeability of a Montney Formation sample to helium was measured at a wide range of pore pressures and confining pressures, including pore pressures low enough to easily recognize gas slippage.

Experimental Method

Permeability measurements were performed using the pressure pulse decay technique (Brace et al., 1968). Permeability was measured over a confining pressure range of 8.6–65.5 MPa and a pore pressure range of 1.7–17.2 MPa, as per the pressure schedule presented in Figure 2. Permeability measurements at higher confining pressures were not possible with the experimental setup due to limitations of the confining cell, and permeability measurements at higher pore pressures were not possible due to limitations of the permeameter.

Results and Discussion

One of the most characteristic symptoms of gas slippage is the linear relationship between apparent permeability (not Klinkenberg corrected) and inverse pore pressure (Figure 3; E.A. Letham and R.M. Bustin, unpublished data, 2015). Because mean free path decreases linearly with decreasing inverse pore pressure, gas slippage and therefore apparent permeability also decreases linearly with decreasing inverse pore pressure. Permeability data in the present study was first analyzed under the simplest assumption that effective stress was the difference between confining pressure and pore pressure (referred to as simple effective stress herein, Equation 1), and Klinkenberg plots were generated for each simple effective stress (Figure 4). The strong linear
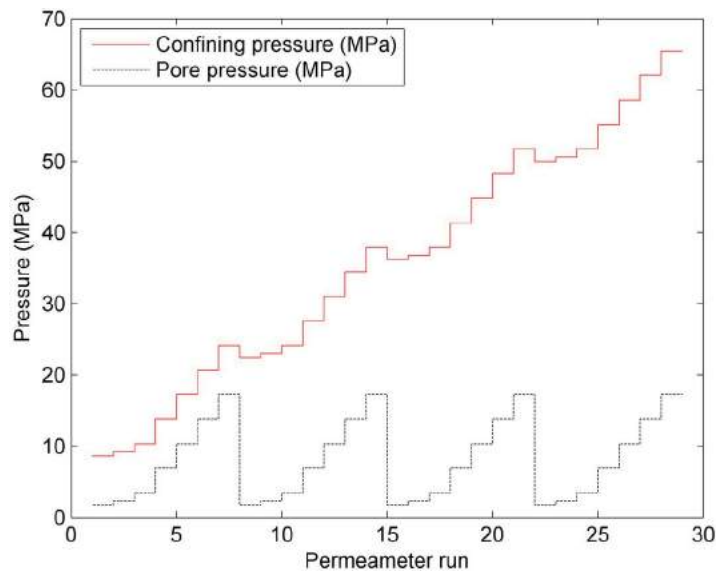
Figure 2. Schedule of confining pressure and pore pressure conditions for permeability measurements (modified from E.A. Letham and R.M. Bustin, unpublished paper, 2015). Abbreviation: MPa, megapascal.
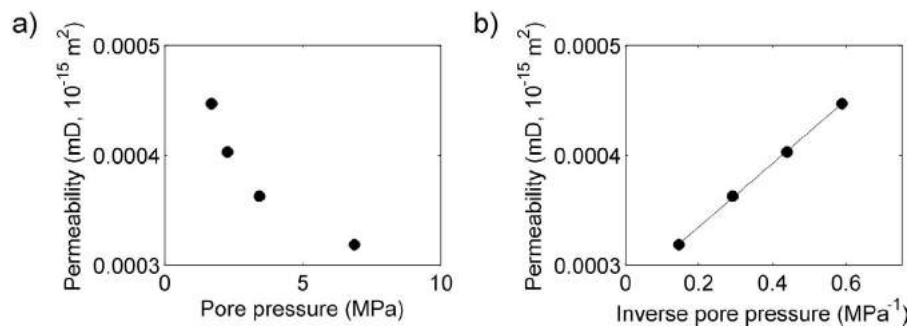
Figure 3. Data for a sample from the Eagle Ford Formation, Texas, U.S. (E.A. Letham and R.M. Bustin, unpublished data, 2015). **a)** Permeability variation with pore pressure. **b)** Klinkenberg plot that shows linear relationship of inverse pore pressure and permeability. The mean free path of the gas varies linearly with the inverse of pressure, which is why permeability varies linearly with inverse pore pressure. Abbreviations: mD, millidarcy; MPa, megapascal.
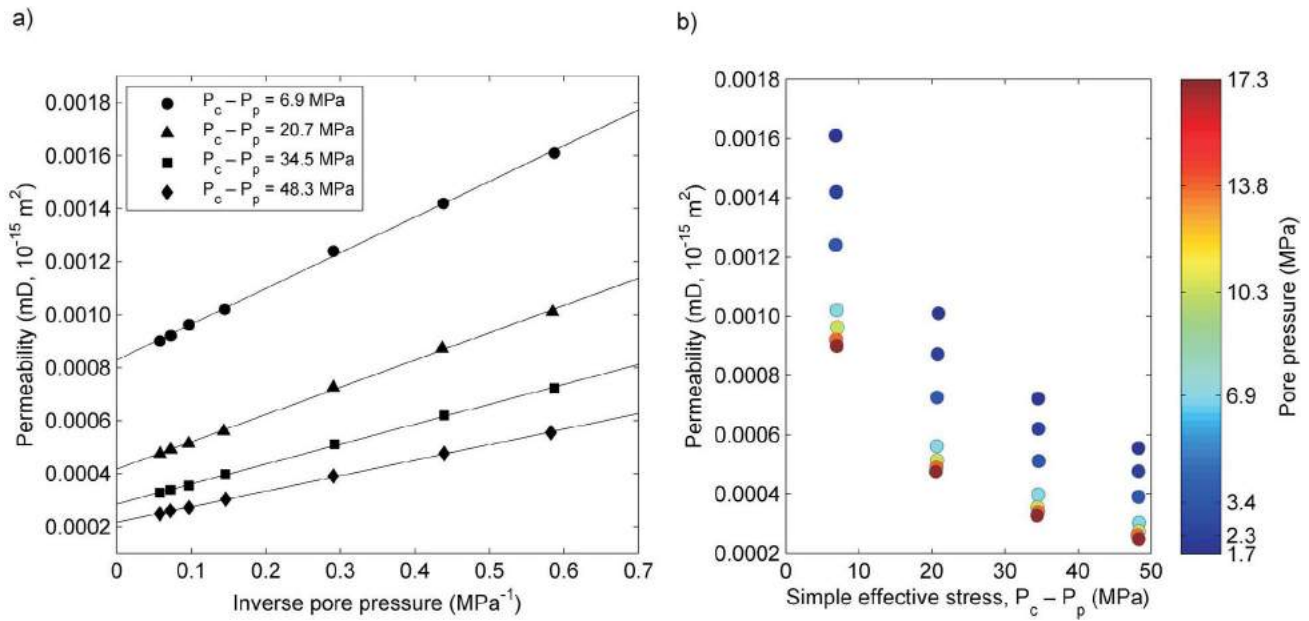
Figure 4. a) Klinkenberg plots for permeability measurements at each simple effective stress. **b)** Permeability variation due to gas slippage at each simple effective stress (modified from E.A. Letham and R.M. Bustin, unpublished paper, 2015). Abbreviations: mD, millidarcy; MPa, megapascal; P_C, confining pressure; P_P, pore pressure.
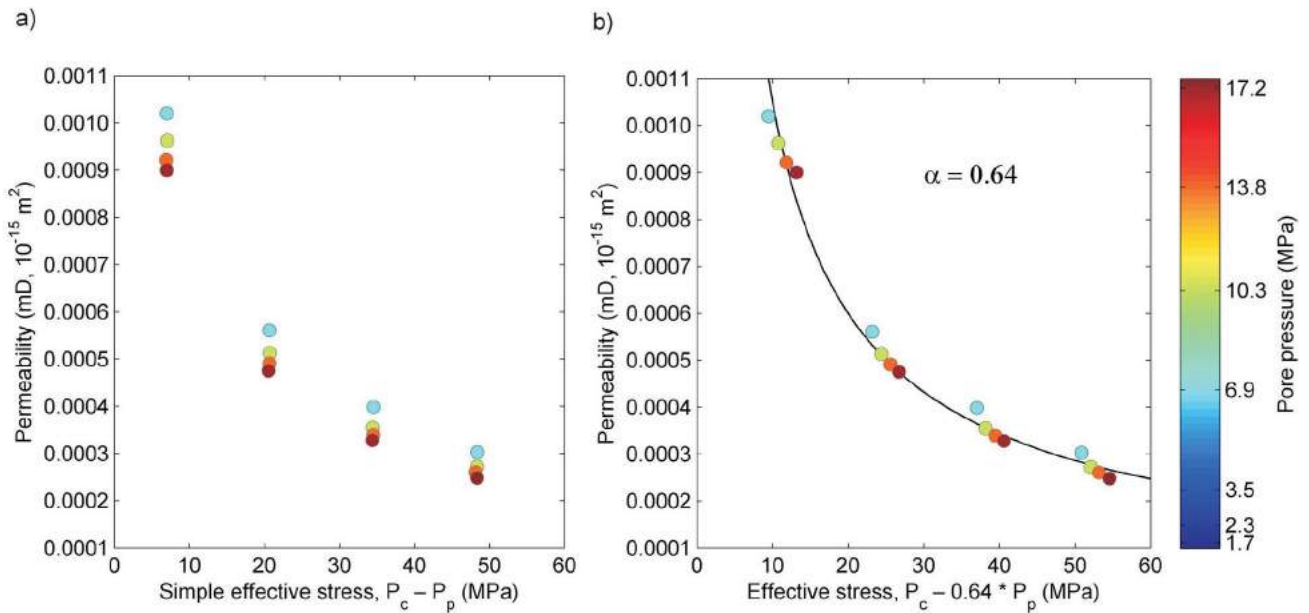
Figure 5. **a)** Permeability variation resulting from gas slippage at individual simple effective stress states for permeability measurements made at pore pressures ≥7 megapascals (MPa). **b)** Apparent permeability effective stress law for data fit to a power function (modified from E.A. Letham and R.M. Bustin, unpublished paper, 2015). Abbreviations: mD, millidarcy; P_C, confining pressure; P_P, pore pressure.

relationships indicate gas slippage is the cause of permeability variation at each simple effective stress. If the assumption was incorrect and pore structure varied significantly at different combinations of confining pressure and pore pressure that equate to the same simple effective stress, then nonlinear Klinkenberg plots would be expected. The simplest form of permeability effective stress law (Equation 1) therefore holds for this particular sample.

Having concluded gas slippage was the cause of permeability variation at each individual simple effective stress, high pore pressure (>7 MPa) data was then analyzed without correcting for gas slippage to determine the impact of gas slippage on what would be the experimentally derived permeability effective stress law (Figure 5). Curve fitting of a power law yielded a permeability effective stress law with

an α value of 0.64 (Figure 5b). This is an apparent permeability effective stress law, as the permeability variation that the fitted curve represents is a combination of both apparent permeability variation due to gas slippage at each single simple effective stress, and permeability variation due to pore structure change when stepping from one simple effective stress to the next. Using the apparent permeability effective stress law to determine input values for reservoir models would hence result in inaccurate production predictions.

Conclusions

Gas slippage was found to significantly impact an experimentally derived permeability effective stress law for a shale-gas sample from the Montney Formation, even when only high pore pressure (>7 megapascals) data was analyzed. The resulting apparent permeability effective stress law would lead to inaccurate matrix permeability estimations and therefore inaccurate production predictions if the matrix permeability estimations were used in a reservoir simulator. The common assumption that gas slippage can be neglected at pore pressures higher than 7 megapascals when determining a permeability effective stress law using a gaseous probing fluid needs to be abandoned for fine-grained rocks and previous studies that utilized this assumption should be thoroughly re-examined.

Acknowledgments

References

Brace, W.F., Walsh, J.B. and Frangos, W.T. (1968): Permeability of granite under high pressure; Journal of Geophysical Research, v. 73, p. 2225–2236, doi:10.1029/JB073i006p02225

Clarkson, C., Nobakht, M., Kaviani, D. and Ertekin, T. (2012): Production analysis of tight-gas and shale-gas reservoirs using the dynamic-slippage concept; Society of Petroleum Engineers Journal, v. 17, p. 230–242.

Cui, X., Bustin, A.M.M. and Bustin, R.M. (2009): Measurements of gas permeability and diffusivity of tight reservoir rocks: different approaches and their applications; Geofluids, v. 9, p. 208–223.

Heller, R., Vermylen, J. and Zoback, M. (2014): Experimental investigation of matrix permeability of gas shales; American Association of Petroleum Geologists, AAPG Bulletin, v. 98, p. 975–995, doi:10.1306/09231313023

Klinkenberg, L.J. (1941): The permeability of porous media to liquids and gases; *in* Drilling and Production Practice, American Petroleum Institute, p. 200–213.

Li, M., Bernabé, Y., Xiao, W.-I., Chen, Z.-Y. and Liu, Z.-Q. (2009): Effective pressure law for permeability of E-bei sandstones; Journal of Geophysical Research, v. 114, B07205, 13 p., doi:10.1029/2009JB006373

Robin, P.Y.F. (1973): Note on effective pressure; Journal of Geophysical Research, v. 78, p. 2434–2437, doi:10.1029/JB078i014p02434

Warpinski, N.R. and Teufel, L.W. (1992): Determination of the effective-stress law for permeability and deformation in low-permeability rocks; SPE Formation Evaluation, v. 7, p. 123–131, doi:10.2118/20572-PA

Interpretation of Quaternary Sediments and Depth to Bedrock, Peace Project Area, Northeastern British Columbia: Project Update

B.J.R. Hayes, Petrel Robertson Consulting Ltd., Calgary, AB, bhayes@petrolrob.com

V. Levson, Quaternary Geosciences Inc., Victoria, BC

J. Carey, Petrel Robertson Consulting Ltd., Calgary, AB

Y. Mykula, Petrel Robertson Consulting Ltd., Calgary, AB

Introduction

Montney Formation tight siltstone reservoirs in northeastern British Columbia are being developed intensively for gas, liquids and oil production using horizontal drilling and multiple hydraulic fracture completions. Drilling and completions operations require substantial volumes of water, which must be obtained while minimizing impacts on other stakeholders, such as First Nations, and agricultural and municipal consumers. As well, costs to source and transport water can be critical components of project economics.

Geoscience BC has worked in partnership with industry, government agencies and local stakeholders to assess available water resources in the BC Montney play fairway; results to date are summarized on the Montney Water Project website (http://www.geosciencebc.com/s/Montney.asp). Even though substantial progress has been made in understanding water resources in deep saline aquifers and in surface water bodies, nonsaline groundwater resources in unconsolidated aquifers and shallow bedrock are not as well known.

The Peace Project has been undertaken to map groundwater resources in an area of more than 8000 km^2 in the Peace Region through the use of airborne geophysics (Figure 1; Brown et al., 2016). Information from the project will serve as a key component of the Northeast Water Strategy, currently under development by the provincial government in partnership with local governments, regulatory bodies, Treaty 8 First Nations, Geoscience BC and industry, by providing knowledge to enable the Northeast Water Strategy's enhanced water monitoring system.

The Peace Project is a collaborative effort involving Geoscience BC, BC Ministry of Forests, Lands and Natural Resource Operations, BC Ministry of Environment, BC Oil and Gas Commission, BC Ministry of Natural Gas Development, Progress Energy Canada Ltd., ConocoPhillips Canada, Northern Development Initiative Trust, and BC Oil and Gas Research and Innovation Society with additional support from the Peace River Regional District and the Canadian Association of Petroleum Producers.

The current report reviews the initial phase of the Peace Project, in which Quaternary sediments and shallow bedrock are assessed and interpreted using existing surficial geology maps and information from petroleum boreholes. Results will be used to calibrate interpretations from the airborne geophysical data to provide the most complete possible assessment of shallow aquifers and the contained groundwater resources.

Project Summary – Initial Phase

Petrel Robertson Consulting Ltd. and Quaternary Geosciences Inc. have undertaken the investigation of Quaternary and other near-surface bedrock formations in the Peace Project area, using cased-hole gamma logs run through surface casings in petroleum boreholes. Properly interpreted, these logs can yield valuable information about the depth to bedrock (and hence thickness of Quaternary cover) and the nature and distribution of Quaternary aquifers and aquitards.

The objective of the initial phase of the project is to generate a map of Quaternary sediment thickness, and to identify potential groundwater aquifers and aquitards in the Quaternary section. The following steps are being undertaken to meet this objective:

1) Compile a digital surficial geology map for the project area from available sources, including the Geological Survey of Canada, BC Geological Survey and the BC Ministry of Environment (Figure 2). The scale of the original source maps varies from 1:20 000 to 1:250 000,
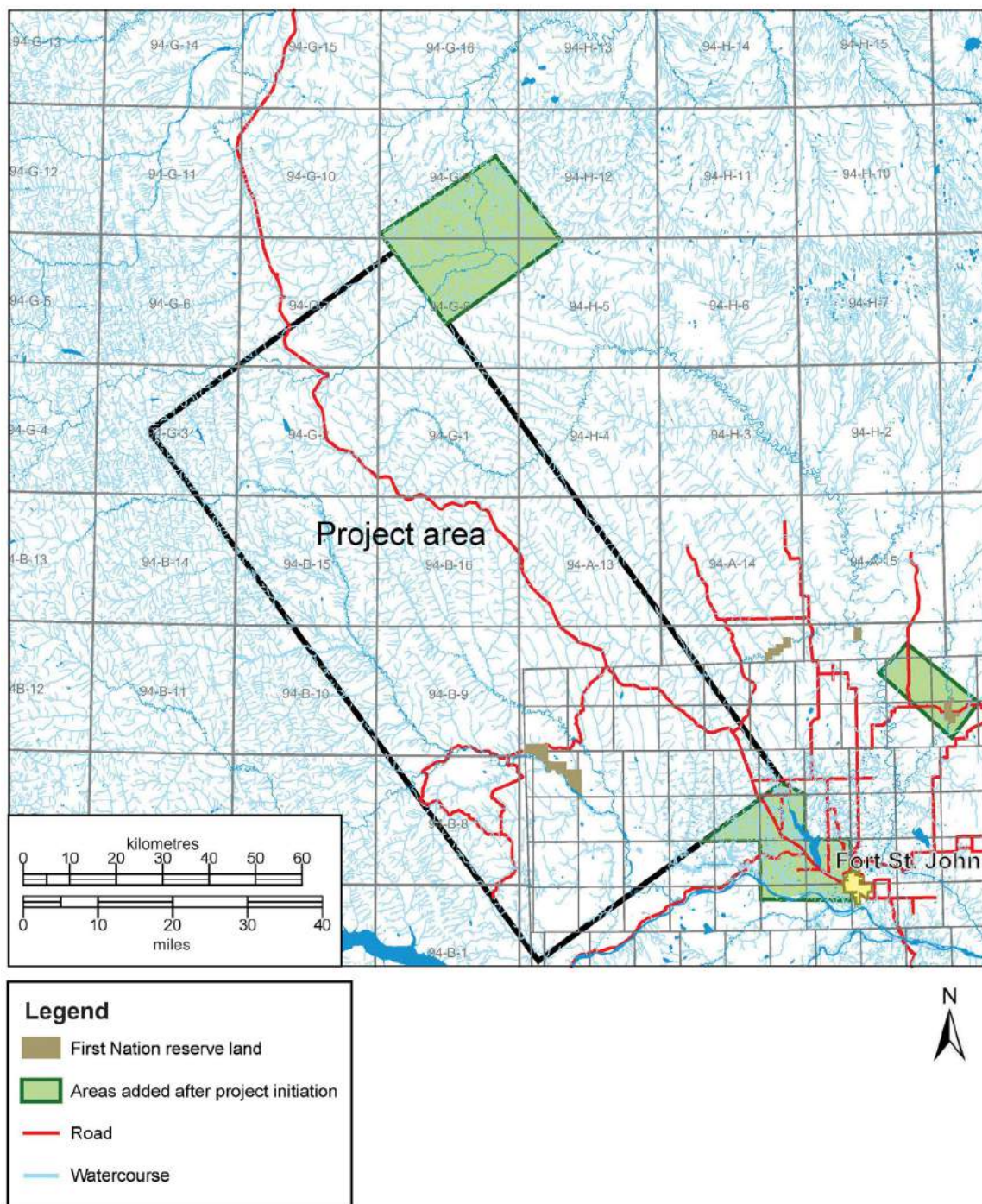
Figure 1. Peace Project area, northeastern British Columbia. Note that supplemental areas were added to the project scope after project initiation.

so units on more detailed maps have been simplified to provide reasonable uniformity. Map boundary issues arise from using a wide range of map scales, and there are varied legends arising from the different purposes of the original mapping. Note that the project area shown in Figure 2 reflects the original Peace Project area, prior to the addition of areas after project initiation (compare to Figure 1).

2) Compile a Quaternary stratigraphy database for the project area, including BC Ministry of Environment water well data and stratigraphic sections described by government and university researchers. Depth-to-bedrock data are extracted for all available sites in the project area. From these datasets, preliminary depth-to-bedrock interpretations have been made. Areas of near-surface bedrock are readily identified from units mapped as till
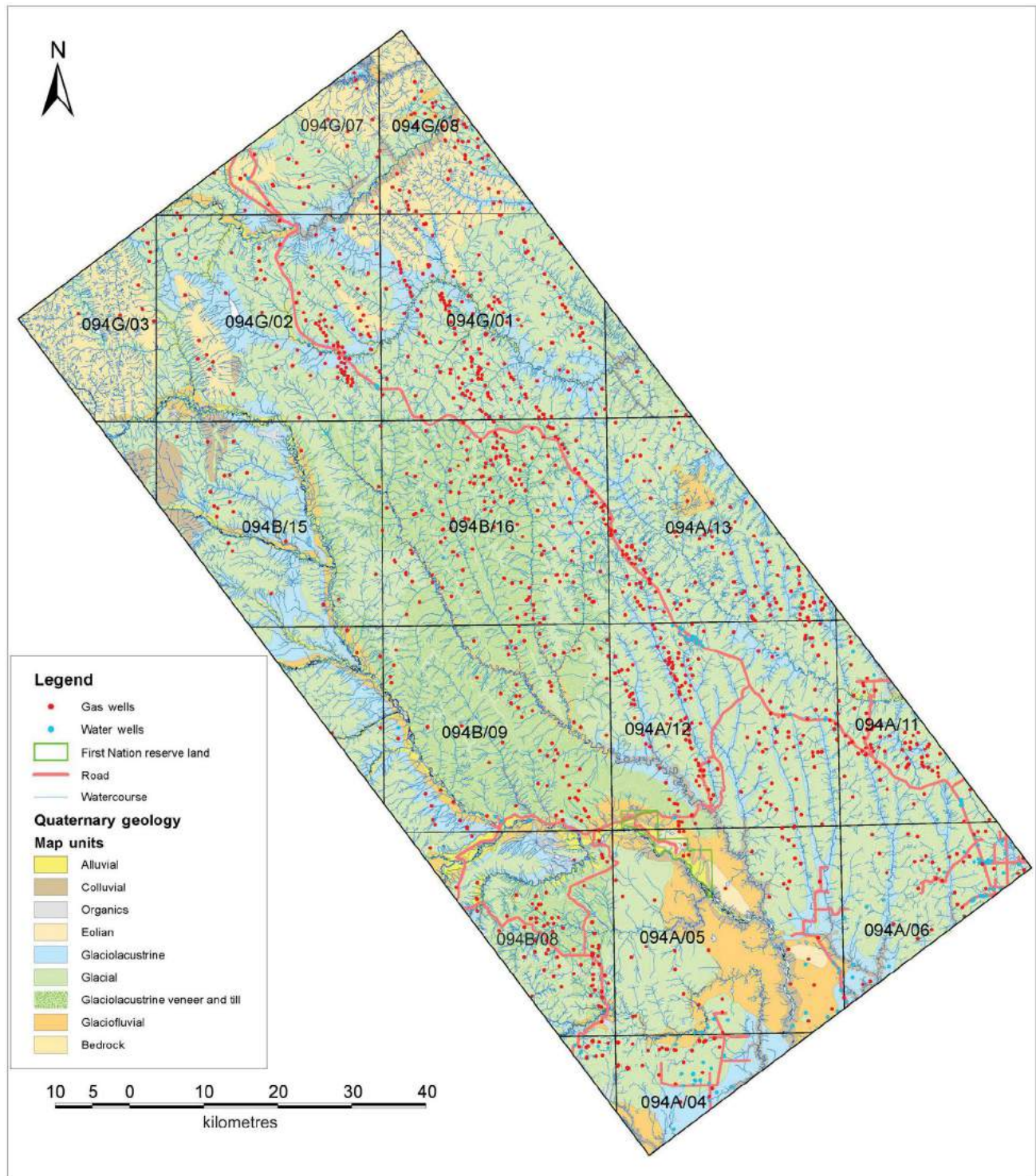
Figure 2. Preliminary surficial geology map, Peace Project area, assembled from existing maps (Lord and Green, 1971, 1986; Lord, 1973, 1977; Green and Lord, 1975; Mathews et al., 1975; Mathews, 1978; BC Ministry of Environment, 1980, 1986, 1987, 1988a, b; Bednarski, 1999, 2000, 2001). Map reflects the original Peace Project area, prior to addition of supplemental areas after project initiation. Surficial geology for the final modified map area will be included in the final project report.
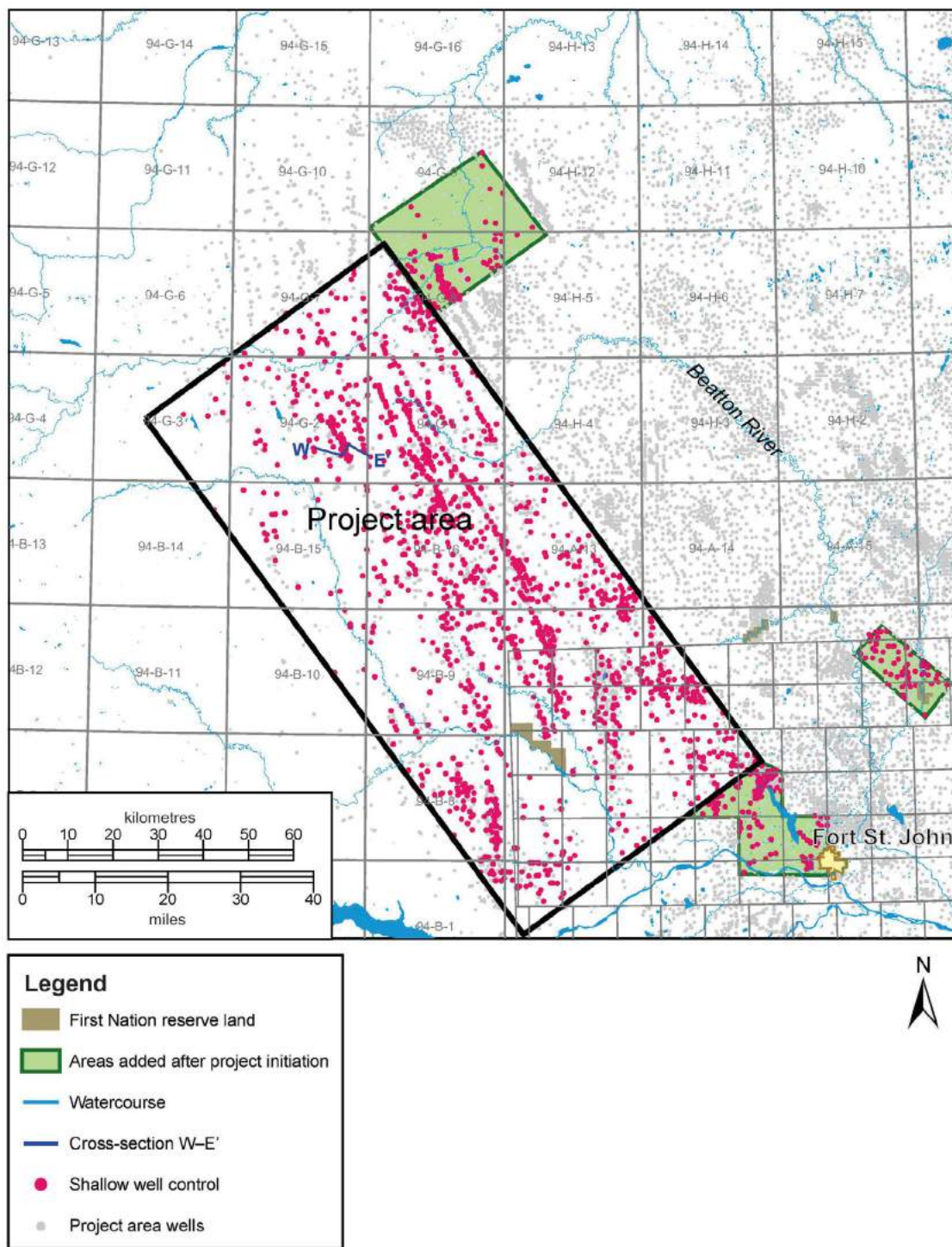
Figure 3. Petroleum borehole wells in Peace Project area. Wells highlighted with red have suitable cased-hole gamma-ray logs and were used in the project. Location of cross-section in Figure 5 is shown.

veneers or as outcrop/subcrop. Approximately 45% of the wells in the study area have been determined, to date, to be in areas of near-surface bedrock.

3) Review all available cased-hole gamma-ray logs from petroleum boreholes in the project area, and select those that have coverage above 50 m true vertical depth

(TVD; Figure 3). A significant number of wells do not have gamma-ray–log data shallower than 50 m depth, and are therefore not usable.

- Particular attention was paid to areas where 3-D seismic data may be available to calibrate mapping. A small number of twinned wells, or wells very close to

wells already selected, were not digitized, as they would add little significant information to the study.

- A final well count of approximately 1300 is anticipated across the entire project area, including the supplemental areas added after project initiation.

- The statistical technique of Quartero et al. (2014) is applied to each cased-hole gamma-ray curve to correct for attenuation effects, thus producing a corrected gamma-ray curve. For each well, the upper portion of the uncorrected open-hole gamma-ray curve is merged with the corrected cased-hole gamma-ray curve to create sufficient stratigraphic coverage to complete stratigraphic correlations in the bedrock section. Results are presented as .pdf images (Figure 4) showing both original and corrected curves, and as final corrected curves in .las format.

4) Interpret each corrected gamma-ray curve to identify the unconsolidated sediment-bedrock contact. This is being done using two techniques:

- from the bottom up, following the bedrock stratigraphy to identify the capping unconformity surface, where the regional succession is truncated; and

- from the top down, identifying the contact by the contrast in gamma-ray log API values between bedrock and the Quaternary section.

5) Interpret aquifer and aquitard intervals within the Quaternary section, and relate them to the available Quaternary geology data compiled for this project.

In most boreholes, the Quaternary section appears to be very thin, and could not be detected despite log coverage as shallow as about 10 m below surface. Stratigraphic cross-section W-E′, near the Beatton River in the northern part of the study area, illustrates the correlation of Cretaceous markers in the Buckinghorse through Dunvegan formations and the top bedrock surface (Figure 5). Note marked incision of the upper Sully Formation shales on well-logs 200/d-077-A 094-G-02/00 and 200/a-096-A 094-G-02/00, whereas identification of the unconformity surface is less definitive on well-log 200/b-086-B 094-G02/00.
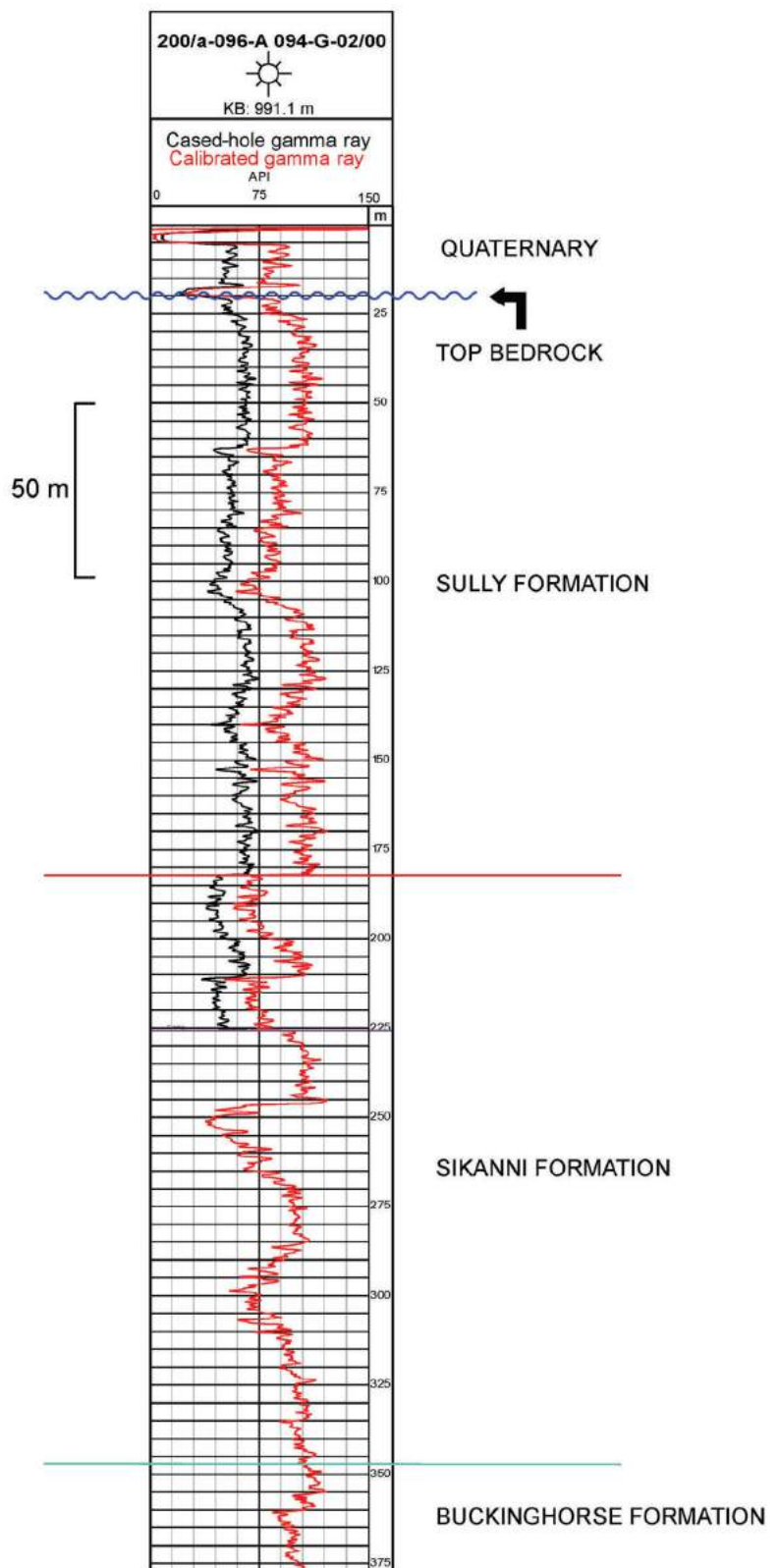
Figure 4. Sample gamma-ray log, well 200/a-096-A 094-G-02/00. Base of surface casing is at drill depth 229 m; the open-hole gamma-ray log is shown below that depth. Above, the cased-hole gamma-ray log is shown in black, whereas the log corrected with the Quartero method (Quartero et al., 2014) is shown in red. Stratigraphic picks can be readily made on the composite red curve. Abbreviation: KB, kelly bushing.
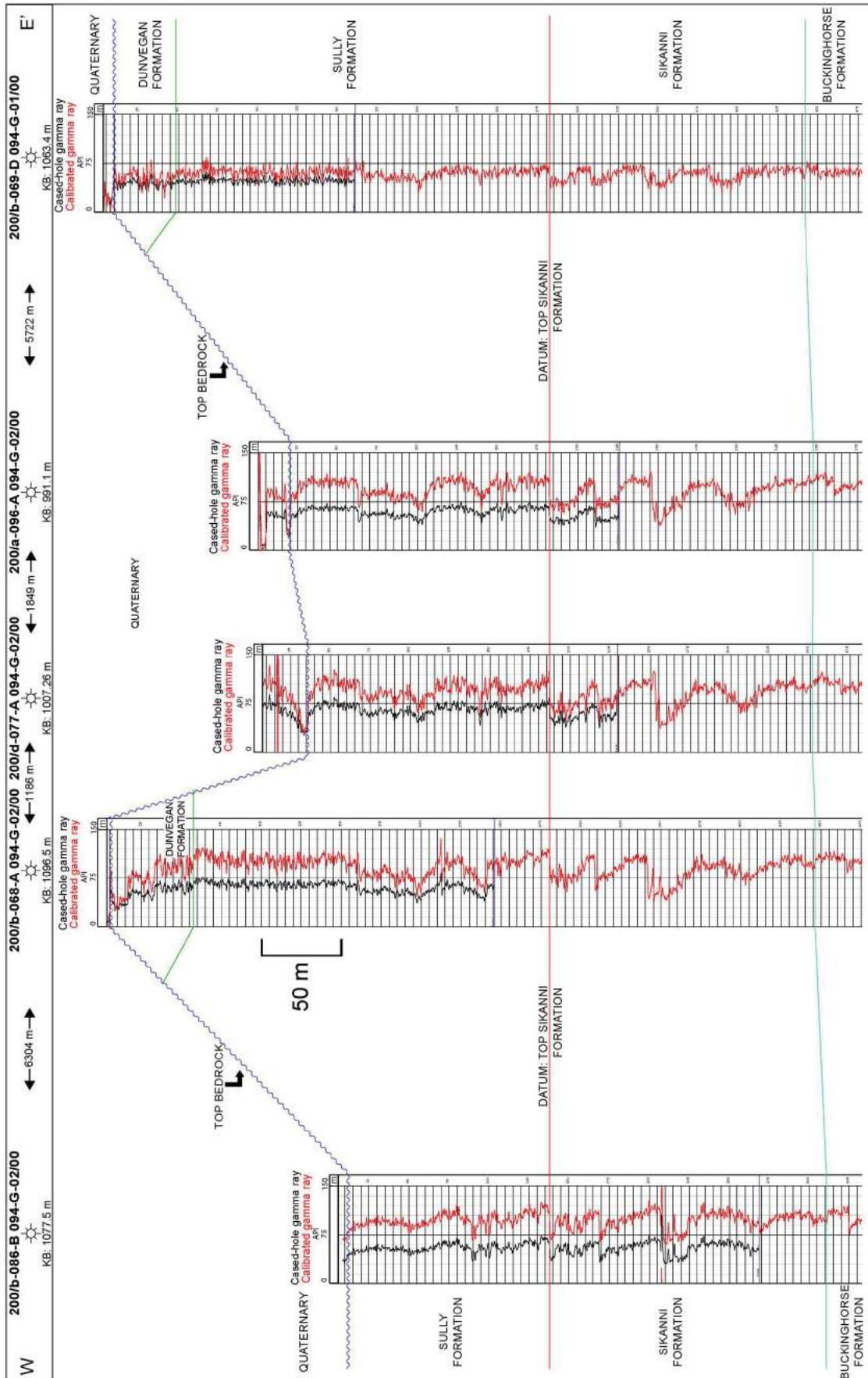
Figure 5. Well-log cross-section, showing erosional relief on the pre-Quaternary unconformity (wavy line). Location of cross-section shown on Figure 3. Abbreviation: KB, kelly bushing.

Next Steps

Completion of the initial phase of the project is scheduled for the end of December 2015, after which comparison and calibration with airborne geophysics results can be undertaken.

Acknowledgments

References

BC Ministry of Environment (1980): Soils and surficial geology, NTS map 94B/NE; BC Ministry of Environment, Terrain Inventory Mapping Project 4421, scale 1:100 000.

BC Ministry of Environment (1986): Soils and landforms (terrain) of the Cypress Creek map area (NTS 94B/15); BC Ministry of Environment, Terrestrial Ecosystem Information Map K15-2750, scale 1:50 000.

BC Ministry of Environment (1987): Soils, Kobes Creek, NTS map 94B/08; BC Ministry of Environment, Terrestrial Ecosystem Information Map K15-2744, scale 1:50 000.

BC Ministry of Environment (1988a): Soils and landforms (terrain) of the Blair Creek map area (NTS 94B/16); BC Ministry of Environment, Terrestrial Ecosystem Information Map K15-2752, scale 1:50 000.

BC Ministry of Environment (1988b): Soils, Dunlevy Creek, NTS map 94B/01; BC Ministry of Environment, Terrestrial Ecosystem Information Map K15-2738, scale 1:50 000.

Bednarski, J.M. (1999): Preliminary report of the Quaternary geology of the Trutch map area, northeastern British Columbia; in Current Research 1999A, Geological Survey of Canada, p. 35–43.

Bednarski, J.M. (2000): Surficial geology, Trutch, British Columbia, (NTS 94G); Geological Survey of Canada, Open File 3885, scale 1:250 000.

Bednarski, J.M., compiler (2001): Drift composition and surficial geology of the Trutch map area (94G), northeastern British Columbia; Geological Survey of Canada, Open File D3815, 1 CD-ROM.

Brown, B., Gisselø, P. and Best, M. (2016): SkyTEM airborne electromagnetic systems for hydrogeological mapping in northeastern British Columbia; in Geoscience BC Summary of Activities 2015, Geoscience BC, Report 2016-1, p. 43–48.

Green, A.J. and Lord, T.M. (1975): Soils of the Nig Creek–Big Arrow Creek map areas, British Columbia; Canada Department of Agriculture, British Columbia Soil Survey Report No. 19, Terrestrial Ecosystem Information maps K15-2778 and K06-2770, scale 1:125 000.

Lord, T.M. (1973): Soils of the Halfway River, British Columbia; Canada Department of Agriculture, British Columbia Soil Survey Report No. 18, Terrestrial Ecosystem Information Map K06-2757, scale 1:125 000.

Lord, T.M. (1977): Soils of the Gold Bar, Dunlevy Creek and Chinaman Lake map areas (94B/SE); Canada Department of Agriculture, Terrestrial Ecosystem Information Map K06-2763, scale 1:100 000.

Lord, T.M. and Green, A.J. (1971): Soils of the Rose Prairie–Blueberry River area of BC (94A/NW); Canada Department of Agriculture, British Columbia Soil Survey Report No. 17, Terrestrial Ecosystem Information Map K06-2718, scale 1:125 000.

Lord, T.M. and Green, A.J. (1986): Soils and landforms of the Fort St. John–Dawson Creek area, British Columbia; Canada Department of Agriculture, British Columbia Soil Survey Report 42, scale 1:125 000.

Mathews, W.H. (1978): Surficial geology, Charlie Lake, Peace River District, British Columbia, (NTS 94A); Geological Survey of Canada, Map 1460A, scale 1:250 000.

Mathews, W.H., Gabrielse, H. and Rutter N.W. (1975): Glacial map, Beatton River (2139), British Columbia; Geological Survey of Canada, Open File 274, scale 1:1 000 000.

Quartero, E.M., Bechtel, D., Leier, A.J. and Bentley, L.R. (2014): Gamma-ray normalization of shallow well-log data with applications to the Paleocene Paskapoo Formation, Alberta; Canadian Journal of Earth Sciences, v. 51, p. 452–465.

Investigating the Potential for Direct-Use Geothermal Resources in British Columbia: A New Geoscience BC Project

C.J. Hickson, Tuya Terra Geo Corp., Burnaby, BC, ttgeo@telus.net

G. Huttrer, Geothermal Management Company Inc., Frisco, CO

T. Kunkel, Tuya Terra Geo Corp., Burnaby, BC

J. Majorowicz, Tuya Terra Geo Corp., Burnaby, BC

R. Yehia, Tuya Terra Geo Corp., Burnaby, BC

J. Lund, Geothermal Management Company Inc., Frisco, CO

K. Raffle, Tuya Terra Geo Corp., Burnaby, BC

M. Moore, Tuya Terra Geo Corp., Burnaby, BC

G. Woodsworth, Tuya Terra Geo Corp., Burnaby, BC

T. Boyd, Geothermal Management Company Inc., Frisco, CO

L. Hjorth, Tuya Terra Geo Corp., Burnaby, BC

INTRODUCTION

Direct-use geothermal resources are an underutilized potential asset in British Columbia. The development hurdles for direct-use applications are significantly lower than for electrical applications, thus there are untapped resources that could be developed. This project will provide the Province of British Columbia (BC) with evaluations of these underutilized resources and will suggest their potential for development. The project will comprise reviews of existing geoscience information for BC and will also work with communities to assess their levels of understanding of direct-use applications. The project will help them identify potential direct-use projects in their regions, as well as ascertain barriers to development. As one of the aids to overcome barriers, the project will create a 'Road Map' for community-development use. Tuya Terra Geo Corp., a BC-based company, and Geothermal Management Company Inc. have combined forces to complete this evaluation and document the results. The project will be carried out over the next six months, with products expected in mid-2016.

Geothermal energy in BC has long been discussed as a potential renewable- (i.e., green) energy source for the prov-

ince. The recent study by Kerr Wood Leidal and GeothermEx (2015) evaluated 18 geothermal sites and provided more detailed information regarding 11 of those sites deemed 'favourable' for electrical generation. They reported that the combined potential for the 11 sites was up to 400 MWe of power. However, the hurdle for economically viable, geothermal, electrical-power–generation development is not just the confirmation of suitable resources, but also the need to identify acceptable financial and economic factors. Electrical generation can have significant long-term payback but it entails very high upfront costs. In addition, the length of time to develop a resource can also be protracted (Figure 1). The exploration required for development of high-enthalpy systems is also complex and costly (Figure 2). In contrast, direct-use applications can typically utilize lower temperature, more easily attainable resources with simpler and lower cost exploration strategies. This study will seek to quantify and evaluate these aspects to determine the potential for direct-use in BC communities from a resource and development-potential perspective.

Using existing compilations of the geothermal resources in BC (e.g., Fairbanks and Faulkner, 1992; Majorowicz and Grasby, 2010a, b; Kerr Wood Leidal and GeothermEx, 2015) and work carried out by university researchers (e.g., Kimball, 2010; Kunkel, 2014), the project will synthesize and organize the known information, along with community input.

Using a community-based participatory approach with a strong First Nations emphasis, the project will seek to engage as many communities as possible. The compelling emphasis put on First Nations participation is important, as many of the communities with direct-use potential are First Nations or have significant First Nations representation. The community-based approach has in the past been successfully carried out with First Nation communities in BC and has the added advantage of building community-research capacity and resource-development awareness. This approach enhances relationship building, and will pave the way for future community engagement and development of identified resources.

In addition to identifying locations with good potential for direct-use applications, the project team will compile an inventory of current and planned direct-use projects as well as provide communities with a 'Road Map' for evaluating their resource as their first step toward development. This toolkit will provide guidance to communities as to how to move forward on direct-use projects, addressing all technical and nontechnical aspects.

The project will not include geothermal heat-pump (sometimes referred to as 'ground-sourced' geothermal) potential, though most communities in BC could take advantage of this shallow subsurface technique used to store and release heat. However, in the community-based methodological approach, geo-exchange–related topics will be included in a questionnaire sent to communities.

Methodology and Project Structure

This project will be divided into three phases as summarized below.

Phase 1

Phase 1 work will identify regions and communities in BC with potential for direct-use geothermal-energy development. As a first step, a compilation of existing BC geoscience datasets useful for the evaluation of direct-use geothermal energy will be completed. This will provide the basis for the identification of a first list of communities and regions with direct-use potential, used in conjunction with the direct-use diagram (Figure 3). This diagram lists numerous possible uses for low- to medium- (70–356°F; 20–180°C) temperature thermal fluids. In parallel with the compilation, a Geothermal Development Decision Matrix (GDDM; Table 1) will be used as outlined below.

This GDDM framework was originally created by Hickson and her exploration team at Magma Energy Corp. (now
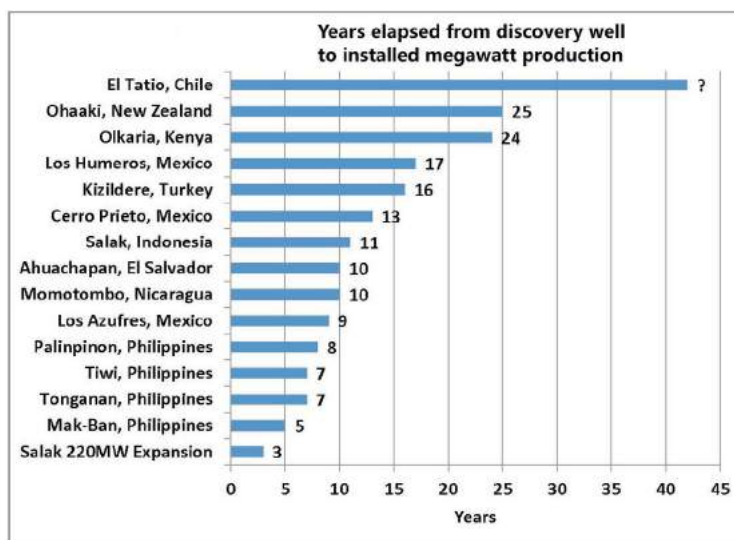
Figure 1. Some of the difficulties faced by developers when dealing with geothermal electrical-generation projects (Sussman and Tucker, 2009). The barriers for direct use are much lower and projects are often completed in less than five years.

Alterra Power Corp.) for use in their global exploration program. It was intended as a way of differentiating between multiple projects in various jurisdictions. Geoscience BC's Geothermal Technical Advisory Committee modified the decision matrix for use in defining the scope of work for its 2014 Request for Proposal on electrical generation.

For the purpose of this study, the matrix will be customized to include more community elements (such as those covered in the 'Traditional use area' in section H) and additional factors related to direct use (section N). Less emphasis will be placed on factors more directly linked to electrical-generation development such as transmission. The project team will then build on the existing geothermal data collected for the 18 locations studied by Kerr Wood Leidal and GeothermEx (2015) for Geoscience BC. These sites are: Canoe Creek–Valemount, Clarke Lake, Clearwater volcanic field, Iskut, Jedney area, King Island, Kootenay, Lakelse Lake, Lower Arrow Lake, Meager Creek/Pebble Creek, Mt. Cayley, Mt. Garibaldi, Silverthrone–Knight Inlet, Nazko Cone, Okanagan, Sloquet Hot Springs, Sphaler Creek and Upper Arrow Lake (Figure 4). The data will be analyzed and compared with the results of earlier studies, such as those by Fairbanks and Faulkner (1992), Pletka and Finn (2009), Kimball (2010), Kunkel (2014), and Woodsworth and Woodsworth (2014).

As the next step, the 11 sites for which detailed economic calculations were completed and additional development information was compiled (Kerr Wood Leidal and GeothermEx, 2015) will be considered as feasible locations for direct-use geothermal-energy development. These sites are Canoe Creek–Valemount, Clarke Lake, Kootenay,
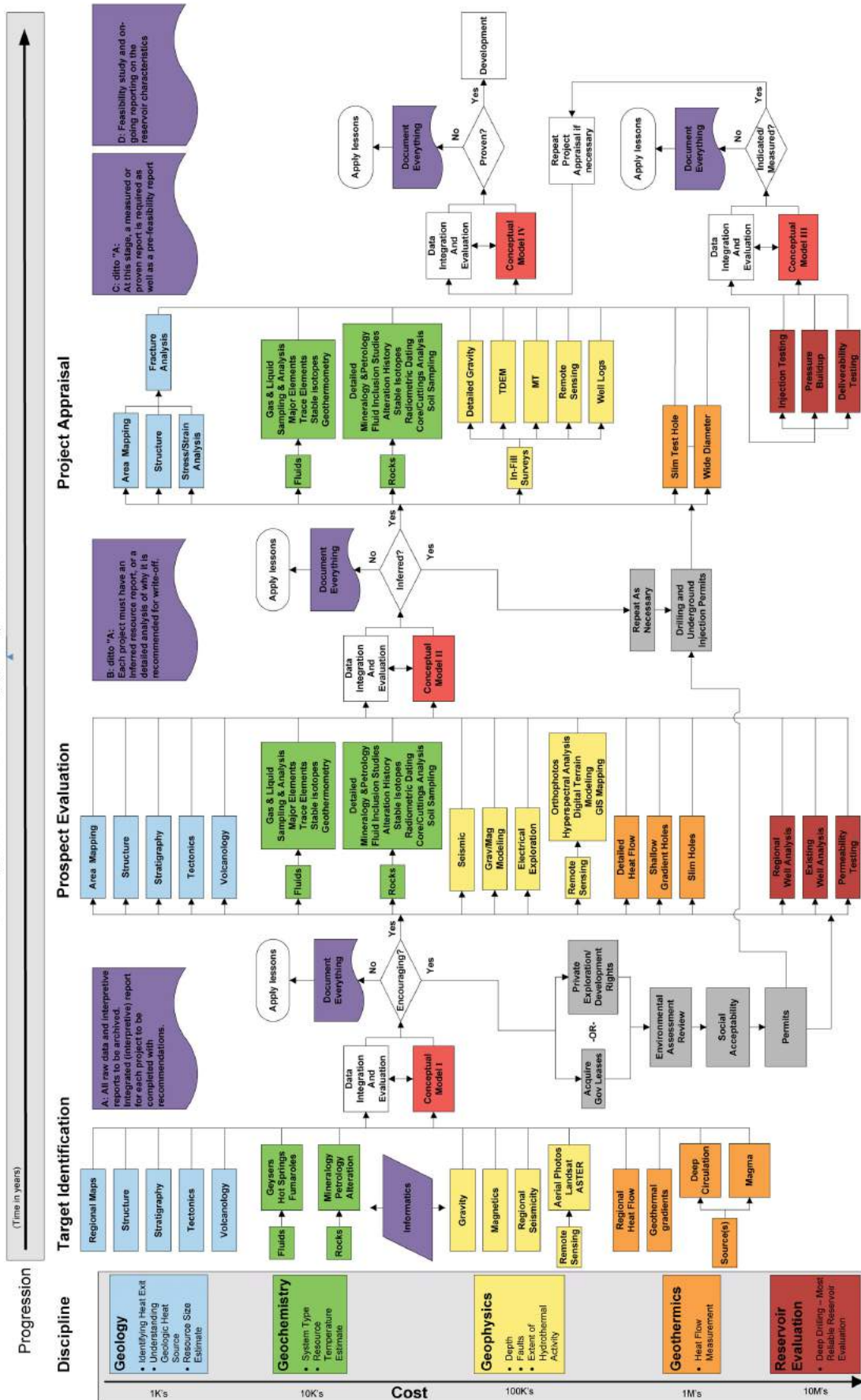
Figure 2. This concept of phased exploration for geothermal resources (Hickson and Yehia, 2014) is applicable to a range of resource temperatures, but the detailed exploration shown here is usually only required for electrical-generation development. Direct use will often be far less complicated and involve far fewer steps. Though technical understanding and parameter quantification are important, a key to economically viable direct-use development is the minimization of 'upfront' costs. The 'Road Map' to accompany the final report will outline the development steps.
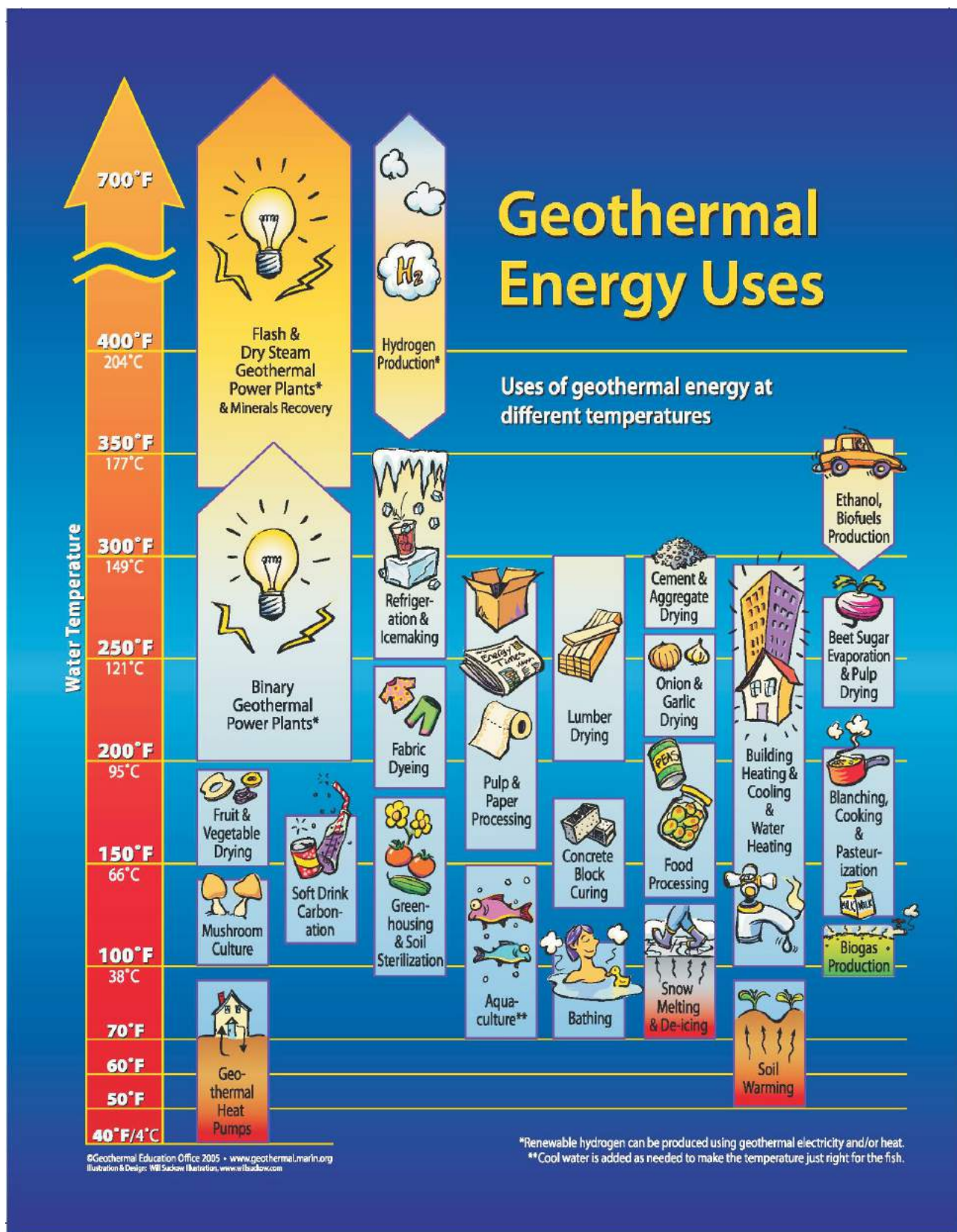
Figure 3. Direct-use diagram of temperature ranges and applications for direct-use geothermal projects (from Geothermal Education Office [2005] and Lund [2010]).

Table 1: Example of a Geothermal Development Decision Matrix (GDDM) to assess development potential. This table and the development-potential index generated were created for prospects having electrical power–generation potential and will be modified for the British Columbia direct-use situation. New information will be gathered where applicable. The weighting factors for direct use have not yet been determined.

|	Area of interest	Numerical favourability index
	Nearest community name	n/a
	Country/state/community	n/a
	Topographic map sheets (name and code)	n/a
	Geological map sheets (name and code)	n/a
A.	**Resource potential**	**Weighting factor**
A.1	General geological setting	TBD
A.2	Size/potential/type	TBD
A.3	Temperature gradient/ Heat flow data	TBD
A.4	Water and gas chemistry	TBD
A.5	Mineral indicators and/or surface alteration	TBD
A.6	Surface thermal features (type, temperature)	TBD
A.7	Surface flow rates and resource recharge	TBD
A.8	3D permeability (heat exchange potential)	TBD
A.9	Recent magmatism	TBD
A.10	Structural setting / seismic / tectonics	TBD
A.11	Geophysics (type and interpretation)	TBD
A.12	Potential resource hostrocks	TBD
A.13	Potential drilling issues	TBD
A.14	Geological setting of thermal features	TBD
B.	**Exploration uncertainty (risk)**	**Weighting factor**
B.1	Degree of identification of resources/reserves	TBD
B.2	Likelihood of covering resource with concession	TBD
B.3	Expected authorization date	TBD
B.4	Specific timing of exploration	TBD
B.5	Previous exploration (can be good or bad)	TBD
B.6	Surface operational capacity	TBD
B.7	Exploration to exploitation (difficult to easy)	TBD
C.	**Environmental issues**	**Weighting factor**
C.1	Protected areas (type and classification)	TBD
C.2	Endangered species	TBD
C.3	Geothermal surface features	TBD
C.4	Other	TBD
D.	**Geothermal area - bidding and/or type of land holding**	**Weighting factor**
D.1	Bidding area	TBD
D.2	Electrical generation potential?	TBD
D.3	Other claim rights(mining and/or oil)	TBD
E.	**Market**	**Weighting factor**
E.1	Potential commodities for direct-use applications	TBD
E.2	Political stability and community relationship to development	TBD
E.3	Time constraints on development	TBD
E.4	Renewal energy 'green value' for potential development	TBD
F.	**Transmission-line infrastructure**	**Weighting factor**
F.1	State of the Infrastructure	TBD
F.2	Transmission route (distance, terrain and costs)	TBD
F.3	Wheeling power	TBD
F.4	Transmission providers	TBD
G.	**Laws governing direct-use renewable energy sources**	**Weighting factor**
G.1	General criteria of the geothermal law	
G.2	General criteria of the water resources law	
G.3	Direct sales possible	
G.4	Carbon credits	
G.5	Lease time and ability to renew or extend exploration licence	
G.6	Conversion from exploration to exploitation	
G.7	Time frame for exploitation licence	

Table 1 (continued)

H.	Community issues	Weighting factor
H.1	Indigenous law and Indigenous development areas	TBD
H.2	Land claims	TBD
H.3	Community action	TBD
H.4	Surface rights	TBD
H.5	Visual considerations	TBD
H.6	Tourism	TBD
H.7	Traditional use area: harvesting	TBD
H.8	Traditional use area: cultural	TBD
H.9	Traditional use area: archeology and other	TBD

I.	Water rights	Weighting factor
I.1	Availability for proposed development	TBD
I.2	Availability for drilling	TBD

J.	Engineering	Weighting factor
J.1	Development proposal and design	TBD
J.2	Construction issues	TBD
J.0	Transportation issues	TBD
J.4	Architectural Issues (design styles)	TBD
J.5	Construction issues (heat exchanger and full injection)	TBD

K.	Non-electrical infrastructure (roads and habitation)	Weighting factor
K.1	Nearest large community > 50 000	TBD
K.2	Nearest community and size	TBD
K.0	Nearest road and condition	TBD
K.4	Current access conditions (restrictions)	TBD
K.5	Terrain and distance factor for road building	TBD

L.	Development finance	Weighting factor
L.1	Development value (greenhouses; tourism; heating)	TBD
L.2	Market price for similar commodities not using direct-use heat	TBD
L.3	Green power premium for commodity?	TBD
L.4	Commodity price	TBD
L.5	Marketing implications	TBD
L.6	Estimated size of resource	TBD
L.7	Are there any green use incentives?	TBD
L.8	Grants	TBD
L.9	Tax holidays	TBD
L.10	Tax relief	TBD
L.11	Loan guarantees	TBD
L.12	Royalties/fees	TBD
L.13	General idea of royalties	TBD
L.14	Private land owner or government land	TBD
L.15	Tax rate in the country	TBD
L.16	Transmission Tariffs	TBD

M.	Maps	Weighting factor
M.1	Regional topographic map of infrastructure (1:500 000?)	n/a
M.2	Regional map land tenure in area (1:500 000?)	n/a
M.3	Regional geological map (1:250 000 or 1:500 000?)	n/a
M.4	Detailed geological maps (1:50 000 or 1:100 000)	n/a

N.	Other issues and considerations	Weighting factor
N.1	Spatial concentration of potential customers	TBD
N.2	Distance to market for prospective commodities	TBD
N.3	Costs to potential customers to receive direct-use benefits	TBD

Abbreviations: n/a, an element that is not evaluated; TBD, to be determined during the course of the project
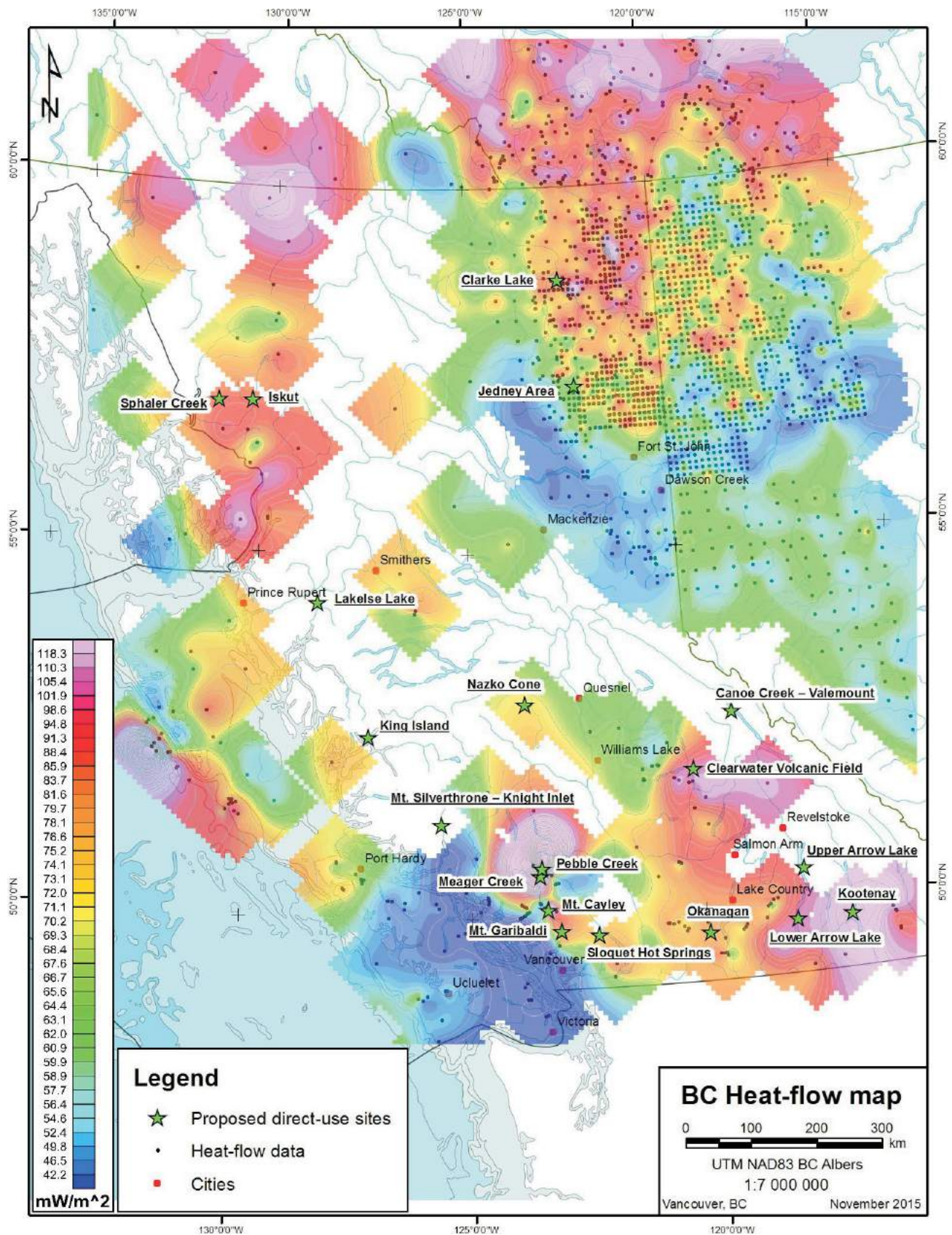
Figure 4: This updated British Columbia heat-flow map uses new data (J. Majorowicz, pers. comm., 2015), as well as results from Lewis (1991) and Majorowicz and Grasby (2010a). It provides a rough guide to regions with potential direct-use resources. Also shown are the 18 sites evaluated by Kerr Wood Leidal and GeothermEx (2015) for electrical generation, which will also be evaluated for direct use.

Lakelse Lake, Lower Arrow Lake, Meager Creek/Pebble Creek, Mt. Cayley, Okanagan, Sloquet Hot Springs, and Jedney (Figure 4). Kerr Wood Leidal and GeothermEx (2015) completed the economic evaluations using the Geothermal Electricity Technology Evaluation Model, a computer modelling system developed by the Office of Energy Efficiency and Renewable Energy (2015); this study will consider additional economic aspects that are suitable for direct-use development (e.g., Beckers et al., 2014).

The compiled GDDM information will then be used to inform and modify the process for the next steps. Following the above process, the remaining seven sites that did not meet the electrical generation–criteria threshold will also be evaluated to see if they might meet more generalized criteria for direct-use applications, using the GDDM (Table 1) and direct-use diagram (Figure 2) as guides.

Additional locations, beyond the initial 18 evaluated for electrical generation, may be identified from available information, as well as any known direct-use projects under development. It is projected that there will likely be another 10–15 sites that might meet the lower temperature threshold necessary for direct-use applications.

Phase 2

Phase 2 will start with a review of the community and technical information gathered for the original 18 sites and any additional sites identified in Phase 1. The direct-use weighting factors for the GDDM (Table 1) will be determined. In the study by Kerr Wood Leidal and GeothermEx (2015), each category (e.g., reservoir potential) was weighted equally and assigned a score by designated experts. The scores to be applied were limited to four: negative one, zero or plus one, as well as a category called 'major barriers', which category was defined as key criteria that eliminated those sites from further consideration.

In this study, the weighting factors will be customized for direct-use development by the designated experts. A priority list will be created comprising the top 10 sites based on the results of the weighting. The factors to be considered include community desire, geothermal potential and economic potential. This aspect of the study is limited to a desktop review of available information, including community input. The Phase 2 processes will be designed to build community-research capacity, and to increase communities' awareness and knowledge of geothermal resources in their region. Questionnaires and information packages will be sent to the communities; this step will then be followed up by telephone interviews with community members. By using inclusionary methods, it is intended that community knowledge of geothermal resources will be increased through the data-gathering and information-dissemination processes.

Phase 3

Phase 3 will entail summarizing and analyzing the community-engagement as well as GDDM results, and completing the geothermal direct-use 'Road Map'. The final report will include conclusions and recommendations regarding the next steps for assisting communities that may wish to move forward with development planning. The 'Road Map' will include, but will not be limited to, information to support such key considerations in the assessment and development of potential direct-use geothermal resources as

- the conduct of ground surface–based activities designed to characterize the resource (geology and geochemistry, possibly some geophysics depending on the cost, location and other circumstances);
- the acquisition of land control;
- the acquisition of all federally, provincially and locally required permits;
- the cost of drilling shallow thermal-gradient holes;
- the cost of drilling either slim hole(s) or production/injection well(s), depending on the amount of money available;
- the testing of wells;
- the design and construction of facilities for beneficial, commercial use and disposal of the produced thermal fluids; and
- the cost of transporting the direct-use product(s) to the potential end user(s).

Conclusions

Through this study, it is anticipated that a great deal more information on geothermal direct-use applications in BC will become available. This information will all be publicly accessible. The updated geoscience and development data, when combined with the geothermal direct-use 'Road Map' and community capacity building, should assist both developers and communities to carry out more cost-effective and timely direct-use geothermal projects.

Acknowledgments

References

Beckers, K.F., Lukawski, M.Z., Anderson, B.J., Moore, M.C. and Tester, J.W. (2014): Levelized costs of electricity and direct-use heat from Enhanced Geothermal Systems; Journal of Renewable and Sustainable Energy, v. 6, no. 1, doi: 10.1063/1.4865575

Fairbank, B.P. and Faulkner, R.L. (1992): Geothermal resources of British Columbia, Geological Survey of Canada, Open File 2526, scale 1:2 000 000.

Geothermal Education Office (2005): Geothermal Energy Uses; Geothermal Education Office, graphic.

Hickson, C.J. and Yehia, R. (2014): The geothermal exploration and development process: graphical representation path to optimal decision making: Geothermal Resources Council, Transactions, v. 38, URL <http://www.geothermal.org/transactions.html> [December 2015].

Kerr Wood Leidal and GeothermEx (2015): An assessment of the economic viability of selected geothermal resources in British Columbia; Geoscience BC, Report 2015-11, 127 p.

Kimball, S. (2010): Favourability map of British Columbia geothermal resources; M.Sc. thesis, University of British Columbia, 175 p.

Kunkel, T. (2014): Aboriginal values, sacred landscapes, and resource development in the Cariboo Chilcotin region of BC; Ph.D. dissertation, University of Northern British Columbia, 296 p.

Lewis, T. J. (1991): Heat flux in the Canadian Cordillera; *in* Neotectonics of North America, Decade Map 1, D. B. Slemmons, E.R. Engdahl, M.D. Zoback and D.D. Blackwell (ed.), Geological Society of America, Boulder, Colorado, p. 445–456.

Lund, J. (2010): Development of direct-use projects; Geo-Heat Center, Oregon Institute of Technology, 7 p.

Majorowicz, J. A. and Grasby, S. (2010a): Heat flow, depth-temperature variations and stored thermal energy for enhanced geothermal systems in Canada; Journal of Geophysical Engineering. v. 7, p. 1–10.

Majorowicz, J. A. and Grasby, S. (2010b): High potential regions for enhanced geothermal systems in Canada; Natural Resources Research, v. 19, no. 3, p. 177–188, doi: 10.1007/s11053-010-9119-8

Office of Energy Efficiency and Renewable Energy (2015): Geothermal Electricity Technology Evaluation Model; Office of Energy Efficiency and Renewable Energy, United States Department of Energy, URL <http://energy.gov/eere/geothermal/geothermal-electricity-technology-evaluation-model> [December 2015].

Sussman, D. and Tucker, R. (2009): Managing the geothermal exploration process with respect to risk and regulations; Geothermal Energy World Conference, Bali, Indonesia, July 22–23, 2009.

Pletka, R. and Finn, J. (2009): Western Renewable Energy Zones, Phase 1: QRA identification technical report; National Renewable Energy Laboratory, Office of Energy Efficiency and Renewable Energy, United States Department of Energy, Subcontract Report NREL/SR-6A2-46877.

Woodsworth, G.J. and Woodsworth, D. (2014): Hot Springs of Western Canada, A Complete Guide; Gordon Soules Book Publishing Ltd., Vancouver, 303 p.

Regional Monitoring of Induced Seismicity in Northeastern British Columbia

A. Babaie Mahani, Geoscience BC, Vancouver, BC, ali.mahani@mahangeo.com

H. Kao, Natural Resources Canada, Geological Survey of Canada-Pacific, Sidney, BC

D. Walker, BC Oil and Gas Commission, Victoria, BC

J. Johnson, BC Oil and Gas Commission, Victoria, BC

C. Salas, Geoscience BC, Vancouver, BC

Introduction

Northeastern British Columbia (NEBC; latitude 55–60°N, longitude 120–125°W) has hosted major hydrocarbon production since the early 1950s (National Energy Board et al., 2013). With the advancement in horizontal drilling and hydraulic fracturing (also known as fracking) in the mid 1990s, unconventional resources of natural gas have been developed within the Montney play and Horn River Basin of NEBC (BC Oil and Gas Commission, 2012b).

The relationship between fluid injection and occurrence of earthquakes has been studied extensively in the past (e.g., Davis and Frohlich, 1993; Ake et al., 2005; Shapiro and Dinske, 2009; Keranen et al., 2014; Dieterich et al., 2015; Hornbach et al., 2015). Injected fluid increases pore fluid pressure and reduces the effective normal stress on a fractured mass of rock. This effect causes shear slip on the preexisting fault planes that are critically stressed (Davies et al., 2013; Holland, 2013). It should be noted that the fluid injected into a well need not travel the entire distance from the injection point to a fault to change the stress condition on the fault plane, as the increased pore pressure can be transmitted to greater distances than the fluid itself (Rubinstein and Babaie Mahani, 2015).

The continuous increase in the number of hydraulic fracturing completions in recent years and the occurrence of new clusters of seismicity have motivated the BC Oil and Gas Commission (BCOGC) to regulate oil and gas operations in NEBC. A fundamental goal of these regulations is to prevent the emergence of seismic hazards from larger magnitude events. Current permit conditions (traffic light system) require the immediate reporting of seismic events that are either felt or recorded with a magnitude of 4.0 and higher. Felt events have initiated deployments of several dense

seismic networks and could lead to suspension of operations (BC Oil and Gas Commission, 2012a, 2014).

To improve the overall understanding of induced seismicity in NEBC, the British Columbia Seismic Research Consortium was initiated in 2012 with funding from Geoscience BC and the Canadian Association of Petroleum Producers and with technical support from Natural Resources Canada (NRCan) and BCOGC. As the first step of this joint effort, eight broadband seismograph stations have been established in NEBC since 2013 to complement the monitoring capability of the Canadian National Seismic Network (CNSN) for induced seismicity (Salas et al., 2013; Salas and Walker, 2014).

The aim of this paper is to evaluate the performance of the regional seismic network in NEBC, which is done by calculating the minimum magnitudes (smallest earthquakes) that can be detected by the network. For each seismic station, the level of background noise (signals due to sources such as traffic, wind, ocean waves), above which earthquake signals (primary [P], secondary [S], surface waves) can be distinguished, was analyzed and used for calculating the magnitude of an event. Then at each station, the peak ground-motion amplitude was simulated from earthquakes with different magnitudes across NEBC. By calculating the ratio of simulated ground motion to the background noise, maps of the minimum magnitudes that can be detected by the regional network were generated. The assessment of minimum detectable magnitude is important for future development of the regional monitoring network in areas with significant shale-gas production.
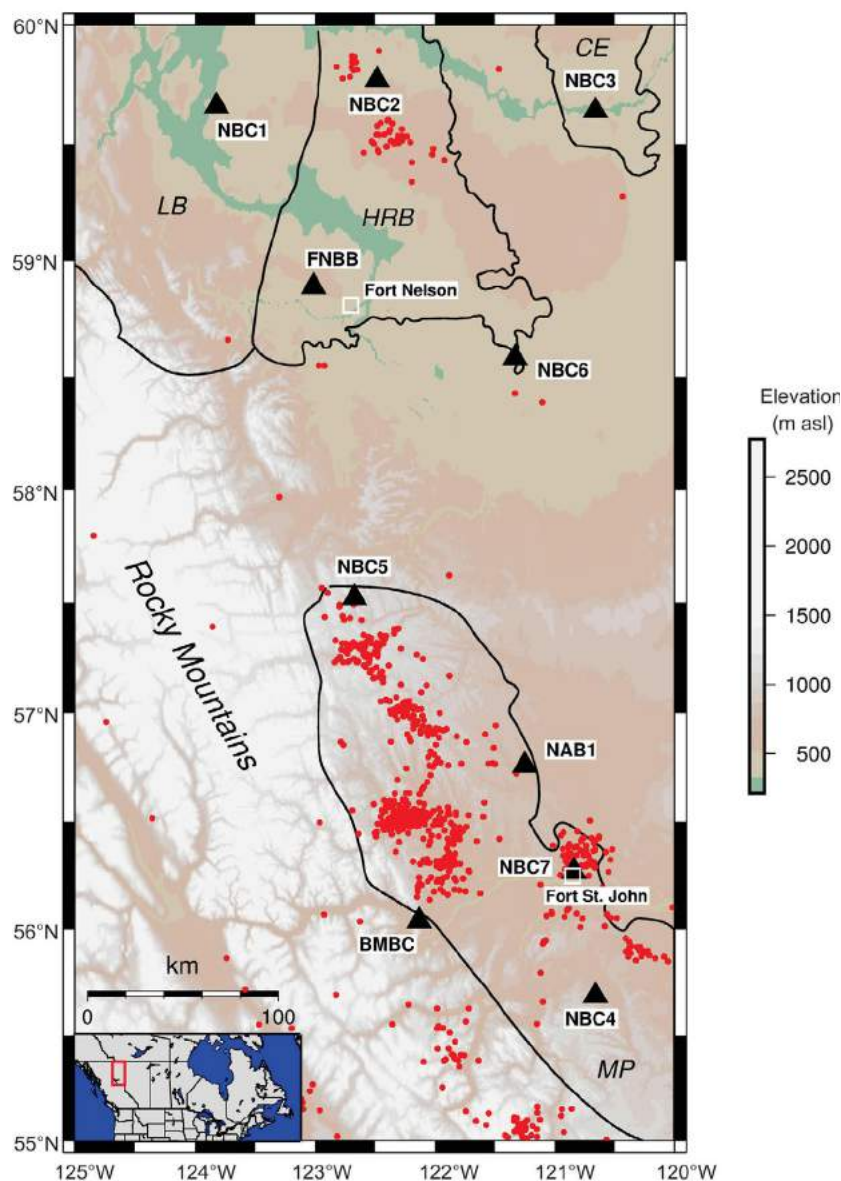
Evaluation Method and Results

Figure 1 shows seismicity in NEBC between 1985 and 2015 from the NRCan earthquake catalogue (Natural Resources Canada, 2015). Also shown on this figure are the locations of regional broadband seismic stations. The two stations BMBC and FNBB have been operating in this region since 1998 and 1999, respectively, whereas stations

Figure 1. Map of seismic events (red dots) in northeastern British Columbia from 1985 to 2015. Black triangles indicate the locations of regional seismic stations in this area. Boundaries of the major shale gas plays are shown with black outlines. Abbreviations: CE, Cordova embayment; HRB, Horn River Basin; LB, Liard Basin; MP, Montney play. The inset shows the location of the study area (red box) on the national map. Background image from Lindquist et al. (2004).

NBC1–6 were established in 2013. Stations NBC7 and NAB1 were installed in 2014. In general, seismicity in NEBC appears to be clustered within specific areas to the east of the Rocky Mountains. These clusters coincide with the location of hydraulic fracturing completions and long-term disposal wells (Horner et al., 1994; BC Oil and Gas Commission, 2012a, 2014; Farahbod et al., 2015). Note that the earthquakes shown in Figure 1 were located using all the available stations in NEBC and environs.

The performance of a seismic network depends on many factors including sensor type, network geometry, instru-mental and ambient noise level, and the condition of data transmission. D'Alessandro et al. (2011a) proposed the method of seismic network evaluation through simulation (SNES) to evaluate the performance of seismic networks. Based on the analysis of ambient noise level at each seismic station, the method simulates the regional distribution of ground motion to estimate variations in the source parameters of a seismic event (epicentre, depth, magnitude) as well as their uncertainties. The SNES method has been used to evaluate a variety of different seismic networks including those in Italy, Greece, Montana, Alaska, Romania and Spain (D'Alessandro et al., 2011a, b, 2012, 2013a, b;

D'Alessandro and Ruppert, 2012; D'Alessandro and Stickney, 2012). In this study, the SNES methodology has been followed to quantitatively evaluate the magnitude detection capability of the regional seismic network in NEBC.

Level of Ambient Noise

Evaluation of the ambient background noise is the first step in the assessment of the performance of a seismic network. It forms the baseline for detection of earthquake phases (P and S) used in magnitude calculations and event location.

There are different sources of noise that can affect seismic signals at different frequencies. Microseisms are ocean-generated noise that can be observed at all stations worldwide, although it is generally less at stations in the interior of continents. The predominant frequency range of microseisms is 0.06–0.25 hertz (Hz). On the other hand, cultural noise due to traffic and machinery has higher frequency content (1–10 Hz), which tends to attenuate quickly with distance and depth (Havskov and Alguacil, 2004).

Conventionally, the noise level is represented by the power spectral density (PSD) of ground acceleration for the frequency range of interest. It is common to represent the units of the PSD (originally in units of $(m/s^2)^2/Hz$) in decibels, which is a logarithmic unit from a ratio of two values. The noise level is therefore converted to decibels (Havskov and Alguacil, 2004) as

$$10 \log [PSD / (m/s^2)^2 / Hz] \qquad (1)$$

To obtain PSD, one year of continuous waveform data (between May 1, 2014 and April 30, 2015) was downloaded from the Data Management Center of the Incorporated Research Institutions for Seismology (Incorporated Research Institutions for Seismology, 2015) for all newly established stations in NEBC (NBC1–7 and NAB1). The waveform data were then cut into one-hour segments. For each segment, PSD of acceleration were calculated using the PQLX software of McNamara and Boaz (2011). Probability density functions (PDF) of each power bin (in decibels, as given by the program) were then obtained at each frequency to better analyze the variation of noise and its probability of occurrence for each station and the three components of motion (two horizontal and one vertical; McNamara and Buland, 2004). Figure 2a shows an example of the noise PDF for the vertical component at station NBC7 in Fort St. John. Also plotted are the global low and high noise models of Peterson (1993) for comparison to the local noise. Since the continuous data was not screened for different types of waveforms, earthquake signals, system transients and instrumental glitches are all included in the calculated PSD. These signals, however, have low probability of occurrence (pink lines) compared to the higher-probability ambient noise (blue portion of the PDF, Figure 2a). For the purpose of this study, the ambient noise level of the ver-

tical component for each station was extracted from their noise PDF, and the results are shown in Figure 2b.

Simulation of Ground Motion

Ground-motion amplitudes were generated for different earthquakes with a range of magnitude (0–4) and epicentral distance (from the earthquake to seismic station; 0–1000 km) values. The simulated values represent the velocity of ground motion in units of m/s (peak ground velocity, PGV). To generate the ground-motion amplitudes, a stochastic approach was followed for simulation of earthquake waveforms. In brief, this approach assumes that earthquake ground motion is a band-limited, finite-duration, white Gaussian noise that can be adjusted by a theoretical model of source (representing the shape and amplitude of the source spectrum), path (representing wave attenuation) and site (representing site amplification) to generate high-frequency motions from an earthquake (Boore, 2003). In this study, the stochastic simulation program SMSIM (Boore, 2003, 2009) was used to produce PGV using input models for western North America (Boore and Thompson, 2012, 2015).

The average level of ambient noise at each station was estimated for the frequency band of 0.5–12 Hz from the vertical components of PSD (Figure 2b). The frequency band of 0.5–12 Hz is used here because it represents the widest detectable frequency band for regional earthquakes (Atkinson and Kraeva, 2010). The PSD were converted from decibel to ground velocity (in m/s) using the conversion methods described in Havskov and Alguacil (2004). Specifically, the relationship between a spectral amplitude at a given frequency to a time domain amplitude in a given frequency band is defined as

$$a = 1.25 a_{RMS} = 1.25 (P(f_2 - f_1))^{1/2} \qquad (2)$$

where a is the true average peak amplitude, a_{RMS} is the root mean squared amplitude, and P is the power spectrum in the frequency range of f_1 to f_2. Here, P has the unit of m/s and is obtained by converting the acceleration PSD in decibels to their equivalent amplitude in m/s^2, then divided by the square of angular frequency. Equation (2) holds true under the assumption that the power spectrum is indeed a constant P if the frequency range of f_1 to f_2 is narrow (Havskov and Alguacil, 2004). For stations BMBC and FNBB the average ambient noise was obtained based on the nearby stations.

## Theoretical Threshold for Locating Earthquakes in NEBC

In this step, a theoretical 100 by 100 grid was generated for the study area. By placing seismic sources of variable magnitudes (0–4 with 0.2 increments) at each grid point, the PGV was estimated at the location of each station using the simulated values as obtained above. For each grid point–

station pair, the ratio of simulated PGV to the average background noise was calculated for all magnitudes. The source signal at any given station was considered identifiable if the signal-to-noise ratio (S/N) exceeded 10. Figure 3a and b show the number of stations with S/N ≥10 when the magni-

tude of the source was 1.6 and 2.6, respectively. For an event to be considered locatable, it is required to have identifiable signals (i.e., S/N ≥10) at four or more stations. In the case of magnitude 1.6, the event can be located only if the source is within the areas that are well covered by the re-
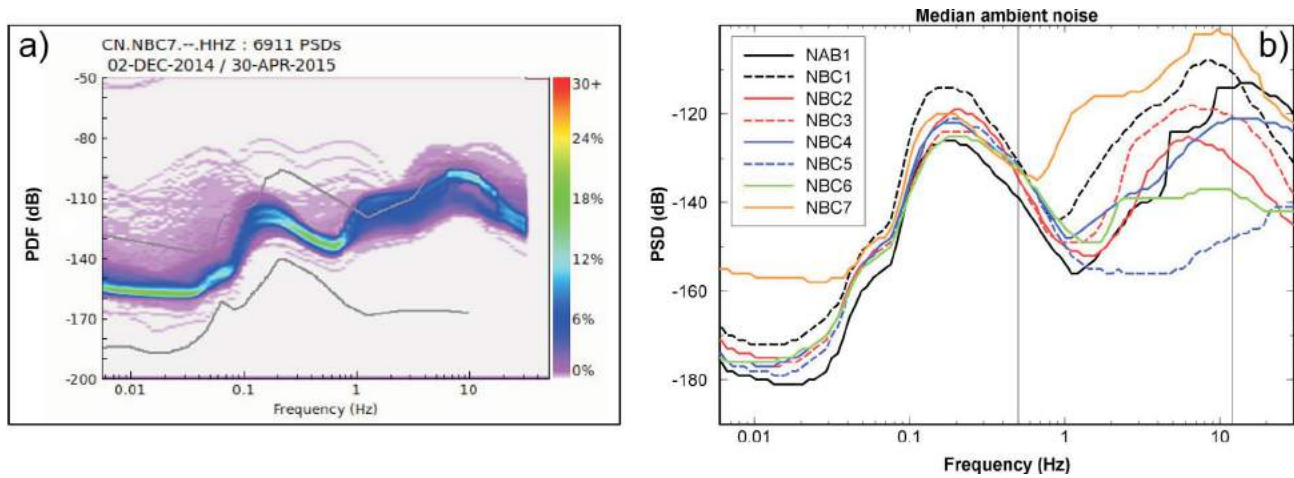
Figure 2. Noise spectra of seismic stations in northeastern British Columbia: **a)** Vertical component of probability density function (PDF) of each acceleration power bin (in decibels [dB]) at station NBC7. The colour bar shows noise probability at each frequency. **b)** Median power spectral density (PSD; vertical component) of all newly established stations (NAB1, NBC1–7) versus frequency. The two vertical lines mark the frequency range used in simulation of ground-motion amplitudes and averaging of the ambient noise. Abbreviation: Hz, hertz.
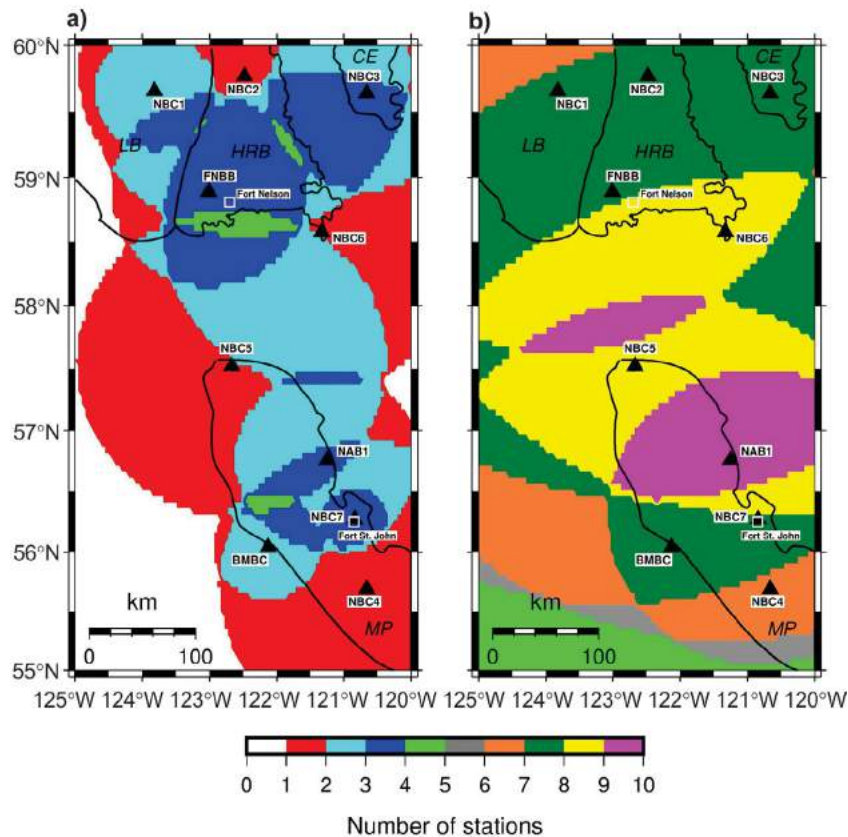
Figure 3. Number of stations with signal-to-noise ratio of ≥10 for **a)** magnitude 1.6 and **b)** magnitude 2.6. Black triangles indicate the locations of regional seismic stations in northeastern British Columbia. Boundaries of the major shale gas plays are shown with black outlines. Abbreviations: CE, Cordova embayment; HRB, Horn River Basin; LB, Liard Basin; MP, Montney play.

gional network. In contrast, a magnitude 2.6 event any-where inside the study area can be detected and located as at least four stations with identifiable signals are available.

Based on the same criterion, the variability of minimum detectable magnitude of regional earthquakes in NEBC was mapped and the results are shown in Figure 4. The minimum detectable magnitude can be considered as the theoretical threshold for any seismic event to be located by the regional seismic network. Overall, the theoretical magnitude threshold for NEBC is below 2.6 and it can be as low as 1.6 for areas of the Montney play and Horn River Basin that are well covered by the regional network.

Future Improvement of the Regional Network

The seismic network in NEBC plays a critical role in detecting and locating seismic events that are potentially linked to hydraulic fracturing or deep injection for the purpose of wastewater disposal. The data of earthquake source parameters (e.g., epicentre, depth, magnitude) obtained from the regional network are used for regulatory purposes. The un-
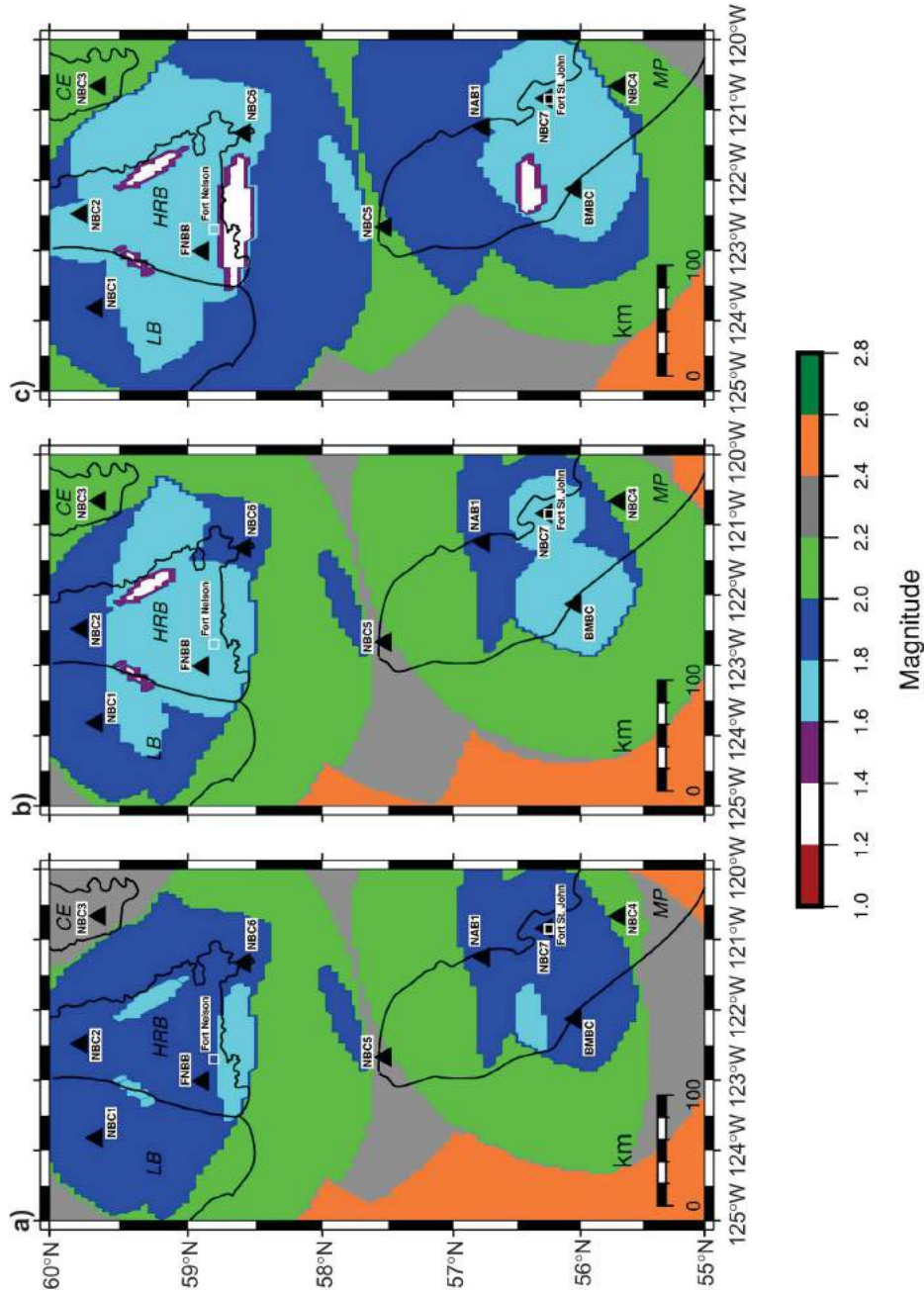

Figure 4. Spatial distribution of the minimum detectable magnitude in northeastern British Columbia based on signal-to-noise ratio of ≥10 at four or more stations. Black triangles indicate the locations of regional seismic stations in this area. Boundaries of the major shale gas plays are shown with black outlines. Abbreviations: CE, Cordova embayment; HRB, Horn River Basin; LB, Liard Basin; MP, Montney play.

certainties in source parameters, however, make hazard mitigation a challenging task. In this section, some options are considered to improve the capability of the current regional seismic network.

The improvement of the regional seismic network in NEBC can be achieved from different approaches in order to reduce the uncertainties in the earthquake parameters. One of the most straightforward ways is to increase the S/N at existing stations such that signals from smaller events can be clearly identified. This is possible by replacing the near-surface sensors with deep borehole ones or by relocating noisy stations to places with better site conditions. Figure 5 shows the hypothetic results if the level of background noise is reduced by 10, 25 and 50%. In comparison to the current network configuration (Figure 4), an overall reduction of noise by 10% (Figure 5a) would lower the detection threshold by ~0.2 magnitude unit for most of the Liard Basin, northeast of the Horn River Basin, southern Montney play, and the area to the west of Montney play. For a 25% noise reduction (Figure 5b), the magnitude detection threshold could be improved to ~2.0 magnitude unit for almost the entire NEBC. The Horn River Basin and central Montney play could have a value down to ~1.6 magnitude. When the noise level is reduced by 50% (Figure 5c), the regional network could detect seismic events with magnitude ≥1.8 for most of NEBC. The area with a magnitude detection threshold of ~1.6 would expand to cover the entire Horn River Basin, most of the Liard Basin and the central Montney play (i.e., the Fort St. John area).

The performance of the regional seismic network in NEBC can also be improved by installing additional stations at critical locations. The exact location of new stations depends on the expected goal of the earthquake monitoring. Given the relatively higher injection activity in the Montney play in recent years, one desirable improvement is to lower the local earthquake detection threshold for more effective monitoring and mitigation of seismic hazard. In Figure 6, the hypothetical scenarios of improvement are presented with up to four additional stations in the Montney play. The area corresponding to the detection threshold of ~1.6 magnitude could expand significantly even with the addition of just one station in the central Montney play (Figure 6a versus Figure 4). Moreover, the addition of this station might help to reduce the azimuthal gap between stations NBC5 and BMBC for events that occurred in the northern and central Montney play. By adding stations to the south and east of station NBC5 in the northern Montney play (Figure 6b, c), the network's monitoring capability could be dramatically improved for the entire Montney play from 1.6–2.2 magnitude to 1.2–1.8 magnitude. The regional network would require four additional stations in the central and northern Montney play to achieve an overall magnitude detection threshold of ~1.2 magnitude (Figure 6d).
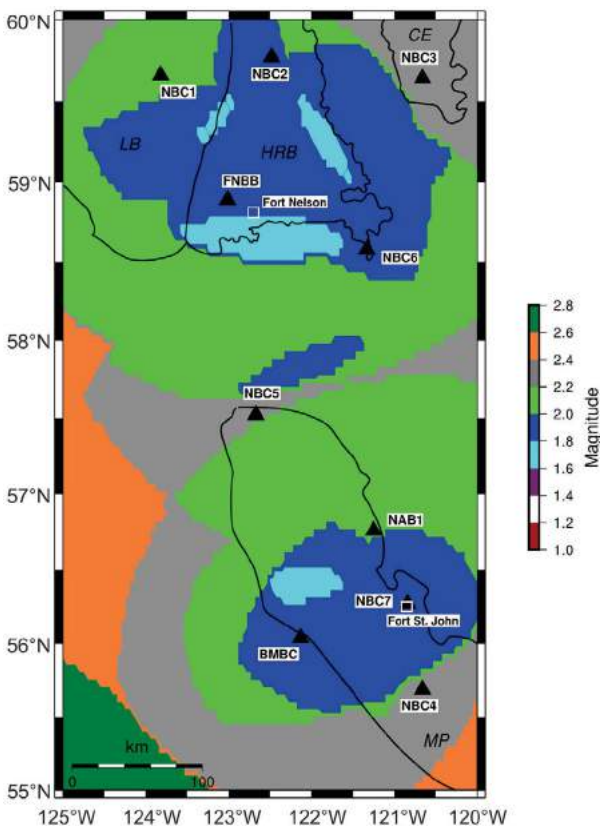
Figure 5. Spatial distribution of minimum detectable magnitude in northeastern British Columbia after reducing the ambient noise levels by **a)** 10%, **b)** 25% and **c)** 50%. Black triangles indicate the locations of regional seismic stations in the area. Boundaries of the major shale gas plays are shown with black outlines. Abbreviations: CE, Cordova embayment; HRB, Horn River Basin; LB, Liard Basin; MP, Montney play.
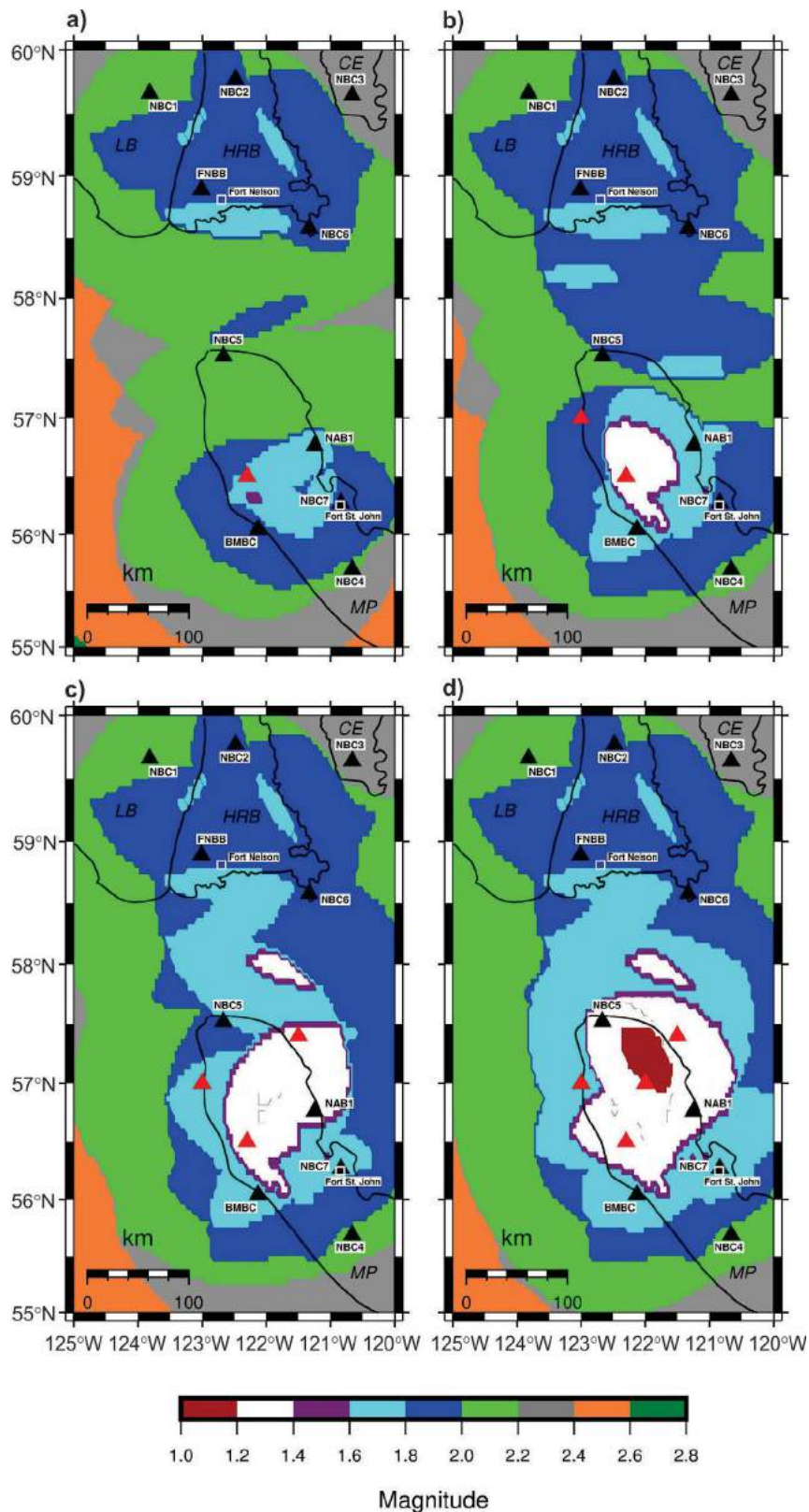
Figure 6. Spatial distribution of the minimum detectable magnitude in northeastern British Columbia after addition of up to four hypothetical stations (red triangles): **a)** one station; **b)** two stations; **c)** three stations; and **d)** four stations. Black triangles indicate the locations of regional seismic stations in the area. Boundaries of the major shale gas plays are shown with black outlines. Abbreviations: CE, Cordova embayment; HRB, Horn River Basin; LB, Liard Basin; MP, Montney play.

Acknowledgments

References

Ake, J., Mahrer, K., O'Connell, D. and Block, L. (2005): Deep-injection and closely monitored induced seismicity at Paradox Valley, Colorado; Bulletin of Seismological Society of America, v. 95, p. 664–683.

Atkinson, G.M. and Kraeva, N. (2010): Ground motions underground compared to those on the surface: a case study from Sudbury, Ontario; Bulletin of Seismological Society of America, v. 100, p. 1293–1305.

BC Oil and Gas Commission (2012a): Investigation of observed seismicity in the Horn River Basin; BC Oil and Gas Commission, technical report, 29 p., URL <https://www.bcogc.ca/node/8046/download> [November 2015].

BC Oil and Gas Commission (2012b): Montney Formation play atlas NEBC; BC Oil and Gas Commission, technical report, 36 p., URL<https://www.bcogc.ca/node/8131/download> [November 2015].

BC Oil and Gas Commission (2014): Investigation of observed seismicity in the Montney trend; BC Oil and Gas Commission, technical report, 32 p., URL <https://www.bcogc.ca/node/12291/download> [November 2015].

Boore, D.M. (2003): Simulation of ground motion using the stochastic method; Pure and Applied Geophysics, v. 160, p. 635–676.

Boore, D.M. (2009): Comparing stochastic point-source and finite-source ground-motion simulations: SMSIM and EXSIM; Bulletin of Seismological Society of America, v. 99, p. 3202–3216.

Boore, D.M. and Thompson, E.M. (2012): Empirical improvements for estimating earthquake response spectra with random-vibration theory; Bulletin of Seismological Society of America, v. 102, p. 761–722.

Boore, D.M. and Thompson, E.M. (2015): Revisions to some parameters used in stochastic-method simulations of ground motion; Bulletin of Seismological Society of America, v. 105, p. 1029–1041.

D'Alessandro, A. and Ruppert, N.A. (2012): Evaluation of location performance and magnitude of completeness of the Alaska regional seismic network by the SNES method; Bulletin of Seismological Society of America, v. 102, p. 2098–2115.

D'Alessandro, A. and Stickney, M. (2012): Montana seismic network performance: an evaluation through the SNES method; Bulletin of Seismological Society of America, v. 102, p. 73–87.

D'Alessandro, A., Badal, J., D'Anna, G., Papanastassou, D., Baskoutas, I. and Ozel, N.M. (2013a): Location performance and detection threshold of the Spanish national seismic network; Pure and Applied Geophysics, v. 170, p. 1859–1880.

D'Alessandro, A., Danet, A. and Grecu, B. (2012): Location performance and detection magnitude threshold of the Romanian national seismic network; Pure and Applied Geophysics, v. 169, p. 2149–2164.

D'Alessandro, A., Gervasi, A. and Guerra, L. (2013b): Evolution and strengthening of the Calabrian regional seismic network; Advances in Geosciences, v. 36, p. 11–16.

D'Alessandro, A., Luzio, D., D'Anna, G. and Mangano, G. (2011a): Seismic network evaluation through simulation: an application to the Italian national seismic network; Bulletin of Seismological Society of America, v. 101, p. 1213–1232.

D'Alessandro, A., Papanastassiou, D. and Baskoutas, I. (2011b): Hellenic unified seismological network: an evaluation of its performance through SNES method; Geophysical Journal International, v. 185, p. 1417–1430.

Davies, R., Foulger, G., Bindley, A. and Styles, P. (2013): Induced seismicity and hydraulic fracturing for the recovery of hydrocarbons; Marine and Petroleum Geology, v. 45, p. 171–185.

Davis, S.D. and Frohlich, C. (1993): Did (or will) fluid injection cause earthquakes? – criteria for a rational assessment; Seismological Research Letters, v. 64, p. 207–224.

Dieterich, J.H., Richards-Dinger, K.B. and Kroll, K.A. (2015): Modeling injection-induced seismicity with the physics-based earthquake simulator RSQSim; Seismological Research Letters, v. 86, p. 1102–1109.

Farahbod, A.M., Kao, H., Walker, D.M. and Cassidy, J.F. (2015): Investigation of regional seismicity before and after hydraulic fracturing in the Horn River Basin, northeast British Columbia; Canadian Journal of Earth Sciences, v. 52, p. 112–122.

Havskov, J. and Alguacil, G. (2004): Seismic noise; *in* Instrumentation in Earthquake Seismology, Modern Approaches in Geophysics, v. 22, p. 70–77.

Holland, A. (2013): Earthquakes triggered by hydraulic fracturing in south-central Oklahoma; Bulletin of Seismological Society of America, v. 103, p. 1784–1792.

Hornbach, M.J., De Shon, H.R., Ellsworth, W.L., Stump, B.W., Hayward, C., Frohlich, C., Oldham, H.R., Olson, J.E., Magnani, M.B., Brokaw, C. and Luetgert, J.H. (2015): Causal factors for seismicity near Azle, Texas; Nature Communications, v. 6, p. 1–18.

Horner, R.B., Barclay, J.E. and Macrae, J.M. (1994): Earthquakes and hydrocarbon production in the Fort St. John area of northeastern British Columbia; Canadian Journal of Exploration Geophysics, v. 30, p. 38–50.

Incorporated Research Institutions for Seismology (2015): Data management center; Incorporated Research Institutions for Seismology, URL <http://ds.iris.edu/ds/nodes/dmc/> [November 2015].

Keranen, K.M., Weingarten, M., Abers, G.A., Bekins, B.A. and Ge, S. (2014): Sharp increase in central Oklahoma seismicity since 2008 induced by massive wastewater injection; Science, v. 345, p. 448–451.

Lindquist, K.G., Engle, K., Stahlke, D. and Price, E. (2004): Global topography and bathymetry grid improves research efforts; Eos, Transactions, American Geophysical Union, v. 85, no. 19, p. 186, URL <http://www.agu.org/pubs/crossref/2004/2004EO190003.shtml> [November 2015].

McNamara, D.E. and Boaz, R.I. (2011): PQLX: a seismic data quality control system description, applications, and user's manual; United States Geological Survey, Open-File Report 2010-1292, 41 p.

McNamara, D.E. and Buland, R.P. (2004): Ambient noise levels in the continental United States; Bulletin of Seismological Society of America, v. 94, p. 1517–1527.

National Energy Board, BC Oil and Gas Commission, Alberta Energy Regulator and BC Ministry of Natural Gas Development (2013): Energy briefing note: the ultimate potential for unconventional petroleum from the Montney Formation of British Columbia and Alberta; National Energy Board, BC Oil and Gas Commission, Alberta Energy Regulator and BC Ministry of Natural Gas Development, 17 p., URL <https://www.neb-one.gc.ca/nrg/sttstc/ntrlgs/index-eng.html> [November 2015].

Natural Resources Canada (2015): Earthquakes Canada; Natural Resources Canada, URL <http://earthquakescanada.nrcan.gc.ca/> [November 2015].

Peterson, J. (1993): Observations and modeling of seismic background noise; United States Geological Survey, Open-File Report 93-322, 94 p.

Rubinstein, J.L. and Babaie Mahani, A. (2015): Myths and facts on wastewater injection, hydraulic fracturing, enhanced oil recovery, and induced seismicity; Seismological Research Letters, v. 86, p. 1060–1067.

Salas, C.J. and Walker, D. (2014): Update on regional seismograph network in northeastern British Columbia (NTS 094C, G, I, O, P); in Geoscience BC Summary of Activities 2013, Geoscience BC, Report 2014-1, p. 123–126.

Salas, C.J., Walker, D. and Kao, H. (2013): Creating a regional seismograph network in northeast British Columbia to study the effect of induced seismicity from unconventional gas completions (NTS 094C, G, I, O, P); in Geoscience BC Summary of Activities 2012, Geoscience BC, Report 2013-1, p. 131–134.

Shapiro, S.A. and Dinske, C. (2009): Fluid-induced seismicity: pressure diffusion and hydraulic fracturing; Geophysical Prospecting, v. 57, p. 301–310.

Permafrost Ecosystems in Transition: Understanding and Predicting Hydrological and Ecological Change in the Southern Taiga Plains, Northeastern British Columbia and Southwestern Northwest Territories

W.L. Quinton, Cold Regions Research Centre, Wilfrid Laurier University, Waterloo, ON, wquinton@wlu.ca

J.R. Adams, Cold Regions Research Centre, Wilfrid Laurier University, Waterloo, ON

J.L. Baltzer, Cold Regions Research Centre, Wilfrid Laurier University, Waterloo, ON

A.A. Berg, Department of Geography, University of Guelph, ON

J.R. Craig, Department of Civil and Environmental Engineering, University of Waterloo, Waterloo, ON

E. Johnson, Northeast Water Strategy, Government of British Columbia, Victoria, BC

Introduction

The southern Taiga Plains ecoregion is one of the most rapidly warming regions on Earth, and is experiencing unprecedented rates of industrial expansion and related human disturbance. The permafrost in this region is relatively warm (e.g., between –1 and 0°C), thin and discontinuous. As a result, permafrost thaw is widespread and often leads to the transformation of forested permafrost terrains to permafrost-free, treeless wetlands. Such land-cover change, induced by permafrost thaw, has the potential to disrupt the hydrological cycle. Despite the demonstrated pan-arctic occurrence of this effect, the hydrological implications of this land-cover transformation remain poorly understood. As a result, there is an urgent need for an improved understanding of, and ability to predict, permafrost thaw and its hydrological consequences.

This paper describes the Consortium for Permafrost Ecosystems in Transition (CPET)—a new project that arose in direct response to these challenges. The CPET will develop and mobilize new knowledge on permafrost-thaw–induced land-cover change and the resulting hydrological and ecological impacts, and will use this new knowledge to develop a new suite of predictive hydrological modelling tools. Field measurements will concentrate on observatories located on an approximately 170 km long south-to-north transect that extends over the peatland-dominated southern fringe of discontinuous permafrost (Figure 1). This transect is ideally suited for the study of permafrost-
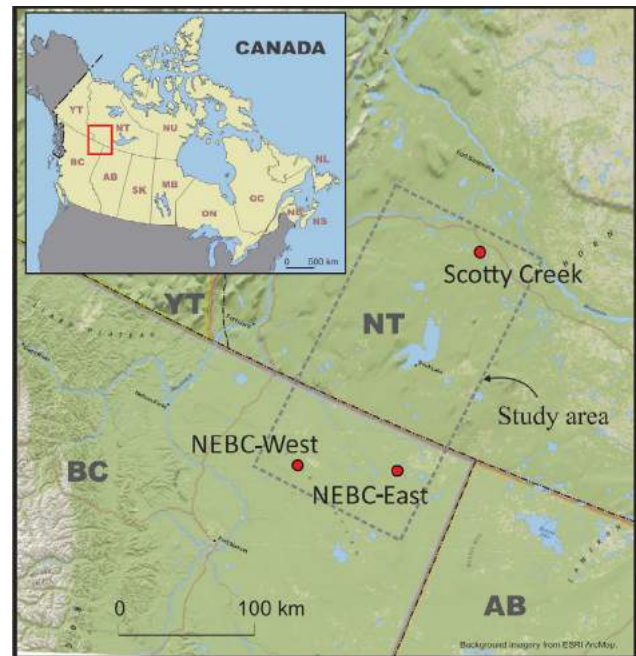
Figure 1: The Consortium for Permafrost Ecosystems in Transition (CPET) project transect extending in a north-south direction over the southern margin of discontinuous permafrost, northeastern British Columbia and southwestern Northwest Territories.

thaw–induced changes to ecosystems and the resulting impacts on surface hydrology, since it covers a wide range of permafrost ecosystem characteristics along a climate gradient. Improved knowledge and predictive capacity of permafrost thaw patterns, rates, impacts and feedbacks will improve water planning, management and security by reducing the uncertainty of the future availability of freshwater, and enable better mitigation strategies to offset negative impacts.

Background

In recent decades, the Taiga Plains ecoregion in northwestern Canada has become one of the most rapidly warming regions on Earth (Jorgenson et al., 2010). This warming is most pronounced in the southern Taiga Plains, including northeastern British Columbia (NEBC) and the adjacent southwestern Northwest Territories (NWT). There is mounting evidence that this warming is affecting the water cycle throughout the Taiga Plains. For example, the frequency of mid-winter melt events has increased (Semmens et al., 2013), end-of-winter snow melt occurs earlier (Francis and Vavrus, 2012) and key variables, such as snowpack depth (Cohen et al., 2014), snow cover extent (Derksen and Brown, 2012), surface water storage (Kurylyk et al., 2014a), groundwater flows (Bense et al., 2012) and seasonal precipitation patterns (Intergovernmental Panel on Climate Change, 2013), have deviated from long-term means. These changes are reflected in basin hydrographs throughout the Taiga Plains, where runoff in streams and rivers has steadily risen since the mid-1990s (St. Jacques and Sauchyn, 2009).

The current understanding of water flow and storage processes in wetland-dominated, discontinuous permafrost terrains, and how climate warming and the resulting ecological changes and feedbacks affect such processes, cannot explain this rise in flows, nor is it sufficient to predict future flows. Rising flows from subarctic rivers are often attributed to reactivation of groundwater systems (e.g., St. Jacques and Sauchyn, 2009), but the very low hydraulic conductivity of the glacial sediments of the border region, precludes appreciable groundwater input. Permafrost-thaw–induced changes to basin flow and storage processes offer a more plausible explanation for rising flows from rivers and streams in this region (Quinton et al., 2011; Connon et al., 2014).

Permafrost thaw is one of the most important and dramatic manifestations of climate warming (Rowland et al., 2010) in the Taiga Plains, yet its influence on runoff and streamflow is unclear. The southern Taiga Plains contain the southern fringe of permafrost (Kwong and Gan, 1994), where ice-rich permafrost, in the form of tree-covered peat plateaus, occurs as islands within a wetland-dominated, treeless, permafrost-free terrain of flat bogs, channel fens and other wetlands (Robinson, 2002). Because the permafrost underlying peat plateaus is relatively warm and thin (<10 m), less energy is required for permafrost thaw in this region than at higher latitudes, and as a result, the highest rates of permafrost thaw are found within the southern fringe (Camill, 2005). This permafrost is discontinuous and, therefore, its thaw is driven not only by vertical heat flows from the ground surface (Zhang et al., 2003), but also by horizontal heat conduction and advection from the permafrost margins (McClymont et al., 2013). As permafrost thaws, the overlying ground surface subsides and is engulfed by surrounding wetlands (Jorgenson and Osterkamp, 2005). This process gradually transforms permafrost terrains with forests into treeless, permafrost-free wetlands. Between 30 and 65% of the permafrost in the fringe zone has degraded or disappeared over the last 100–150 yr (Beilman and Robinson, 2003), with concomitant increases in wetland coverage (Quinton et al., 2011), and with forest-to-wetland conversion rates increasing in recent decades (Patankar et al., 2015).

Given that permafrost exerts a primary control on surface (Woo, 1986) and subsurface (Kurylyk et al., 2014a, b) hydrological processes, its disappearance has profound implications to the overall water cycle, including runoff, from local (Quinton and Baltzer, 2013) to regional (Rowland et al., 2010) scales. Rapid climate warming at high latitudes is projected to continue (Intergovernmental Panel on Climate Change, 2013) and model simulations suggest that this warming will produce greater discharge from drainage basins through the intensification (i.e., increased flow rates) of the hydrological cycle (Rawlins et al., 2013). It is also projected that accelerated permafrost thaw (Schaefer et al., 2011; Lawrence et al., 2012) may lead to the disappearance of permafrost throughout much of the southern fringe (Delisle, 2007; Zhang et al., 2008) over the next half century. However, simulations of permafrost loss are largely one-dimensional, run on large (e.g., 0.5 by 0.5°C) grids, and do not consider the co-occurrence of permafrost and nonpermafrost landscapes. The simulations do not explicitly account for the effects of subgrid processes, such as the lateral conductive and advective heat transfer between adjacent permafrost and permafrost-free terrains. Recent advances have enabled the modelling of discontinuous permafrost thaw using new three-dimensional numerical simulations of subsurface mass and energy transport. These simulations include freeze-thaw processes (e.g., Endrizzi et al., 2014; Kurylyk et al., 2014a,b) coupled to land-surface models (e.g., Zhang et al., 2003) and driven by general circulation model (GCM) output or higher resolution regional climate models (RCMs) following statistical downscaling (e.g., Wilby and Dawson, 2013) and bias correction (e.g., Bordoy and Burlando, 2013). These developments offer an important new opportunity to combine detailed field-based process studies with numerical modelling in order to improve the understanding of and ability to predict basin hydrographs that account for permafrost thaw and the resulting land-cover changes.

In the NEBC–NWT border region (hereafter border region), climate-warming–induced changes are exacerbated by unprecedented rates of industrial expansion. New roads and highways, pipelines, seismic lines, airstrips, drill pads and other infrastructure have the potential to profoundly affect permafrost, ecosystems and the hydrological cycle at local scales. Knowledge of permafrost thaw impacts are

important to the petroleum industry since permafrost thaw greatly increases infrastructure construction and maintenance costs by causing pipeline ruptures, pad instabilities, foundation cracks from subsidence and the need for road resurfacing. Activities such as drilling wells and creating borrow pits, water storage ponds and linear features (e.g., winter roads, seismic lines, pipelines) all increase thaw rates by disturbing the insulating surface layer. Permafrost thaw and the resulting land-cover changes add uncertainty to the future availability of freshwater in the region. Industry requires both improved capacity to predict future water supplies and mitigation strategies to reduce the costs associated with industrial expansion in areas of permafrost.

Permafrost thaw is also of concern to local communities, including First Nations, especially with regard to its impact on the long-term health of water resources and natural ecosystems. In particular, unconventional gas extraction by hydraulic fracturing (fracking) has increased dramatically in the border region in recent years. Since hydraulic fracturing requires large volumes of water, industrial water use has also increased rapidly and is raising pressures on ecosystems and water supplies. However, the current lack of knowledge and predictive capacity of the rates, patterns, impacts and ecosystem feedbacks of permafrost thaw prevents communities from rigorous, science-based decision making on water resource and ecosystem planning and management, water and land permit approval and environmental impact assessment.

Both industry and governments acknowledge the lack of data on water resources and hydrology in the border region, and that water management in this region lacks sufficient information on permafrost thaw impacts. In response, the authors proposed CPET, a three-year (2015–2018) regional consortium of industry, provincial, territorial and federal government agencies, non-governmental organizations (NGOs), First Nations and other communities and stakeholders who will collaborate to improve the understanding of and ability to predict the impacts of permafrost thaw on shared water resources. The consortium approach is keenly supported by all participants and is fundamental to this project. The CPET was conceived from discussion with the Horn River Basin Producers Group (HRPG), Petroleum Technology Alliance of Canada, Fort Nelson First Nation, Liidlii Kue First Nation, BC Ministry of Forests, Lands and Natural Resource Operations, Geoscience BC, NWT Department of Environment and Natural Resources and the Water Survey of Canada. By contributing knowledge on permafrost thaw impacts to the implementation of both the BC Water Sustainability Act and NWT Water Stewardship Strategy, CPET will improve the scientific basis of the framework within which all water users of the border region will manage their shared resource, and will reduce the uncertainty of water

futures by putting into the hands of trained end-users, customized science-based tools that will increase their predictive capacity.

CPET Research Direction

The CPET has five specific objectives:

1) Map the changing spatial distribution of permafrost, wetland and forest coverage over the past 60 years using aerial photography, satellite and light detection and ranging (LiDAR) images.

2) Conduct field studies for different ground thaw and moisture conditions to improve the understanding of the volume and timing of runoff from a) peat plateau–bog complexes and b) the adjacent channel fens, which convey the runoff that they receive from plateau–bog complexes to streams and rivers. For each setting, the water flux and storage processes that control runoff will be examined.

3) Simulate the major water flux and storage processes controlling runoff from the plateau–bog complexes using the cold regions hydrological model (CRHM) and the Raven hydrological modelling framework and, where needed, make improvements to both models based on the improved process understanding arising from objective 2.

4) Improve the ability to characterize permafrost impacts at larger scales through field investigation and subsequent adaptation of the northern ecosystem soil temperature (NEST) regional-scale permafrost model to handle the unique thaw response of bogs, fens and plateaus.

5) Use information generated from the improved hydrological models (objective 3) and the permafrost model (objective 4) to estimate future quantities of runoff and surface water storage within boreal and subarctic landscapes with discontinuous permafrost under possible scenarios of climate warming and human disturbance.

Study Sites

The CPET field studies will focus on three study sites (Table 1). Sites NEBC-East and Scotty Creek are the end-members of a 170 km long north-south transect through the fringe zone over which the wetland to forest ratio, permafrost concentration, climate and eco-hydrology vary. Site

Table 1: Location information for three study sites, northeastern British Columbia and southwestern Northwest Territories.

Site ID	Latitude	Longitude	Location	Area
NEBC-West	59° 29.056' N	122° 16.105' W	4.5 km east of Two-Island Lake	Horn River Basin, BC
NEBC-East	59° 42.460' N	120° 53.760' W	6 km west of July Lake	Cordova region, BC
Scotty Creek	61° 18.207' N	121° 17.628' W	50 km south of Fort Simpson	NWT

NEBC-West is wetland-dominated, with standing water and small lakes, but with greater topographic variation, greater variety of tree species and more mineral soil. The 1981–2010 climate normals indicate that Fort Simpson and Fort Nelson (located just south of the study area) have dry continental climates with short, dry summers and long, cold winters. Fort Simpson has an average annual air temperature of –2.8°C, and receives 388 mm of precipitation annually, of which 38% is snow (Environment Canada, 2013). Fort Nelson has an average annual air temperature of –0.4°C, and receives 452 mm of precipitation annually, of which 31% is snow (Environment Canada, 2013). The landscape at both Scotty Creek and NEBC-East are dominated by discontinuous permafrost (Heginbottom, 2000) and plateau–bog complexes, typical of the southern fringe of discontinuous permafrost. Both NEBC-East and Scotty Creek have experienced rapid and widespread permafrost thaw in recent decades.

Previous Work and Progress to Date

Recent work by CPET and others in the wetland-dominated, southern fringe of discontinuous permafrost or fringe zone (Kwong and Gan, 1994), has demonstrated that a) major land-cover types have contrasting hydrological functions, b) the relative proportions and spatial arrangement of these land-cover types is changing due to climate warming, and c) this warming-induced land-cover change is changing the water balance of drainage basins.

Contrasting Hydrological Functions

Ice-rich permafrost in the form of tree-covered peat plateaus dominates much of the fringe zone, where plateaus occur as forested permafrost islands within a wetland terrain of flat bogs and channel fens. The contrasting biophysical properties of these peatland types, gives each a specific role in the water cycle. Plateaus have a limited capacity to store water, a relatively large snowmelt water supply and an ability to direct excess water into adjacent wetlands (Wright et al., 2009). They have been found to function primarily as runoff generators, with runoff occurring predominately through the thawed, saturated layer between the water table and the relatively impermeable frost table below. Bogs are entirely surrounded by raised permafrost and are therefore unable to exchange surface or near-surface water with the basin drainage network. However, recent field studies at Scotty Creek, NWT, found that certain bogs can produce runoff, specifically, cascade bogs and open bogs. A cascade bog is one bog that belongs to a series of bogs connected by ephemeral channels. During periods of high moisture supply and/or limited ground thaw, such bogs cascade water through the series and into a fen. An open bog is one where the permafrost that once separated it from an adjacent fen has since thawed so that the bog is now open (i.e., connected) to the fen. This process of bog capture, as described in Connon et al. (2014), enables surface and near-surface flow between fens and open bogs during wet periods. Channel fens collect water from surrounding peatlands and convey it laterally along their broad (~50–100 m wide), hydraulically rough channels to streams and rivers (Quinton et al., 2003).

Warming-Induced Land-Cover Changes

As permafrost thaws, peat plateau surfaces subside and are flooded by the adjacent bogs or fens (Jorgenson and Osterkamp, 2005), a process leading to loss of forest and expansion of wetlands. At the Scotty Creek location, the proportion of a 1 km^2 area underlain by permafrost decreased from 70 to 43% between 1947 and 2008 (Quinton et al., 2011) and, currently, the fragmentation of peat plateaus is accelerating thaw rates (Baltzer et al., 2014). Electrical resistivity imaging across the width of plateaus at Scotty Creek indicated that permafrost is on the order of 10 m thick with edges that are close to vertical making the transition from permafrost to non-permafrost terrain abrupt (McClymont et al., 2013). Permafrost thaw involves simultaneous recession of these vertical edges and thickening of the active layer (Quinton et al., 2011).

Changes to the Water Balance of Drainage Basins

At Scotty Creek, field observations and image analyses suggest that plateaus contain two distinct runoff source areas separated by a break in slope approximately 10 m inland from the fen–plateau edge. Primary runoff drains from the sloped edges of plateaus directly into the basin drainage network (i.e., a channel fen). Field measurements suggest that the entire primary area supplies runoff to fens throughout the thaw season. Secondary runoff enters fens through a bog or a bog cascade, where the degree of hydrological connection with fens varies seasonally. As such, secondary runoff is neither direct nor continuous. The rate of secondary runoff is greatest during periods of high moisture supply and minimal ground thaw, when the hydrological connection among the bogs of a cascade, and also between individual bogs and their contributing areas (i.e., bog-sheds), is maximized. As the active layer thaws and drains, the contributing area shrinks and secondary runoff decreases. Large rain events can temporarily reverse this decrease.

In comparing historical images of Scotty Creek, a basin typical of the border region, numerous bogs that were isolated from the drainage network in 1977 had become connected to it by 2008. This bog capture process increases basin runoff by increasing the basin's runoff contributing area (Connon et al., 2014). Specifically, bog capture adds to the basin drainage network through a) runoff arising from direct precipitation falling onto the captured bog (i.e., bog drainage), and b) runoff from the captured bog's watershed (i.e., slope drainage). As captured bogs expand due to per-

mafrost thaw at their margins, they merge into other bogs. This process increases both the bog and slope drainage contributions to fens.

Future Work

Scotty Creek and NEBC-East are the primary sites for on-going process studies and model development. This work will be supported by well-developed field research infrastructure and extensive data archives (1999–present) at Scotty Creek and new data at NEBC-East. The transferability of processes and models will be tested at intervening drainage basins along the north-south transect. However, this transect does not include upland forests and some of the peatland types typical of the Horn River Basin, which has a greater topographic variation. For this reason, NEBC-West was established as a study site to explicitly examine the permafrost thaw impacts on hydrology and ecology of biophysical units not represented along the north-south transect.

Acknowledgments

References

Baltzer, J.L., Veness, T., Chasmer, L.E., Sniderhan, A. and Quinton, W.L. (2014): Forests on thawing permafrost: fragmentation, edge effects, and net forest loss; Global Change Biology, v. 20, no. 3, p. 824–834, doi:10.1111/gcb.12349

Beilman, D.W. and Robinson, S.D. (2003): Peatland permafrost thaw and landform type along a climate gradient; *in* Proceedings of the Eighth International Conference on Permafrost, M. Phillips, S.M. Springman and L.U. Arenson (ed.), A.A. Balkema, July 21–25, 2003, Zurich, Switzerland, v. 1, p. 61–65.

Bense, V.F., Kooi, H., Ferguson, G. and Read, T. (2012): Permafrost degradation as a control on hydrogeological regime shifts in a warming climate; Journal of Geophysical Research, Earth Surface, v. 117, no. 03036, 18 p., doi:10.1029/2011JF002143

Bordoy, R. and Burlando, P. (2013): Bias correction of regional climate model simulations in a region of complex orography; Journal of Applied Meteorology and Climatology, v. 52, no. 1, p. 82–101, doi:10.1175/JAMC-D-11-0149.1

Camill, P. (2005): Permafrost thaw accelerates in boreal peatlands during late-20th century climate warming; Climatic Change, v. 68, no. 1–2, p. 135–152, doi:10.1007/s10584-005-4785-y

Cohen, J., Screen, J.A., Furtado, J.C., Barlow, M., Whittleston, D., Coumou, D., Francis, J., Dethloff, K., Entekhabi, D., Overland, J. and Jones, J. (2014): Recent Arctic amplification and extreme mid-latitude weather; Nature Geoscience, v. 7, p. 627–637, doi:10.1038/NGEO2234

Connon, R.F., Quinton, W.L., Craig, J.R. and Hayashi, M. (2014): Changing hydrologic connectivity due to permafrost thaw in the lower Liard River valley, NWT, Canada; Hydrological Processes, v. 28, no. 14, p. 4163–4178, doi:10.1002/hyp.10206

Delisle, G. (2007): Near-surface permafrost degradation: how severe during the 21st century?; Geophysical Research Letters, v. 34, no. L09503, 4 p., doi:10.1029/2007GL029323

Derksen, C. and Brown, R. (2012): Spring snow cover extent reductions in the 2008–2012 period exceeding climate model projections; Geophysical Research Letters, v. 39, no. L19504, 6 p., doi:10.1029/2012GL053387

Endrizzi, S., Gruber, S., Dall'Amico, M. and Rigon, R. (2014): GEOtop 2.0: simulating the combined energy and water balance at and below the land surface accounting for soil freezing, snow cover and terrain effects; Geoscientific Model Development, v. 7, no. 6, p. 2831–2857, doi:10.5194/gmd-7-2831-2014

Environment Canada (2013): Canadian climate normals; Environment Canada, URL <http://climate.weather.gc.ca/climate_normals/index_e.html> [December 2013].

Francis, J. and Vavrus, S. (2012): Evidence linking Arctic amplification to extreme weather in mid-latitudes; Geophysical Research Letters, v. 39, no. L06801, 5 p., doi:10.1029/2012GL051000

Heginbottom, J.A. (2000): Permafrost distribution and ground ice in surficial materials; *in* The Physical Environment of the Mackenzie Valley, Northwest Territories: a Base Line for the Assessment of Environmental Change, L.D. Dyke and G.R. Brooks (ed.), Geological Survey of Canada, Bulletin 547, p. 31–39.

Intergovernmental Panel on Climate Change (2013): Summary for policymakers; *in* Climate Change 2013: The Physical Science Basis, Contribution of Working Group I to the Fifth Assessment Report of the Intergovernmental Panel on Climate Change, T.F. Stocker, D. Qin, G.-K. Plattner, M. Tignor, S.K. Allen, J. Boschung, A. Nauels, Y. Xia, V. Bex and P.M. Midgley (ed.), Cambridge University Press, Cambridge, United Kingdom and New York, New York, 27 p.

Jorgenson, M.T. and Osterkamp, T.E. (2005): Response of boreal ecosystems to varying modes of permafrost degradation; Canadian Journal of Forest Research, v. 35, no. 9, p. 2100–2111, doi:10.1139/X05-153

Jorgenson, M.T., Romanovsky, V., Harden, J., Shur, Y., O'Donnell, J., Schuur, E., Kanevskiy, M. and Marchenko, S. (2010): Resilience and vulnerability of permafrost to climate change; Canadian Journal of Forest Research, v. 40, no. 7, p. 1219–1236, doi:10.1139/X10-060

Kurylyk, B., MacQuarrie, K. and McKenzie, J. (2014a): Climate change impacts on groundwater and soil temperatures in cold and temperate regions: implications, mathematical theory, and emerging simulation tools; Earth-Science Reviews, v. 138, p. 313–334, doi:10.1016/j.earscirev.2014.06.006

Kurylyk, B.L., McKenzie, J.M., MacQuarrie, K.T.B. and Voss, C.I. (2014b): Analytical solutions for benchmarking cold regions subsurface water flow and energy transport models: one-dimensional soil thaw with conduction and advection; Advances in Water Resources, v. 70, p. 172–184, doi:10.1016/j.advwatres.2014.05.005

Kwong, J.Y.T. and Gan, T.Y. (1994): Northward migration of permafrost along the Mackenzie Highway and climate warming; Climate Change, v. 26, no. 4, p. 399–419, doi:10.1007/BF01094404

Lawrence, D.M., Slater, A.G. and Swenson, S.C. (2012): Simulation of present-day and future permafrost and seasonally frozen ground conditions in CCSM4; Journal of Climate, v. 25, no. 7, p. 2207–2225, doi:10.1175/JCLI-D-11-00334.1

McClymont, A.F., Hayashi, M., Bentley, L.R. and Christensen, B.S. (2013): Geophysical imaging and thermal modelling of subsurface morphology and thaw evolution of discontinuous permafrost; Journal of Geophysical Research, Earth Surface, v. 118, no. 3, p. 1826–1837, doi:10.1002/jgrf.20114

Patankar, R., Quinton, W.L., Hayashi, M. and Baltzer, J.L. (2015): Sap flow responses to seasonal thaw and permafrost degradation in a subarctic boreal peatland; Trees – Structure and Function, v. 29, no. 1, p. 129–142, doi:10.1007/s00468-014-1097-8

Quinton, W.L. and Baltzer, J.L. (2013): The active-layer hydrology of a peat plateau with thawing permafrost (Scotty Creek, Canada); Hydrogeology Journal, v. 21, no. 1, p. 201–220, doi:10.1007/s10040-012-0935-2

Quinton, W.L., Hayashi, M. and Chasmer, L.E. (2011): Permafrost-thaw-induced land-cover change in the Canadian subarctic: implications for water resources; Hydrological Processes (Scientific Briefing), v. 25, no. 1, p. 152–158, doi:10.1002/hyp.7894

Quinton, W.L., Hayashi, M. and Pietroniro, A. (2003): Connectivity and storage functions of channel fens and flat bogs in northern basins; Hydrological Processes, v. 17, no. 18, p. 3665–3684, doi:10.1002/hyp.1369

Rawlins, M.A., Nicolsky, D.J., McDonald, K.C. and Romanovsky, V. (2013): Simulating soil freeze/thaw dynamics with an improved pan-Arctic water balance model; Journal of Advances in Modeling Earth Systems, v. 5, no. 4, p. 659–675, doi:10.1002/jame.20045

Robinson, S.D. (2002): Peatlands of the Mackenzie Valley: permafrost, fire, and carbon accumulation; in Long-Term Dynamics and Contemporary Carbon Budget of Northern Peatlands, Z.C. Yu, J.S. Bhatti and M.J. Apps (ed.), Proceedings of International Workshop on Carbon Dynamics of Forested Peatlands: Knowledge Gaps, Uncertainty and Modelling Approaches, March 23–24, 2001, Edmonton, Alberta, p. 21–24.

Rowland, J.C., Jones, C.E., Altmann, G., Bryan, R., Crosby, B.T., Hinzman, L.D., Kane, D.L., Lawrence, D.M., Mancino, A., Marsh, P., McNamara, J.P., Romanovsky, V.E., Toniolo, H., Travis, B.J., Tochim, E., Wilson, C.J. and Geernaert, G.L. (2010): Arctic landscapes in transition: responses to thawing permafrost; Eos, Transactions, American Geophysical Union, v. 91, no. 26, p. 229–236, doi:10.1029/2010EO260001

Schaefer, K., Zhang, T., Bruhwiler, L. and Barrett, A.P. (2011): Amount and timing of permafrost carbon release in response to climate warming; Tellus Series B, Chemical and Physical Meteorology, v. 63, no. 2, p. 165–180, doi:10.1111/j.1600-0889.2011.00527.x

Semmens, K., Ramage, J., Bartsch, A. and Liston, G. (2013): Early snowmelt events: detection, distribution, and significance in a major sub-arctic watershed; Environmental Research Letters, v. 8, no. 1, no. 0.14020, 11 p., doi:10.1088/1748-9326/8/1/014020

St. Jacques, J.M. and Sauchyn, D.J. (2009): Increasing winter baseflow and mean annual streamflow from possible permafrost thawing in the Northwest Territories, Canada; Geophysical Research Letters, v. 36, no. L01401, 6 p., doi:10.1029/2008GL035822

Wilby, R.L. and Dawson, C.W. (2013): The statistical downscaling model: insights from one decade of application; International Journal of Climatology, v. 33, no. 7, p. 1707–1719, doi:10.1002/joc.3544

Woo, M.K. (1986): Permafrost hydrology in North America; Atmosphere-Ocean, v. 24, no. 3, p. 201–234, doi:10.1080/07055900.1986.9649248

Wright, N., Hayashi, M. and Quinton, W.L. (2009): Spatial and temporal variations in active-layer thawing and their implication on runoff generation; Water Resources Research, v. 45, no. W05414, 13 p., doi:10.1029/2008WR006880

Zhang, Y., Chen, W.J. and Cihlar, J. (2003): A process-based model for quantifying the impact of climate change on permafrost thermal regimes; Journal of Geophysical Research Atmospheres, v. 108, no. D22, 13 p., doi:10.1029/2002JD003355

Zhang, Y., Chen, W. and Riseborough, D.W. (2008): Transient projections of permafrost distribution in Canada during the 21st century under scenarios of climate change; Global and Planetary Change, v. 60, no. 3–4, p. 443–456, doi:0.1016/j.gloplacha.2007.05.003

Quantifying the Water Budget for a Northern Boreal Watershed: The Coles Lake Study, Northeastern British Columbia

S. Abadzadesahraei, University of Northern British Columbia, Prince George, BC, sina@unbc.ca

S.J. Déry, University of Northern British Columbia, Prince George, BC

J. Rex, British Columbia Ministry of Forests, Lands and Natural Resource Operations, Prince George, BC

Introduction

Northeastern British Columbia is undergoing rapid development for oil and gas extraction and this depends largely on subsurface hydraulic fracturing (fracking), which depends on the available freshwater. Even though this industrial activity has made substantial contributions to regional and provincial economies, it is important to ensure that sufficient and sustainable water supplies are available for all those dependent on the resource, including ecological systems. This in turn demands comprehensive understanding of how water in all its forms interacts within the watershed, and of the potential impacts of changing climatic conditions on these processes. The aim of this study is to characterize and quantify all components of the water budget in the small watershed of Coles Lake, northeastern BC through a combination of fieldwork, observational data analysis and numerical modelling. Baseline information generated from this project will support the assessment of the sustainability of current and future plans for freshwater extraction in the region by the oil and gas industry.

This research will not only quantify the short-term water budget (hydrological year 2013–2014) for Coles Lake but will also examine its historical and regional context, research which aims to benefit the larger northeastern region. Historical water balance quantification can help to identify and assess climatic and biophysical features that contribute to uncertainties in water balance components, such as climate change. Specifically, historical estimates of the water balance can assist in identifying climate change signals on air temperature, precipitation patterns and evapotranspiration. This paper will only provide the latest results of fieldwork and observational analysis for the short-term (hydrological year 2013–2014) water budget. The outcomes of a modelling study will be published separately.

Water and Natural Gas in Northeastern British Columbia

Natural gas development has increased globally, but particularly in North America. Natural gas is considered by many to be a reliable, secure and environmentally acceptable fuel. According to the Canadian Association of Petroleum Producers, Canada is the world's third largest producer of natural gas and has access to extensive reserves that are concentrated in the largest producing regions of the western provinces (BC, Alberta and Saskatchewan; Canadian Association of Petroleum Producers, 2015). Within northeastern BC, the Montney shale gas play and Horn River Basin are two regions that have come into prominence in the past few years because of their unconventional natural gas resources. Intensive unconventional development of these shale- and tight-gas reservoirs requires large quantities of freshwater (Chapman et al., 2012).

Overview of Past Research

Shale-gas exploration and development near Fort Nelson has increased demand for surface water in these wetland-dominated landscapes, prompting several studies to assess the sustainable function of such natural ecosystems. Recently, Johnson (2010) developed a conceptual water-balance model for the Horn River Basin near Fort Nelson and identified knowledge gaps. To fill these gaps would require the identification of wetlands, delineation of fens and bogs, location and distribution of permafrost, spatial distribution of evapotranspiration and increased monitoring of discharge. Further contributions to water allocation planning efforts have also been made by Chapman et al. (2012) with the development of the northeast water tool (NEWT)—a web-based hydrological model and planning tool for prediction of water availability based on modelled annual, seasonal and monthly runoff. Recent studies indicate that the combination of gentle topography, relatively fine-textured surficial materials, extensive wetlands, discontinuous permafrost and seasonally frozen ground make hydrological studies in the Fort Nelson area particularly challenging (Golder Associates, 2010; Johnson, 2010). Several studies have explored these concerns, but there are many gaps that

still need to be addressed. The current research will consist of short-term monitoring to identify if there is ecosystem change associated with water use and to obtain more knowledge about boreal wetland dynamics by identifying the water balance of the Coles Lake watershed.

Study Area Characteristics

Coles Lake is part of the Peace River Land District and it is situated at 59°46′57″N latitude and 122°36′27″W longitude with an area of 1.715 km^2 (Figure 1). The watershed is about 140 km northeast of Fort Nelson and has a drainage area of approximately 227 km^2. Its elevation ranges from 311 to 550 m asl with an average elevation of 523.9 m asl and contains an elevated central highland, which acts as a drainage divide. Coles Lake is a small and shallow water body with a maximum depth of 2.2 m. The southern and western side of the project area drains to the west and north through Emile Creek and flows into the Petitot River, whereas the northern and eastern side of the project area drains to the east and north through Fortune Creek and flows into the Petitot River.

The Coles Lake watershed is located in the moist and cool boreal white and black spruce subzone (Delong et al., 2011). This subzone is characterized by black and white spruce forests and wetland complexes of discontinuous permafrost, fens, bogs, swamps and marshes on a glaciolacustrine plain, with extensive organic deposits and a lesser component of streamlined tills (Golder Associates, 2010; Johnson, 2010; Huntley et al., 2011; Kabzems et al., 2012).

The banks of Coles Lake are covered by fen-type vegetation, which transitions to mixed wood forest up moderately steep slopes away from the banks. Based on the most recent vegetation resource inventory (VRI) and the BC Land Cover Classification Scheme, approximately 43.3% of this watershed is open, 51.4% has a mixed vegetation canopy and 5.3% has a closed vegetation canopy. Only crown closure (%) of VRI is used to identify open, mixed and closed vegetation canopies (≤25% open, >25–61% mixed, >61% closed). Based on data from the automated weather station (UF) installed near Coles Lake for this study (latitude 59°47′22.2″N, longitude 122°36′42.8″W, elevation 480.0 m asl), the mean annual air temperature was –1.2°C, ranging from –4.0 to 1.0°C, with a total annual precipitation of 372.0 mm in the 2013–2014 hydrological year. Permanent snow cover lasts from early November until early to mid-May, depending on the year, and maximum snow accumulation occurs either in December, January or February.

Methodology

Estimating the Water Balance

The water cycle of Coles Lake is composed of several water fluxes and stocks that need to be quantified. Precipitation (rain and snow) and stream inflow to the lake are considered the two main inputs; evaporation, stream outflow and water extraction from the lake are considered outputs. In addition to surface water flows, the potential role of shallow groundwater flow to the lake is investigated. As a first step, an appropriate water budget equation must be defined
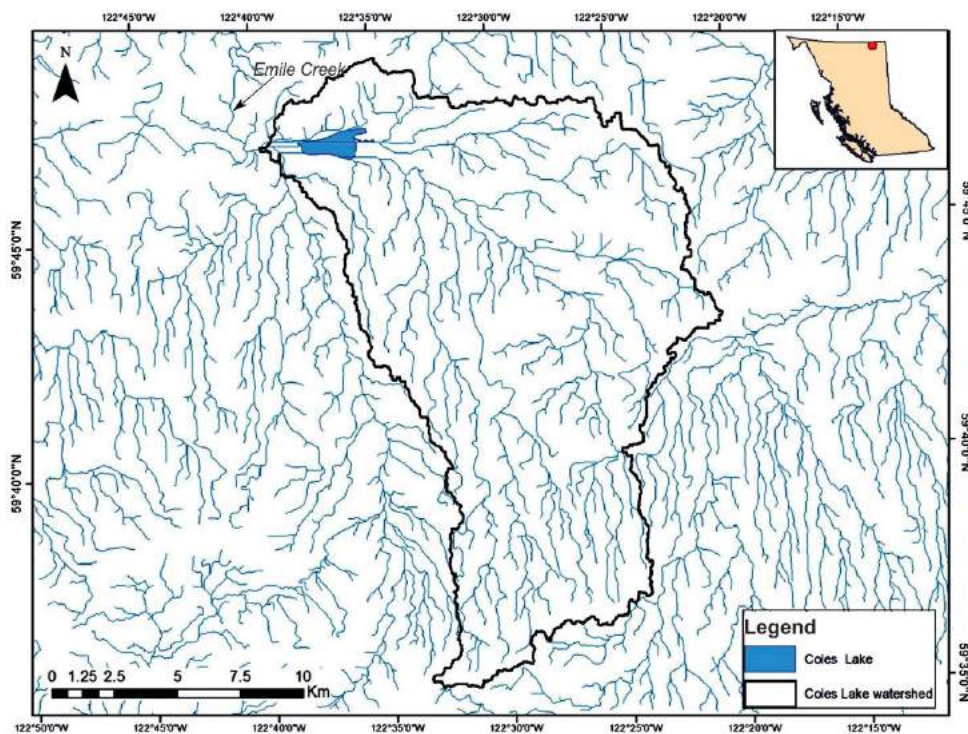

Figure 1. Location of Coles Lake and its watershed boundary, northeastern British Columbia.

to represent these components. Hence, the Coles Lake water balance is defined as follows:

$$\Delta S = P + I \pm G - E - Q - W \qquad (1)$$

Where, ΔS is the change in stored water, P is precipitation (P = R + S, where R denotes rainfall and S represents snowfall), I is the mean annual stream inflow to Coles Lake, G is the groundwater exchange, E is evaporation (maximum evaporation), Q is discharge (outflow) and W is the licensed withdrawal of water. Although the water balance has been computed for the entire Coles Lake watershed, results presented here are for the lake itself. All terms are expressed in units of millimetres. A water-year from October 1, 2013 to September 30, 2014 was used as the temporal framework within which to estimate the balance, as this period begins and ends when both discharge and storage are at their minimum levels (Winkler et al., 2010).

Data Collection

Fieldwork was conducted from May 2012 to September 2014 to examine the hydrological components of this watershed in detail. Challenges to the field efforts included the remoteness of the basin and difficult access to the area, as well as frequent severe weather conditions. The results of this work will support the quantification and understanding of the Coles Lake water budget. A general description of each field procedure used and its purpose is outlined below:

- A Campbell Scientific, Inc. weather station (CR1000 data logger) was installed in a large clearing area approximately 400 m from Coles Lake (Figure 2). The purpose was to record the meteorological information used to compute the hydrological components that contribute to Coles Lake and its watershed.

- In addition to the rain gauge at the weather station, three Davis Instruments tipping-bucket rain gauges were deployed under the three different vegetation canopies. The purpose was to identify how different amounts of rainfall contribute to the watershed for the different vegetation canopies (R parameter).

- Three snow survey sites were established at the rain gauge locations. The purpose was to capture the contribution of snowfall to the watershed for the different vegetation canopies (S parameter).

- Nine piezometers equipped with the Odyssey™ capacitance water level recorders (Dataflow Systems Limited) were installed at three transects around the shore of Coles Lake. The purpose was to examine the variability of seasonal shallow groundwater flows and to quantify the contribution of shallow groundwater to Coles Lake (G parameter).

- Two Onset Computer Corporation hydrometric stations (HOBO® data logger) were established, one at the inflow and another at the outflow of the lake (Figure 2). The purpose was to measure the streamflow discharge at the inflow and the outflow stations (I and Q parameters).

- Quicksilver Resources Canada Inc. (Quicksilver) established a hydrometric station on Emile Creek, 4 km downstream of the lake outflow (Figure 2). The purpose was to measure the runoff from the Coles Lake watershed.

- A skin sensor temperature probe (Eclo's iBCod 22L) was installed in the middle of Coles Lake. The purpose was to monitor the water skin temperature and the data was used to compute the amount of evaporation from Coles Lake (E parameter).

- Amounts of water extracted for Quicksilver Resources Canada Inc.'s (Quicksilver) exploration operations were collected. The purpose was to quantify the total amount of water withdrawal from the lake (W parameter).

- Staff gauges were installed in Coles Lake by Quicksilver. The purpose was to record lake water levels.

- A Coles Lake bathymetric map (0.25 m interval) was produced by Quicksilver. The purpose was to provide morphometry information for Coles Lake including surface area, maximum length and width, shoreline length and volume—all crucial to understanding how a lake system functions.

Results

Rainfall (R)

Local rainfall data were collected every 15 min at the UF weather station and then

Figure 2. Western view of Coles Lake with location of automated weather and hydrometric stations, northeastern British Columbia.

summed for a daily total. At the three rainfall gauges, which were installed in open, mixed and closed vegetation canopies, every rainfall event was recorded and daily totals were obtained. Although all four gauges were used to compute total rainfall for the whole watershed using the Thiessen method, only recorded data from the UF station were used to calculate the total contribution of mean rainfall on Coles Lake itself. Rainfall data from November to May are considered to be zero, since most of the precipitation reported during this period is from snow and ice melt rather than rainfall. In total 243.9 mm of rainfall is reported, with maximum rainfall occurring in June (73.9 mm) and July (61.9 mm).

Snowfall (S)

Based on Environment Canada standard equivalences, 1 cm of snow is assumed to correspond to 1 mm of water. Therefore, total snow water equivalent (SWE) for the Coles Lake station equals 167.4 mm. In addition, a manual snow sampling procedure was performed at the three canopy sites to measure the SWE and snow depth and will later be used as input to a hydrological model.

Evaporation (E)

Multiple steps were required to compute the total evaporation over the Coles Lake area. The first step was to identify the ice-free period. Landsat images were downloaded and reviewed to determine the start and end time of freezing and melting at Coles Lake. Based on the Landsat images, Coles Lake began freezing on November 1, 2013, and the melting period began by May 15, 2014. The profile method, which was shown by Granger (1991) to provide reliable estimates of latent heat fluxes, was selected to estimate evaporation from the lake surface. To use the profile method, air and water temperature, wind speed, relative humidity and air pressure were collected for the duration of the open-water period. In addition to employing the profile method, several assumptions were made, such as fluxes are constant with height and stability is neutral. The results suggested that maximum evaporation occurred in July and minimum in September, with a total loss of 148.6 mm during the ice-free months. Finally, the potential contribution of blowing snow sublimation to the water budget of Coles Lake was assessed using the Piektuk blowing snow model (Déry et al., 1998). The model indicates that blowing snow sublimation does not contribute significantly to the water budget of Coles Lake and can be safely neglected in this study.

Inflow and Outflow (I, Q)

Discharge measurements were made at both the inflow and the outflow stations. The plot between the discharge and the stage of the river is referred to as the stage–discharge relation or rating curve. The plot helps to obtain the discharge by simply reading the stage and finding out the corresponding discharge. That is, measurement of discharge involves a two-step procedure. First, the development of the stage–discharge relationship, and, second, obtaining the corresponding discharge for each stage. Unfortunately, it was not possible to use the stage–discharge relationship to measure the streamflow because of beaver dams. Since these structures blocked water, the water level recorded by transducers in July, August and September mostly stayed the same. As a result of this natural phenomenon, water levels were raised in the upstream stage, and therefore rendered the rating curve invalid. In light of this challenge, an alternative method to obtaining representative streamflow data was employed. To compute the amount of discharge, the streamflow data from the Emile Creek and two Coles Lake stations was compared. The Emile Creek hydrometric station is located about 4 km downstream from Coles Lake. Four days of onsite discharge measurements of inflow and outflow using the mid-point method were correlated with data for the same day from the Emile Creek station. A high degree of correspondence is demonstrated between the Emile Creek station and each of the inflow and outflow stations. The high correlation coefficients show that discharge measurements are consistent (Table 1).

The obtained regression allowed extrapolation of the daily discharges (I = 106.6 mm and Q = –198.5 mm) at each site for each day of the study period. The total amount of water withdrawal is zero because there was no water extracted during this study period due to low natural gas prices (Quicksilver Resources Canada Inc., pers. comm., 2013). The final result of the Coles Lake water balance compo-

Table 1. The t- and p-values between Coles Lake and Emile Creek stations with the computed Pearson's product-moment correlation coefficients. The t-value reflects the value of the 't' test statistic for the test, and the p-value reflects whether the significance of the correlation (<0.05) is significant.

	t-value	p-value	Correlation
Between inflow station and Emile Creek station	9.39	0.011	0.99
Between outflow station and Emile Creek station	9.78	0.010	0.99

Table 2. Summary of water balance components, hydrological year 2013–2014, Coles Lake, northeastern British Columbia.

Component	Total (mm)
Rainfall (R)	243.9
Snowfall (S)	167.4
Inflow (I)	106.6
Outflow (Q)	-198.5
Evaporation (E)	-148.6
Groundwater (G)	In progress
Water withdrawal (W)	0
Change in stored water (ΔS)	In progress

nents are listed in Table 2. Assessment of the interactions between lake and shallow groundwater is in progress.

Summarys

The main goal of this project is to advance and improve the knowledge of the hydrological cycle in northeastern BC and to estimate the water balance for Coles Lake. In this paper, the water budget for Coles Lake is quantified including its inputs, outputs and storage terms. However, the contribution of shallow groundwater as the last remaining hydrological component of the water budget is yet to be quantified. Once the 2013–2014 water budget for Coles Lake is completed, it will be placed into its historical context using a hydrological model—MIKE SHE (DHI Water & Environment, 2007). These historical results will be compared to other watersheds to investigate the differences/similarities of the Coles Lake watershed with the other watersheds in the northeastern region.

The results of this research can be considered a good source of knowledge for decision-makers to better understand water fluxes of Coles Lake (and similar water bodies in northeastern BC). The aim is to determine how much freshwater can be extracted by oil and gas operations by forecasting balance thresholds and avoiding the over-allocation of local water resources.

Acknowledgments

References

Canadian Association of Petroleum Producers (2015): Canadian oil and natural gas; Canadian Association of Petroleum Producers website, URL <http://www.capp.ca/canadian-oil-and-natural-gas> [September 2015].

Chapman, A., Kerr, B. and Wilford, D. (2012): Hydrological modelling and decision-support tool development for water allocation, northeastern British Columbia; in Geoscience BC Summary of Activities 2011, Geoscience BC, Report 2012-1, p. 81–86.

DeLong, C., Banner, A., MacKenzie, W.H., Rogers, B.J. and Kaytor, B. (2011): A field guide to ecosystem identification for the boreal white and black spruce zone of British Columbia; BC Ministry of Forests, Lands and Natural Resource Operations, BC Land Management Handbook No. 65, 250 p., URL <www.for.gov.bc.ca/hfd/pubs/Docs/Lmh/Lmh65.htm> [August 2013].

Déry, S.J., Taylor, P.A. and Xiao, J. (1998): The thermodynamic effects of sublimating, blowing snow in the atmospheric boundary layer; Boundary-Layer Meteorology, v. 89, no. 2, p. 251–283.

DHI Water & Environment (2007): MIKE SHE user manual, volume 2: reference guide; DHI Water & Environment, Horsholm, Denmark, 386 p.

Golder Associates (2010): Surface water study – Horn River Basin; draft report prepared for BC Ministry of Natural Gas Development, Oil and Gas Division, 61 p., URL <http://www.geosciencebc.com/i/pdf/RFP/App2_Water_Supply_in_HRB_Mar31_2010_1.pdf> [November 2015].

Granger, R.J. (1991): Evaporation from natural non saturated surfaces; Ph.D. thesis, University of Saskatchewan, 141 p.

Huntley, D., Hickin, A., and Chow, W. (2011): Surficial geology, geomorphology, granular resource evaluation and geohazard assessment for the Maxhamish Lake map area (NTS 94-O), northeastern British Columbia; Geological Survey of Canada, Open File 6883, 20 p., doi:10.4095/289306

Johnson, E. (2010): Conceptual water model for the Horn River Basin, northeast British Columbia (NTS 094O, parts of 094P, J); Geoscience Report 2010, BC Ministry of Natural Gas Development, p. 99–121.

Kabzems, R., D'Aloia, M., Rex, J., Geertsema, M., Maloney, D. and MacKenzie, W. (2012): Monitoring indicators of wetland dynamics and hydrologic function in Fort Nelson watersheds; unpublished report prepared for BC Ministry of Forest, Lands and Natural Resource Operations, 26 p.

Winkler, R.D., Moore, R.D., Redding, T.E., Spittlehouse, D.L., Carlyle-Moses, D.E. and Smerdon, B.D. (2010): Hydrologic processes and watershed; in Compendium of Forest Hydrology and Geomorphology in British Columbia, R.G. Pike, T.E. Redding, R.D. Moore, R.D. Winkler and K.D. Bladon (ed.), BC Ministry of Forests, Lands and Natural Resource Operation and FORREX Forum for Research and Extension in Natural Resources, BC Land Management Handbook 66, v. 1, p. 133–177.

Integration of Surface Regolith Mapping and Soil Field Measurements with Geochemistry in a Till-Covered Terrain, Lara Volcanogenic Massive-Sulphide Deposit, Southern Vancouver Island (NTS 092B/13)

M.M. Bodnar, Mineral Deposit Research Unit, University of British Columbia, Vancouver, BC, mbodnar@eos.ubc.ca

P.A. Winterburn, Mineral Deposit Research Unit, University of British Columbia, Vancouver, BC

Introduction

A technical challenge faced by mineral exploration is the detection of mineral deposits buried under younger exotic geological units. Conventional surface-media geochemical methods using strong acid digestion examines endogenic mineral particles. Sample types such as soil, stream sediment and till are capable of detecting a primary metal signal that has been eroded and dispersed from a bedrock source (McClenaghan and Cabri, 2011); however, this method may not be appropriate if mineralization is buried by thick or complex cover (Eppinger et al., 2013).

Advances in analytical equipment have made accessible relatively rapid and affordable multi-element analyses with reduced lower detection limits. Using weak acid digestions and selective extractions, subtle geochemical signatures have been shown as accumulations of labile ions thought to be weakly bonded to components in the soil (Cameron et al., 2004; Kelley et al., 2006; Hamilton, 2007; Aspandiar et al., 2008; van Geffen et al., 2012). The authors propose that the labile ions migrate vertically from an oxidizing sulphide body by a combination of mechanisms including electrochemical transport, diffusion and gaseous or biological activity, eventually accumulating near the surface (Figure 1; Aspandiar et al., 2008; Anand et al., 2016). While anomalous responses have been observed above buried mineral deposits, there remains a fundamental lack of understanding of the processes that control ion dispersion. Identification of these processes will improve survey design and analyses and interpretation of geochemical datasets, including the recognition of misleading or false positive signatures and situations where false negatives may arise.

The total concentration of a trace element at surface is a function of many factors that promote or inhibit ion mobility. These factors include overburden chemistry (redox state, pH) and texture, surface vegetation, topography and hydrology. As part of the Exploration Geochemistry Initiative at the Mineral Deposit Research Unit (MDRU) at the University of British Columbia (UBC), ongoing research will map major-, minor- and trace-element distribution at the surface above a massive-sulphide target to identify the processes and controls on labile ion mobility. This research is a study of processes with widely applicable results. This paper will describe surface regolith mapping and soil sampling fieldwork completed in May–September 2015.

Background

Research is centred on the Lara volcanogenic massive-sulphide (VMS) deposit in the Cowichan Valley Regional District of southern Vancouver Island (NTS 092B/13; Figure 2). The landscape is characterized by moderately rugged mountains (1000–1200 m) flanking the Sully creek valley (600 m). The area is covered by an approximately 70 year old mature second-growth forest with a 125 m wide clearing down the axis of the valley for a high-voltage electric power transmission line.

The Lara VMS deposit was selected for this study on the basis of satisfying three criteria: sulphide mineralization in bedrock; widespread, relatively uniform surface cover; and minimal anthropogenic surface disturbance. Available geographic and drillhole data was consulted in order to select the optimal sampling area with proven mineralization and the least surface disturbance.
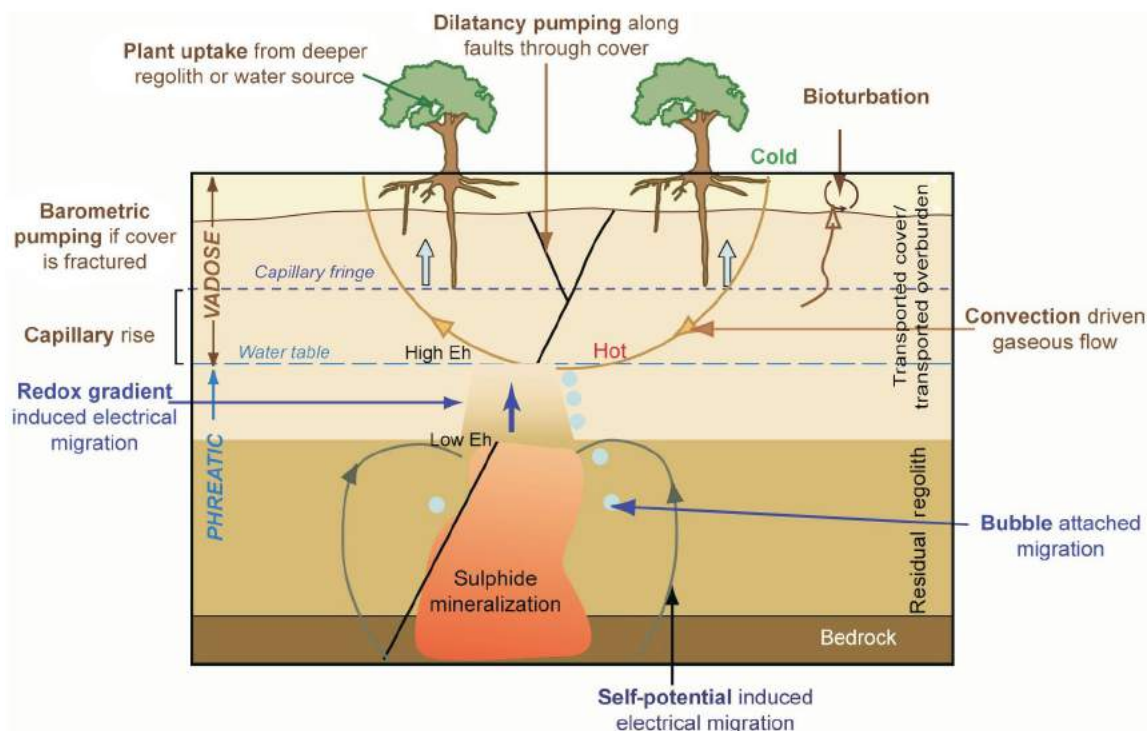
Bedrock Geology

The Lara deposit (MINFILE 092B 129: BC Geological Survey, 2015) is an unmined Zn-Cu-Pb resource hosted in the mid-Paleozoic Sicker Group volcanic rocks of the Wrangell terrane (Massey, 1995a, b; Yorath et al., 1999). The rocks underlying the study area comprise intermediate to felsic volcanic and fine-grained tuffaceous volcani-
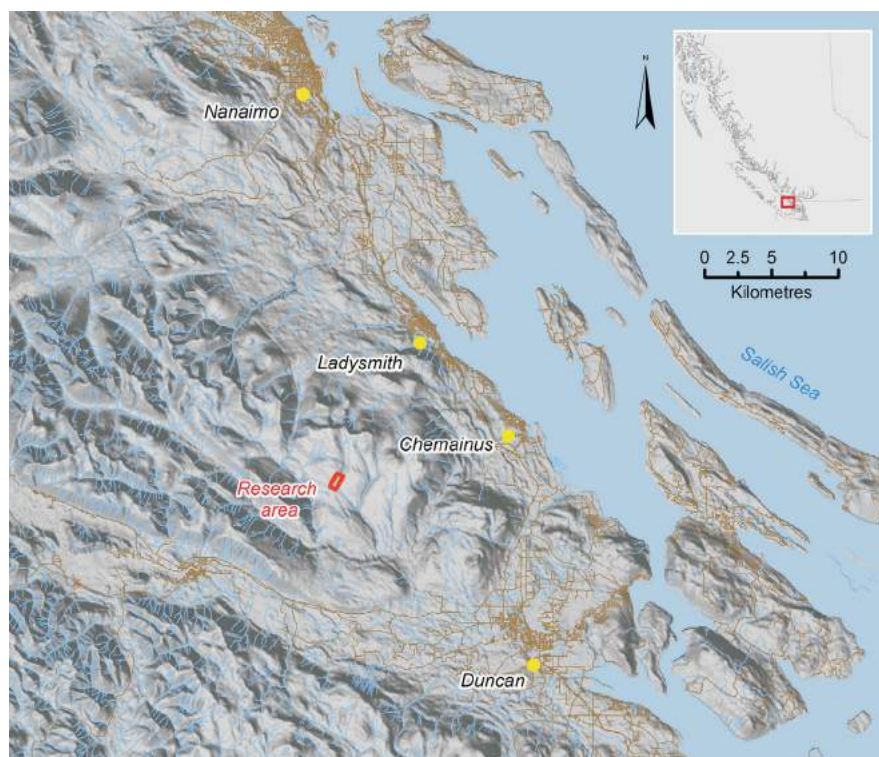
Figure 1. Schematic of proposed mechanisms of element migration in a buried mineralization setting (Aspandiar et al., 2008).


Figure 2. Location of the research area (outlined in red).

clastic rocks of the McLaughlin Ridge Formation intruded by late Triassic dikes and sills of the Mount Hall gabbro (Figure 3; Massey, 1995a, b). Mineralization is hosted within the McLaughlin Ridge Formation, which also hosts numerous other VMS showings along strike. The current indicated resource of approximately 1.2 Mt at 3% Zn, 1% Cu, 0.6% Pb, 33 g/t Ag and 2 g/t Au at a 1% Zn cut-off is hosted by strongly silicified, coarse-grained rhyolite crystal tuff and ash tuff (Kelso et al., 2007). Mineralization comprises banded and laminated accumulations of sulphide minerals up to 16 m thick with occasional sulphide stringers and breccia with a sulphide matrix. Disseminated sulphide minerals are also noted in hostrocks. Historical trenching along strike from the study area identified a massive-sulphide lens with 25 g/t Au, 500 g/t Ag, 3% Cu, 43% Zn and 8% Pb over 3.5 m. (Kelso et al., 2007). Mapping by Ruks et al. (2008) further described the local mineralization as dark grey to black, medium-grained massive sulphides dominated by black sphalerite with lesser chalcopyrite and pyrite with scattered 2 cm by 10 cm carbonate blebs hosted by intensely silica-sericite–altered felsic ash tuff.

Surficial Geology

The Quaternary sediments of southern Vancouver Island record a dynamic glacial history. Up to three glacial advances and interglacial periods have deposited and locally reworked sediments across the region (Mathews et al., 1970; Armstrong and Clague, 1977; Alley, 1979; Alley and Chatwin, 1979; Clague et al., 1980). The surficial materials in the study area potentially range in age from >125 000 to 15 000 years BP but most were likely deposited during the Vashon stage of the Fraser Glaciation (25 000–15 000 years BP; van Vliet et al., 1987; Easterbrook, 1992). The area is considered to have been free of ice by about 13 000 years BP (Alley and Chatwin, 1979). The study area is characterized by a blanket of basal till in the valley base; till mixed with colluvium is interpreted to dominate the upslope regions (Blyth and Rutter, 1993). Overburden cover is between 2 and 15 m thick based on drill records (Kapusta et al., 1987).
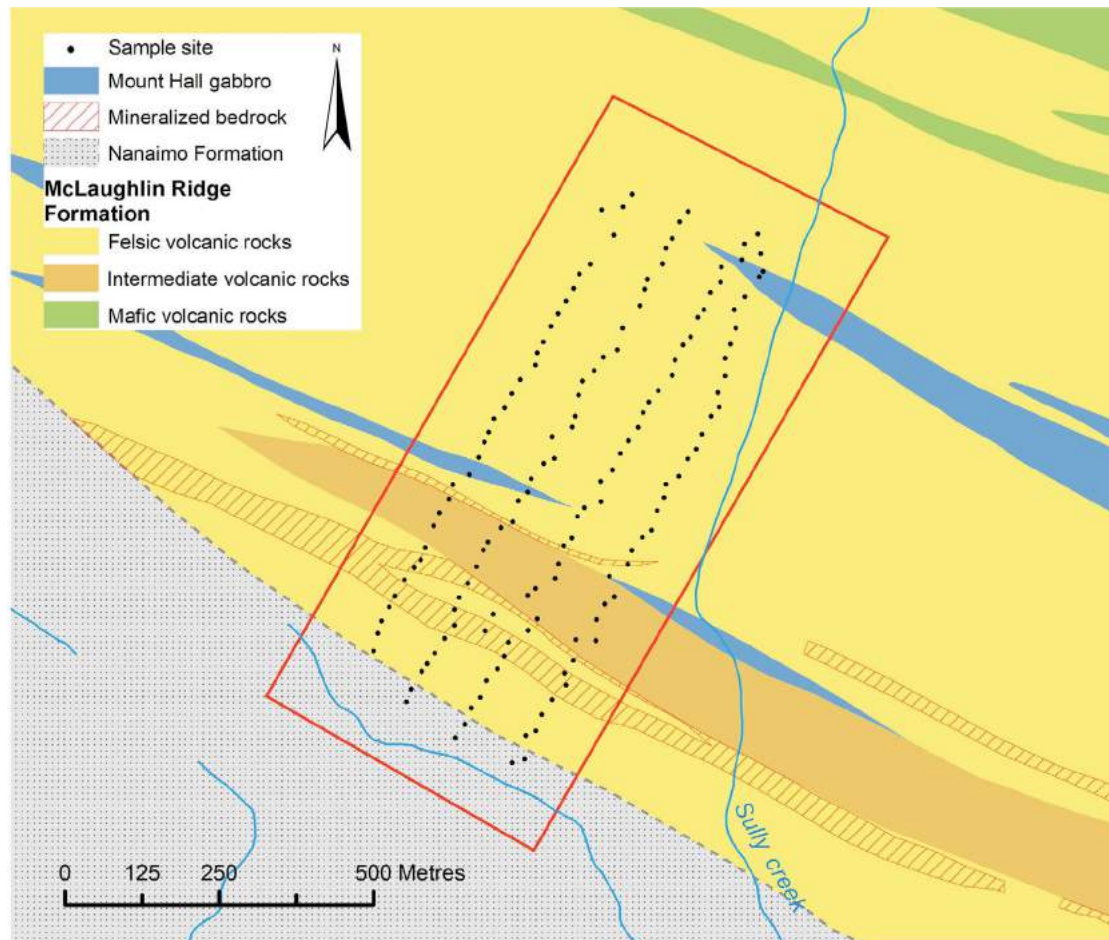
Figure 3. Geology of the study area with interpreted surface projection of mineralized bedrock (after Wetherup, 2010). Soil sample locations are shown as dots. Place names with the generic in lower case are unofficial.

Research Project

Fieldwork was undertaken to support the following research objectives:

- identify the processes and controls on labile ion mobility
- identify processes contributing to false positive or false negative signatures
- develop a process-based model of trace-element dispersion in the near-surface environment above massive-sulphide mineralization

The following work was completed to characterize the composition and variability in the surface environment and characterize the chemistry and physical properties of the shallow soil.

Surface Mapping

Comprehensive surface mapping was completed prior to the soil sampling program. An area of approximately 0.6 km^2 was included in this exercise, with a 100 m buffer beyond the proposed limits of sampling. Airphoto and geographic data from the TRIM database were used for preliminary mapping and fieldwork strategy, with a total of five days of field data collection.

A series of traverses were completed along the boundary of the study area and proposed sampling lines to map glacial sediments, geomorphology, dominant vegetation and anthropogenic disturbances. Mapping was done directly into mobile GIS software with integrated global navigation satellite system (GNSS) positioning. A total of 48 surface pits and roadcut sections were compiled to generate a map of major surficial domains that were used to modify soil sampling locations as appropriate. The mapped units were further refined following sampling, adding a further 150 control points.

The area is densely vegetated by Douglas fir with lesser western hemlock and western red cedar tree cover. Fern, salal and Oregon grape bushes cover much of the exposed forest floor. Rare 20 by 50 m stands of cedar provide a distinctive surface environment of relatively little sunlight exposure, loose litter or floor vegetation. Alder is the sole broadleaf tree growing in recent clearings or large drainages where sunlight and moisture are readily available.

Four domains of surficial material are observed in the study area (Figure 4): the original till blanket making up the residual surface, erosional gullies and depositional materials (fluvial and alluvial deposits). All materials have been modified by anthropogenic activity.

Till

The prevailing material at the surface is a basal till blanket. This unit is relatively unmodified from original deposition except for localized overturn by fallen trees. The till is poorly sorted with mixed clasts of variable grain size and angularity. Locally derived felsic volcanic clasts are generally angular due to their schistose fabric and rarely exceed 10 cm in diameter. The remaining clasts are a mixture of subangular to rounded granodiorite, gabbro and siltstone up to 30 cm in diameter. Although most locations indicate a massive till blanket, one roadcut section revealed a 30 cm bed of coarse sand between till blankets, suggesting intermittent local fluvial activity (Figure 5). A bed of well-sorted coarse sand between till blankets may alter the local hydraulic regime.

Erosional Gullies

Erosional gullies are generally steep (~45°) with patchy salal bush cover and exposed soil. Profiles within the erosional slope reveal a mixture of oxidized B horizon with patches of less oxidized relict C horizon, suggesting reworking with downslope movement. This latter till appears to bury antecedent masses of roots. Soil sampling was avoided in drainage gullies due to the recent reworked surface materials.

Fluvial Deposits

Fluvial deposits were observed in the active Sully creek channel and in a smaller stream that crosses the southwestern corner of the map area. These deposits are composed of boulders, cobbles, pebbles and sand deposited in a braided channel. This unit is considered to represent the coarse lag of till slumping into the creek channel where clay and silt are carried downstream. Bedrock exposures were observed in the Sully creek gully basin. Sampling this unit was avoided due to the recent reworked surface materials.

Alluvial Deposits

Alluvial deposits was the most difficult unit to recognize in the field. Located near the base of hill slopes where slope angle decreases, alluvial sand and gravel appeared to be a result of seasonal water flow as a network of channels across the forest floor (Figure 6). These networks begin at the terminus of erosional gullies representing the redeposition of material from the erosional gully slope. Samples were not collected in obvious corridors of water flow and deposition.

Anthropogenic Clearings

Anthropogenic activity was evident across the research site as decomposing tree stumps from logging old-growth forest are common. Clearings younger than the second-growth forest could be identified by alder and thick fern with a lack of coniferous forest. Road berms and clearings from previous logging activities and more recent exploratory drilling were mapped in detail to guide sample placement. Most drillhole locations are clearly marked with a labelled sign and casing removed.
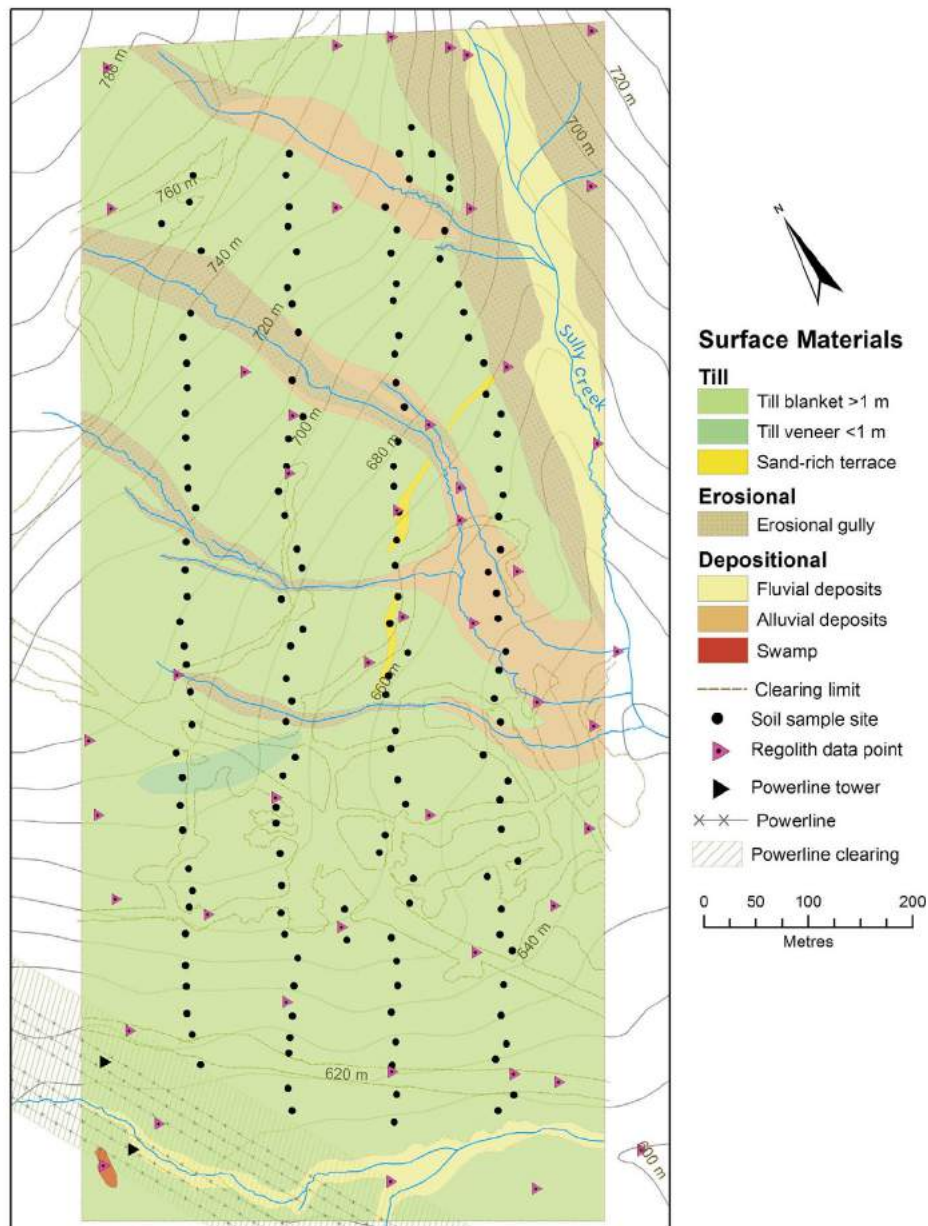
Figure 4. Preliminary map of surficial materials in the research area. Place names with the generic in lower case are unofficial.

Soil Profiles

Soil profiles are well developed with notable variability in horizon thicknesses. Many sites show an excellent O-Ah-Ae-B-C progression (Figure 7a, b); however, complex profiles were occasionally noted (Figure 7c, d). Development of a grey-white powdery Ae horizon appeared to preferentially form around larger root systems and follow along the surface of boulders 2–8 cm below the general base of the Ae horizon.

Sampling and Field Measurements

The sampling grid included four lines, 100 m apart, and was approximately 1 km long with soil samples collected at 25 m intervals. The grid was designed to cut mineralization perpendicular to strike and cover the hostrocks. By crosscutting different hostrock types (mafic to felsic), additional insights into the formation of false anomalies may be identified. At each sample site a suite of in situ and slurry-based physical properties were measured. The first measurements taken were electrical conductivity (EC), soil moisture and pH of the undisturbed pit wall in each of the soil horizons (Figure 8a).

Samples were then collected from the upper B horizon at the pit wall. The B-horizon soil was chosen because it is consistently present and suited to routine sample collection. Using clean nitrile gloves and a nylon trowel, soil was
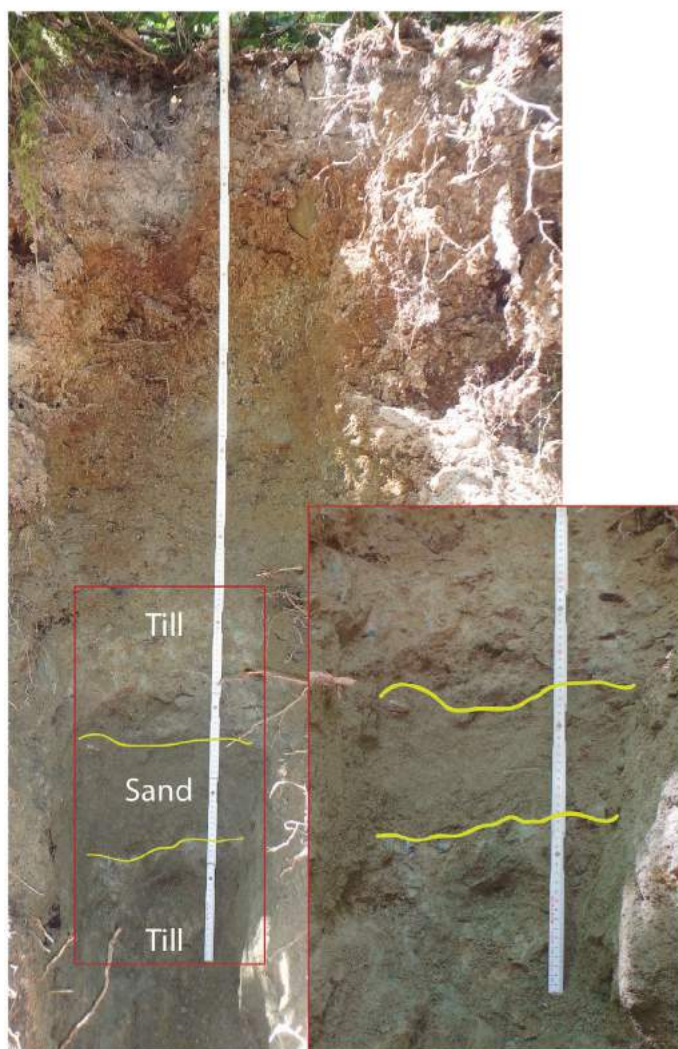
Figure 5. Roadcut section showing a 30 cm bed of well-sorted, coarse sand between till. Total pit depth is 160 cm; the top of the sand layer is 120 cm from the top of the pit. Note the extended weathering profile, including a mottled transitional zone between B and C horizons.

Figure 6. Typical shallow-angle gravel depositional channel.

removed from between 3 and 13 cm below the base of the Ae horizon. The soil was sieved to –6.3 mm using a stainless steel screen until approximately 1.5 kg was collected. A small air-tight zip polythene bag of sieved material (~500 g) was collected for hydrocarbon analysis and a second was collected for microbial analysis (Figure 8b). A further 60 ml was taken for slurry-based measurements and the remainder packaged for chemical analysis in a polythene bag sealed by zip tie. Oxidation-reduction potential (ORP), pH, pH following acidification, total dissolved solids (TDS) and free chlorine measurements were taken on 1:1 de-ionized water:soil slurries (Figure 8c).

Samples were submitted to ALS Minerals (North Vancouver, BC) for drying at <60°C, screening to –180 µm followed by multi-element inductively coupled plasma–mass spectrometry (ICP-MS) analysis with aqua-regia digestion and again with de-ionized water extraction. A split of the original sample and the screened fraction was retained for further research. Total organic carbon of the 180 µm fraction was measured by combustion furnace and infrared spectrometry at ALS Minerals. Samples for hydrocarbon and microbial analysis have been retained by the authors for further research.

Soil Hydrocarbon Measurements

A passive hydrocarbon collection module was deployed at each sample location. The module is composed of activated carbon wrapped in waterproof but vapour-permeable expanded polytetrafluoroethylene (ePTFE) tubing (Anderson, 2006). A narrow punch was used to penetrate the soil at the base of the sample pit. The modules were inserted in a vertical orientation and covered with soil. After 60 days, the modules were recovered, placed in air-tight glass vials and submitted for analysis of up to C_{20} hydrocarbons at Amplified Geochemical Imaging (Newark, Delaware, United States).

Self-Potential Survey

Self-potential describes naturally occurring electrical fields at the Earth's surface, useful for identifying bodies of sulphide mineralization at depth. A 4175 m line survey was conducted over the research area using a pair of nonpolarizing Cu-CuSO$_4$ porous ceramic electrodes, 1000 m of 12-gauge cable and a high-impedance voltmeter. A base electrode was installed at the north corner of the site and a second roving electrode was moved to each sample location downslope. Normal- and reverse-polarity resistance and DC voltage measurements were recorded. Each sampling line was surveyed separately followed by tie lines at the top and bottom of the survey. Due to a high-voltage electrical
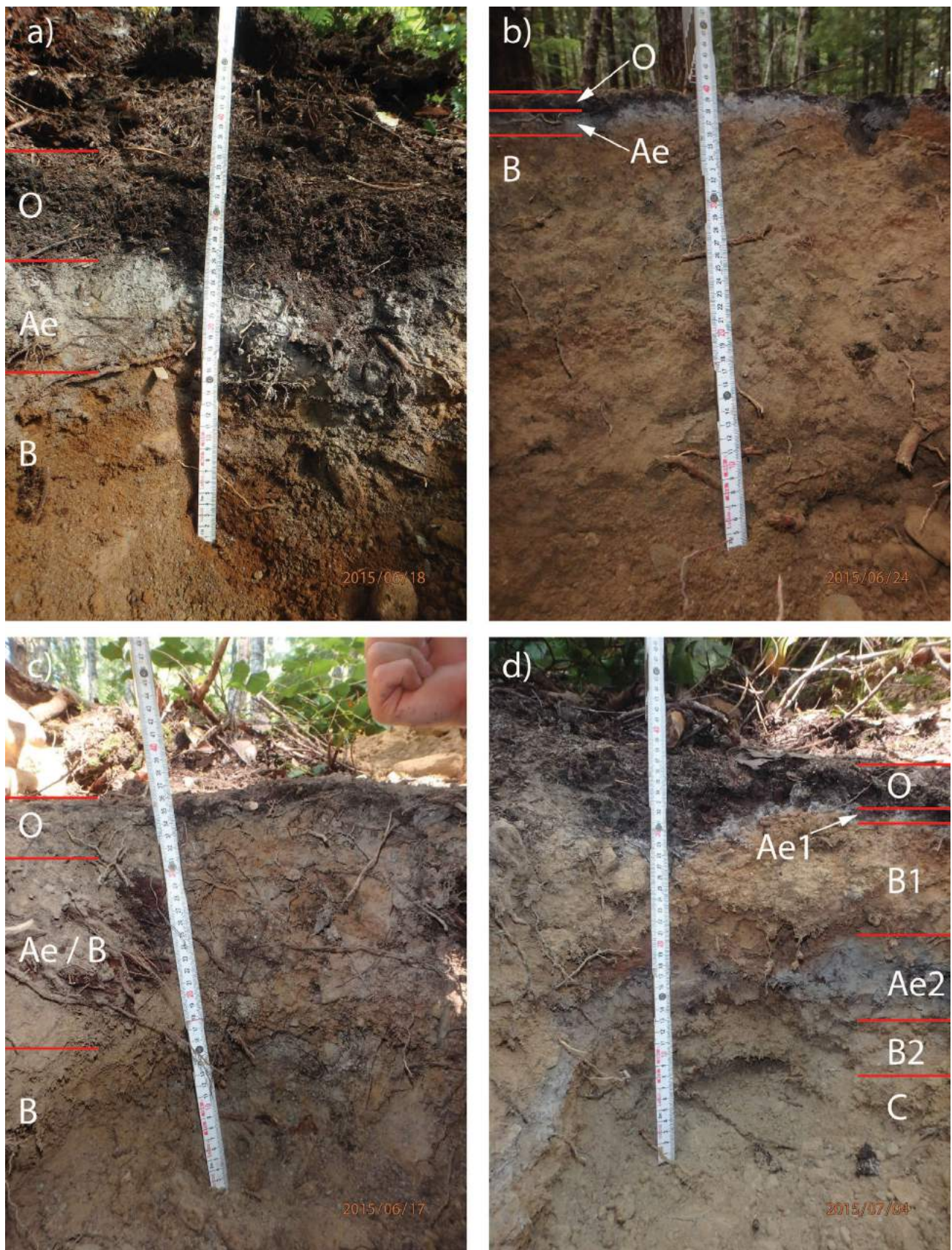
Figure 7. Variability in soil profile development: **a)** a typical idealized profile; **b)** a similar profile with less organic surface litter; **c)** a poorly developed soil profile; **d)** the rare occurrence of duplicated horizons.

Figure 8. Sampling procedure: **a)** the direct soil measurement of electrical conductivity; **b)** a completed sample with the pit showing a portion of the B horizon removed; **c)** slurry-based measurements in the field, including free chlorine on the left and pH on the right.

transmission line at the southern end of the grid, additional processing is required to reduce or eliminate noise.

Conclusions and Future Work

Mapping the surficial materials present in the research area prior to sampling was valuable in eliminating inappropriate areas of younger reworked material. Future work will integrate the field observations and measurements with analytical results to evaluate the chemical variability of the surface environment unrelated to the presence of mineralization and, hence, clarify the anomalous response above mineralization. Additional sampling of selected sites for vegetation and other horizons will be undertaken to clarify potential anomaly formation mechanisms. The research will be completed in August 2016.

Acknowledgments

References

Alley, N.F. (1979): Middle Wisconsin stratigraphy and climatic reconstruction, southern Vancouver Island, British Columbia; Quaternary Research, v. 11, p. 213–237.

Alley, N.F. and Chatwin, S.C. (1979): Late Pleistocene history and geomorphology, southwestern Vancouver Island, British Columbia; Canadian Journal or Earth Sciences, v. 16, p. 1645–1657.

Anand, R.R., Aspandiar, M.F. and Noble, R.R.P. (2016): A review of metal transfer mechanisms through transported cover with emphasis on the vadose zone within the Australian regolith; Ore Geology Reviews, v. 73, no. 3, p. 394–416, doi:10.1016/j.oregeorev.2015.06.018

Anderson, H. (2006): Amplified geochemical imaging: an enhanced view to optimize outcomes; in First Break, EAGE, v. 24, p. 77–81, URL <https://www.agisurveys.net/uploads/Amplified_small.pdf> [November 2015].

Armstrong, J.E. and Clague, J.J. (1977): Two major Wisconsin lithostratigraphic units in southwest British Columbia; Canadian Journal of Earth Sciences, v. 14, p. 1471–1480.

Aspandiar, M.F., Anand, R.R. and Gray, D.J. (2008): Geochemical dispersion mechanisms through transported cover: implications for mineral exploration in Australia; Cooperative Research Centre for Landscape Environments and Mineral Exploration (CRC-LEME), Commonwealth Scientific and Industrial Research Organisation (CSIRO) Open File Report 246, 84 p., URL <http://crcleme.org.au/Pubs/OPEN%20FILE%20REPORTS/OFR246/OFR246.pdf> [November 2015].

BC Geological Survey (2015): MINFILE BC mineral deposits database; BC Ministry of Energy and Mines, URL <http://minfile.ca/> [October 2015].

Blyth, H.E. and Rutter, N.W. (1993): Quaternary geology of southeastern Vancouver Island and Gulf Islands (92B/5, 6, 11, 12, 13 and 14); in Geological Fieldwork 1992, BC Ministry of Energy and Mines, Paper 1993-1, p. 407–413, URL <http://www.empr.gov.bc.ca/Mining/Geoscience/PublicationsCatalogue/Fieldwork/Documents/1992/407-414-blyth.pdf> [October 2015].

Cameron, E.M., Hamilton, S.M., Leybourne, M.I., Hall, G.E.M. and McClenaghan, M.B. (2004): Finding deeply buried deposits using geochemistry; Geochemistry Exploration Environment Analysis, v. 4, p. 7–32.

Clague, J.J., Armstrong, J.E. and Mathews, W.H. (1980): Advance of the late Wisconsin Cordilleran Ice Sheet in southern British Columbia since 22,000 yr B.P.; Quaternary Research, v. 13, p. 322–328.

Easterbrook, D.J. (1992): Advance and retreat of Cordilleran Ice Sheets in Washington, U.S.A.; Géographie Physique et Quaternaire, v. 46, p. 51–68.

Eppinger, R.G., Fey, D.L., Giles, S.A., Grunsky, E.C., Kelley, K.D., Minsley, B.J., Munk, L. and Smith, S.M. (2013): Summary of exploration geochemical and mineralogical studies at the Giant Pebble porphyry Cu-Au-Mo deposit, Alaska: implications for exploration under cover; Society of Economic Geologists, v. 108, p. 495–527.

Hamilton, S.M. (2007): Major advances in soil geochemical exploration methods for areas of thick glacial drift cover: advances in prospect-scale geochemical methods; in Proceedings of Exploration 07: Fifth Decennial International Conference on Mineral Exploration, p. 263–280.

Kapusta, J.D., Blackadar, D.W. and McLaughlin, A.D. (1987): 1987 Report for drilling conducted on the Lara group 1 and Lara group 2; BC Ministry of Energy and Mines, Assessment Report 17 857, 873 p., URL <https://aris.empr.gov.bc.ca/search.asp?mode=repsum&rep_no=17857> [November 2015].

Kelley, D.L., Kelley, K.D., Coker, W.B., Caughlin, B. and Doherty, M.R. (2006): Beyond the obvious limits of ore deposits: the use of mineralogical, geochemical, and biological features for the remote detection of mineralization; Society of Economic Geologists, v. 101, p. 729–752.

Kelso, I., Wetherup, S. and Takats, P. (2007): Independent technical report and mineral resource estimation, Lara polymetallic property, British Columbia, Canada; unpublished company report prepared by Caracle Creek International Consulting for Laramide Resources Ltd, URL <http://www.sedar.com/GetFile.do?lang=EN&docClass=24&issuerNo=00003540&fileName=/csfsprod/data85/filings/01191450/00000001/v%3AAPOLLOLAM-Technical-Report.pdf> [December 2015]

Massey, N.W.D. (1995a): Geology and mineral resources of the Duncan sheet, Vancouver Island 92B/13; BC Ministry of Energy and Mines, Paper 1992-4, 112 p., URL <http://www.empr.gov.bc.ca/Mining/Geoscience/PublicationsCatalogue/Papers/Documents/Paper1992-4.pdf> [November 2015].

Massey, N.W.D. (1995b): Geology and mineral resources of the Cowichan Lake sheet, Vancouver Island 92C/16; BC Ministry of Energy and Mines, Paper 1992-3, 112 p., URL <http://www.empr.gov.bc.ca/Mining/Geoscience/PublicationsCatalogue/Papers/Documents/Paper1992-3.pdf> [November 2015].

Mathews, W.H., Fyles, J.G. and Nasmith, H.W. (1970): Postglacial crustal movements in southwestern British Columbia and adjacent Washington State; Canadian Journal of Earth Sciences, v. 7, p. 690–702.

McClenaghan, M.B. and Cabri, L.J. (2011): Review of gold and platinum group element (PGE) indicator minerals methods for surficial sediment sampling; Geochemistry Exploration Environment Analysis, v. 11, p. 251–263.

Ruks, T., Mortensen, J.K. and Cordey, F. (2008): Preliminary results of geological mapping, uranium-lead zircon dating, and micropaleontological and lead isotopic studies of volcanogenic massive sulphide–hosting stratigraphy of the Middle and Late Paleozoic Sicker and Lower Buttle Lake groups on Vancouver Island, British Columbia (NTS 092B/13, 092C/16, 092E/09, /16, 092F/02, /07); in Geoscience BC Summary of Activities 2008, Geoscience BC, Report 2009-1, p. 103–122, URL <http://www.geosciencebc.com/i/pdf/SummaryofActivities2008/SoA2008-Ruks_original.pdf> [November 2015].

van Geffen, P.W.G., Kyser, T.K., Oates, C.J. and Ihlenfeld, C. (2012): Till and vegetation geochemistry at the Talbot VMS Cu-Zn prospect, Manitoba, Canada: implications for mineral exploration; Geochemistry Exploration Environment Analysis, v. 12, p. 67–68.

van Vliet, L.J.P., Green, A.J. and Kenney, F.A. (1987): Soils of the Gulf Islands of British Columbia – soils of Saltspring Island; Agriculture Canada, Report 43, v. 1.

Wetherup, S. (2010): Structural mapping and whole rock geochemical sampling, Lara polymetallic property. Lara polymetallic property, British Columbia, Canada; BC Ministry of Energy and Mines, Assessment Report 31 578, 58 p., URL <https://aris.empr.gov.bc.ca/search.asp?mode= repsum&rep_no=31578> [November 2015].

Yorath, C.J., Sutherland Brown, A. and Massey, N.W.D. (1999): LITHOPROBE, southern Vancouver Island, British Columbia: geology; Geological Survey of Canada, Bulletin 498, 145 p.

Facies Analysis and Ichnology of the Upper Montney Formation in Northeastern British Columbia

A.E. Gegolick, University of Alberta, Edmonton, AB, agegolic@ualberta.ca

C.M. Furlong, University of Alberta, Edmonton, AB

T.L. Playter, University of Alberta, Edmonton AB

D.T. Prenoslo, University of Alberta, Edmonton, AB

M.K. Gingras, University of Alberta, Edmonton, AB

J.-P. Zonneveld, University of Alberta, Edmonton, AB

Introduction

The Lower Triassic Montney Formation is a world-class unconventional hydrocarbon reservoir hosted primarily in low-permeability siltstone and to a lesser extent, very fine grained sandstone. To date, most published research has focused on conventional plays in the eastern part of the basin, such as the Montney Formation turbidite interval and shoreface clastic and bioclastic units proximal to the Triassic subcrop edge (Davies et al., 1997; Moslow, 2000; Zonneveld et al., 2010a). These targets have been explored since the 1950s (Zonneveld et al., 2010a), whereas the low-permeability siltstone that constitutes the bulk of the Montney Formation was largely overlooked. Over the past decade, however, advances in horizontal drilling and multistage hydraulic fracturing made it possible to exploit hydrocarbons from this unconventional siltstone reservoir (National Energy Board et al., 2013). As a result, British Columbia has become a leading province in the exploration and development of unconventional gas resources (BC Oil and Gas Commission, 2012). The Montney Formation is the foremost gas-producing formation in BC and is believed to house 449 trillion cubic feet of marketable natural gas along with high volumes of gas liquids and condensate (National Energy Board et al., 2013).

The processes that control reservoir characteristics in this western unconventional trend are less well known than for plays situated to the east. Despite the relatively restricted grain size, the sedimentary facies of the Montney Formation are very heterogeneous. This refers to the several sedimentological and ichnological factors that result in highly variable reservoir characteristics (e.g., Clarkson et al., 2012; Wood, 2013). Subtle changes in the rock fabric both laterally and vertically result in the compartmentalization of resources within zones of distinctly different porosity and permeability values. Another controlling factor on reservoir properties is the occurrence of bioturbation. Biogenic permeability is important to reservoir properties because it has the ability to either enhance or reduce permeability or porosity (Pemberton and Gingras, 2005; Baniak et al., 2015). Bioturbation can influence the porosity and permeability by changing the distribution of grains and affecting the geochemistry thus affecting diagenetic processes (Gingras et al., 2012). A study done by Wood (2013) identified the degree of bioturbation in relation to the water saturation in the Montney Formation. Upper Montney Formation samples with a higher degree of bioturbation had a higher vertical permeability and water saturation (Wood, 2013). Bioturbated fabrics tend to enhance the permeability and vertical transmissivity of the rock (Pemberton and Gingras, 2005).

The purpose of this study is to understand the variability in bioturbated intervals in the Montney Formation and its affect on the porosity and permeability of this siltstone reservoir. This study will integrate sedimentology, ichnology and petrography from core studies with various petrophysical analyses to develop predictive models.

Regional Setting and Stratigraphy

The Montney Formation was deposited during the early Triassic on the western margin of Pangea (Davies, 1997). The Montney Formation succession in the study area is dominated by fine-grained clastic sediment as a result of an arid climate and long transport distances during the Triassic

(Zonneveld et al., 2011). The Montney Formation is dominated by siltstone and very fine grained sandstone and determining depositional environments is challenging due to this restriction in grain size (Zonneveld et al., 2011). The Montney Formation is laterally extensive, spanning across Alberta and northeastern BC (Figure 1). It reaches thicknesses of over 300 m in the west and thins to 0 m at the subcrop edge in the east (Davies et al., 1997). Armitage (1962) defined Texaco's NFA Buick Creek No. 7 well (L.S. 6, Sec. 26, Twp. 87, Rge. 21, W 6th Mer) as the type well for the Montney Formation. From this well, the Montney Formation was originally described as dark argillaceous siltstone and interbedded shale. It has been interpreted that the Montney Formation in the study area represents deposition in an offshore, basin-centred setting (Gibson and Barclay, 1989; Edwards et al., 1994; Davies et al., 1997). Core studies do not support this interpretation and the upper Montney Formation shows evidence of deposition in a shallow marine environment with most deposition occurring within a couple hundred metres of maximum water depth (Zonneveld et al., 2011).

Different workers have formally and informally assigned the Montney Formation, and units within it, to different stratigraphic levels. Also, correlations can differ significantly across the Alberta and BC border. Thus far no lithostratigraphic subdivision has been widely accepted but for the purpose of this research, the Montney Formation in the study area is divided into the upper and lower Montney Formation (Figure 2). The upper Montney Formation spans from the informally named mid-Montney marker (MMM)

to the base of the Doig phosphate zone. The MMM is interpreted as a flooding surface and it approximates the Smithian–Spathian boundary (Golding et al., 2014). It is easily identifiable on well logs as a sharp increase in gamma-ray levels. The Doig phosphate zone has a very high signal on gamma-ray logs as result of phosphate-rich siltstone (Golding et al., 2014).

Ichnology

The Montney Formation includes the earliest Triassic strata in the subsurface of the Western Canada Sedimentary Basin and provides valuable information about life during the recovery interval after the end of the Permian mass extinction (Zonneveld et al., 2010b). Trace fossils provide a record of in situ activities of infaunal and epifaunal organisms (Zonneveld et al., 2010b). Environmental conditions during this time were stressed and as a result the ichnofossil assemblages observed are characterized by low diversity, high abundance and reduced body size (Zonneveld et al., 2010b).

Bioturbation is important to reservoir properties because it has the ability to either enhance or reduce permeability or porosity (Pemberton and Gingras, 2005; Baniak et al., 2015). In recent literature, ichnology of the Montney Formation has been discussed, however, its affects on reservoir properties has received little attention. Analyzing bioturbated intervals includes the identification of fossil traces, assessment of bioturbation intensities and burrow size (Figure 3).
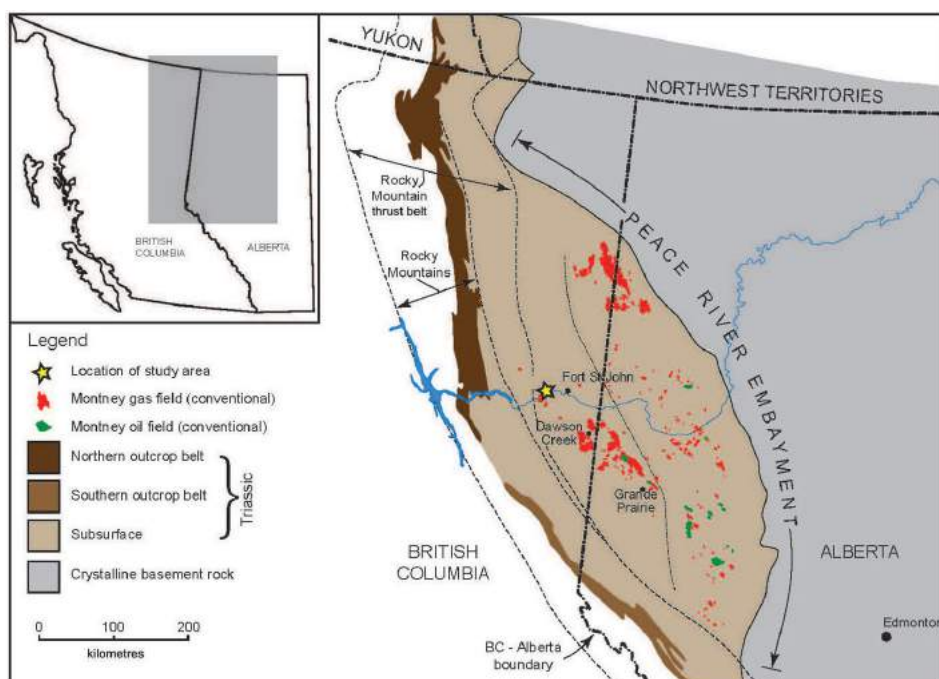
Figure 1. Regional map indicating the extent of Triassic strata in the Western Canada Sedimentary Basin. Montney Formation oil fields, unconventional gas fields and location of the study area are indicated. Figure modified from Zonneveld et al. (2011).
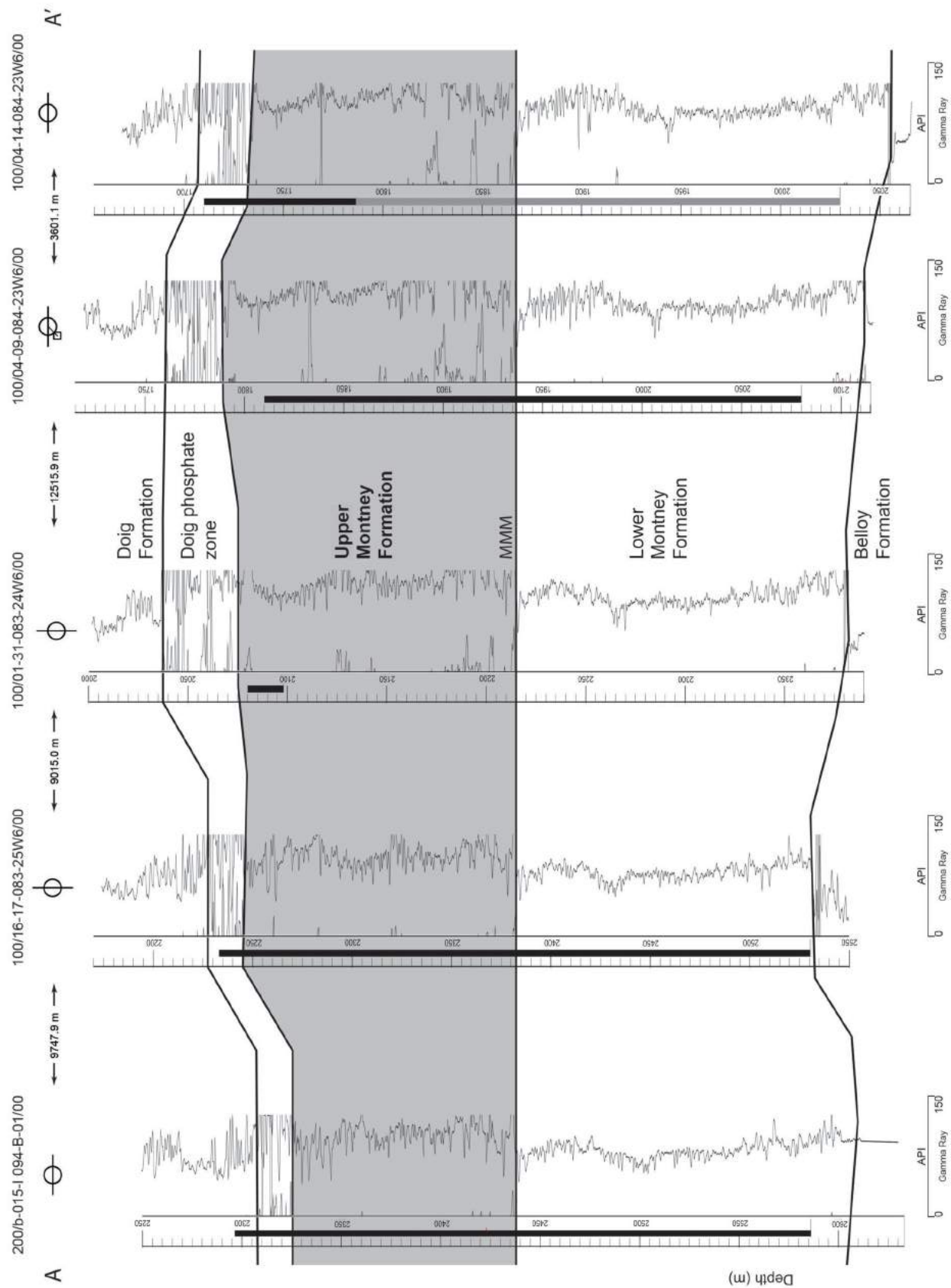
Figure 2. Well-log cross-section through study area indicating log picks informally designating the upper Montney Formation, northeastern British Columbia. See Figure 4 for cross-section location. Abbreviation: MMM, mid-Montney marker.
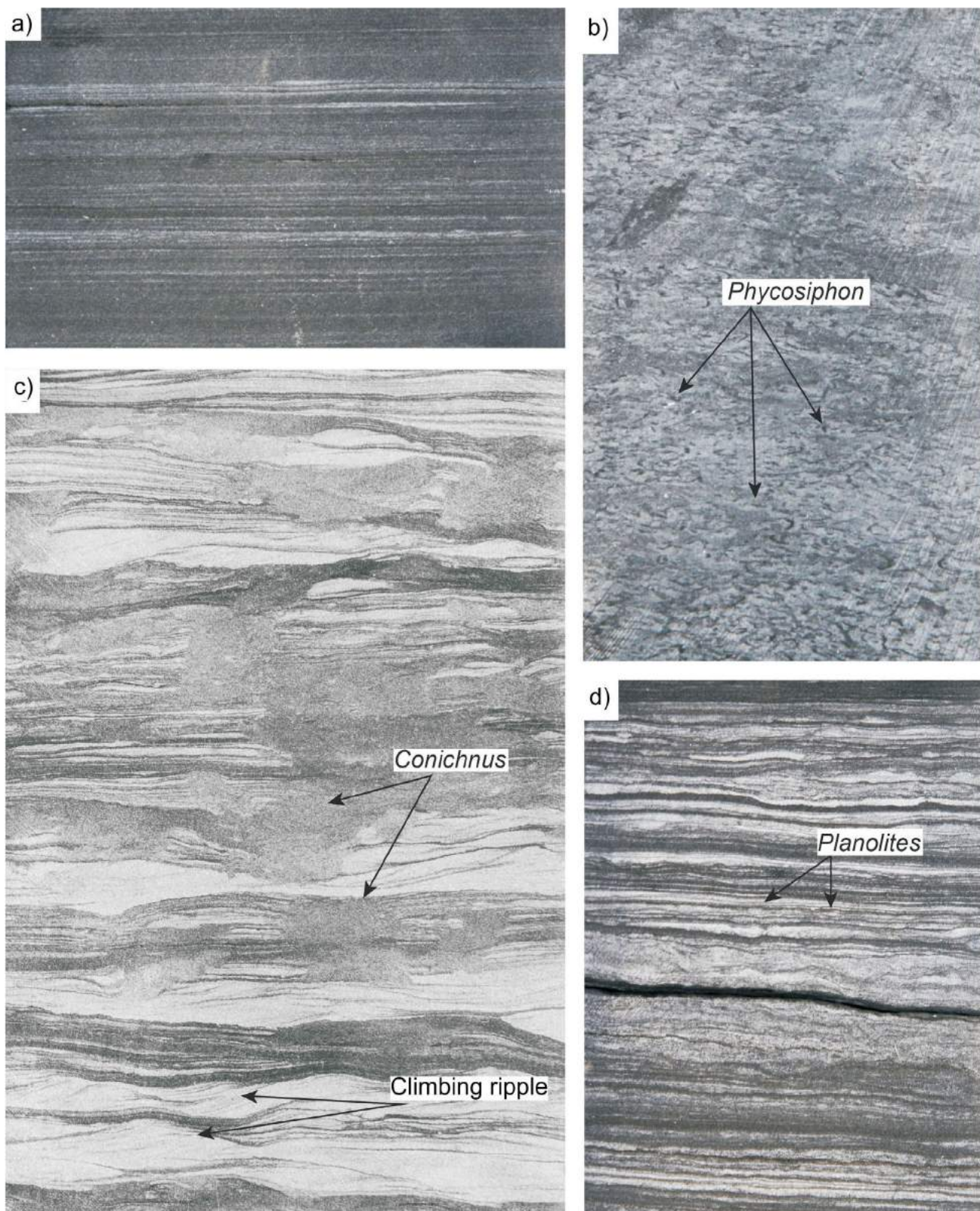
**Figure 3.** Example images of different bioturbated facies: **a)** parallel laminated siltstone, no bioturbation present, in well C-033-C/094-B-09 at 2226.40 m; **b)** sample of bioturbated fabric completely dominated by *Phycosiphon*, in well C-024-K/094-B-08 at 2229.70 m; **c)** *Conichnus* traces interpenetrate and disrupt the sedimentary structures, climbing ripples are present, in well D-067-J.094-B-09 at 1901.70 m; and **d)** bioturbated fabric with small diminutive traces of *Planolites*, in well C-033-C/094-B-09 at 2202.40 m.
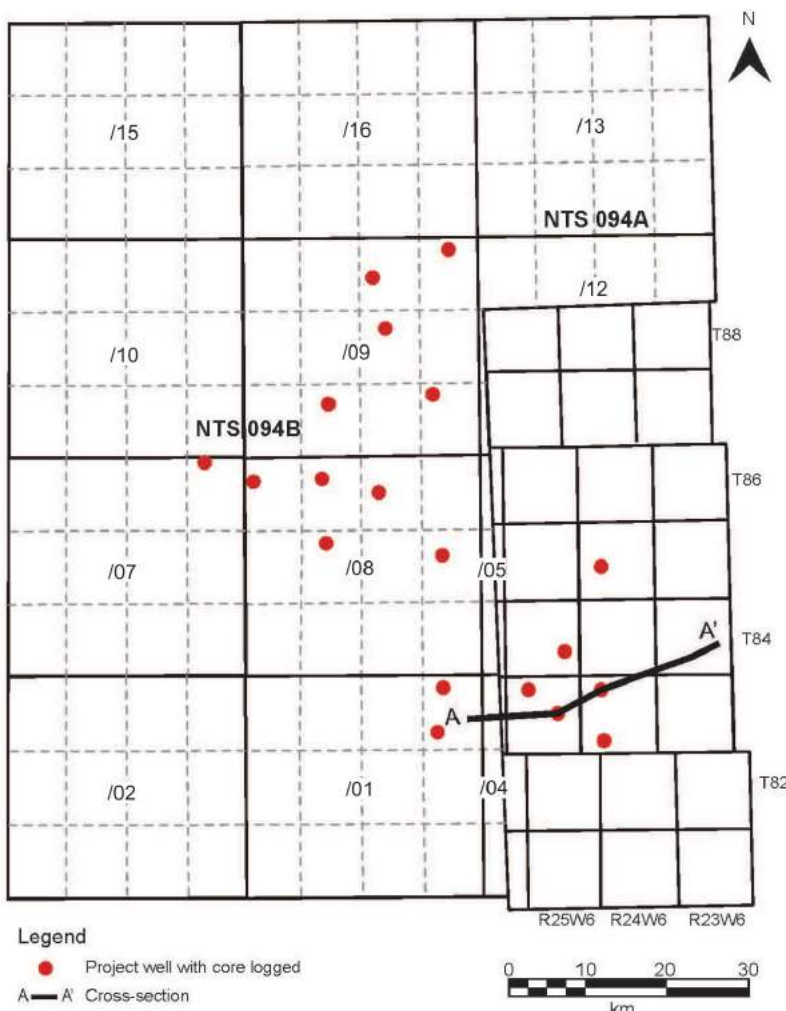
Figure 4. Map of study area, northeastern British Columbia. The red dots indicate the location of wells from which core of the upper Montney Formation has been sampled and analyzed in detail.

Study Area

The study area is commonly referred to as the northern Montney within the Montney play trend and is part of the dry gas fairway (BC Oil and Gas Commission, 2012). The Montney Formation in this northern region has not been extensively studied and facies distributions and relationships to the rest of the basin are not well understood. The area of interest lies within Twp. 82 to 84, Rge. 24 to 25, W 6th Mer. and includes areas on NTS map areas 094A and 094B (Figure 4). There are approximately 1900 wells that penetrate the top of the Montney Formation over this 10 300 km^2 area. Within the upper Montney Formation, there are 87 wells that have cores preserved and stored at the BC Oil and Gas Commission Core Research Facility in Fort St. John. A subset of 19 wells has been described in detail and provides the primary data for this study (Table 1).

Project Work

To develop a predictive geological model of reservoir characteristics and quality, this study will integrate the results of sedimentological, ichnological and petrographic analysis. This work will be completed over an 18-month period, with the results to be reported as an M.Sc. thesis.

Table 1. List of wells from which core of the upper Montney Formation was analyzed. See Figure 4 for map of the well locations.

Location (UWI)	Well name	Pool name	Year drilled
200/b-017-I 094-B-01/00	CANBRIAM HZ W FARRELL B-017-I/094-B-01	Farrell	2009
200/c-085-I 094-B-01/00	PROGRESS ET AL ALTARES C-085-I/094-B-01	Altares	2008
200-d-094-I 094-B-07/00	PROGRESS ET AL GRAHAM D-094-I/094-B07	Graham	2012
200/c-065-F 094-B-08/00	PROGRESS ET AL GRAHAM C-065-F/094-B-08	Graham	2013
202/c-003-H 094-B-08/00	CANBRIAM HZ ALTARES B-B034-H/094-B-08	Altares	2012
200/c-007-J 094-B-08/00	PROGRESS HZ ALTARES C-007-J/094-B-08	Altares	2011
200/c-024-K 094-B-08/00	PROGRESS HZ GRAHAM C-024-K/094-B-08	Graham	2011
200/c-006-L 094-B-08/00	PROGRESS ET AL GRAHAM C-006-L/094-B-08	Graham	2013
200/d-048-A 094-B-09/00	SUNCOR PC HZ KOBES D-048-A/094-B-09	Kobes	2006
200/c-033-C 094-B-09/00	CNRL GRAHAM C-033-C/094-B-09	Graham	2009
200/c-074-G 094-B-09/00	SUNCOR PC HZ KOBES C-074-G/094-B-09	Kobes	2008
200/b-093-I 094-B-09/00	SHELL HZ BLUEBERRY B-093-I/094-B-09	Blueberry	2011
200/d-067-J 094-B-09/00	PROGRESS KOBES D-067-J/094-B-09	Kobes	2009
100/04-20-084-24W6/00	ARCRES HZ ALTARES 04-20-084-24	Altares	2011
100/01-31-083-24W6/00	CANBRIAM FARRELL 01-31-083-24	Farrell	2008
100/05-05-083-24W6/00	CANBRIAM FARRELL 05-05-083-24	Farrell	2008
100-01-32-083-25W6/00	PROGRESS ET AL HZ ALTARES A01-32-083-25	Altares	2011
100-12-36-083-25W6/02	PROGRESS ET AL HZ ALTARES 12-36-083-25	Altares	2011
100/16-17-083-25W6/00	PROGRESS ET AL ALTARES 16-17-083-25	Altares	2009

Abbreviation: UWI, unique well identifier.

The specific research methods to generate inputs to the model are outlined below:

- analyzing the core, focusing on sedimentological and ichnological characteristics (bioturbation intensities, mineralogy, sedimentary structures, biogenic structures, body fossils and grain size), work completed this past season;
- mapping the distribution of bioturbated fabrics, stratigraphically and regionally;
- analyzing the thin sections to study lithology, porosity and trace fossils;
- obtain permeability measurements using a Core Laboratories pressure-decay profile permeameter;
- identifying log signatures associated with specific ranges of porosity and permeability; and
- correlating core data with downhole wireline logs and extrapolate information to wells that are underrepresented with core.

Acknowledgments

References

Armitage, J.H. (1962): Triassic oil and gas occurrences in northeastern British Columbia, Canada; Bulletin of Canadian Petroleum Geology, v. 10, no. 2, p. 35–56.

Baniak, G.M., Gingras, M.K., Burns, B.A. and Pemberton, S.G. (2015): Petrophysical characterization of bioturbated sandstone reservoir facies in the Upper Jurassic Ula Formation, Norwegian North Sea, Europe; Journal of Sedimentary Research, v. 85, no. 1, p. 62–81.

BC Oil and Gas Commission (2012): Montney Formation play atlas NEBC; BC Oil and Gas Commission, technical report, 36 p.

Clarkson, C.R., Wood, J., Burgis, S., Aquino, S. and Freeman, M. (2012): Nanopore-structure analysis and permeability predictions for a tight gas siltstone reservoir by use of low-pressure adsorption and mercury-intrusion techniques; SPE Reservoir Evaluation & Engineering, v. 15, no. 6, p. 648–661.

Davies, G.R. (1997): The Triassic of the Western Canada Sedimentary Basin: tectonic and stratigraphic framework, paleogeography, paleoclimate and biota; Bulletin of Canadian Petroleum Geology, v. 45, no. 4, p. 434–460.

Davies, G.R., Moslow, T.F. and Sherwin, M.D. (1997): The lower Triassic Montney Formation, west-central Alberta; in Triassic of the Western Canada Sedimentary Basin, T.F. Moslow and J. Wittenberg (ed.), Bulletin of Canadian Petroleum Geology, v. 45, p. 474–505.

Edwards, D.E., Barclay, J.E., Gibson, D.W., Kvill, G.E. and Halton, E. (1994): Triassic strata of the Western Canada Sedimentary Basin; in Geological Atlas of the Western Canada Sedimentary Basin, G.D. Mossop and I. Shetsen (comp.), Canadian Society of Petroleum Geologists, Calgary, Alberta and Alberta Research Council, Edmonton, Alberta, p. 257–275.

Gibson, D.W. and Barclay, J.E. (1989): Middle Absaroka Sequence - the Triassic stable craton; in Western Canada Sedimentary Basin, B.E. Ricketts (ed.), Canadian Society of Petroleum Geologists, Special Publication 30, p. 219–232.

Gingras, M.K., Baniak, G., Gordon, J., Hovikoski, J., Konhauser, K.O., La Croix, A., Lemiski, R., Mendoza, C., Pemberton, S.G., Polo, C. and Zonneveld, J.-P. (2012): Porosity and permeability in bioturbated sediments; in Trace Fossils as Indicators of Sedimentary Environments, D. Knaust and R. Bromley (ed.), Developments in Sedimentology, v. 64, p. 837–868.

Golding, M.L., Orchard, M.J., Zonneveld, J.-P., Henderson, C.M. and Dunn, L. (2014): An exceptional record of the sedimentology and biostratigraphy of the Montney and Doig formations in British Columbia; Bulletin of Canadian Petroleum Geology, v. 62, no. 3, p. 157–176.

Moslow, T.F. (2000): Reservoir architecture of a fine-grained turbidite system: Lower Triassic Montney Formation, Western Canada Sedimentary Basin; in Deep-Water Reservoirs of the World, P. Weimer, R.M. Slatt, J. Coleman, N.C. Rosen, H. Nelson, A.H. Bouma, M.J. Styzen and D.T. Lawrence (ed.), Society of Economic Paleontologists and Mineralogists, Gulf Coast Section, Conference Proceedings, December 3–6, 2000, Houston, Texas, p. 686–713.

National Energy Board, BC Oil and Gas Commission, Alberta Energy Regulator and BC Ministry of Natural Gas Development (2013): Energy briefing note: the ultimate potential for unconventional petroleum from the Montney Formation of British Columbia and Alberta; National Energy Board, BC Oil and Gas Commission, Alberta Energy Regulator and BC Ministry of Natural Gas Development, 17 p.

Pemberton, S.G. and Gingras, M.K. (2005): Classification and characterizations of biogenically enhanced permeability; American Association of Petroleum Geologists, AAPG Bulletin, v. 89, no. 11, p. 1493–1517.

Wood, J.M. (2013): Water distribution in the Montney tight gas play of the Western Canadian Sedimentary Basin: significance for resource evaluation; SPE Reservoir Evaluation & Engineering, v. 16, no. 3, p. 290–302.

Zonneveld, J.-P., Beatty, T.W., MacNaughton, R.B., Pemberton, S.G., Utting, J. and Henderson, C.M. (2010a): Ichnology and sedimentology of the Lower Montney Formation in the Pedigree-Ring/Border-Kahntah River area, northwestern Alberta and northeastern British Columbia; in Bulletin of Canadian Petroleum Geology, v. 58, no. 2, p. 115–140.

Zonneveld, J.-P., Gingras, M.K. and Beatty, T.W. (2010b): Diverse ichnofossil assemblages following the PT mass extinction, Lower Triassic, Alberta and British Columbia, Canada: evidence for shallow marine refugia on the northwestern coast of Pangaea; Palaios, v. 25, no. 6, p. 368–392.

Zonneveld, J.-P., Golding, M., Moslow, T.F., Orchard, M.J., Playter, T. and Wilson, N. (2011): Depositional framework of the Lower Triassic Montney Formation, west-central Alberta and northeastern British Columbia; in recovery – 2011 CSPG CSEG CWLS Convention, p. 1–4.

Advanced Geoscience Targeting via Focused Machine Learning Applied to the QUEST Project Dataset, British Columbia

J. Granek, Geophysical Inversion Facility, University of British Columbia, Vancouver, BC, jgranek@eos.ubc.ca

E. Haber, Geophysical Inversion Facility, University of British Columbia, Vancouver, BC

Introduction

As mineral exploration matures in the technological age, new methods for leveraging computational resources for prospecting continue to gain popularity. One such advance has been the widespread adoption of geographic information systems (GIS) for geoscientific-data management and integration, and the associated interest in spatial-data analysis. At the forefront of this effort is the emerging field of mineral-prospectivity mapping (MPM). With origins in Bayesian probability in the 1980s (Hart et al., 1978; Agterberg et al., 1990), the concept of linking numerous georeferenced datasets to derive a map of mineral potential has evolved to a suite of machine-learning algorithms, ranging from weights of evidence (WofE; Bonham-Carter et al., 1988; Agterberg et al., 1990; Carranza 2004) to neural networks (NN; Singer and Kouda, 1997; Porwal et al., 2003; Barnett and Williams, 2006) and support vector machines (SVM; Porwal et al., 2010; Zuo and Carranza, 2011; Abedi et al., 2012). Although many solution methods have been presented, certain characteristics of the MPM problem present difficulties related to uncertainty management and computational efficiency that have yet to be fully addressed. As a test case for this problem, the algorithm is run on the Geoscience BC QUEST (**Qu**esnellia **E**xploration **St**rategy) dataset that covers parts of NTS 093A, B, G, H, J, K, N and O, and comprises, amongst other available public data, airborne gravity, magnetics and electromagnetics, geochemical analysis, geological mapping and a database of known mineral occurrences in the region.

Mineral-Prospectivity Mapping

Mineral-prospectivity mapping (MPM) was first proposed in the late 1980s by geoscientists as a statistical method for the integration and interpretation of spatial patterns in geoscience data (Bonham-Carter et al., 1988). The concept

was to determine the link between various geoscience datasets (i.e., geology, geophysics and geochemistry) and the existence or absence of economic mineralization (Figure 1).

The problem can be stated as follows: given training pairs of geoscience data $\mathbf{X}$, where the columns of $\mathbf{X}$ represent the different types of field measurements and the rows represent the different sample locations, and known mineralization occurrences $\mathbf{y}$ (binary indicator; mineralization or no mineralization), find some mapping function $f(\mathbf{X})$ that can approximate the relationship between the data and the mineralization occurrences such that it can be used to predict mineral potential on new data $\mathbf{X}^{new}$. In general, the mapping function $f(\sim)$ can be anything; Agterberg's original formulation, termed Weights of Evidence (Agterberg et al., 1990), used posterior probability as the mapping function. Numerous other approaches have been taken since, including fuzzy logic (Porwal et al., 2003), logistic regression (Harris and Pan, 1999), neural networks (Singer and Kouda, 1997; Barnett and Williams, 2006) and support vector machines (SVM; Zuo and Carranza, 2011; Abedi et al., 2012).

Due to the difficulty in field testing algorithms for this application and the relatively slow adoption of these methods by industry, most of the work—both past and present—on MPM has been primarily academic, although examples of governments and major mining companies using related methods do exist. That being said, some of the more commonly adopted methods include weights of evidence, fuzzy logic and neural networks. The popularity of these methods can be attributed to ease of use, flexibility and successful application in other fields. The primary challenge for this application is that geoscientific data are prone to errors, but none of the work mentioned above addresses this issue explicitly. This paper will do so by following the SVM approach and reformulating the problem as a total least squares optimization. In this way, the errors in the data can be faithfully and robustly treated.
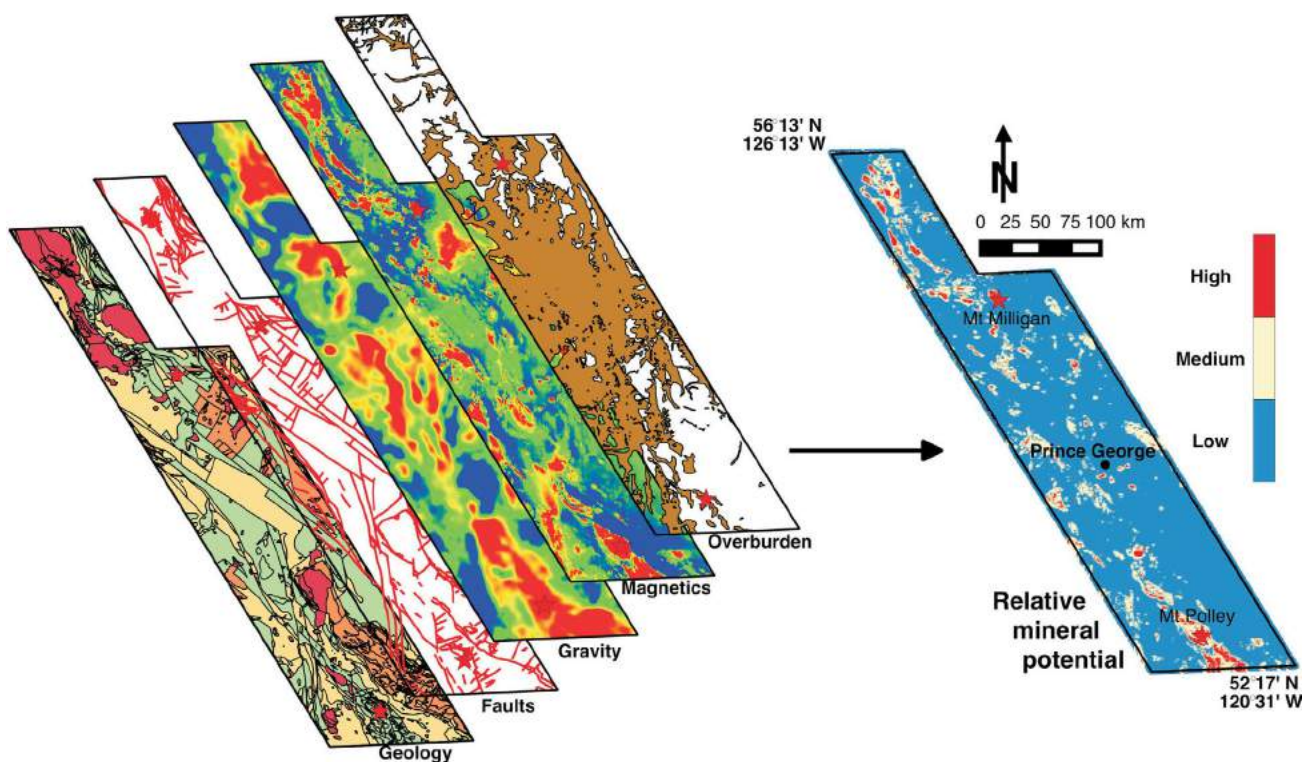
Problem Characteristics

Although many black-box software packages exist for various machine-learning algorithms, the optimization problem presented by MPM has a number of practical character-

Figure 1. Combining numerous geoscientific datasets to produce a map of mineral relative potential using datasets from the QUEST study area (Barnett and Kowalczyk, 2007; Jackaman and Balfour, 2007).

istics that should be considered when implementing a solver. Many of these issues have been addressed individually by previous authors at one time or another; to date, however, a comprehensive solution for the MPM problem has yet to be discussed.

Imbalanced Training Data

In most supervised machine learning environments, an unbiased training is achieved by approximately sampling uniformly from each class. When this is not true, the problem is termed '**imbalanced**' (Chawla et al., 2004) and can lead to poor generalization of the resulting predictor. A number of methods exist to handle imbalanced data, including boosting (Guo and Viktor, 2004; Chawla et al., 2011) and rebalancing (Kubat and Matwin, 1997; Raskutti and Kowalczyk, 2004; Tang et al., 2009). As might be expected, mineral occurrences are relatively rare, resulting in an extremely imbalanced set of training labels. This problem is further exacerbated when one restricts the problem to a specific type of mineralization (e.g., porphyry deposits), as is often the case for prospectivity studies.

Training-Label Uncertainty

On top of the imbalanced nature of the MPM problem is the large degree of uncertainty associated with the training labels. In this regard, there are two fundamental problems:
- the crucial distinction that, in most cases, a label of 'no mineralization' simply means that mineralization has

not been discovered, and not necessarily that there is none
- within each class (mineralized and not mineralized) exists a large range in certainty

For example, in many mineral occurrence databases, 'mineralization' encompasses occurrences ranging from producing mines all the way down to anomalies and prospects. Also, it is easy to understand how a classification of 'no mineralization' has very different implications in the middle of a highly explored mining district than it does in a remote location miles from the nearest field-sample site.

Training Data Uncertainty

As with any observed data, the training data in the MPM problem are associated with uncertainty from various sources. Some data, such as a magnetic-total-field measurement, will have numerical uncertainties associated with detection limits and processing procedures. Others, such as geological mapping of bedrock units, will have qualitative uncertainties associated with expert interpretation and sampling bias. Additionally, some data can have a spatially correlated uncertainty introduced by different exploration environments in the field (e.g., beneath thick deposits of overburden, it becomes prohibitively difficult to map bedrock). Unlike many machine-learning problems, where both the data and the labels can be trusted, it is known in mineral-prospectivity mapping that both have as-

sociated errors. Furthermore, the errors on the different data types can have very large statistical differences.

Big Data

Because mineral occurrences are rare events, the regions considered for MPM are often quite large. Combined with the large number of data n and the ever-growing number of predictive data sources (e.g., magnetic total field, fault locations, bedrock age), the data matrix $\mathbf{X}$ quickly becomes large and dense. Algorithms for solving this problem need to be able to handle large-scale learning of nonlinear relationships without prohibitive computational requirements.

Geoscience Datasets

Before one can contemplate how best to integrate numerous geoscience datasets, an understanding of the data is required. A typical exploration program will employ data from three primary disciplines: geology, geochemistry and geophysics. The variety of data within each of these is broad, comprising qualitative and quantitative measurements, inferred or interpreted values, and a large range in data resolution and uncertainty.

In an idealized exploration environment, all datasets would be densely sampled in the same locations, giving uniform coverage of the area of interest with an associated known uncertainty for each survey. The reality is more commonly represented by a scenario in which each survey was run independently, with highly varied sampling schemes, areas of coverage and target resolutions. The uncertainty on the data

is typically a combination of numerous factors that also vary from survey to survey—many of which are either qualitative, inferred or simply unknown.

The integration of such surveys requires that the following considerations be properly handled:
- Data coverage may vary by survey, resulting in overlaps, holes or missing data.
- Nomenclature may vary amongst qualitative datasets describing the same parameters, resulting in either redundant or incompatible descriptions.
- Survey parameters may vary amongst quantitative datasets describing the same parameters, resulting in different sensitivities and measured values.
- Data quality and value can vary greatly, depending on such factors as age of the survey, sampling technique and environmental conditions.

Spatial Data

As one begins to collect various datasets for a given region, the first issue encountered is the discrepancy between the two data coverage plots shown in Figure 2. In most exploration environments, the available data will span multiple exploration programs, each potentially having a different area of interest. Even within a single exploration program, each survey will likely have a different sampling scheme based on the specific parameter being measured (e.g., bedrock geology will often be sampled wherever outcrop is available, whereas geophysical data are typically collected at predetermined grid points).
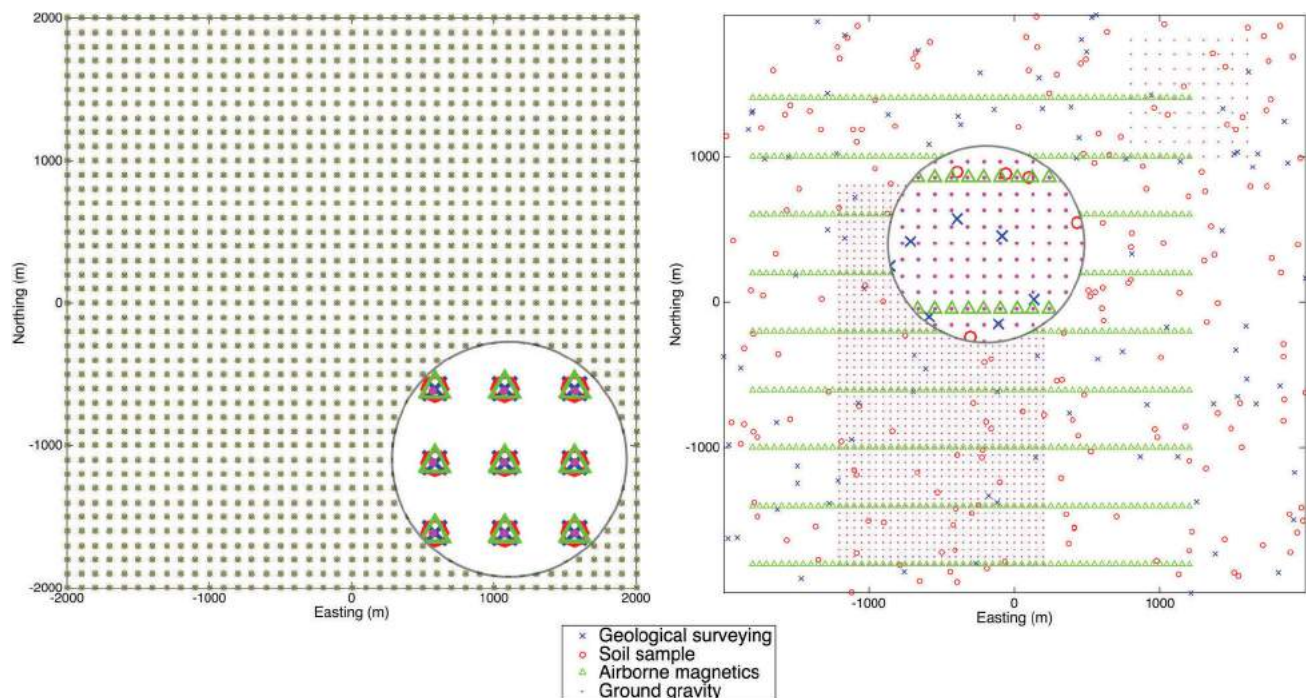
Figure 2. Idealized versus realistic data coverage for a representative suite of geoscience datasets.

To train the learning algorithm, the different measurements must have some geographic basis and, therefore, a domain must be specified. Traditional methods of prospectivity mapping, such as weights of evidence, handled this by reducing all field measurements—be they point measurements or polygons—to a series of overlapping polygons, each with a single value for each parameter (Agterberg et al., 1990).

The approach used in this project is to define a sample grid that specifies the target resolution of the prospectivity map. Continuous point measurements (i.e., geophysical fields or geochemical assays) can then be interpolated and resampled at the grid points, and discrete or categorical polygon layers (i.e., geological units) can simply be sampled at the specified locations. In this way, it is possible to define a spatial uncertainty for each data layer based on the distance from the field measurements to each grid point. Under this approach, sparse or missing data are easily handled as well, since they will simply have very large uncertainty, thus effectively removing their impact on the training of the algorithm.

Levelling/Reinterpreting Data

The other major challenge in integrating datasets occurs when multiple independent surveys are measuring the same parameters (e.g., ground magnetics and airborne magnetics). In such cases, it is important that steps be taken to ensure that all measurements of a given parameter are represented on the same scale or dictionary. For continuous measurements, such as geophysical fields or geochemical assays, this is commonly referred to as levelling (Luyendyk, 1997). For discrete or categorical data, this might be more complex and involve interpreting and reassigning labels to avoid redundant or incompatible descriptions (e.g., [volcanic rocks, intrusive rocks,…, dioritic intrusive rocks] → [volcanic rocks, intrusive rocks,…, intrusive rocks]).

Data Representation

For much of the continuous data (geophysics and geochemistry), representation simply consists of gridding the data and extracting values at points of interest. For some data, however, the question of data representation is more delicate. Take, for example, the bedrock class: this is a categorical variable where only one of the possible options can be true (sedimentary, volcanic, metamorphic or intrusive). If these data are represented as a single input with values ranging from 1 to 4 (mapping each of the four rock classes to a number), an inherent relationship is implied that states that sedimentary rocks are more similar to volcanic rocks than they are to intrusive rocks (since 1 is closer to 2 than it is to 4). This is not the desired behaviour. Instead, an approach has been taken to convert each of the classes to a separate binary input that states whether it is the specified rock type or not.

Another type of data that can be difficult to properly represent is point or line data (e.g., faults or mineralization occurrences). Because of the grid-sampling approach taken, data that are only defined on a point or a line can easily be misrepresented (if the data support is between the grid points) or simply saturated by the majority of the grid points that have no value. For these types of data, the approach taken is to define a range of influence or some other spatial function, such as distance to a fault or density of faults. This is done using different point-spread functions (e.g., Gaussians) to extend the support of these data from a single point or line to a continuous variable that can be sampled on the grid.

Support Vector Machines

Support vector machines (SVMs) were first formally introduced in the 1990s by Vapnik, Boser and Guyon (Boser et al., 1992; Vapnik, 2013) as a machine-learning algorithm structured on the statistical-learning theory (VC theory) developed by Vapnik and Chervonenkis during the 1960s and 1970s (Vapnik and Chervonenkis, 1971). The basic principle of SVMs is to construct an optimal margin classifier that has complexity based not on the dimensionality of the feature space, but rather on the number of support vectors, thus allowing for sparse solutions in high dimensions (Figure 3). The SVM is an optimal margin classifier because the goal is to learn the equation for a hyperplane that separates the different data classes with as large a margin as possible (subject to the constraints). A classifier with complexity independent of the data dimensionality can be a powerful advantage when dealing with large, highly dimensional datasets, since only a small subset is necessary in constructing the SVM classifier.
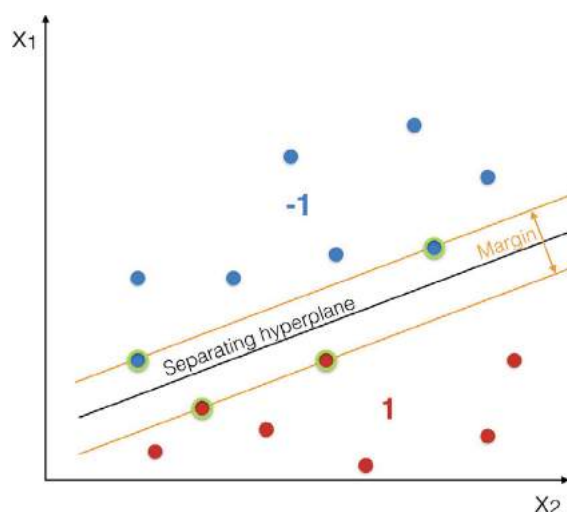
Figure 3. Optimal margin classification using the support vector machine (SVM); the separating hyperplane (black) is determined by maximizing the margin (yellow) between a few sparse support vectors (outlined in green).

The SVM falls under the branch of machine learning known as supervised learning, in which a predictor is taught using training data and training labels (Friedman et al., 2001). In the simplest case, one can consider training data with binary labels. The SVM can also easily be modified to handle regression on continuous or multivalued labels—binary classification is simply the most intuitive to visualize and illustrate the algorithm. The data and labels can therefore be represented as

$$[(\mathbf{X}_1, \mathbf{y}_1), (\mathbf{X}_2, \mathbf{y}_2),\ldots, (\mathbf{X}_n, \mathbf{y}_n)] \text{ with } \mathbf{X_i}R^m, y_i \{-1, 1\}$$

For mineral-prospectivity mapping, $\mathbf{X}_i$ would be a vector of different field measurements (e.g., magnetic total field, bedrock age, distance to fault) for a given sample location and $\mathbf{y}_i$ would signify 'mineralization' or 'no mineralization' for that location. If the data are linearly separable, then one can define a separating hyperplane:

$$f(\mathbf{X}) = \mathbf{Xw} + \mathbf{b}$$

where $\mathbf{w}$ and $\mathbf{b}$ are weights with normalization $|\mathbf{X}_n\mathbf{w} + \mathbf{b}| = 1$. The problem then becomes one of maximizing the margin between training points of opposing classes –1 and 1 (see Figure 3). This is equivalent to the following optimization problem (Burges, 1998; Friedman et al., 2001):

$$\underset{w}{\text{minimize}} \quad \frac{1}{2}\boldsymbol{w}^T\boldsymbol{w}$$
$$\text{subject to} \quad y_i(X_i\boldsymbol{w} + b) \geq 1, i = 1, \ldots, n$$

which can be solved using quadratic programming (Burges, 1998; Platt, 1998; Smola and Schölkopf, 2004; Chang and Lin, 2011) or a number of iterative gradient-based methods (Joachims, 2006; Chapelle, 2007; Chang et al., 2008; Shalev-Shwartz et al., 2011). To solve this in the primal form using gradient-based methods, one typically casts the problem as a regularized risk minimization with unknown regularization parameter and iterates through perturbations of the model weights $\mathbf{w}$

$$\underset{w}{\text{minimize}} \quad \frac{\lambda}{2}\|\boldsymbol{w}\|_2^2 + \boldsymbol{e}^T\text{max}(0, 1 - \text{diag}(\boldsymbol{y})(X\boldsymbol{w} + \boldsymbol{b}))$$

where $\mathbf{e}$ is a vector of ones. This formulation is preferred not only due to its simplicity, but also because it is scalable with number of data n. Traditionally, however, the SVM problem was solved via quadratic programming using the primal-dual optimality conditions (KKT)

$$\underset{w}{\text{minimize}} \quad \frac{1}{2}\alpha^T\boldsymbol{Q}\alpha + (\mathbb{I}^T + \beta\boldsymbol{y}^T)\alpha$$

where $\mathbf{Q} = \text{diag}(\mathbf{y})\mathbf{X}^T\mathbf{X}\text{diag}(\mathbf{y})$. The primal and dual formulations were equally popular, however, until the dual formulation recently became more prevalent due to the natural extension to nonlinear transformations via the kernel trick (Figure 4; Boser et al., 1992). Since the data only appear as inner products in the dual form, a transformation $K(\mathbf{X},\mathbf{X}^T)$ can be applied and yet the size of K remains $n \times n$. This has powerful implications, allowing for transformations to very high dimensional spaces without penalty, but it is easy to see that this becomes computationally expensive when n is large.

This fact, combined with the realization that kernel methods can be applied in the primal form via the representer theorem (Chapelle 2007), has led to a resurgence of primal SVM methods in the past 10 years. With the advance of iterative optimization techniques, primal SVM methods have gained in speed and popularity to accommodate the growing size of applied datasets. Extensions of the algorithm to many specific problems have also taken place, including imbalanced datasets (Raskutti and Kowalczyk, 2004; Tang et al., 2009; Pant et al., 2011), density estimation (Chen et al., 2001; Manevitz and Yousef, 2002; Mordelet and Vert, 2010) and the incorporation of uncertainties for robust estimation (Zhang, 2005; Carrizosa, 2007; Pant et al., 2011; Huang et al., 2012).

SVM for Prospectivity Mapping

Beginning from the primal SVM formulation previously discussed, it is straightforward to adapt the problem to handle the characteristics specific to mineral-prospectivity mapping, namely by adding uncertainties on the data and
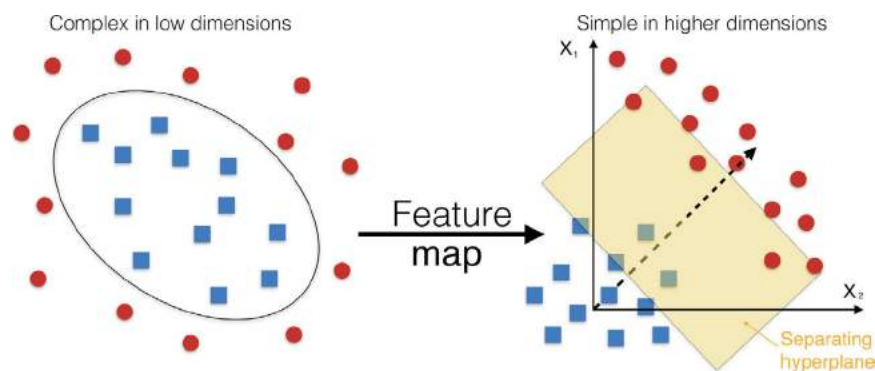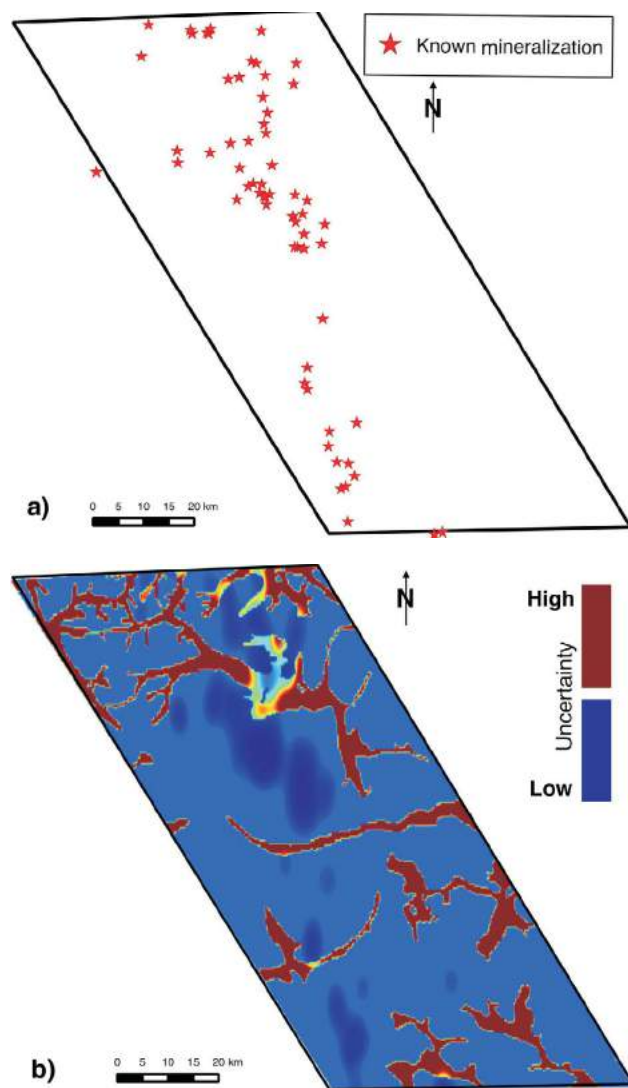

Figure 4. Nonlinear mapping via the kernel trick; classes may not be linearly separable in original dataspace, but easily separable in the transformed dataspace.

labels. In the simplest case, this can be done by adding weighting terms that penalize highly uncertain values, although more sophisticated algorithms can also be developed, such as in Granek and Haber (2015). In the simplest case (linearly separable SVM classification), training label uncertainty can be incorporated with the addition of a weighting term in the objective function

$$\text{minimize}_{w} \quad \frac{\lambda}{2}\|w\|_2^2 + \left(\frac{1}{\varepsilon}\right)^T \max(0, 1 - \text{diag}(y)(Xw + b))$$

where $\mathring{a}_i$ is proportional to the uncertainty on the ith training label. In this way, labels with low confidence are used less to train the classifier because they do not contribute as much to the misfit. Similarly, uncertainties in the training data can be handled by adding an extra penalty term (in red) to the objective function

$$\text{minimize}_{w} \quad \frac{\lambda}{2}\|w\|_2^2 + \left(\frac{1}{\varepsilon}\right)^T \max(0, 1 - \text{diag}(y)(Xw + b))$$
$$+ \frac{\beta}{2}(X - X_{obs})^T \text{diag}\left(\frac{1}{\Sigma}\right)(X - X_{obs})$$

It is now assumed that the observed data $\mathbf{X_{obs}}$ are incorrect, and the true data are $\mathbf{X}$. Treating the uncertainties (Ó) as a proxy for the variance of the difference between these two data, and assuming Gaussian distribution, this bares a striking resemblance to the total least squares (Golub and Loan, 1980) problem.

Results

Finally, to demonstrate the utility of such an algorithm for mineral-prospectivity mapping (MPM), the following example from the QUEST (**Que**snellia **E**xploration **St**rategy) project in central British Columbia is presented. This work was funded by NEXT Exploration Inc. and Mitacs, so the results are currently confidential. For demonstration purposes, permission has been given to show preliminary results from a subset of the QUEST area (Figures 5, 6). This region is known to host a number of large, economic, copper-porphyry deposits. Through a government-sponsored program, a large amount of geoscientific data (including geological mapping, geochemical analysis and geophysical-data acquisition) was acquired between 2008 and 2012 in order to stimulate mineral exploration. Included in the large multidimensional dataset are covariates such as total-magnetic-field intensity, age of bedrock, geological rock class and copper content. Since each dataset was collected independently with its own sampling scheme, all layers were resampled to a base grid of 300×300 m, resulting in
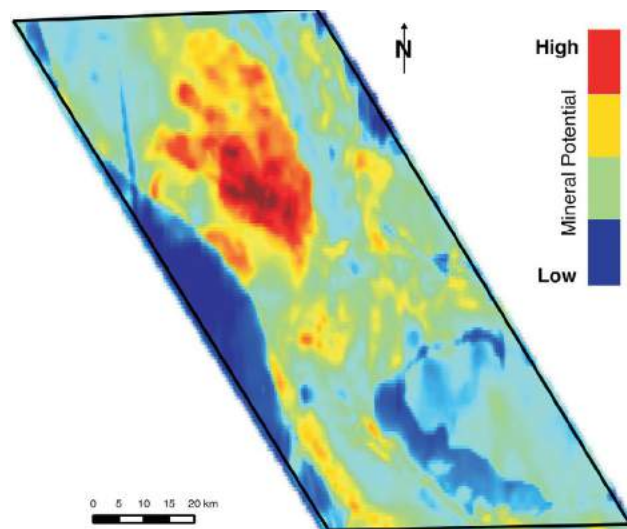

Figure 5. Examples of input layers for a subset of data from the QUEST project area: **a)** known mineralization locations, and **b)** uncertainty estimates for the mineralization labels (red is more uncertain). NEXT Exploration Inc. is thanked for permission to publish these preliminary results.

Figure 6. Prediction for prospective mineral regions in a portion of the QUEST area (red is more prospective, blue is less). NEXT Exploration Inc. is thanked for permission to publish these preliminary results; final prospectivity maps and locations are confidential under the terms of the funding agreement with NEXT Exploration Inc.

Geoscience BC Summary of Activities 2015

more than 700 000 sample points. When all data were assembled and properly processed for training, 91 distinct input layers were used, including both continuous and discrete values.

Uncertainty on these inputs can vary widely, depending on the data source. For example, most geophysical data can bear uncertainty in the form of a noise floor plus an acceptable standard deviation, whereas it is less obvious for geological data due to the subjective, interpreted nature of the measurements. In these cases, estimates can still be made based on confidence in the expert and the availability of field measurements.

As previously mentioned, the labels for the MPM problem present a suite of practical issues. The lack of confident negative labels (no mineralization) results in an imbalanced learning problem, and the sparse subjective nature of the positive labels (mineralization) results in a large range in confidence that can be adequately quantified using a framework of uncertainty estimates. For the QUEST dataset, 155 alkalic copper-porphyry–style mineral occurrences were used to generate a set of binary labels on the base grid. Each occurrence has associated with it a status ranging from 'Showing' to 'Producer' (six unique statuses are possible), indicating the confidence in the mineral occurrence being economic. Combining this with other factors such as the extent of the overburden (concealing potentially mineral-bearing bedrock), uncertainty estimates for the labels (see Figure 5b) were generated, ranging from 1 (confident label) to 50 (not confident label). The final result is a predicted mineral-prospectivity map (Figure 6) that indicates which regions are more favourable for copper-porphyry mineralization than others. As one can see, the algorithm was able to successfully predict the known prospective regions, as well as highlight potential new areas for exploration. The addition of uncertainty estimates in the algorithm provides a more robust framework for the incorporation of multidisciplinary data that possess a large range in data quality.

Discussion and Future Work

In the mineral-prospectivity–mapping literature, much has been made of the difference between knowledge-driven and data-driven methods. Although SVM automates the learning process and is therefore considered a data-driven approach, it is important to acknowledge that, without properly informed data processing prior to learning, the entire methodology is doomed to poor performance. This is not a short-coming of SVM but rather a well-known idiom of machine learning in general: "garbage in, garbage out!" In this sense, it is advisable to employ a data-driven approach, such as SVM, but with deliberate consultation of field experts when processing the data prior to learning.

A major shortcoming of many prospectivity-mapping methods, including SVM, is the insensitivity to spatial patterns in the data. One can think of the example of a typical porphyry halo, in which the presence of a large ring in the geophysical data is indicative of a target in the centre. In such a case, the actual value at each point location is not nearly as important as the structure it represents.

One promising new algorithm designed to handle the challenge is the convolutional neural network (CNN; LeCun and Bengio, 1995). An extension of the well-known neural network family of learning algorithms, CNNs implicitly build in sensitivity to spatial structures via use of convolutional kernels that are optimized to detect key structures in the input data. Developed and popularized in the last decade primarily for image, text and speech recognition, CNNs present an exciting new algorithm ideally suited for recognizing complex patterns in spatial geoscience datasets.

Conclusions

This work has explored the rapidly developing field of mineral-prospectivity mapping from an algorithmic and data-processing point of view. Although much work has been done in the fields of machine learning, geoscience and GIS independently, the intersection of all three has left a suite of challenges that remain to be fully addressed. Using a subset of the data from Geoscience BC's QUEST project, this study addresses several challenges through the modification and application of a primal support-vector-machine algorithm, incorporating uncertainties in both the labels and the data. In conjunction with this work, much effort has been directed at the proper understanding and use of data processing prior to learning. Going forward, the authors are exploring different algorithms that are better able to handle the spatial and structured nature of many geoscience datasets; most notably, current research is working on developing a convolutional neural network for mineral-prospectivity mapping. Such algorithms show promise as tools for geoscientists, both in the early stages of exploration by allowing for critical appraisal of which datasets are most valuable, and in the later stages to extract maximum value from existing data-rich environments.

Acknowledgments

References

Abedi, M., Norouzi, G.-H. and Bahroudi, A. (2012): Support vector machine for multi-classification of mineral prospectivity areas; Computational Geoscience, v. 46, p. 272–283.

Agterberg, F., Bonham-Carter, G. and Wright, D. (1990). Statistical pattern integration for mineral exploration; *in* Computer Applications in Resource Estimation Prediction and Assessment for Metals and Petroleum, G. Gaál and D.F. Merriam (ed.), Pergamon Press, Toronto, p. 1–21.

Barnett, C.T. and Kowalczyk, P.L. (2007): Airborne electromagnetics and airborne gravity in the QUEST project area, Williams Lake to Mackenzie, British Columbia; *in* Geoscience BC Summary of Activities 2007, p. 1–6.

Barnett, C. and Williams, P. (2006): Mineral exploration using modern data mining techniques; First Break, v. 24, no. 7, p. 295–310.

Bonham-Carter, G., Agterberg, F. and Wright, D. (1989): Integration of geological datasets for gold exploration in Nova Scotia; Photogrammetric Engineering and Remote Sensing, v. 54, no. 11, p. 1585–1592.

Boser, B., Guyon, I. and Vapnik, V. (1992): A training algorithm for optimal margin classifiers; Proceedings of the Fifth Annual Workshop on Computational Learning Theory, p. 144–152.

Bottou, L. and Lin, C. (2007): Support vector machine solvers; *in* Large Scale Kernel Machines, L. Bottou, L. Chapelle, D. DeCoste and J. Weston (ed.), MIT Press, Boston, p. 301–320.

Burges, C.J.C. (1998): A tutorial on support vector machines for pattern recognition; Data Mining Knowledge Discovery, v. 2, p. 121–167, URL <http://research.microsoft.com/pubs/67119/svmtutorial.pdf> [November 2015].

Carranza, E.J.M. (2004): Weights of evidence modeling of mineral potential: a case study using small number of prospects, Abra, Philippines; Natural Resource Reserves, v. 13, no. 3, p. 173–187.

Carrizosa, E. and Plastria, F. (2007): Support vector regression for imprecise data; Vrije University, MOSI Working Paper 35, 35 p.

Chang, C.-C. and Lin, C.-J. (2011): LIBSVM: a library for support vector machines; ACM Transactions on Intelligent Systems and Technology, v. 2, no. 27, p. 1–27.

Chang, K.-W., Hsieh, C.-J. and Lin, C.-J. (2008): Coordinate descent method for large-scale L2-loss linear support vector machines; Journal of Machine Learning, v. 9, p. 1369–1398.

Chapelle, O. (2007) Training a support vector machine in the primal; Neural Computation, v. 19, no. 5, p. 1155–1178.

Chawla, N., Bowyer, K., Hall, L. and Kegelmeyer, W. (2011): SMOTE: synthetic minority over- sampling technique; Journal of Artificial Intelligence Research, v. 16, p. 321–357.

Chawla, N., Japkowicz, N. and Kotcz, A. (2004): Editorial: special issue on learning from imbalanced data sets; SIGKDD Explorations, v. 6, no. 1, p. 1–6.

Chen, Y., Zhou, X. and Huang, T. (2001): One-class SVM for learning in image retrieval; *in* Proceedings of the International Conference on Image Processing, v. 1, p. 34–37.

Friedman, J., Hastie, T. and Tibshirani, R. (2001): The Elements of Statistical Learning; Springer, Berlin, Springer Series in Statistics, Volume 1.

Golub, G. and Loan, C.V. (1980): An analysis of the total least squares problem; SIAM Journal Numerical Analysis, v. 17, no. 6, p. 883–893.

Guo, H. and Viktor, H. (2004): Learning from imbalanced data sets with boosting and data generation: the DataBoost-IM approach; SIGKDD Explorations, v. 6, no. 1, p. 30–39.

Granek, J. and Haber, E. (2015): Data mining for real mining: a robust algorithm for prospectivity mapping with uncertainties; *in* Proceedings of the 2015 SIAM International Conference on Data Mining, p. 145–153. doi:10.1137/1.9781611974010.17

Harris, D. and Pan, G. (1999): Mineral favorability mapping: a comparison of artificial neural networks, logistic regression, and discriminant analysis; Natural Resource Research., v. 8, no. 2, p. 93–109.

Hart, P., Duda, R. and Einaudi, M. (1978): PROSPECTOR—a computer-based consultation system for mineral exploration; Mathematical Geology, v. 10, no. 5, p. 589–610. doi:10.1007/bf02461988

Huang, G., Song, S., Wu, C. and You, K. (2012): Robust support vector regression for uncertain input and output data; IEEE Transactions on Neural Networks and Learning Systems v. 23, no. 11, p. 1690–1700.

Jackaman, W. and Balfour, J.S. (2008): QUEST project geochemistry: field surveys and data re-analysis (parts of NTS 93A, B, G, H, J, K, N and O); *in* Geoscience BC Summary of Activities 2007, Geoscience BC, Report 2008-1, p. 7–10.

Joachims, T. (2006): Training linear SVMs in linear time; *in* Proceedings of the 12th ACM SIGKDD International Conference Knowledge Discovery and Data Mining (KDD), 10 p.

Kubat, M. and Matwin, S. (1997): Addressing the curse of imbalanced training sets: one-sided selection; *in* Proceedings of the Fourteenth International Conference on Machine Learning, p. 179–186.

LeCun, Y. and Bengio, Y. (1995): Convolutional networks for images, speech, and time series; *in* The Handbook of Brain Theory and Neural Networks, M.A. Arbib (ed.), MIT Press, Boston, p. 255–258.

Luyendyk, A.P.J. (1997): Processing of airborne magnetic data; AGSO Journal of Australian Geology and Geophysics, v. 17, p. 31–38.

Manevitz, L. and Yousef, M. (2002): One-class SVMs for document classification; Journal of Machine Learning Research, v. 2, p. 139–154.

Mordelet, F. and Vert, J. (2010): A bagging SVM to learn from positive and unlabeled examples; Pattern Recognition Letters, v. 37, p. 201–209.

Pant, R., Trafalis, T. B. and Barker, K. (2011): Support vector machine classification of uncertain and imbalanced data using robust optimization; *in* Proceedings of the 15th World Scientific and Engineering Academy and Society (WSEAS) International Conference on Computers, p. 369–374.

Platt, J. (1998): Sequential minimal optimization: a fast algorithm for training support vector machines; Microsoft Technical Research, Technical Report MSR-TR-98-14, 21 p., URL <http://research.microsoft.com/pubs/69644/tr-98-14.pdf > [November 2015].

Porwal, A., Carranza, E. and Hale, M. (2003): Artificial neural networks for mineral-potential mapping: a case study from Aravalli Province, western India; Natural Resources Research, v. 12, no. 3, p. 155–171.

Porwal, A., Yu, L. and Gessner, K. (2010): SVM-based base-metal prospectivity modeling of the Aravalli Orogen, northwestern India; EGU General Assembly, Conference Abstracts, v. 12, p. 15171.

Raskutti, B. and Kowalczyk, A. (2004). Extreme re-balancing for SVMs: a case study; SIGKDD Explorations, v. 6, no. 1, p. 60–69.

Shalev-Shwartz, S., Singer, Y., Srebro, N. and Cotter, A. (2011): Pegasos: Primal Estimated sub-GrAdient SOlver for SVM; Mathematical Programming, v. 127, no. 1, p. 3–30.

Singer, D.A. and Kouda, R. (1997): Use of a neural network to integrate geoscience information in the classification of mineral deposits and occurrences; *in* Proceedings of Exploration 97, Fourth Decennial International Conference on Mineral Exploration, A.G. Gubins (ed.), p. 127–134.

Smola, A.J. and Schölkopf, B. (2004): A tutorial on support vector regression; Statistics and Computing, v. 14, no. 3, p. 199–222.

Tang, Y., Zhang, Y.Q., Chawla, N.V. and Krasser, S. (2009): SVMs modeling for highly imbalanced classification; Systems, Man and Cybernetics, Part B: Cybernetics, IEEE Transactions, v. 39, no. 1, p. 281–288.

Vapnik, V.N. and Chervonenkis, A.Y. (1971): On the uniform convergence of relative frequencies of events to their probabilities; Theory of Probability and its Applications, v. 16, no. 2, p. 264–280.

Vapnik, V. (2013): The Nature of Statistical Learning Theory; Springer Science and Business Media.

Zhang, J.B.T. (2005): Support vector classification with input data uncertainty; *in* Proceedings of Advances in Neural Information Processing Systems Conference, v. 17, p. 161–168.

Zuo, R. and Carranza, E.J.M. (2011): Support vector machine: a tool for mapping mineral prospectivity; Computers and Geoscience, v. 37, no. 12, p. 1967–1975.

Structure of a High-Grade, Electrum-Bearing, Quartz-Carbonate Vein Stockwork at the Brucejack Deposit, Northwestern British Columbia (NTS 104B)

N.J. Harrichhausen, Department of Earth and Planetary Sciences, McGill University, Montréal, QC,
nicolas.harrichhausen@mail.mcgill.ca

C.D. Rowe, Department of Earth and Planetary Sciences, McGill University, Montréal, QC

W.S. Board, Pretium Resources Inc., Vancouver, BC

C.J. Greig, Pretium Resources Inc., Vancouver, BC

Introduction

One of the most commonly cited mechanisms for the formation of gold deposits invokes transport of gold in aqueous solution through the Earth's crust and localized precipitation due to changes in physical conditions or solution chemistry. Numerous examples of epithermal and orogenic deposits, where gold is contained in hydrothermal vein systems, have been explained by dissolved transport (e.g., Krupp and Seward, 1987; Simmons and Browne, 1990; Mikucki, 1998; Hayashi et al., 2001; Williams-Jones et al., 2009). However, solubility of gold in hydrothermal solutions is low (approximately 1–10 ppb in vapour and 100–1000 ppb in liquid; Heinrich et al., 2004; Williams-Jones et al., 2009; Zezin et al., 2011) and, in deposits where gold concentrations are highly variable and range locally to extremely high grades, it may be worthwhile to search for an alternative mechanism for gold transport and enrichment.

At the Brucejack deposit of Pretium Resources Inc. in northwestern British Columbia, gold is present as electrum, a gold-silver alloy, within epithermal quartz-carbonate veins. These veins locally show extremely high grades of gold (up to 41 500 ppm), occurring as porous or dendritic blebs of visible electrum approximately 0.5–5 cm in size. However, the adjoining wallrock and vein material are typically low grade (<1 ppm Au). The extreme 'nugget effect', or inherent unpredictability, of the spatial statistics of the gold-assay population presents complications for estimating the mineral resource. In order to help with resource estimation and further exploration, controls on gold mineralization, in particular the local enrichment of electrum within the quartz-carbonate veins, must be understood. The

extreme concentration gradients of gold seen at Brucejack have led the authors to investigate the possibility that additional transport mechanisms may aid in localizing gold enrichment. One suggested mechanism is the transport of gold in colloidal suspension (e.g., Saunders 1990; Herrington and Wilkinson, 1993; Saunders and Schoenly, 1995; Hough et al., 2011).

The purpose of the study at Brucejack reported herein is to test the potential for colloidal deposition and contextualize the role of colloidal transport within the vein system by examining both quartz and electrum for evidence of relict colloids (cf. Saunders, 1990; Hough et al., 2011; Kirkpatrick et al., 2013; Faber et al., 2014). An essential aspect of the study is to describe and interpret the structural relationships within the faults, extensional veins and stockworks that constitute the vein system, and to understand the roles of hydrofracture, fault slip and static fluid flow in controlling vein-mineral precipitation and gold distribution. The aim of the project is to understand the specific deformational context of the formation of enriched veins, including the differentiation of sites of structural dilation that may have contributed to precipitation of electrum and quartz, and the identification of structural-trapping sites (e.g., vein jogs and intersections) where colloids may have ponded or adhered during hydrothermal flow.

This paper presents preliminary field observations from detailed vein mapping of a surface outcrop and underground intersections of mineralized quartz-carbonate stockwork systems that extend to depth within the Brucejack mineral resource. These observations led the authors to believe that quartz-carbonate stockwork veining is a result of multiple episodes of cyclic fault motion, with vein precipitation occurring between slip/fracture events.

Tectonic Setting

The Brucejack deposit is hosted by rocks of the Early Jurassic lower Hazelton Group, a package of arc-related vol-

cano-sedimentary rocks within Stikinia. Stikinia, along with other Paleozoic–Mesozoic arc and oceanic terranes of the Intermontane Belt, is interpreted to have accreted to ancestral North America by mid-Jurassic time (Monger et al., 1982; Nelson and Colpron, 2007; Gagnon et al., 2012). Following accretion, Stikinia was subjected to at least one major episode of compressional deformation during the mid-Cretaceous formation of the northeast-verging, sinistral-transpressive Skeena fold-and-thrust belt (Evenchick, 1991, 2001). This deformation gave rise to the McTagg anticlinorium (Figure 1; Henderson et al., 1992), where the thickness of the lower Hazelton Group decreases considerably from the east to the west limb. The change in strati-

graphic thickness is interpreted by Nelson and Kyba (2014) to represent the presence of a paleostructural highland along the axis of the McTagg anticlinorium and a volcano-sedimentary basin to the east. Hazelton Group deposition within this basin was coeval with displacement along basin-bounding faults. Several large mineral deposits, including the Kerr-Sulphurets-Mitchell (KSM) copper-gold porphyries and the epithermal Brucejack gold vein-stockwork system, are located along a narrow south-southeast trend just west of the McTagg anticlinorium and are interpreted to relate to Jurassic magmatic and hydrothermal systems controlled by the basin-bounding faults (Nelson and Kyba, 2014; Febbo et al., 2015).
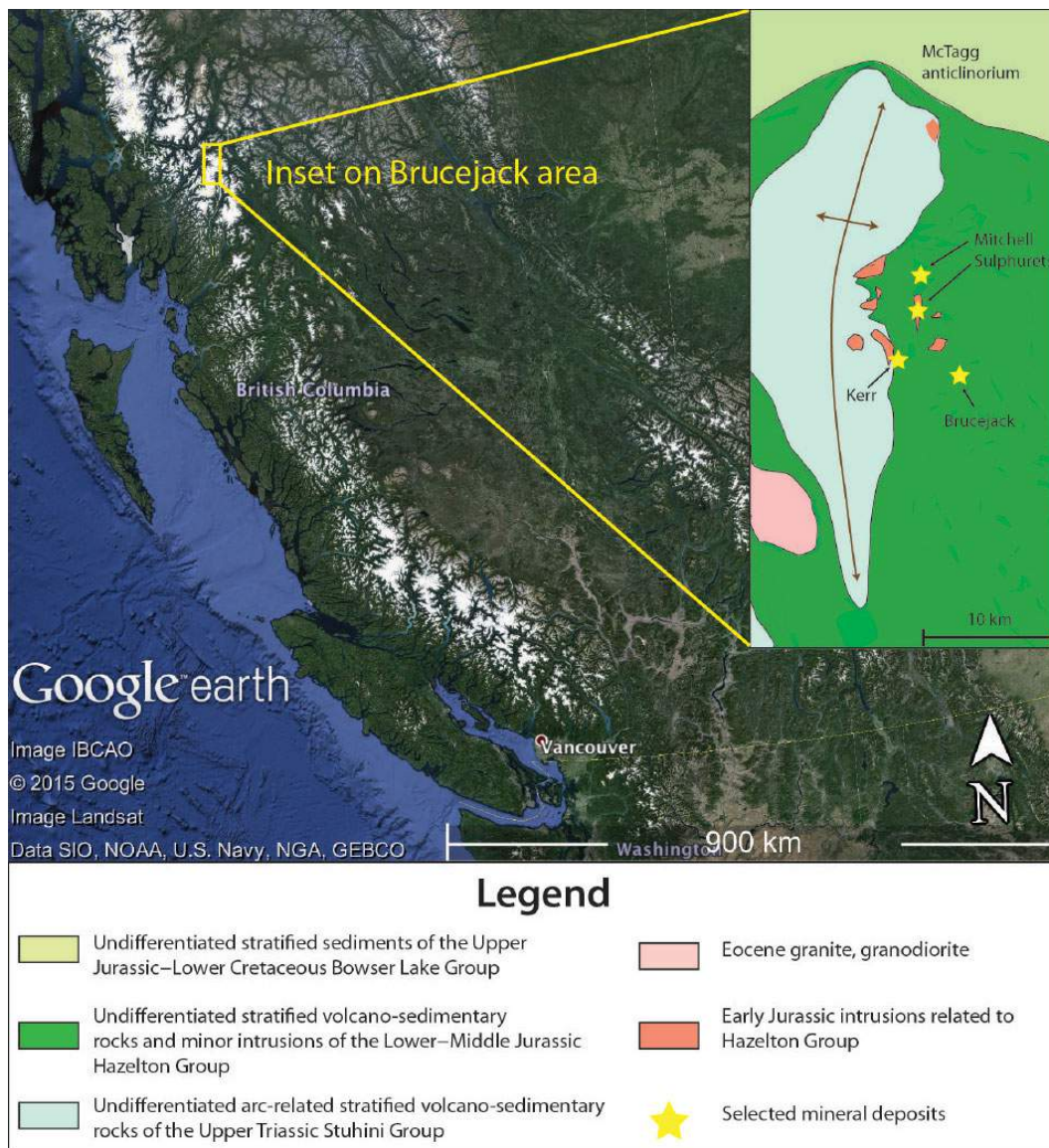
Figure 1. Google Earth™ image of the location of the Brucejack deposit in northwestern British Columbia. Inset on the left shows a simplified regional geology map with the location of the McTagg anticlinorium. The stars show the locations of three major copper-gold porphyry deposits, as well as the Brucejack gold-silver epithermal deposit. Geology contacts from Erdmer and Cui (2009) and legend modified from Nelson and Kyba (2014).

Deposit Geology

Quartz-carbonate stockwork veining in the Brucejack deposit hosts the majority of a total mine reserve of 7.3 million oz. gold and 35.3 million oz. silver (proven and probable reserves; Jones, 2013). Previous work at Brucejack has documented electrum-bearing quartz-carbonate vein networks that crosscut latite lavas and breccias, and associated immature volcaniclastic rocks (Board and McNaughton, 2013; Jones, 2013). The mineralized veins are found within a band of quartz-sericite-pyrite (QSP) alteration that follows the outline of broad easterly plunging folds. These fold axes are folded by a north-trending syncline, suggesting that polyphase deformation has occurred (Board and McNaughton, 2013; Jones, 2013). This coincides with polyphase-deformation interference patterns recorded in mid-Jurassic to early Cretaceous clastic sequences within the Bowser Basin that overlies Hazelton Group strata (Evenchick, 2001), and three phases of deformation recorded within the nearby Mitchell copper-gold porphyry deposit (Febbo et al., 2015). Peak metamorphism, up to lower-greenschist facies, within the Brucejack deposit coincided with the beginning of the formation of the Skeena fold-and-thrust belt at 110 Ma (Kirkham and Margolis, 1995; Evenchick, 2001). This later deformation has affected all of the early Jurassic mineralized-vein generations at Brucejack (Kirkham and Margolis 1995; Board and McNaughton, 2013; Jones, 2013). Lenses of silicified conglomerate have been correlated as a marker horizon that outlines the stratigraphy within the band of QSP alteration. Stockwork-vein systems follow an east-northeast trend and dip subvertically, subparallel to hostrock foliation, however, this foliation is believed to postdate vein formation (Kirkham, 1992; Davies et al., 1994; Board and McNaughton, 2013; Jones, 2013). Within stockwork zones, veins may occur in many different orientations. Although mineralization is hosted within veins, higher grades are not clearly correlated with vein intensity because diffuse stockwork zones with a smaller percentage of vein material may contain significant electrum.

Several generations of veining have been documented in the Brucejack deposit (Board and McNaughton, 2013; Jones, 2013; Tombe, 2015); pyrite veins that are suggested to be associated with early QSP alteration are crosscut by electrum-bearing quartz-carbonate veins. These quartz-carbonate veins exist as dense stockwork and stockwork breccia, and as parallel, decimetre- to metre-spaced, layered vein sets. They, in turn, are cut by quartz-carbonate veins containing base-metal sulphide (sphalerite, galena, chalcopyrite), electrum and silver sulphide mineralization. A third generation of manganoan carbonate-quartz veins contains local high-grade electrum mineralization. Quartz-chlorite fibrous slicken veins and tension gashes associated with later (probably Skeena fold-and-thrust belt) shortening crosscut all earlier vein systems. They contain limited chalcopyrite and no reported electrum.

Fluid-inclusion thermobarometry completed by Tombe (2015) yielded mineralized vein formation temperatures of approximately 160°C and co-trapping of liquid and vapour inclusions, indicating that boiling probably occurred during quartz precipitation. Rhenium-osmium dates on molybdenite suggest some of the initial veining occurred at 188 Ma (Tombe, 2015), and crosscutting relationships between an electrum-bearing generation of veins and 182.7 Ma, late syn- to postmineralization monzonite dikes suggest that the latest electrum-mineralizing event may have occurred at approximately this time (Pretium Resources Inc., 2013). Volcanic rocks on the property range in age from 196 to 182 Ma (U-Pb zircon; Pretium Resources Inc., 2013), and porphyritic intrusions related to copper-gold mineralization at the nearby KSM deposit have yielded U-Pb zircon ages of 197–189.9 Ma (Bridge, 1993; Febbo et al., 2015). If the deposits are related to the same magmatic activity, these dates suggest a long-lived magmatic-hydrothermal system lasting up to 15 million years.

Observations

In order to document the scale and geometry of the vein system at Brucejack, detailed maps were prepared of individual and composite vein orientations, lithology and patterns of alteration, at a scale of tens of metres, on surface exposures of major vein systems. These were then linked, in part using drillhole intersections, to structural measurements underground, where the same vein systems were intersected by active workings. Aerial photographs were acquired using a lightweight drone (DJI Phantom3 Advanced). Low-altitude airphotos were used to construct a three-dimensional surface model from which a detailed georeferenced orthophoto was extracted (methods described in Johnson et al., 2014). The orthophotos have a scale of approximately 1–2 pixels/cm, depending on the size of the outcrop. Veins were then mapped directly onto these orthophotos using a tablet, with locations of structural measurements and vein descriptions denoted by station names. Rock types were mapped directly onto paper printouts of the outcrop orthophotos. Three outcrop map areas (one shown in Figure 2) were chosen to get a good representation of the stockwork systems at Brucejack. Each of these areas is located around stockwork systems of different size and orientation, and within different hostrocks or alteration assemblages. The first location (Figure 3a, map area 1) was also chosen because this vein system may be correlative with 'Domain 20', an important gold-bearing vein system that is well exposed in the underground workings of the Brucejack mine. The focus of this preliminary paper is on observations of this vein system from surface and underground mapping.
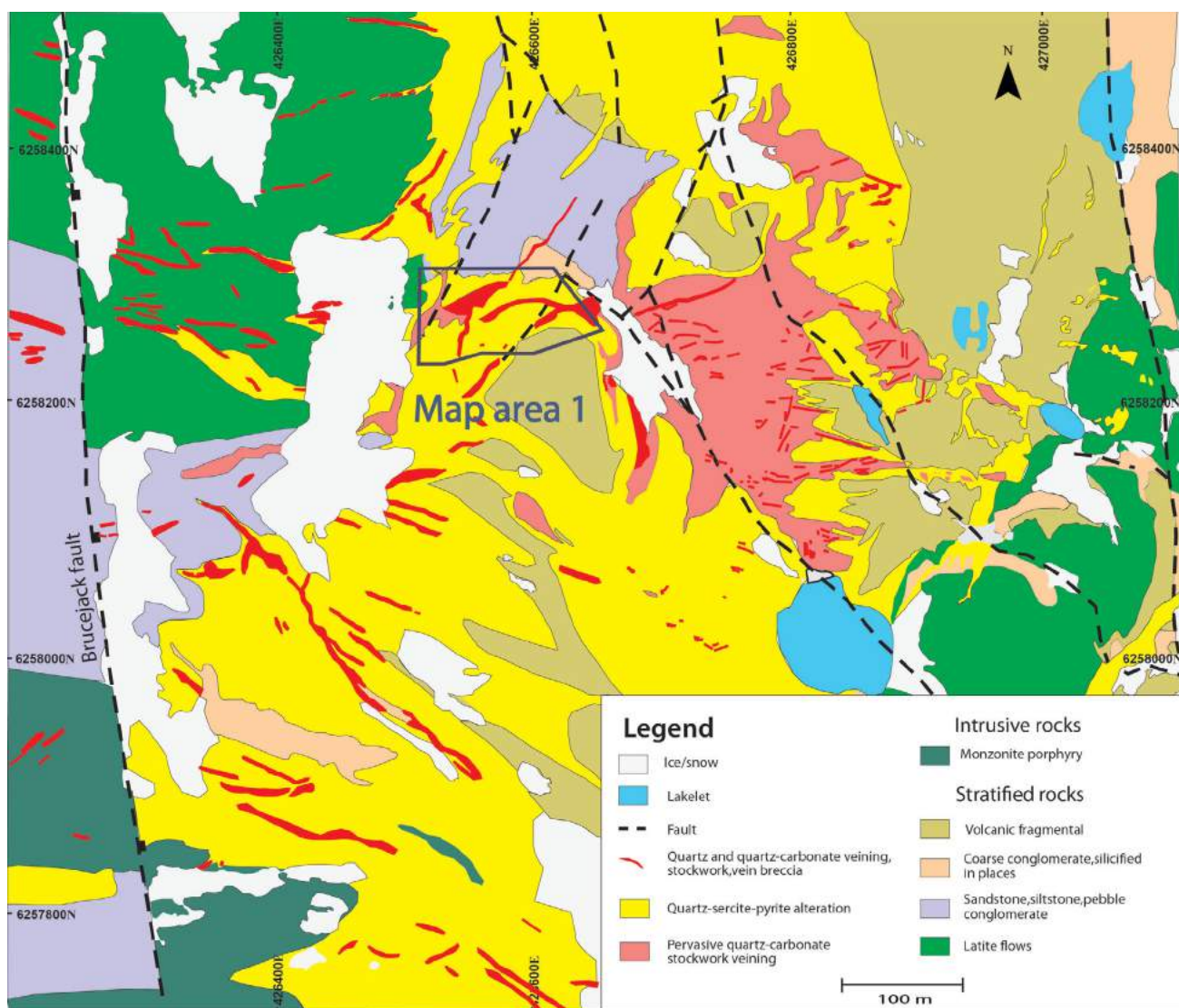
Figure 2. Simplified deposit geology of the Brucejack gold-silver deposit (modified from Pretium Resources Inc., unpublished data, 2015), with schematic representation of quartz-carbonate veining, stockwork and breccia (true thickness of veins approximately 0.5–10 m). Detail of map area 1 is shown in Figure 3. Stockwork system shown in map area 1 extends to the southeast as a broad zone of stockwork with both southeast- and east-striking veins.

Figure 3a presents the detailed outcrop geology of map area 1 (location shown in Figure 2). This outcrop is part of a large, steeply south-dipping stockwork system that strikes east-southeast to the west of the map area. Directly east of map area 1, Figure 2 shows northeast- to east-trending veins that are part of an area of pervasive quartz-carbonate stockwork that extends east and southeast for several hundred metres. This system may be linked to Domain 20 (see discussion), a stockwork zone that drillcore and underground workings show extends underground for 400 m along strike (east-southeast) and at least 400 m vertically (steeply south dipping; Pretium Resources Inc., unpublished data, 2015). Previous detailed surface mapping (Figure 2) shows that the stockwork system in map area 1 may actually consist of several large, en échelon stockwork zones (Pretium Resources, unpublished data, 2015). Figure 3a depicts one of these large zones and subsidiary stockwork.

Figure 3a shows that map area 1 contains several composite quartz veins, the largest of which is up to 10 m wide and strikes ~240° for at least 60 m. The boundaries of the smaller individual veins that form the composite 10 m wide zone can be distinguished only on the weathered surface of outcrop. Some of these individual veins are subhorizontal, creating a cap with less susceptibility to erosion that may enhance the strong positive relief of the vein in outcrop. On the southern edge of the intensely veined zone is 10–20 m of less intense stockwork and vein networks cutting intact wallrock, where several additional parallel stockwork zones, up to 4 m in width, were mapped. At the eastern edge of the mapped area, there is a 2–3 m wide stockwork zone
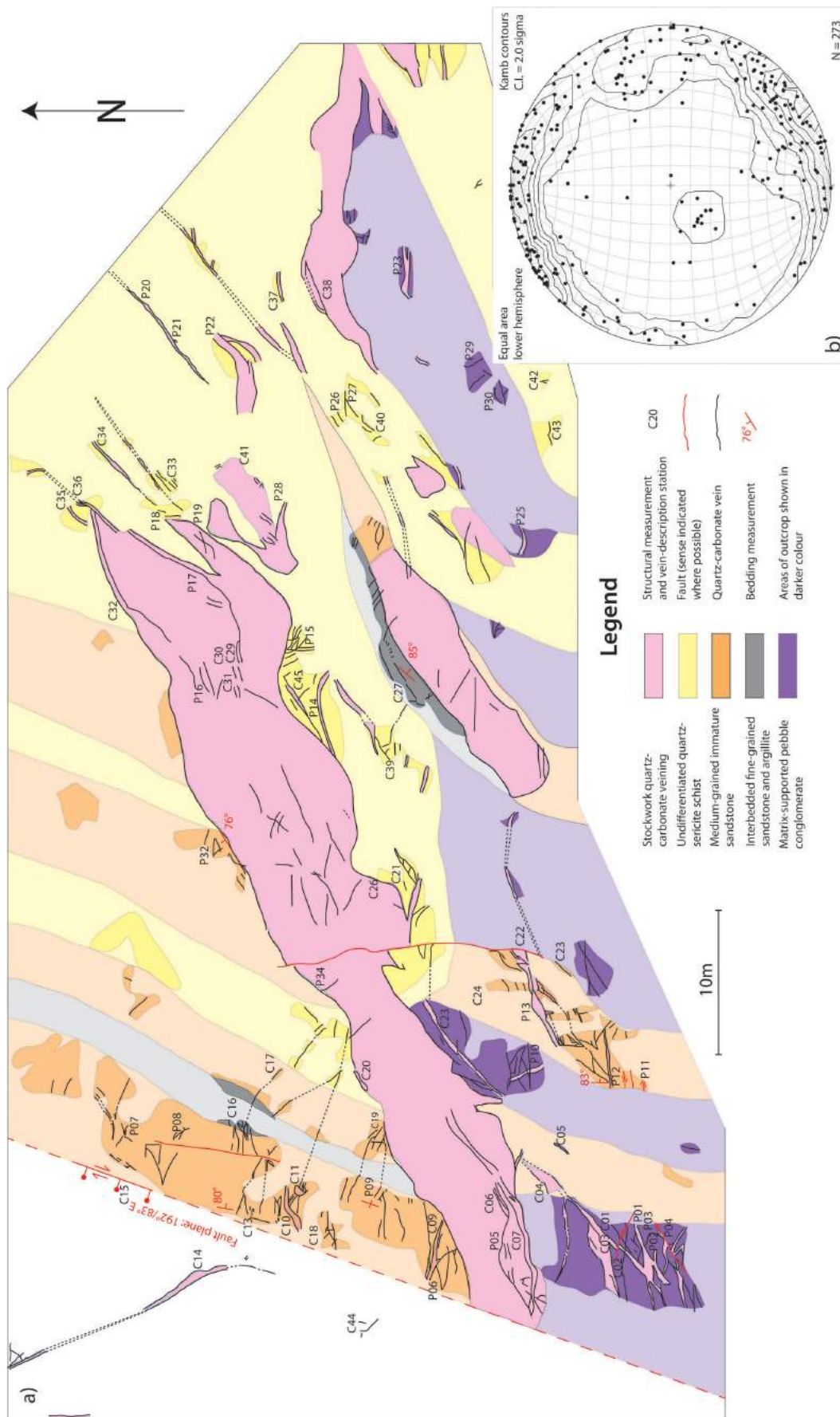
Figure 3. a) Lithology, stockwork quartz-carbonate veining and faults in map area 1 of the Brucejack gold-silver deposit (see Figure 2 for location). **b)** Equal-area projection of poles to vein orientations measured at stations indicated in (a); Kamb contours indicate concentration of poles. See text for further description.

that strikes east. At the western edge of the main stockwork zone, a 2 m wide fault zone offsets veining by reverse right-lateral motion (Figure 3a, station C15). To the north of the main stockwork zone, there are several veins that join with the main stockwork zone. These east-southeast-trending veins can be up to a metre wide. The surrounding zone of stockwork is typically not symmetric about the core (Figure 3a) and may consist of subsidiary zones of dense stockwork veining ~1 m wide. Along strike to the northeast from the largest stockwork zone, several continuous quartz-carbonate veins up to 1 m in width continue out of the map area at the same 060° azimuth as the main zone (station C34).

In total, 273 vein orientations were measured at indicated stations throughout the map area (Figure 3a, b). Mapping and equal-area projection plots of these veins indicate at least three sets of orientations: 1) continuous, east- to northeast-striking veins, up to 1 m wide, that are parallel with the main (en échelon) stockwork zones; 2) discontinuous, north-trending veins and veinlets (many below map scale on Figure 3a) located mainly in the eastern half of the map area; and 3) centimetre-scale, subhorizontal veins associated with dense stockwork zones. Many of the quartz-carbonate veins throughout the area of surface outcrop change orientation near intersections with other veins. Intersections where several veins coalesce are common, with each vein bending or following a previous fracture or vein toward a single intersection (Figure 4a). This geometry is evidence that at least some of the veins were open fractures when subsequent veins formed, acting as free surfaces to reorient the local stress field during crack propagation.

Lithological mapping is difficult due to the intensity of the QSP alteration around the stockwork veining, which serves to obliterate diagnostic rock textures. The rock type close to the intense veining is predominantly undifferentiated quartz sericite schist. However, there are areas with mappable units of immature medium-grained sandstone, interbedded finer grained sandstone and argillite, and matrix-supported pebble conglomerate. To the north of the main stockwork zone, there are regular 3–10 m wide beds of coarse sandstone, interbedded sandstone and undifferentiated quartz-sericite schist. To the south, there are irregular beds of pebble conglomerate. This juxtaposition of dissimilar rock sequences across the stockwork zone suggests that it coincides with a fault. Measurements and contact traces indicate that stratigraphy is steeply dipping and strikes north-northeast to northeast. Northeast-striking units are situated proximally southeast of the main stockwork zone and may trend closer to north farther along strike to the southwest, away from the large stockwork zone. To the north and southwest of the main stockwork zone, the unit contacts strike north-northeast. This pattern may indicate dextral drag of bedding along the southern contact of the stockwork zone, suggesting shear along the vein system.
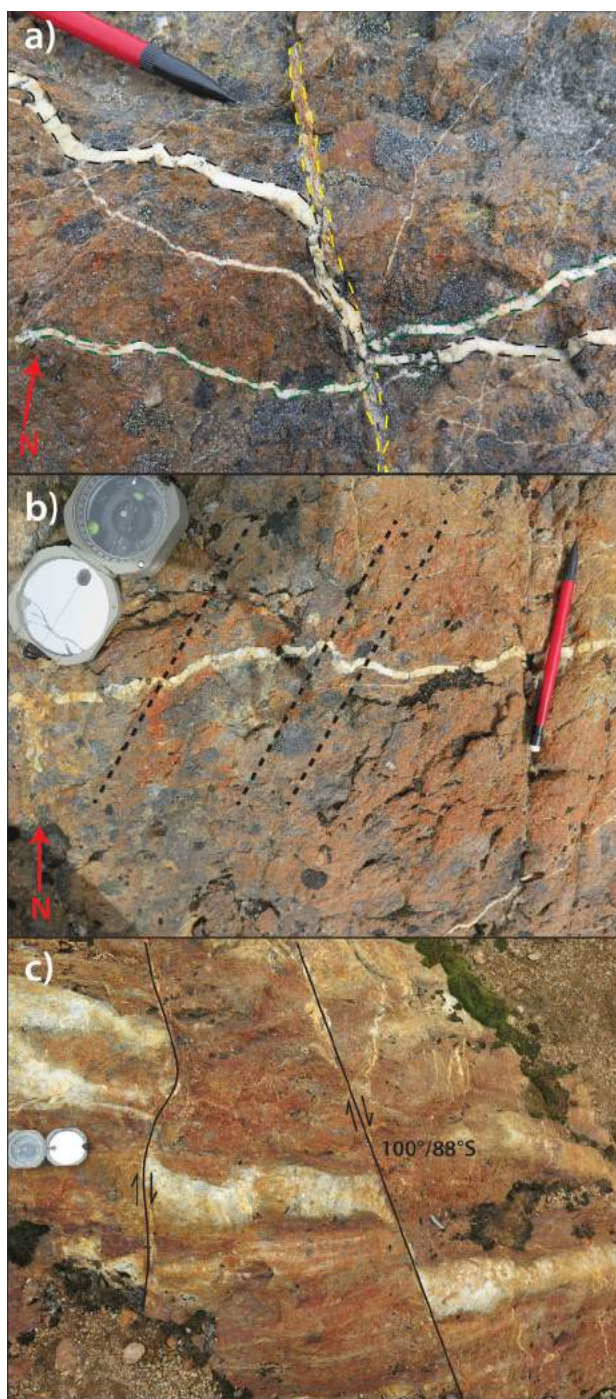
Figure 4. Photographs showing textures and geometry of veins and faults in map area 1 of the Brucejack gold-silver deposit: **a)** syntaxial quartz-carbonate veins bending and coalescing (green and black) along the surface of an earlier vein (yellow), station P10 (Figure 3a); **b)** disharmonic folding of a quartz-carbonate vein, the axial planes of the folds trending approximately 035°, station P10 (Figure 3a); **c)** two subvertical faults showing approximately 20 cm of apparent dextral offset of sandstone beds, station P11 (Figure 3a).

Minor faults mapped to the south of the main stockwork zone show minor left- and right-lateral apparent offset on the 10–50 cm scale. Only 12 exposed fault planes were measured in map area 1, which is not enough to construct a kinematic analysis, but a distinct set of faults was observed that is parallel to the large fault cutting the main stockwork zone on the western side of the map area. These faults strike east-southeast and dip steeply to the east. A few steeply dipping faults subparallel to the main stockwork are also exposed. They show both right-lateral (Figure 4b) and left-lateral apparent offset (Figure 3a, stations P01, P04, P11). Several veins were deformed into disharmonic folds (Figure 4c). The axial plane of these folds strikes ~35° with approximately subvertical dip, indicating some southeast-directed shortening that postdates vein formation.

Veins in map area 1 (Figure 3a) are predominantly quartz with minor calcite, although a small stockwork zone with 0.5–1 m thick, grey-weathering blocky calcite was mapped directly southeast of the main stockwork (Figure 3a, station C31). These carbonate veins show multiple phases of mineralization, with quartz layers in the centre and along the wallrock, as well as along fractures within the grey calcite. Quartz in this area displays a bladed crystal habit similar to that of calcite, suggesting that it pseudomorphed after calcite. Within the main stockwork zone, multiple phases of veining crosscut one another and are locally brecciated. Similarly, large bull quartz veins were observed in the underground workings crosscutting early-silicified wallrock and breccia, as well as early veins of banded colloform quartz with local cores of cryptocrystalline silica. Quartz growth in most veins, where it can be observed, is syntaxial, with symmetric crystal growth away from the wallrock toward the centre of the vein (e.g., Bons et al., 2012). Similar euhedral to blocky quartz is also found as rims on many of the breccia clasts, with radial quartz growth occurring from clast boundaries into pore space. Both of these textures suggest there was open-space growth of quartz.

Electrum mineralization is not observed in the outcrop of map area 1 due to weathering and gossan formation on the surface. However, it can be seen in multiple locations underground (Figure 5). It is located in predominantly quartz-carbonate vein breccia within or proximal to the main stockwork zones (Figure 5c). Electrum can be present in reworked quartz-carbonate vein clasts within vein stockwork (Figure 5c), as well as in more continuous veins and sheeted veins. At least one location shows electrum crosscut by a later syntaxial quartz vein, indicating that stockwork formation occurred for some time after some electrum precipitation or deposition. Base metal–sulphide (galena, sphalerite, chalcopyrite) quartz-carbonate veins are visible underground. They contain silver sulphosalts and silver-rich electrum, and can be tabular and continuous over tens of metres.

Where the tentatively related stockwork system (named 'Domain 20' by Pretium Resources Inc.) is exposed in the walls of underground workings down-dip from map area 1, patterns similar to those observed on surface emerge (Figure 5a). However, with a much smaller number of measurements underground, the clustering is less clear in equal-area projections (Figure 5b), and the measured vein orientations do not belong to the same population shown in Figure 3b. The thickest veins may dominate the pattern seen in outcrop, which makes it visible in outcrop but obscured on the equal-area projection that includes all vein measurements. Underground, a distinct set of vertical veins parallel to and south of the main stockwork can be seen. Sigmoidal tension gashes that crosscut steep veins can be seen in the footwall of a significant reverse fault. However, these definitive fault-related veins are the latest stage of veining seen in Figure 4a and do not appear to be related to the stockwork veining in Domain 20.

Discussion

The vein systems seen in map area 1 and in the underground workings of the Brucejack deposit show a textural relationship. Both show a (5–10 m wide) core zone with intense stockwork consisting of several generations of quartz-carbonate veins whose contacts are difficult to discern. Away from this core zone, vein intensity diminishes, and a sharper boundary is observed on the north contact (footwall) of the core stockwork. To the south, large, steeply dipping veins with associated stockwork are spaced centimetres to decimetres apart within a region up to 20 m away from the core, in the hangingwall of the stockwork system. These large parallel veins can be seen close to the south contact (hangingwall) of the core zone in both the ~80 m long (strike-parallel) surface map and the ~15 m long (dip-parallel) underground exposure. Measured vein orientations underground and on surface, however, are different (Figures 3b, 5b), with the underground veins showing a distinct southeast trend compared to the east-northeast trend of those in map area 1. Also, a direct projection of the Domain 20 stockwork system to surface (Pretium Resources Inc., unpublished data, 2015), using both drillhole intercepts and underground measurements, would lie 100 m to the south of map area 1. There is a distinct possibility that the two sites do not expose the same continuous vein system; they may be linked, however, via one of the following three scenarios:

- The Domain 20 system could branch updip, meaning that the stockwork seen in map area 1 may represent a northern branch of Domain 20 (Figure 6a).

- To the east of map area 1, an extensive stockwork zone that extends both east and southeast (Figure 2) contains en échelon east-trending veins (Figure 2). This type of en échelon pattern may also extend downdip from map

area 1, causing the stockwork system to step south downdip (Figure 6b).

- The stockwork has been displaced along one or more north-verging thrust faults (Figure 6c). Figure 4a shows a steeply south-dipping reverse fault cutting the main stockwork zone of Domain 20 underground. Motion is deduced from tension gashes and offsets on tension gashes along a conjugate fault below the main through-going fault plane. Late north-verging thrust faults that could be related to formation of the Skeena fold-and-thrust belt have been mapped elsewhere in underground workings, on surface and using drillholes (Board and McNaughton, 2013; Jones, 2013). Combined north-ward heave on several of these faults between the outcrop and the exposures in the underground workings may result in an offset between the projected location of Domain 20 and the outcrop in map area 1 (Figure 6c).
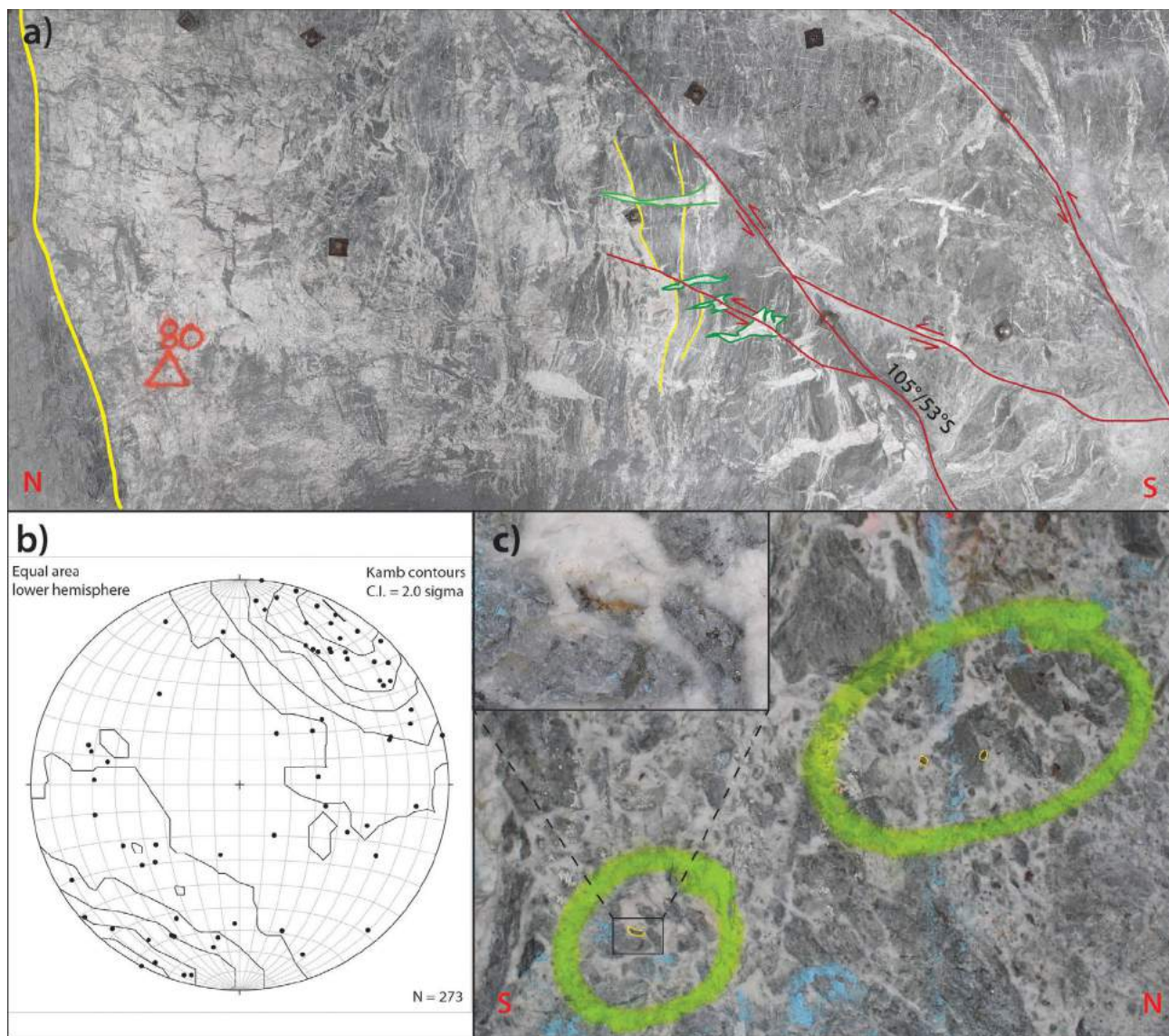
Figure 5. Photographs and measurements of stockwork exposure in the underground workings at the Brucejack gold-silver deposit: **a)** Domain 20 exposure in the east wall of a crosscut; view of vertical wall is approximately 8 m wide and faces east; yellow lines indicate subvertical veining and the sharp northern contact of the core stockwork zone of Domain 20; location of the subvertical veins highlighted in yellow on the south side shows where there is a transition from the core stockwork zone to less intense quartz-carbonate veining; red lines show late faults with associated tension-gash veins that crosscut subvertical veins highlighted in green; **b)** equal-area projection shows poles to 71 veins; Kamb contour interval is 2σ; measurements were taken from both the east and west walls of the photographed crosscut, as well as both the east and west walls of another exposure updip (85 m vertically above photo); **c)** quartz-carbonate breccia along the north (footwall contact) of Domain 20; small yellow circles indicate electrum-quartz vein fragments that form clasts in the breccia; circle spray-painted green in bottom left of photo is approximately 15 cm in diameter; inset in top left corner shows electrum within a clast of older grey quartz surrounded by younger white quartz that forms cement within the breccia.
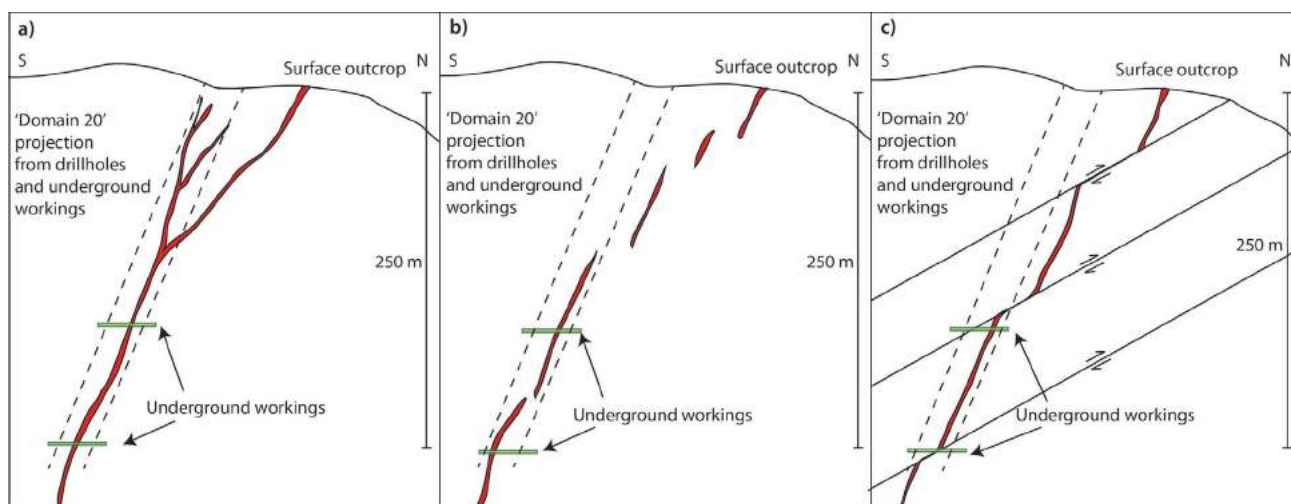
Figure 6. Schematic representation of the projection of Domain 20 from underground workings, drillhole intercepts and surface outcrop of stockwork to the north (map area 1), being offset by **a)** branching stockwork geometry, **b)** en échelon stockwork veining, or **c)** north-verging thrust faults.

However, these scenarios do not explain the differing orientations of veins between map area 1 and the underground exposure (Figures 3b, 5b).

A number of observations suggest that the stockworks of map area 1 and Domain 20 occupy fault/shear zones. The offset in rock units across the stockwork zone, and the similarities in geometry of the stockwork and surrounding zone of veining to fault-zone cores and damage zones described in the literature (e.g., Chester and Logan, 1986; Smith et al., 1990; Forster et al., 1991; Caine et al., 1996), indicate that these types of stockwork features (which include Domain 20) formed along fault zones. In the case of the mapped outcrop, the massive composite quartz vein is the fault core and the surrounding steep veining is the damage zone, with veins appearing to follow fracture sets with Andersonian fault geometry (e.g., Caine et al., 2010). Figure 3a shows several areas (stations C03, C09, P10) where sets of steeply dipping conjugate veins may exist. Equal-area projection plots of poles to vein orientation from both the underground workings and the surface outcrop show predominantly steep veining, and the range in strike of these veins reflects varied damage-zone fracture geometry. At least one of the exposures of the Domain 20 stockwork system in the underground workings shows an abrupt contact between stockwork and wallrock on the north contact (the footwall) of the main stockwork zone. On the south (hangingwall) contact, there is an extensive zone of less intense stockwork veining. Similarly, the north contact on the surface map displays a significant drop in stockwork-vein intensity (Figure 3a). Here, several large veins are mapped, but vein size and intensity are less than to the south, where 10–20 m of less intense stockwork veining is mapped.

These outcrop patterns show an asymmetry in veining about the core stockwork zone. Asymmetry in damage zones around faults due to asymmetric strain distribution can be a result of lithological or structural contrast across a fault zone (e.g., Aydin and Johnson, 1978; Antonellini and Aydin, 1995; Nelson et al., 1999; Mitra and Ismat, 2001; Clausen et al., 2003; Doughty, 2003; Berg and Skar, 2005). Mapped rock units in Figure 3a show a pronounced bend near the southern contact of the core stockwork zone. This may be due to drag folding of strata during apparent dextral fault motion. Exposures in the underground workings show areas of brecciation along the contacts of the core stockwork zone (Figure 5a, c) that could also be a result of faulting. Clasts within this breccia include quartz-carbonate vein and wallrock, indicating that the fault zone was active during the formation of stockwork vein systems such as Domain 20.

Although the overall geometry of the stockwork in map area 1 is suggestive of shear offset, many of the veins within the stockwork do not show measurable offset across them and are interpreted as opening-mode veins. Syntaxial quartz growth indicates open-space quartz crystallization, which may be evidence of supra-lithostatic fluid pressure (Wilson, 1994; Bons et al., 2012). This syntaxial texture is seen in all orientations of veins, including subhorizontal veins, further supporting the suggestion of extremely high pore pressure. As most of the quartz is syntaxial and euhedral, and there is a lack of consistent offset across veins, the authors deduce that quartz-crystal growth did not occur during periods of major slip along faults. Much of the quartz precipitation occurred during periods of static high fluid pressure between slip and fracturing events, or within pressurized fracture networks in the damage zone of the fault. However, cryptocrystalline quartz within some vein cores may also indicate that rapid silica precipitation occurred during changes in temperature or pressure caused by seismic events. As there are many crosscutting relation-

ships between isolated veins, large composite veins and vein breccias containing clasts of quartz-carbonate vein material (including electrum-mineralized veins), it can also be deduced that the formation of stockwork veining occurred during multiple seismic events. These seismic events must predate later Cretaceous transpression during emplacement of the Skeena fold-and-thrust belt.

Examination of the electrum mineralization in the Domain 20 stockwork system underground does not show that it occurs at any preferred structural traps. This may be due to the fact that electrum is locally observed in clasts and vein fragments within the core stockwork zone, and so was inherited from older vein systems that have been reworked into the present vein geometry. Consequently, deducing the original location of electrum precipitation when it occurs as a clast may be difficult. Instances of electrum mineralization being crosscut by later syntaxial quartz-carbonate veining indicate that the mineralization was not an isolated later event. Instead, the electrum mineralization is considered to have formed both early in the development of the stockwork and coeval with the stockwork development.

Conclusions

Vein mapping and observations on selected large quartz-carbonate stockwork zones in outcrop and underground workings (e.g., Domain 20) show similarities in vein texture and geometry, indicating that they may be part of the same stockwork system. However, the surface projection of Domain 20 is approximately 100 m south of the outcrop investigated in map area 1. This offset could be due to branching stockwork veining, an en échelon stockwork vein network or previously mapped north-verging thrust faults. Previously described fault-zone geometry has similarities to mapped stockworks at the Brucejack deposit, and offset of lithological units across the main stockwork in map area 1 suggests shear offset. This leads the authors to believe that the described stockwork formed within a fault zone. Quartz-vein formation occurred within open space in fractures where the static fluid pressure was above that of lithostatic pressure. Multiple slip events have caused several generations of fractures, with quartz growth within veins occurring mainly between fracturing events (i.e., earthquake slip) and lesser cryptocrystalline quartz precipitation occurring during seismic slip. The fault core consists of recycled vein material, which also indicates that cyclic seismicity occurred during vein formation. This seismicity must predate later Cretaceous polyphase deformation during emplacement of the Skeena fold-and-thrust belt. Electrum occurring within recycled clasts of quartz-carbonate veining, and electrum occurrences that are cut by syntaxial quartz-carbonate veining, show that at least one of the mineralizing event(s) at Brucejack was early to coeval with stockwork emplacement.

Future Work

Further investigation of field data and analysis of samples is required to achieve the ultimate goal of investigating the role of colloidal transport in the formation of high-grade quartz-carbonate veins. The structural setting of electrum occurrence is still not fully understood. The pattern of displacement across faults and veins will be further analyzed to constrain stress orientation during fault-zone and vein formation within the mapped stockwork systems. Maps and structural data for the two other outcrop locations will be compared to the information presented here in order to generalize stockwork geometries on the deposit scale. The structural setting in which electrum mineralization occurs within Domain 20 is difficult to determine due to complexity of the stockwork and the existence of electrum within clasts. Electrum occurrences elsewhere in the underground workings at the Brucejack deposit have been documented within smaller continuous veins where the structural setting may be more easily deduced. Several of these locations were described in the field in August 2015 and will be further analyzed to determine if electrum mineralization at Brucejack occurs in a preferred structural setting. Additionally, millimetre- to micrometre-scale analysis of both electrum and vein quartz will be used to investigate whether relict colloid textures exist, which might confirm colloidal transport and deposition.

References

Antonellini, M. and Aydin, A. (1995): Effect of faulting on fluid flow on porous sandstones: geometry and spatial distribution; American Association of Petroleum Geologists Bulletin, v. 79, no. 5, p. 642–671.

Aydin, A. and Johnson, A.M. (1978): Development of faults as zones of deformation bands and slip surfaces in sandstone; Pure and Applied Geophysics, v. 116, p. 931–942.

Berg, S.S. and Skar, T. (2005): Controls on damage zone asymmetry of a normal fault zone: outcrop analyses of a segment of the Moab fault, SE Utah; Journal of Structural Geology, v. 27, no. 10, p. 1803–1822.

Board, W.S. and McNaughton, K.C. (2013): The Brucejack high-grade gold project, northwest British Columbia, Canada; *in* Proceedings of NewGenGold Conference, November 26–27, Perth, Australia, p. 177–191.

Bons, P.D., Elburg, M.A. and Gomez-Rivas, E. (2012): A review of the formation of tectonic veins and their microstructures; Journal of Structural Geology, v. 43, 33–62.

Bridge, D.J. (1993): The deformed Early Jurassic Kerr copper-gold porphyry deposit, Sulphurets gold camp, northwestern British Columbia; M.Sc. thesis, University of British Columbia.

Caine, J.S., Bruhn, R.L. and Forster, C.B. (2010): Internal structure, fault rocks, and inferences regarding deformation, fluid flow, and mineralization in the seismogenic Stillwater normal fault, Dixie Valley, Nevada; Journal of Structural Geology, v. 32, no. 11, p. 1576–1589.

Caine, J.S., Evans, J.P. and Forster, C.B. (1996): Fault zone architecture and permeability structure; Geology, v. 24, no. 11, p. 1025–1028.

Chester, F.M. and Logan, J.M. (1986): Implications for mechanical properties of brittle faults from observations of the Punchbowl fault zone, California; Pure and Applied Geophysics, v. 124, no. 1–2, p. 79–106.

Clausen, J.A., Gabrielsen, R.H., Johnsen, E. and Korstgård, J.A. (2003): Fault architecture and clay smear distribution: examples from field studies and drained ring-shear experiments; Norwegian Journal of Geology, v. 83, no. 2, p. 131–146.

Davies, A., Macdonald, A.J. and Lewis, P.D. (1994): Stratigraphic and structural setting of mineral deposits in the Brucejack Lake area, northwestern British Columbia; *in* Current Research 1994-A, Geological Survey of Canada, p. 37–43.

Doughty, P.T. (2003): Clay smear seals and fault sealing potential of an exhumed growth fault, Rio Grande Rift, New Mexico; American Association of Petroleum Geologists Bulletin v. 87, no. 3, p. 427–444.

Erdmer, P. and Cui, Y. (2009): Geological map of British Columbia; BC Ministry of Energy, Mines and Petroleum Resources, Geoscience Map 2009-1, scale 1:1 500 000.

Evenchick, C.A. (1991): Geometry, evolution, and tectonic framework of the Skeena fold belt, north-central British Columbia; Tectonics, v. 10, no. 3, p. 527–546.

Evenchick, C.A. (2001): Northeast-trending folds in the western Skeena Fold Belt, northern Canadian Cordillera: a record of Early Cretaceous sinistral plate convergence; Journal of Structural Geology, v. 23, no. 6, p. 1123–1140.

Faber, C., Rowe, C.D., Miller, J.A., Fagereng, Å. and Neethling, J.H. (2014): Silica gel in a fault slip surface: field evidence for palaeo-earthquakes? Journal of Structural Geology, v. 69A, p. 108–121.

Febbo, G.E., Kennedy, L.A., Savell, M., Creaser, R.A. and Friedman, R.M. (2015): Geology of the Mitchell Au-Cu-Ag-Mo porphyry deposit, northwestern British Columbia, Canada; *in* Geological Fieldwork 2014, BC Ministry of Energy and Mines, BC Geological Survey, Paper 2015-1, p. 59–86.

Forster, C.B. and Evans, J.P. (1991): Hydrogeology of thrust faults and crystalline thrust sheets: results of combined field and modeling studies; Geophysical Research Letters, v. 18, no. 5, p. 979–982.

Gagnon, J.F., Barresi, T., Waldron, J.W., Nelson, J.L., Poulton, T.P. and Cordey, F. (2012): Stratigraphy of the upper Hazelton Group and the Jurassic evolution of the Stikine terrane, British Columbia; Canadian Journal of Earth Sciences, v. 49, no. 9, p. 1027–1052.

Hayashi, K.I., Maruyama, T. and Satoh, H. (2001): Precipitation of gold in a low-sulfidation epithermal gold deposit: insights from a submillimeter-scale oxygen isotope analysis of vein quartz; Economic Geology, v. 96, no. 5, p. 211–216.

Heinrich, C.A., Driesner, T., Stefánsson, A. and Seward, T.M. (2004): Magmatic vapour contraction and transport of gold from the porphyry environment to epithermal ore deposits; Geology, v. 32, no. 9, p. 761–764.

Henderson, J.R., Kirkham, R.V., Henderson, M.N., Payne, J.G., Wright, T.O. and Wright, R.L. (1992): Stratigraphy and structure of the Sulphurets area, British Columbia; *in* Current Research, Part A: Cordillera and Pacific Margin, Geological Survey of Canada, Paper 82-1A, p. 323–332, URL <http://ftp2.cits.rncan.gc.ca/pub/geott/ess_pubs/132/132780/pa_92_1a.pdf> [November 2015].

Herrington, R.J. and Wilkinson, J.J. (1993): Colloidal gold and silica in mesothermal vein systems; Geology, v. 21, no. 6, p. 539–542.

Hough, R.M., Noble, R.R.P. and Reich, M. (2011): Natural gold nanoparticles; Ore Geology Reviews, v. 42, p. 55–61.

Johnson, K., Nissen, E., Saripalli, S., Arrowsmith, J., McGarey, P., Scharer, K., Williams, P. and Blisniuk, K. (2014): Rapid mapping of ultrafine fault zone topography with structure from motion; Geosphere, v. 10, no. 5, p. 969–986.

Jones, I.W.O. (2014): Pretium Resources Inc.: Brucejack Project, Mineral Resources Update Technical Report, Effective Date – 19 December 2013; NI 43-101 report prepared by Snowden Mining Industry Consultants for Pretium Resources Inc., 194 p., URL <http://www.sedar.com/GetFile.do?lang=EN&docClass=24&issuerNo=00030613&fileName=/csfsprod/data149/filings/02160428/00000001/C%3AacsedarPVGPVG43101TechReport.pdf> [November 2015].

Kirkham, R.V. (1992): Preliminary geological map of the Brucejack Creek area, British Columbia; Geological Survey of Canada, Open File 2550, scale 1:5000, URL <http://geoscan.nrcan.gc.ca/starweb/geoscan/servlet.starweb?path=geoscan/downloade.web&search1=R=133465> [November 2015].

Kirkham, R.V. and Margolis, J. (1995): Overview of the Sulphurets area, northwestern British Columbia; *in* Porphyry Deposits of the Northwestern Cordillera of North America, Canadian Institute of Mining, Metallurgy and Petroleum, Special Volume 46, p. 473–483.

Kirkpatrick, J.D., Rowe, C.D., White, J.C., and Brodsky, E.E. (2013): Silica gel formation during fault slip: evidence from the rock record; Geology, v. 41, no. 9, p. 1015–1018.

Krupp, R.E. and Seward, T.M. (1987): The Rotokawa geothermal system, New Zealand: an active epithermal gold-depositing environment; Economic Geology, v. 82, no. 5, p. 1109–1129.

Mikucki, E.J. (1998): Hydrothermal transport and depositional processes in Archean lode-gold systems: a review; Ore Geology Reviews, v. 13, no. 1, p. 307–321.

Mitra, G. and Ismat, Z. (2001): Microfracturing associated with reactivated fault zones and shear zones: what can it tell us about deformation history? *in* The Nature and Tectonic Significance of Fault Zone Weakening, R.E. Holdsworth, R.A. Strachan, J.F. Magloughlin and R.J. Knipe (ed.), Geological Society, London, Special Publications, v. 186, p. 113–140.

Monger, J., Price, R. and Tempelman-Kluit, D. (1982): Tectonic accretion and the origin of the two major metamorphic and plutonic welts in the Canadian Cordillera; Geology, v. 10, no. 2, p. 70–75.

Nelson, E.P., Kullman, A.J. and Gardner, M.H. (1999): Fault-fracture networks and related fluid flow and sealing, Brushy Canyon Formation, West Texas; *in* Faults and Subsurface Fluid Flow in the Shallow Crust, L.B. Goodwin, P.S. Mozley, J.M. Moore and W.C. Haneberg (ed.), American Geophysical Union, Geophysical Monograph 113, p. 69–81.

Nelson, J. and Colpron, M. (2007): Tectonics and metallogeny of the British Columbia, Yukon and Alaskan Cordillera, 1.8 Ga to the present; *in* Mineral Deposits of Canada: A Synthesis of Major Deposit-Types, District Metallogeny, the Evolution of Geological Provinces, and Exploration Methods, W.D. Goodfellow (ed.), Geological Association of Canada, Mineral Deposits Division, Special Publication 5, p. 755–791.

Nelson, J. and Kyba, J. (2014): Structural and stratigraphic control of porphyry and related mineralization in the Treaty Glacier–KSM–Brucejack–Stewart trend of western Stikinia; *in* Geological Fieldwork 2013, BC Ministry of Energy and Mines, BC Geological Survey, Paper 2014-1, p. 111–140.

Pretium Resources Inc. (2013): Geology of the Brucejack property; Pretium Resources Inc., URL <http://www.pretivm.com/files/doc_downloads/geology/2013429_Geology_for_website_APRIL2013_WSB.pdf> [October, 2015].

Saunders, J.A. (1990): Colloidal transport of gold and silica in epithermal precious-metal systems: evidence from the Sleeper deposit, Nevada; Geology, v. 18, p. 757–760.

Saunders, J.A. and Schoenly, P.A. (1995): Boiling, colloid nucleation and aggregation, and the genesis of bonanza Au-Ag ores of the Sleeper deposit, Nevada; Mineralium Deposita, v. 30, no. 3–4, p. 199–210.

Simmons, S.F. and Browne, P.R. (1990): Mineralogic, alteration and fluid-inclusion studies of epithermal gold-bearing veins at the Mt. Muro prospect, central Kalimantan (Borneo), Indonesia; Journal of Geochemical Exploration, v. 35, no. 1, p. 63–103.

Smith, L., Forster, C.B. and Evans, J.P. (1990): Interaction between fault zones, fluid flow and heat transfer at the basin scale; *in* Hydrogeology of Low Permeability Environments, S.P. Newman and I. Neretnieks (ed.), International Association of Hydrological Sciences Selected Papers in Hydrogeology, v. 2, p. 41–67.

Tombe, S.P. (2015): The Brucejack epithermal Au-Ag deposit, northwestern British Columbia; M.Sc. thesis, University of Alberta.

Williams-Jones, A.E., Bowell, R.J. and Migdisov, A.A. (2009): Gold in solution; Elements, v. 5, p. 281–287.

Wilson, C.J.L. (1994): Crystal growth during a single-stage opening event and its implications for syntectonic veins; Journal of Structural Geology, v. 16, no. 9, p. 1283–1296.

Zezin, D.Y., Migdisov, A.A. and Williams-Jones, A.E. (2011): The solubility of gold in H_2O-H_2S vapour at elevated temperature and pressure; Geochimica et Cosmochimica Acta, v. 76, p. 5140–5153.

Stratigraphic and Lithological Constraints of Late Cretaceous Volcanic Rocks in the TREK Project Area, Central British Columbia (NTS 093E)

R.S. Kim, Mineral Deposit Research Unit, University of British Columbia, Vancouver, BC, rsykim@eos.ubc.ca

C.J.R. Hart, Mineral Deposit Research Unit, University of British Columbia, Vancouver, BC

J.J. Angen, Mineral Deposit Research Unit, University of British Columbia, Vancouver, BC

J.M. Logan, Consulting Geologist, Victoria, BC

Introduction

The TREK (**T**argeting **R**esources for **E**xploration and **K**nowledge) project aims to facilitate mineral exploration in the northern Interior Plateau in central British Columbia by using a multidisciplinary approach to improve geological confidence and knowledge (Clifford and Hart, 2014). The TREK area is considered to have high mineral exploration potential with numerous epithermal and porphyry deposits documented in the region, including New Gold Inc.'s Blackwater Au-Ag epithermal deposit. The hostrocks for the Blackwater orebody, and other epithermal occurrences in the region, are interpreted to be Late Cretaceous Kasalka Group volcanic rocks (Christie et al., 2014; Looby, 2015); consequently this volcanic rock package is highly prospective. However, extensive Eocene and Neogene magmatism, along with glacial till, obscure older bedrock exposure, leading to considerable uncertainty in the distribution of the Kasalka Group across central BC.

Fieldwork conducted in 2015 focused on the correlation of geophysical signatures to rock units and structures in the TREK area, as well as their relationships to mineral occurrences in the region (Angen et al., 2016). Comparisons to the Late Cretaceous Kasalka Group type section, defined by MacIntyre (1977, 1985, 1988) in the Tahtsa and Whitesail Lake areas (NTS 093E), will be made to better define the regional distribution of Late Cretaceous volcanic rocks throughout central BC. This project is a joint initiative between the Mineral Deposit Research Unit (MDRU) at the University of British Columbia (UBC) and Geoscience BC to characterize the Kasalka Group and to distinguish Late Cretaceous volcanic rocks from visually comparable Jurassic and Eocene volcanic suites in the area. The results from

new regional 1:20 000 scale bedrock mapping, aided by high-resolution geophysical surveys (Angen et al., 2015), along with geochronological and geochemical analysis of field samples, will enable easier identification of the Kasalka Group rocks, thereby aiding in future exploration targeting initiatives within the TREK project area.

Regional Geology

Tectonic Framework

British Columbia consists predominantly of several tectonic blocks that accreted onto the western margin of ancestral North America during the Mesozoic Era (Monger, 1977). Much of central BC is underlain by the Intermontane Belt that comprises the amalgamated Stikine, Cache Creek and Quesnel terranes (Monger and Price, 2002). The Stikine and Quesnel terranes formed as volcanic-oceanic island arcs that may have been part of the same Late Triassic arc that enclosed the Cache Creek terrane during accretion onto the continental margin (Mihalynuk et al., 1994). The underlying units in the study area are Late Triassic to Middle Jurassic arc volcanic rocks of the Stikine terrane and their erosional products. Overlap basinal assemblages of the Bowser Lake Group record marine deposition from the Late Jurassic until the mid-Cretaceous, with subsequent deposition of the Skeena Group in the Early Cretaceous (Riddell, 2011). Continental volcanic arcs formed episodically through the Late Cretaceous to the Eocene and produced the Kasalka, Ootsa Lake and Endako groups of volcanic strata (Evenchick, 1991). The younger rocks exposed in central BC are dominantly the extensive Eocene Endako Group and basalt flows of the Neogene Chilcotin Group (Bevier et al., 1983).
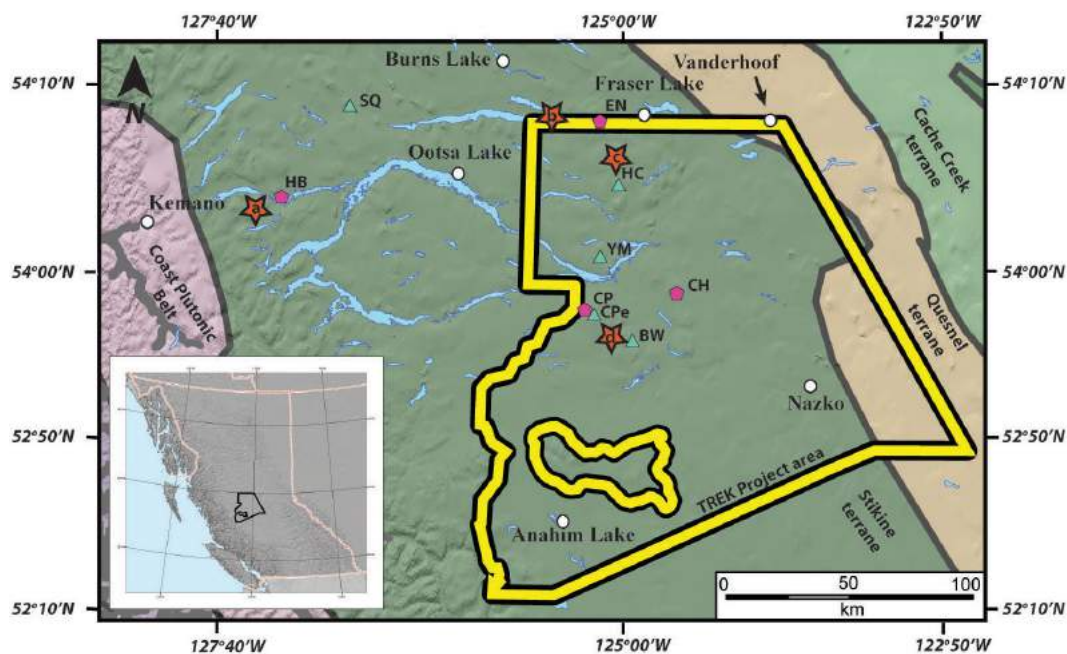
Late Cretaceous Volcanic Rocks

Late Cretaceous volcanic rocks in the TREK project area are closely associated with several mineral deposits and occurrences, including hostrocks to the Blackwater deposit, with its epithermal style Au-Ag mineralization (Christie et

Figure 1. The TREK project area, central British Columbia, modified from Colpron et al. (2007). Stars indicate the locations of stratigraphic sections (See Figure 2) that are based on mapping of Late Cretaceous Kasalka Group rocks. Green triangles indicate locations of epithermal mineralization hosted in Late Cretaceous volcanic packages: BW, Blackwater; CPe, Capoose; HC, Holy Cross; SQ, Silver Queen; YM, Yellow Moose. Pink pentagons indicate porphyry deposits in the region. Jurassic: EN, Endako; Cretaceous: CP, Capoose; HB, Huckleberry; Eocene: CH, Chu.

al., 2014; Looby, 2015). Similar mineralization styles occur in Late Cretaceous felsic dikes and sills of the Capoose epithermal prospect (Figure 1), 27 km northwest of Blackwater (Andrew, 1988; Bordet et al., 2011). The Newton epithermal deposit, located ~175 km southeast of Blackwater in the Chilcotin Plateau, is hosted in Late Cretaceous felsic fragmental volcanic rocks (McClenaghan, 2013) and represents the most southerly known occurrence of Late Cretaceous epithermal mineralization in central BC. Late Cretaceous rocks of the Tip Top Hill (known informally as Brian Boru) Formation also host the Silver Queen epithermal Au-Ag-Zn-Pb deposit (Leitch et al., 1991) south of the town of Houston (Figure 1). The Huckleberry mine is a Cu-Mo porphyry deposit, hosted in the Late Cretaceous Bulkley intrusive suite and located approximately 120 km southwest of Houston, BC (MacIntyre, 1985; Ferbey and Levson, 2000; Diakow, 2006).

Kasalka Group

The Kasalka Group was first defined in the Whitesail Lake map area (NTS 093E) by D.G. MacIntyre (1977). The type section is characterized by a basal conglomerate that unconformably overlies deformed Lower Cretaceous Skeena Group rocks and is therefore interpreted to be deposited during the Late Cretaceous (MacIntyre, 1977, 1985). The conglomerate is overlain by thick packages of andesitic flows and volcaniclastic rocks. The uppermost members of the Kasalka Group consist of felsic flows and fragmental

units (MacIntyre, 1977, 1985). The descriptions originally made at the type section are also applied to volcanic rocks across the northern half of the TREK project area, which is dominated by andesitic flows with minor felsic components (Anderson et al., 1999, 2000).

The distribution of the felsic flows and fragmental units in the northern half of the TREK project area, indicates their probable formation proximal to an eruptive centre, such as a rhyolite dome or a caldera complex (Looby, 2015). In the area west of the Blackwater deposit, this felsic package was initially interpreted to belong to the Eocene Ootsa Lake Group (Diakow and Levson, 1997), an interpretation supported by the paucity of mineralization compared to the felsic rocks within the Blackwater deposit (R. Whiteaker, pers. comm., 2015). Improved exposure with recent logging activity made it possible to conduct detailed mapping and improve understanding of the stratigraphic relationships of various units in the area, and has resulted in this package being reassigned to the Late Cretaceous (R. Whiteaker, pers. comm., 2015). A capping unit of a variably quartz-bearing rhyolite lithic-ash tuff is common to the Blackwater deposit (Figure 2d). This resistant unit is found to crop out at higher elevations near Blackwater, and was interpreted as part of the Eocene Ootsa Lake Group (Diakow and Levson, 1997). However, lithological similarities to the Late Cretaceous G-Pluton (quartz-eye granite dated at 68.3 ±2 Ma; R. Whiteaker, pers. comm., 2015) sug-
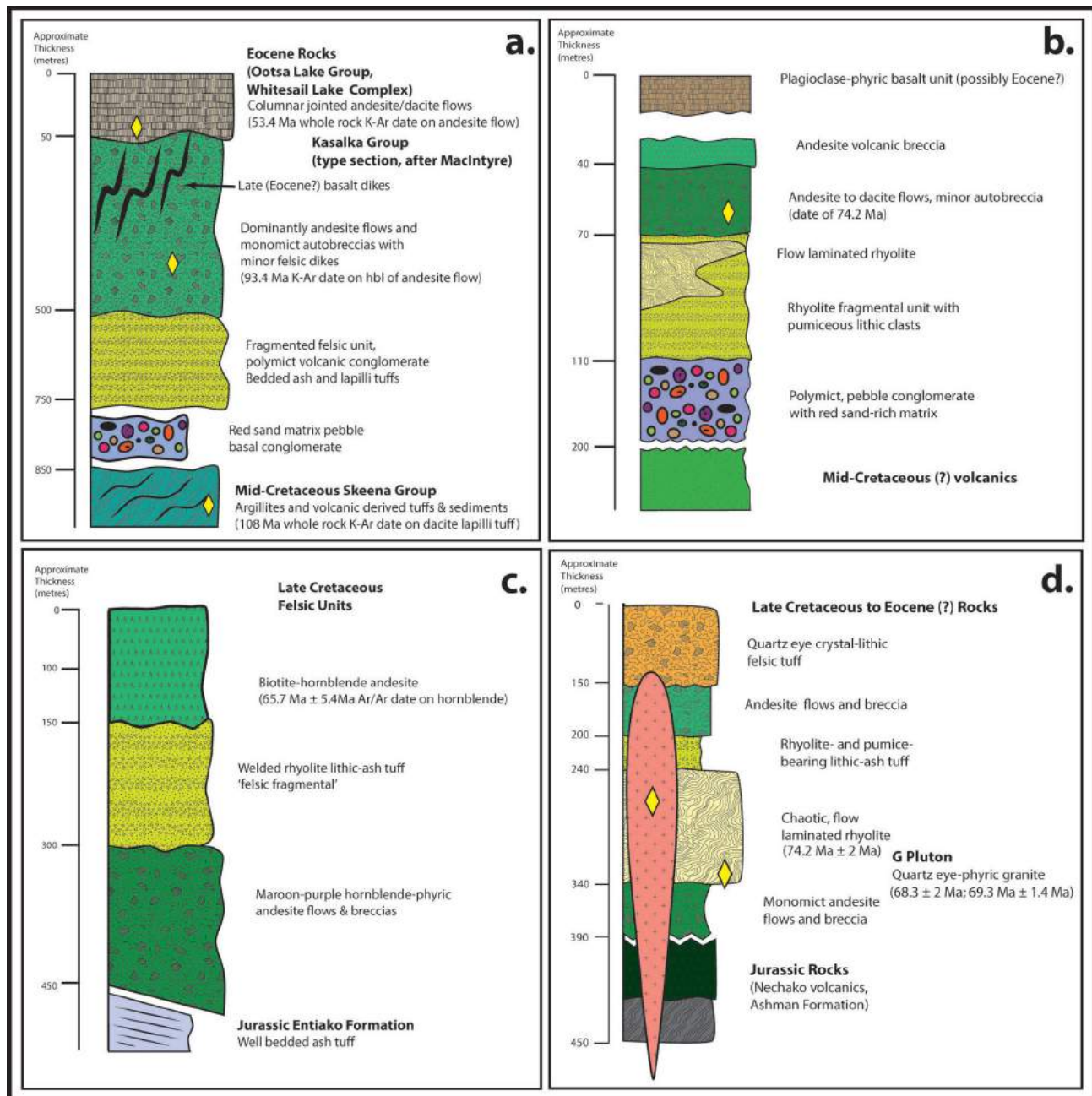
Figure 2. Stratigraphic schematics from the Kasalka type section and other localities in the study area: **a)** type section locality from the Kasalka Ranges (NTS 093E), K/Ar dates compiled in Diakow (2006), modified from MacIntyre (1985); **b)** stratigraphic schematic from Tchesinkut cell tower, north of Francois Lake, U/Pb date from Grainger (2000); **c)** stratigraphic schematic from the Cabin Lake area, in the northwest portion of the TREK project area, south of Francois Lake; Ar/Ar date from Friedman et al. (2001); **d)** stratigraphy west of Blackwater deposit, north of the access road, ages from R. Whiteaker (pers. comm., 2015).

gest that this unit was emplaced at a similar time as the intrusion. Felsic flows underlying this lithic-ash tuff are dated by New Gold Inc. as 74.2 ±2 Ma (R. Whiteaker, pers. comm., 2015) indicating that the underlying rocks also belong to Late Cretaceous stratigraphy.

Late Cretaceous stratigraphy is also observed near Cabin Lake (Figure 2c), where a felsic welded tuff unit underlies a capping sequence of a biotite hornblende andesite that was dated at 65.7 ±5.4 Ma (Friedman et al., 2001). This indicates the tuff must have been deposited prior to the biotite hornblende andesite.

Fieldwork

The fieldwork part of this project included the mapping of four localities (Figure 1). The first location (Figure 2b), was mapped as part of fieldwork conducted in 2014 and described in Kim et al. (2014). In 2015, three additional localities (Figure 2a, c, d) were mapped.

Continuous stratigraphic exposures of all units are rare in the project area. Late Cretaceous to Eocene stratigraphy is presented to correlate the lithological similarities observed at the regional scale. The Kasalka Group type section in the Tahtsa Lake area was sampled to facilitate geochemical and geochronological comparisons with examples of the Kasalka Group farther to the east.

Recent logging and forest fires have improved the surface exposure in the area allowing for detailed 1:20 000 scale mapping and studies of felsic rocks west of the Blackwater deposit. To supplement mapping, geochemical and geochronological samples were collected in the field, the results from which are anticipated to provide a comprehensive assessment of the Kasalka Group from the type section (Figure 3). This framework will then be used to compare the Late Cretaceous volcanic rocks in the TREK area to assess the similarities and/or differences between them.

Geochemistry

Whole-rock lithogeochemistry data were acquired from selected samples collected during the 2014 field season and are presented here (Figure 4). These data are plotted against previously published data (MacIntyre, 1985, 2001) in order to compare rock type and affinity. Geochemical data from the Kasalka Group and other Late Cretaceous volcanic packages indicate two main compositions: mafic to intermediate and felsic end members.

Geochemistry data from rocks in the Kasalka Group type section will be compared to new data to be obtained from rocks observed within the TREK area and collected in 2015. This comparison is expected to provide insights into the composition of, and distinctive element signatures from, each constituent unit.

Geochronology

Previous geochronological studies of Cretaceous and Jurassic rocks in the area were conducted in conjunction with the Nechako NATMAP project (Friedman and Armstrong, 1995; Friedman et al., 2001; Grainger et al., 2001; Struik and MacIntyre, 2001) and ages were largely obtained from K-Ar dating on whole rock, hornblende and/or biotite, in addition to U/Pb geochronology on zircons (Grainger, 2000; Friedman et al., 2001; Ferbey and Diakow, 2012; Christie et al., 2014; Looby, 2015; R. Whiteaker, pers. comm., 2015).

Published geochronological ages for the Kasalka Group show a broad distribution (Figure 5). MacIntyre (1988) reports ages ranging from 105 to 75 Ma suggesting that the Kasalka Group ranges from mid- to Late Cretaceous in age. Friedman et al. (2001) report Late Cretaceous ages ranging from 68.1 to 65.7 Ma for andesitic rocks that were previously mapped as Jurassic and Eocene in the Fawnie Range. At the Blackwater deposit, Late Cretaceous ages ranging from 72 to 70 Ma (Looby, 2015) and also 74.2 Ma (R. Whiteaker, pers. comm., 2015) are reported for felsic flow units.

A total of 20 samples were collected during the 2014 and 2015 field seasons for U-Pb dating on zircons using laser-ablation, multiple-collector inductively coupled plasma–mass spectrometry (LA-MC-ICP-MS) with another 11 samples collected for ^{40}Ar/^{39}Ar dating. The results will contribute to this project's aim to constrain the timing of Late Cretaceous volcanism in the TREK project area, and more specifically to define the age of the Kasalka Group volcanic suite.

Discussion

The volcanic rocks and suites in the northern and western TREK project area presented herein were documented in the field over the 2014–2015 field seasons. Late Cretaceous volcanic packages across the TREK project area are predominantly intermediate to felsic, coherent and fragmental packages.

The compilation of stratigraphic successions across the northern TREK area and at the Kasalka Group type sections show broad similarities in rock units. Figure 2 shows the general trend across each section of a middle felsic unit being under- and overlain by andesite breccias and flows. This package of felsic and intermediate rocks is also shown to overlie Jurassic Ashman Formation and mid-Cretaceous Skeena Group volcano-sedimentary packages. The basal conglomerate described in the Kasalka Group type section is not continuous, possibly the result of paleotopography.

The Kasalka Group rocks have been dated previously by a variety of methods (K-Ar on whole rock, biotite, hornblende; ^{40}Ar/^{39}Ar on hornblende; U-Pb on zircon. More recent geochronology results from zircon show the age range
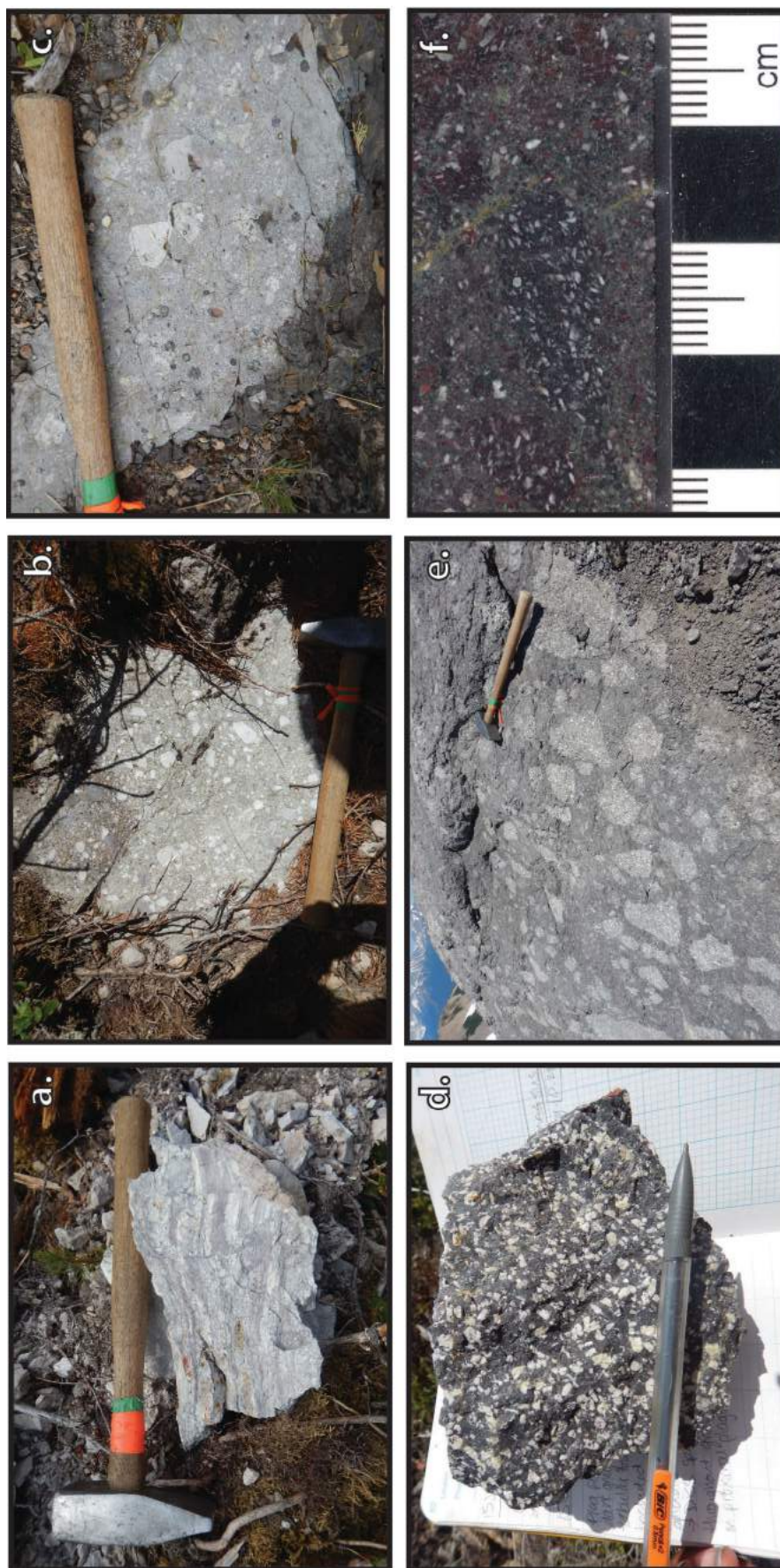
Figure 3. Examples of lithological units of the Kasalka Group: **a)** flow-banded rhyolite west of Blackwater; **b)** 'felsic fragmental', flow-banded rhyolite clast-dominated unit at Blackwater; **c)** andesitic volcanic breccia dominated by felsic clasts; **d)** plagioclase-phyric andesite; **e)** monomict, andesitic volcanic breccia from Kasalka type section; **f)** polymict, plagioclase–hornblende–phyric andesite breccia sampled from north of the Yellow Moose showing.
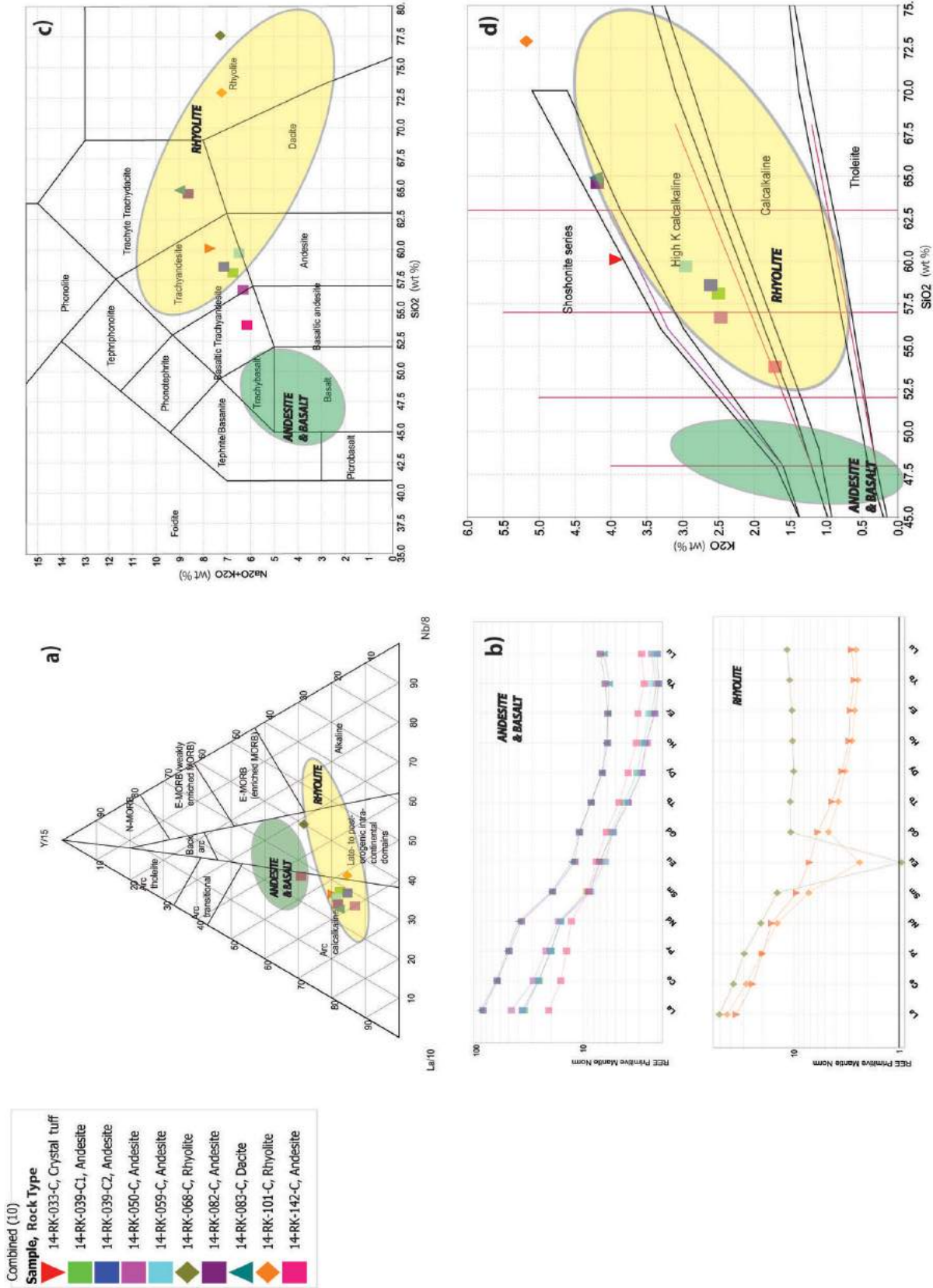
Figure 4. Compilation of geochemistry data collected from Late Cretaceous volcanic rocks across the Stikine terrane; samples collected in the 2014 field season. Ellipses represent Kasalka Group geochemistry data (MacIntyre, 1977, 1985, 2001): **a)** tectonic classification ternary plot, after Cabanis and Lecolle (1989); **b)** primitive mantle-normalized rare-earth element (REE) pattern (Sun and McDonough, 1989) for andesite and basaltic samples (top) and for rhyolite and crystal tuff samples (bottom); **c)** total alkali/silica (TAS) classification for volcanic rocks; **d)** Percillo-Taylor plot of K_2O vs. SiO_2.
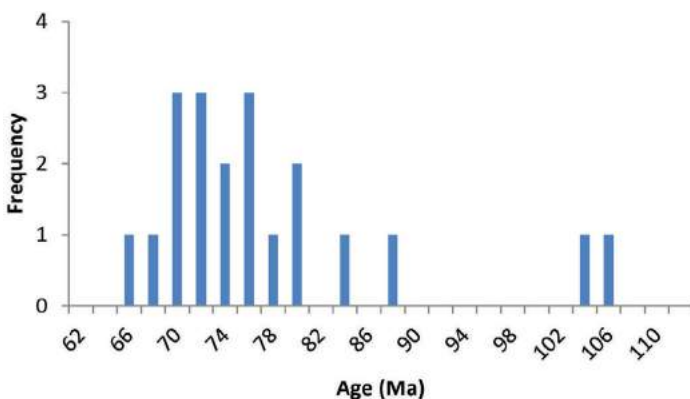
Figure 5. Compiled histogram of published ages for Kasalka Group and similar volcanic suites. Dating methods include K-Ar on whole rock, biotite and hornblende (MacIntyre, 1985; Leitch et al., 1991; Diakow et al., 1997; Friedman et al., 2001), and U/Pb on zircon (Grainger, 2000; Friedman et al., 2001; Ferbey and Diakow, 2012; McClenaghan, 2013; Looby, 2015).

for felsic components of the Kasalka Group to be from ca. 74 to 70 Ma (Friedman et al., 2001; Ferbey and Diakow, 2012; Looby, 2015; R. Whiteaker, pers. comm., 2015). Although the age ranges of these recent dates narrow the timing constraints, correlation to the units and their respective timing is sparse. The rocks mapped as the Kasalka Group in the TREK area may represent a different pulse of volcanism compared to the Kasalka Group type section.

The susceptibility of zircon inheritance in volcanic rocks may have affected the reported dates of older data, so this study will utilize cathodoluminescence imaging and LA-MC-ICP-MS to target both zircon populations and parts of zircon grains that represent the latest stages of growth to enhance the geochronological dataset. Dating using K-Ar methods is also prevalent for rocks associated with the Kasalka Group, particularly at the type section (MacIntyre 1977, 1985; Diakow, 2006). These methods have been proven to be unreliable in some cases, and this study will attempt to re-date these units using more robust methods, including $^{40}Ar/^{39}Ar$ and U-Pb on mineral grains.

Whole rock lithogeochemistry signatures for each unit of the Kasalka Group may provide further contrast when identifying rocks from the Jurassic, Late Cretaceous and Eocene. Rocks of the Late Cretaceous may be difficult to define based solely on whole-rock geochemistry, as indicated by Grainger (2000) who determined that geochemistry data from Kasalka Group rocks are identical to those from Eocene Ootsa Lake Group rocks. The focus of trace-element geochemistry on selected minerals such as hornblende and zircon, in addition to petrographic and geochronological analysis, may allow for a clearer distinction between visually similar units of Eocene, Cretaceous and Jurassic ages. The observations and analyses of samples collected at the Kasalka Group type section are anticipated to provide a geochemical footprint to compare against the Late Cretaceous volcanic packages farther west in the

TREK area. Magnetic-susceptibility measurements taken in the field will also be compared to existing regional geophysical studies to further characterize various volcanic rocks in the study area. At the time of writing the authors await results for lithogeochemical and geochronology data for samples collected in the 2015 field season.

Acknowledgments

References

Anderson, R.G., Snyder, L.D., Grainger, N.C., Resnick, J., Barnes, E.M. and Pint, C.D. (2000): Mesozoic geology of the Takysie Lake and Marilla map areas, central British Columbia; Geological Survey of Canada, Current Research 2000-A12, 11 p., URL <http://ftp2.cits.rncan.gc.ca/pub/geott/ess_pubs/211/211182/cr_2000_a12.pdf> [December 2015].

Anderson, R.G., Snyder, L.D., Resnik, J., Grainger, N.C. and Barnes, E.M. (1999): Bedrock geology of the Knapp Lake map area, central British Columbia; *in* Geological Survey of Canada, Current Research 1999-A, p. 109–118., URL <http://www.em.gov.bc.ca/MINING/GEOSCIENCE/PUBLICATIONSCATALOGUE/OPENFILES/2007/2007-10/PAPERS/CURRENTRESEARCH/Pages/ar991.aspx> [September 2015].

Andrew, K.P.E. (1988): Geology and genesis of the Wolf precious metal epithermal prospect and the Capoose base and precious metal porphyry-style prospect, Capoose Lake area, central British Columbia; M.Sc. thesis, University of British Columbia, 359 p., URL <https://open.library.ubc.ca/cIRcle/collections/ubctheses/831/items/1.0052699> [December 2015].

Angen, J.J., Logan, J.M., Hart, C.J.R. and Kim, R. (2016): TREK geological mapping project, year 2: update on bedrock geology and mineralization in the TREK project area, central British Columbia (parts of NTS 093B, C, F, G); *in* Geoscience BC Summary of Activities 2015, Geoscience BC, Report 2016-1, p. 1–16.

Angen, J., Westberg, E., Hart, C., Kim, R. and Raley, C. (2015): TREK geology project: recognizing Endako Group and Chilcotin Group basalts from airborne magnetic data in the Interior Plateau region, south-central British Columbia (NTS 093B, C, F, G); *in* Geoscience BC Summary of Activities 2014, Geoscience BC, Report 2015-1, p. 21–32, URL <http://www.geosciencebc.com/i/pdf/SummaryofActivities2014/SoA2014_Angen.pdf> [December 2015].

Bevier, M.L. (1983): Regional stratigraphy and age of Chilcotin Group basalts, south-central British Columbia; Canadian Journal of Earth Sciences, v. 20, no. 4, p. 515–524.

Bordet, E., Hart, C.J. and McClenaghan, L. (2011): Epithermal-style Au-Ag mineralization in Cretaceous to Eocene felsic volcanic complexes, central British Columbia, western Canada; Society for Geology Applied to Mineral Deposits, Antofagasta, Chile, Abstract.

Cabanis, B. and Lecolle, M. (1989): The La/10-Y/15-Nb/8 diagram: a tool for discriminating volcanic series and evidencing continental crust magmatic mixtures and/or contamination; Comptes Rendus de l'Academie des Sciences, Serie 2, Sciences de la Terre, v. 309, no. 20, p. 2023–2029.

Christie, G., Lipiec, I., Simpson, R.G., Horton, J. and Bromtraeger B. (2014): Blackwater gold project British Columbia: NI 43-101 technical report on feasibility study; New Gold Inc., 2014, 336 p., URL <http://www.newgold.com/files/documents_properties/blackwater/Blackwater%20Gold%20Project%20Technical%20Report%20January%202014%202014.pdf> [November 2015].

Clifford, A. and Hart, C.J.R. (2014): Targeting Resources through Exploration and Knowledge (TREK): Geoscience BC's newest minerals project, Interior Plateau Region, central British Columbia (NTS 093B, C, F, G); in Geoscience BC Summary of Activities 2013, Geoscience BC, Report 2014-1, p. 13–18, URL <http://www.geosciencebc.com/i/pdf/SummaryofActivities2013/SoA2013_CliffordHart.pdf> [November 2015].

Colpron, M., Nelson, J. and Murphy, D.C. (2007): Northern Cordilleran terranes and their interactions through time; GSA Today, v. 17, no. 4/5, p. 4–10, doi: 10.1130/GSAT01704-5A.1

Diakow, L.J. (2006): Geology of the Tahtsa Ranges between Eutsuk Lake and Morice Lake, Whitesail Lake map area, west-central British Columbia: parts of NTS 93E/5, 6, 7, 9, 10, 12, 13, 14 and 15; BC Ministry of Energy and Mines, BC Geological Survey, Geoscience Map 2006-5, scale 1:50 000, URL <http://www.empr.gov.bc.ca/Mining/Geoscience/PublicationsCatalogue/Maps/GeoscienceMaps/Documents/GM2006-05.pdf> [December 2015].

Diakow, L.J. and V.M. Levson (1997): Bedrock and surficial geology of the southern Nechako Plateau, central British Columbia; BC Ministry of Energy and Mines, BC Geological Survey, Geoscience Map 1997-2, scale 1:100 000, URL <http://www.empr.gov.bc.ca/Mining/Geoscience/PublicationsCatalogue/Maps/GeoscienceMaps/Documents/GM1997-02.pdf> [November 2015].

Diakow, L.J., Webster, I.C.L., Richards, T.A. and Tipper H.W. (1997): Geology of the Fawnie and Nechako ranges, southern Nechako Plateau, central British Columbia (98F/2, 3, 6, 7); in Interior Plateau Geoscience Project: Summary of Geological, Geochemical and Geophysical Studies, L.J. Diakow, J.M. Newell and P. Metcalfe (ed.), BC Ministry of Energy and Mines, BC Geological Survey, Paper 1997-2, p. 7–30, URL <http://ftp2.cits.rncan.gc.ca/pub/geott/ess_pubs/208/208972/of_3448.pdf> [November 2015].

Evenchick, C.A. (1991): Geometry, evolution and tectonic framework of the Skeena Fold Belt, north central British Columbia; Tectonics, v. 10, p. 527–546, URL <http://onlinelibrary.wiley.com/doi/10.1029/90TC02680/pdf> [November 2015].

Ferbey, T. and Diakow, L.D. (2012): U-Pb Isotopic ages from volcanic rocks near Ootsa Lake and François Lake, west-central British Columbia; in Geological Fieldwork 2011, BC Ministry of Energy and Mines, BC Geological Survey, Paper 2012-1, p. 149–156, URL <http://www.empr.gov.bc.ca/Mining/Geoscience/PublicationsCatalogue/Fieldwork/Documents/2011/11_Ferbey_2011.pdf> [September 2015].

Ferbey, T. and Levson, V.M. (2000): Quaternary geology and till geochemistry of the Huckleberry mine area; in Geological Fieldwork 2000, BC Ministry of Energy and Mines, BC Geological Survey, Paper 2001-1, p. 397–410, URL <http://citeseerx.ist.psu.edu/viewdoc/download?doi=10.1.1.176.4906&rep=rep1&type=pdf> [October 2015].

Friedman, R. M. and Armstrong, R. L. (1995): Jurassic and Cretaceous geochronology of the southern Coast Belt, British Columbia, 49°–51°N; in Jurassic Magmatism and Tectonics of the North American Cordillera, D.M. Miller and C. Busby (ed.), Geological Society of America Special Paper 299, p. 95–139.

Friedman, R.M., Diakow, L.J., Lane, R.A. and Mortensen, J.K. (2001): New U-Pb age constraints on latest Cretaceous magmatism and associated mineralization in the Fawnie Range, Nechako Plateau, central British Columbia; Canadian Journal of Earth Sciences, v. 38, p. 619–637, URL <http://www.nrcresearchpress.com/doi/pdf/10.1139/e00-122> [November 2015].

Grainger, N. (2000): Petrogenesis of Middle Jurassic to Miocene magmatism within the Nechako Plateau, central British Columbia: insight from petrography, geochemistry, geochronology and tracer isotope studies; M.Sc. thesis, University of Alberta, 138 p.

Grainger, N.C., Villeneuve, M.E., Heaman, L.M. and Anderson, R.G. (2001): New U-Pb and Ar/Ar isotopic age constraints on the timing of Eocene magmatism, Fort Fraser and Nechako River map areas, central British Columbia; Canadian Journal of Earth Sciences, v. 38, p. 679–696, URL <http://www.nrcresearchpress.com/doi/pdf/10.1139/e00-093> [October 2015].

Kim, R., Hart, C., Angen, J. and Westberg, E. (2015): Characterization of Late Cretaceous volcanic suites in the TREK Project area, Central British Columbia (NTS 093F, K); in Geoscience BC Summary of Activities 2014, Geoscience BC, Report 2015-1, p. 33–40, URL <http://www.geosciencebc.com/i/pdf/SummaryofActivities2014/SoA2014_Kim.pdf> [November 2015].

Leitch, C.H.B., Hood, C.T., Cheng, X.-L. and Sinclair, A.J. (1991): Tip Top Hill volcanics: Late Cretaceous Kasalka Group rocks hosting Eocene epithermal base- and precious-metal veins at Owen Lake, west-central British Columbia; in Canadian Journal of Earth Sciences, v. 29, p. 854–864, URL <http://www.nrcresearchpress.com/doi/citedby/10.1139/e92-073#.VFgHQvnF9DA> [December 2015].

Looby, E.L. (2015): The timing and genesis of the Blackwater gold-silver deposit, central British Columbia: constraints from geology, geochronology and stable isotopes; M.Sc. thesis, University of British Columbia, 172 p., URL <https://open.library.ubc.ca/media/stream/pdf/24/1.0135681.pdf> [November 2015].

MacIntyre, D.G. (1977): Evolution of upper Cretaceous volcanic and plutonic centres and associated porphyry copper occurrences Tahtsa Lake area, British Columbia; Ph.D. thesis, University of Western Ontario, 216 p.

MacIntyre, D.G. (1985): Geology and mineral deposits of the Tahtsa Lake District, west central British Columbia; BC Ministry of Energy and Mines, BC Geological Survey, Bul-

letin 75, URL <http://www.empr.gov.bc.ca/Mining/ Geoscience/PublicationsCatalogue/BulletinInformation/ BulletinsAfter1940/Documents/Bull75.pdf> [December 2015].

MacIntyre, D.G. (2001): The mid-Cretaceous Rocky Ridge Formation—a new target for subaqueous hot-spring deposits (Eskay Creek-type) in Central British Columbia; *in* Geological Fieldwork 2000, BC Ministry of Energy and Mines, BC Geological Survey, Paper 2001-1, p. 253–268.

McClenaghan, L. (2013): Geology and genesis of the Newton bulk-tonnage gold-silver deposit, central British Columbia; Msc. thesis, University of British Columbia, 205 p., URL <https://circle.ubc.ca/bitstream/handle/2429/44008/ ubc_2013_spring_mcclenaghan_lindsay.pdf?sequence=1> [September 2015].

Mihalynuk, M.G., Nelson, J. and Diakow, L.J. (1994): Cache Creek terrane entrapment: oroclinal paradox within the Canadian Cordillera; Tectonics, v. 13, no. 2, p. 575–595, URL <http://www.empr.gov.bc.ca/Mining/Geoscience/Staff/ Documents/MihalynuketAl1994.pdf> [November 2015].

Monger, J. (1977): Upper Paleozoic rocks of the western Canadian Cordillera and their bearing on Cordilleran evolution; Canadian Journal of Earth Sciences, v. 14, no. 8, p. 1832–1859.

Monger, J. and Price, R. (2002): The Canadian Cordillera: geology and tectonic evolution; Canadian Society of Exploration Geophysicists Recorder v. 27, no. 2, p. 17–36, URL <http:// www.geology.ucdavis.edu/~shlemoncourse/html/trips/ Skeena_River/documents/journals/Monger(2002).pdf> [November 2015].

Riddell, J. (2011): Lithostratigraphic and tectonic framework of Jurassic and Cretaceous Intermontane sedimentary basins of south-central British Columbia; Canadian Journal of Earth Sciences, v. 48, p. 870–896, URL <http://www. nrcresearchpress.com/doi/pdf/10.1139/e11-034s> [September 2015].

Struik, L.C. and MacIntyre, D.G. (2001): Introduction to the special issue of Canadian Journal of Earth Sciences: the Nechako NATMAP project of the central Canadian Cordillera; Canadian Journal of Earth Sciences, v. 38, p. 485–494, URL <http://cjes.geoscienceworld.org/content/38/4/ 485.full.pdf+html> [November 2015].

Sun, S.-s. and McDonough, W.F. (1989): Chemical and isotopic systematics of oceanic basalts: implications for mantle composition and processes; Geological Society of London, Special Publications 42, p. 313–345.

Geology of the Cache Creek Terrane in the Peridotite Peak–Menatatuline Range Area, Northwestern British Columbia (Parts of NTS 104K/15, /16)

S. McGoldrick, School of Earth and Ocean Sciences, University of Victoria, Victoria, BC, smcgold@uvic.ca

A. Zagorevski, Natural Resources Canada, Geological Survey of Canada, Ottawa, ON

D. Canil, School of Earth and Ocean Sciences, University of Victoria, Victoria, BC

A.-S. Corriveau, Institut national de la recherche scientifique, Québec, QC

S. Bichlmaier, School of Earth and Ocean Sciences, University of Victoria, Victoria, BC

S. Carroll, School of Earth and Ocean Sciences, University of Victoria, Victoria, BC

Introduction

Ophiolites are ubiquitous features of Phanerozoic orogens around the world, where they are bounded by major suture zones, along which oceanic basins were consumed. The Canadian Cordillera hosts several belts of structurally dismembered Upper Paleozoic–Lower Mesozoic ophiolites, including the Nahlin ultramafic body exposed within the oceanic Cache Creek terrane (Figure 1). Nahlin represents the largest and best preserved of the Cordilleran ophiolites, and provides a glimpse into magmatic processes occurring in suprasubduction-zone–spreading environments and into subduction processes in the Panthalassa Ocean. Establishing clear relationships between mantellic, lower crustal and supracrustal rocks is paramount to understanding the tectonic setting and emplacement of the Nahlin ultramafic body. This in turn has implications for models of terrane accretion and continental growth in the Cordillera. Despite their importance in the Cordillera, detailed studies of the ophiolitic rocks in the Cache Creek terrane in northern British Columbia (BC) and Yukon have been limited in number.

A collaborative Geomapping for Energy and Minerals (GEM-2) project led by the Geological Survey of Canada aims to update the geological framework of the northern Cache Creek terrane through detailed mapping and regional map compilation. This paper presents preliminary results from 1:20 000 scale mapping and sampling of the Cache Creek terrane in 2015. The two study areas for this project are located in northwestern BC, approximately 115 km south of the Yukon border (Figure 1), and are ac-

cessed by helicopter from Atlin, BC. Bedrock mapping focused on the Menatatuline Range (TRIM sheet 104K/099) and Peridotite Peak (TRIM sheet 104K/097) areas, located 80 km and 110 km southeast of Atlin, respectively (Fig-
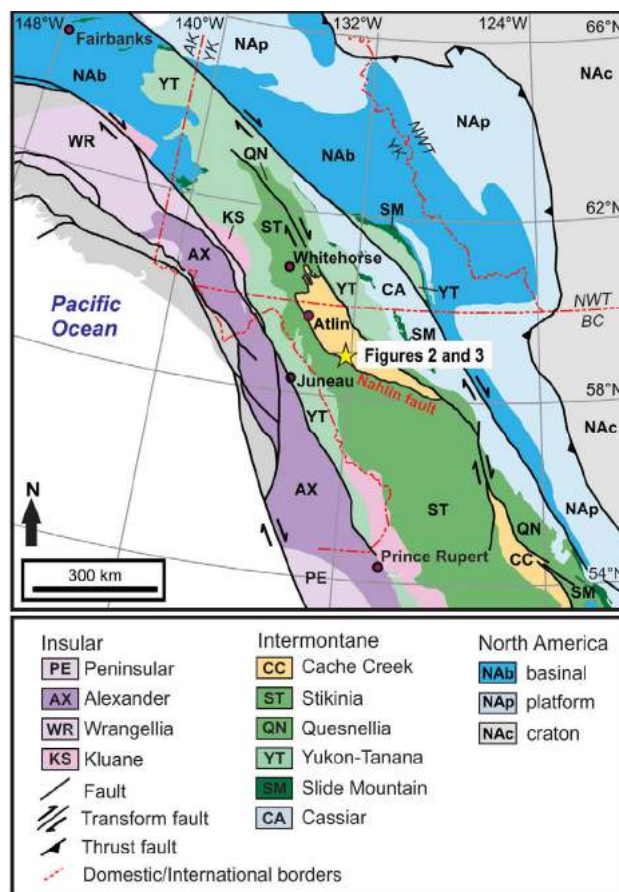
Figure 1: Terranes of the northern Cordillera, in northwestern British Columbia (from Colpron and Nelson, 2011). Star denotes location of Figures 2 and 3 on 1:20 000 TRIM map sheets 104K/097 and /099.

ures 2, 3). The mapping evaluated the regional distribution and relationships between the mantle, intrusive and supracrustal rocks exposed in a northwest-trending series of mountains up to 1960 m in elevation. Low-lying areas are commonly vegetated and marshy, and covered by glaciofluvial sediments, whereas higher elevations yield excellent bedrock exposures with limited vegetation cover.

Samples collected from all units mapped will be the focus of several ongoing projects related to the GEM-2 project. This paper summarizes field descriptions and outlines the results of bedrock mapping, as well as some preliminary interpretations.
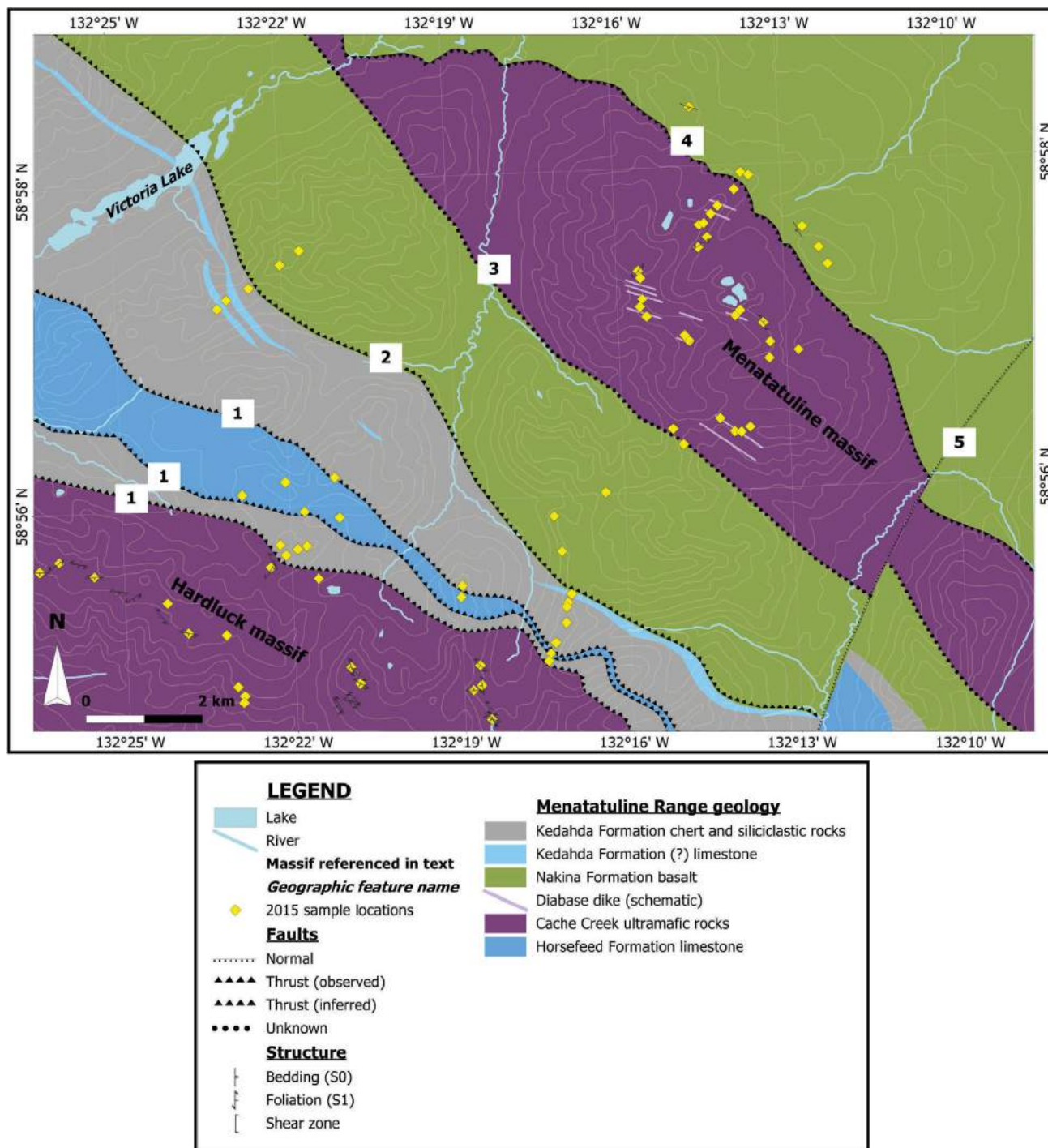
Figure 2: Preliminary bedrock geology of the Menatatuline Range area, based on 2015 mapping and compiled British Columbia Geological Survey data (Mihalynuk et al., 1996). Diabase dikes are shown schematically. Faults, labelled by numbers in white boxes, are discussed under 'Structure' in this paper (background topographic raster image from Natural Resources Canada, 1990a).
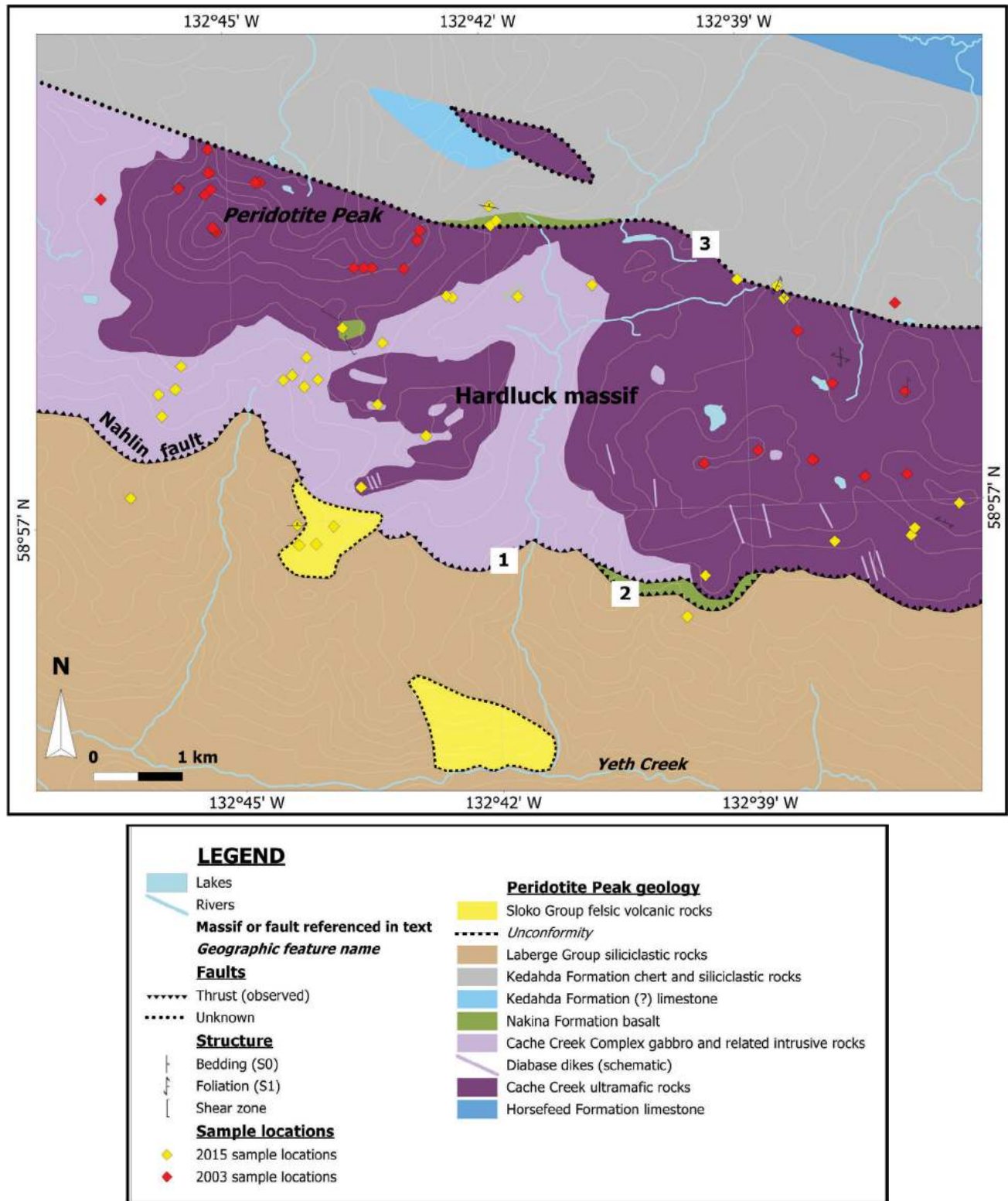
Figure 3: Preliminary bedrock geology of the Peridotite Peak area, based on 2015 mapping and compiled British Columbia Geological Survey data (Mihalynuk et al., 1996). Diabase dikes are shown schematically. Faults, labelled by numbers in white boxes, are discussed under 'Structure' in this paper (background topographic raster image from Natural Resources Canada, 1990b).

Regional Geology

The Mississippian to Lower Jurassic Cache Creek terrane is located within the Intermontane Belt adjacent to the Yukon-Tanana, Quesnel and Stikine terranes (Figure 1). The northern Cache Creek terrane near Atlin, BC has been the focus of a number of studies, ranging from regional to thematic in scope (e.g., Aitken, 1959; Souther, 1971; Monger, 1975; Terry, 1977; Bloodgood and Bellefontaine, 1990; Ash, 1994; Mihalynuk et al., 1994).

The Cache Creek and Stikine terranes were accreted to North America by the Middle Jurassic, as constrained by biostratigraphy, ca.172 Ma crystallization age of crosscutting plutons and timing of peak blueschist-facies metamorphism at 173 Ma (Gabrielse, 1991; Mihalynuk et al., 1992; Mihalynuk et al., 1999). Presence of Tethyan fauna in preophiolitic, Permian–Mississippian carbonate rocks of the Cache Creek terrane contrasts strongly with that of McLeod fauna found in the adjacent Stikine and Quesnel terranes (Monger and Ross, 1971; Orchard et al., 2001), suggesting that parts of the Cache Creek terrane are exotic with respect to Laurentia. The presence of these contrasting faunal assemblages between the accreted terranes and the Jurassic emplacement age have strongly influenced the tectonic models for the northern Cordillera. For example, it has been proposed that the far-travelled Cache Creek terrane and other accreting terranes, including the Stikine and Quesnel, were amalgamated during intra-oceanic collisional events in Panthalassa prior to docking onto the North American plate (Johnston and Borel, 2007). Alternatively, the closure of the Cache Creek ocean may have resulted in Late Triassic to Early Jurassic oroclinal bending of a once continuous Stikine–Quesnel arc system prior to accretion of the terranes with the Laurentian margin (Mihalynuk et al., 1994).

The northern Cache Creek terrane was first recognized to contain a disrupted ophiolite sequence by Monger (1975), an interpretation that was later confirmed by Terry (1977) and Ash (1994); however, several distinct and possibly unrelated subterranes (Monger, 1975) have also been identified including an ophiolite and/or rifted arc (e.g., Childe and Thompson, 1997; English et al., 2010; Schiarizza, 2012; Bickerton et al., 2013), seamounts and/or oceanic plateaus (e.g., English et al., 2010), and a subduction-related accretionary complex (Monger, 1975; Terry, 1977; Ash, 1994; Mihalynuk, 1999; English and Johnston, 2005). The age of the ophiolitic rocks is most reliably constrained by a pyroxenite sample from the Teslin area in southern Yukon that yielded a weighted-average zircon U-Pb age of 245.4 ±0.8 Ma (Gordey et al., 1998). In the Peridotite Peak–Menatatuline Range area, the Cache Creek terrane comprises the dismembered remnants of oceanic lithospheric mantle, mafic intrusions, mafic volcanic rocks and sedimentary basins (e.g., carbonate rocks, chert and siliciclastic rocks).

Geology of the Menatatuline Range Area

Cache Creek Ultramafic Massifs

Aitken (1959) recognized two belts of ultramafic rocks in the Menatatuline Range area, which were subsequently investigated by Terry (1977). Together, these two belts form the Nahlin ultramafic body. The northern belt trends northwest and underlies Nahlin Mountain and the Menatatuline Range (Menatatuline massif; Figure 2). The west-north-west-trending southern belt continues through Peridotite Peak to the Hardluck Peaks (Hardluck massif; Figure 3). Ultramafic rocks in the Menatatuline and Hardluck massifs comprise variably serpentinized harzburgite with pyroxenite dikes, and replacive dunite pods. The harzburgite massifs are fairly homogeneous, with the exception of some across-strike compositional variations observed in the Hardluck massif. Locally, a primary-mantle tectonic fabric (S_1) defined by orthopyroxene elongation and variably developed pyroxene-defined layering is preserved in both massifs.

Harzburgite Tectonite

Menatatuline Massif

The Menatatuline massif consists of massive harzburgite, pyroxenite dikes and replacive dunite. The harzburgite weathers dun brown, with protruding brown to green-brown orthopyroxene and rare emerald-green clinopyroxene. The protruding appearance of the pyroxene crystals is a result of their resistance to serpentinization and alteration, relative to the surrounding olivine crystals. There is little variation in modal mineralogy throughout the massif, with ~25–40% orthopyroxene, lesser clinopyroxene (2%) and rare spinel (<5%). Orthopyroxene, clinopyroxene and olivine grain size varies between 2 and 10 mm, and orthopyroxene grains are commonly subhedral. Anhedral spinel ranges in size from <1 mm to 5 mm. Discrete zones of ophicalcite (<1 m in width) are found throughout the massif and comprise brecciated harzburgite in a carbonate±quartz matrix.

Hardluck Massif

Hardluck massif consists predominantly of layered harzburgite, with lesser amounts of massive harzburgite. The layered harzburgite consists of layers 5–20 cm thick defined by variable proportions of pyroxene. There is an abrupt shift from layered to massive harzburgite along a westerly-trending zone of serpentinite that may define a steeply dipping fault in the northernmost part of the Hardluck massif. Overall, the harzburgite is largely similar to that in the Menatatuline massif; however, in the Hardluck massif, an across-strike increase in modal orthopyroxene toward the north was observed.
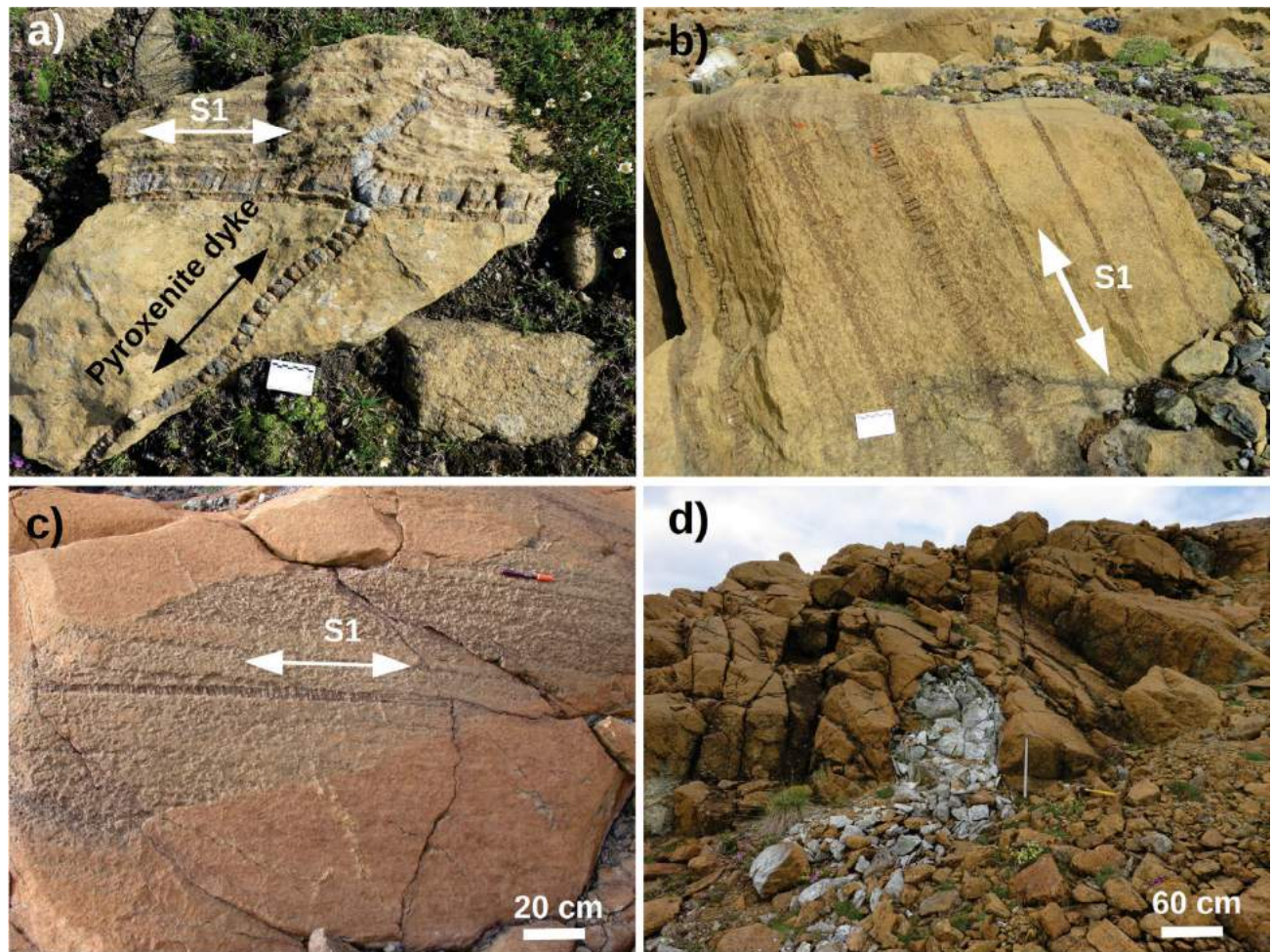
Pyroxenite

Pyroxenite dikes, rarely exceeding 5–10 cm in width, although locally reaching up to 20 cm, crosscut both the Menatatuline and Hardluck massifs. In both massifs, northwest- to north-northwest-striking and steeply dipping pyroxenite dikes can be layer-discordant or concordant with respect to the locally layered harzburgite (Figure 4 a, b) and are locally deformed into metre-scale folds. Small-scale folds and regionally variable dip direction of the pyroxenite dikes likely document regional-scale folding within the Hardluck massif.

Dunite

Discrete, dun-weathering dunite pods comprise as much as 20% of the Menatatuline and Hardluck massifs. These replacive bodies represent melt channels formed as a result of melt-rock interaction in the host harzburgite (Kelemen and Dick, 1995). The size of individual pods is variable, ranging from sub-metre scale up to 100 m across. Dunite bodies have sharp contacts against harzburgite, are locally folded and locally crosscut pyroxenite, indicating that there are likely multiple generations of replacive dunite and pyroxenite dikes (Figure 4c). Establishing temporal relationships between the pyroxenite dikes and dunite pods is not everywhere straightforward; in the Hardluck massif, dunite also appears as centimetre-scale envelopes surrounding the pyroxenite dikes or as orthopyroxene-poor horizons in the layered harzburgite. In both massifs, dunite is mostly homogeneous, consisting of ~95% olivine, with accessory euhedral spinel. Olivine macroscopically appears to be equigranular and fine grained; however, this may be a result of disaggregation of larger crystals along serpentine-veinlet boundaries. The dunite is commonly enriched in spinel relative to the host harzburgite, with modal abundance locally reaching up to 8% and grain size, up to 4 mm.

Figure 4: Field photographs of harzburgite of the Hardluck massif: **a)** a boulder of typical layered harzburgite, crosscut by a pyroxenite dike; dikes are locally deformed into metre-scale folds and can be layer concordant or discordant with respect to locally layered harzburgite; **b)** layered harzburgite defined by variable proportions of orthopyroxene and layer-concordant pyroxenite dikes; **c)** dunite pod replacing layer-concordant pyroxenite dikes in layered harzburgite near Peridotite Peak; **d)** white-weathering listwaenite zone in massive harzburgite of the Hardluck massif in the Menatatuline Range area.

Alteration Assemblages

In both the Menatatuline and Hardluck massifs, the alteration and serpentinization of harzburgite varies from thin millimetre-scale serpentine veinlets to complete replacement of primary olivine by serpentine and talc±carbonate. Serpentinization generally results in darkening of the peridotite from green-grey to black on fresh surfaces, making it easy to identify highly altered samples. Metasomatized and pervasively altered sections (e.g., listwaenite, Figure 4d) are typically associated with faults, gabbro intrusions and diabase dikes; however, irregular and relatively cryptic alteration zones also occur irrespective of faulting and intrusions, implying that the massifs have likely experienced multiple episodes of alteration.

Cache Creek Gabbro

Gabbroic rocks consisting of plagioclase and pyroxene±amphibole are present along the southern margin of the Hardluck massif. Gabbroic dikes and pods with distinctive chill margins commonly intrude serpentinite, especially in proximity to the Nahlin fault. Gabbro is varitextured and ranges from fine grained to pegmatitic (Figure 5a). Foliated amphibolite- and trondhjemite-rich zones are locally present. Gabbroic rocks are clearly visible as light-weathering streaks in scree slopes along gullies. Gabbro becomes less abundant toward the north, where it typically forms thin dikes and reticulated dike and vein swarms within variably serpentinized peridotite. Northernmost exposures of gabbro comprise boudinaged rodingite pods completely enveloped within fresh peridotite. Rodingite locally preserves the primary gabbroic texture, including apparent igneous layering in the gabbro.

Diabase Dikes

West- to northwest-trending and steeply dipping diabase dikes ranging in width from <2 to 20 m occur as a swarm crosscutting the Menatatuline massif. The dikes have chilled margins against the host harzburgite, and core zones typically comprise fine- to medium-grained equigranular plagioclase (40–50%) and pyroxene (1–3 mm). Many of these dikes display ophitic to subophitic textures (Figure 5b) and wider dikes also contain rare (<1%), black, 3-4 mm phenocrysts of pyroxene. Dikes are commonly bordered by serpentinite and/or listwaenite alteration zones.
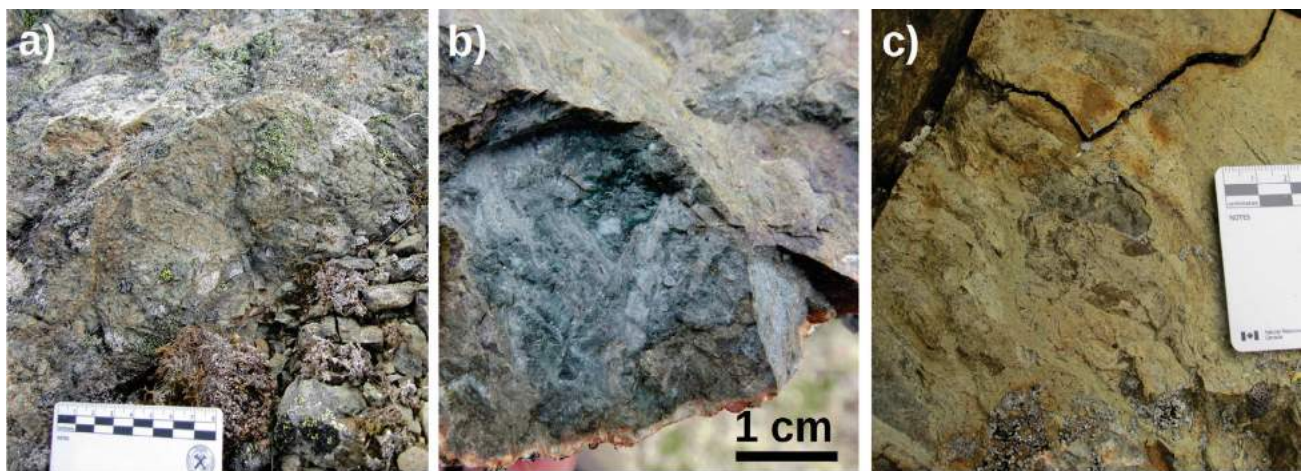
Nakina Formation

Mafic volcanic rocks, previously mapped as part of the Triassic Nakina Formation (Mihalynuk et al., 1996; English et al., 2002; Mihalynuk et al., 2002), are exposed to the northeast of the Menatatuline massif, and between the Menatatuline and Hardluck massifs. To the northeast of the Menatatuline massif, a ~150 m zone of phacoidal serpentinized harzburgite defines a southwest-dipping contact against the mafic volcanic rocks. This contact is interpreted as a thrust fault with volcanic rocks in the footwall. Dark grey-weathering basaltic volcanic rocks crop out sporadically on low hills to the northeast of the Menatatuline massif. The flows are pillowed (Figure 6a) and massive but it is difficult to determine younging direction or contact relations as outcrop quality and exposure are poor. The basaltic rocks are dark green-grey on fresh surfaces and predominantly aphanitic, with the exception of one outcrop of plagioclase- and pyroxene-phyric basalt. The Nakina Formation basalt in this area is chloritized and commonly contains thin quartz veinlets.

A broadly northwest-trending valley separates the Menatatuline massif from the volcanic/volcaniclastic rocks that
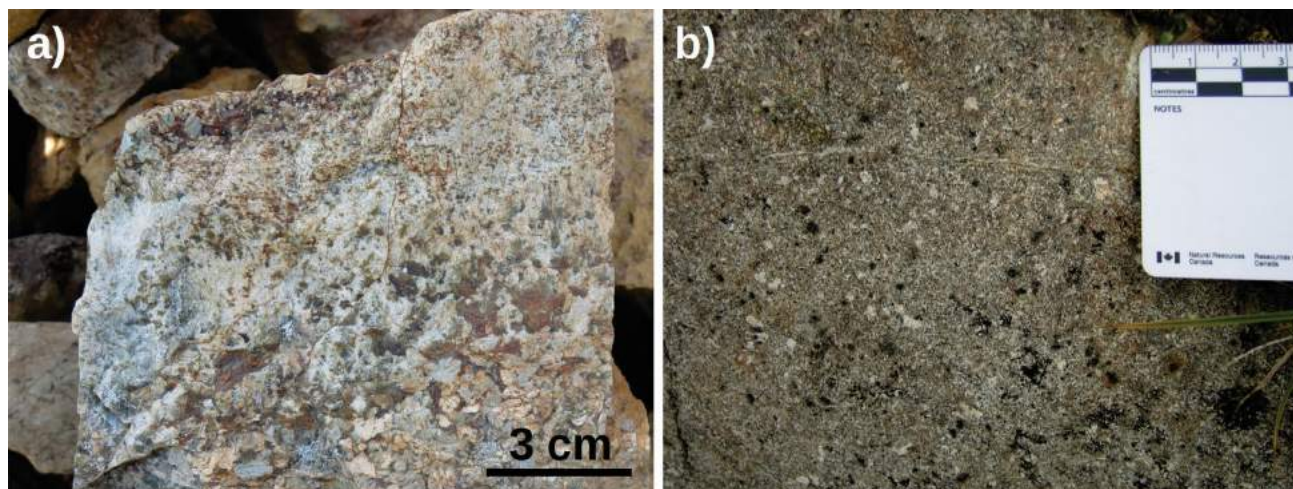
Figure 5: a) Varitextured gabbro intrusion in the Hardluck massif, in the Menatatuline Range area. Grain size within the gabbroic intrusions varies from fine grained to pegmatitic. **b)** Ophitic texture in the medium-grained centre of a ~5 m wide diabase dike crosscutting massive harzburgite in the Menatatuline massif, in the Menatatuline Range area.

Figure 6: Mafic volcanic rocks of the Nakina Formation, in northwestern British Columbia: **a)** dark grey, pillowed, mafic volcanic rocks to the northeast of the mantle section; **b)** light grey-green, pervasively hematite-altered volcanic or volcaniclastic rocks to the southeast of the Menatatuline massif; **c)** locally fragmental texture in the volcaniclastic rocks between the Menatatuline and Hardluck massifs.

form steep cliffs and jagged ridges to the south. A saddle of highly serpentinized and fissile-weathering rock is interpreted as a fault trace that follows this valley. The dip direction and sense of displacement of this fault were not observed, although it is thought to dip steeply because of its apparent interaction with topography (Figure 2). Here, the Nakina Formation volcanic rocks have light grey-green to mint-green fresh surfaces, and locally show signs of pervasive hematite alteration (Figure 6b). These volcanic rocks are fine grained, aphanitic, locally vesicular and flow banded, and commonly fragmental. Fragments are variable in shape, from rounded to elongate or shard-like (Figure 6c), suggesting a proximal volcanic origin. Thin veins and thick zones of chlorite and/or quartz alteration, as well as inclusions of red to green chert, are common.

Horsefeed Formation

A wide belt of fault-bounded limestone extends through the area, thinning significantly to the southeast and widening toward the northwest, where it appears to be continuous with Mississippian–Permian Horsefeed Formation limestone (Monger, 1975; Mihalynuk et al., 2002.). In general, this limestone is massive although it is locally thinly bedded (Figure 7), fetid and oolitic.

Kedahda Formation

Sedimentary rocks, previously mapped as the Kedahda Formation (Monger, 1975; Mihalynuk et al., 1996; Mihalynuk et al., 2002), occur as two belts that are separated by the Mississippian–Permian Horsefeed Formation limestone (Monger, 1975; Mihalynuk et al., 2002). Sedimentary rocks are folded and comprise abundant massive to ribbon chert and argillite that are interbedded with fine-grained sandstone to pebble conglomerate. Siliciclastic rocks contain abundant free quartz, suggesting a source region that contains felsic volcanic and/or plutonic rocks. Lateral ex-

tent of the siliciclastic rocks is difficult to determine due to folding and lack of exposures between ridges. Thin lenses of massive limestone are present within the siliciclastic sequence; in the absence of age constraints, these lenses may be part of the Horsefeed Formation or Kedahda Formation limestone (see Mihalynuk et al., 2003).

Geology of the Peridotite Peak Area

Cache Creek Ultramafic Rocks

Ultramafic rocks in the Peridotite Peak area and along-strike continuation of the Hardluck massif are largely similar to those in the Menatatuline Range area, comprising variably serpentinized harzburgite and lherzolite, with pyroxenite dikes, websterite and replacive dunite pods (Mihalynuk et al., 2004). Harzburgite and lherzolite are mostly massive and are locally foliated in the centre of the

Figure 7: Bedded limestone of the Mississippian–Permian Horsefeed Formation, in northwestern British Columbia (Monger, 1975; Mihalynuk et al., 2002).

mapped area, where west-striking, steeply dipping layering was observed.

On the northern side of Peridotite Peak, layers of lherzolite contain up to 25% emerald-green clinopyroxene (Mihalynuk et al., 2004). Exposures of harzburgite in the southern sections of the Hardluck massif at Peridotite Peak contain variable amounts of clinopyroxene (5–7%, 2–3 mm across) and orthopyroxene (up to 20%, 4–5 mm across). Disseminated 1–3 mm spinel grains make up 1% of the lherzolite. In one outcrop, a dunite pod is cut by a 1 m wide, anastomosing pegmatitic websterite dike. In the eastern part of the map area, sparse orthopyroxenite dikes 3–10 cm wide are both concordant and locally crosscutting with respect to layering, where present, in the harzburgite and lherzolite. As in the Menatatuline Range area, the ultramafic rocks are cut by abundant thin serpentine veinlets and are locally highly serpentinized. The latter is particularly apparent in proximity to gabbro bodies on the western side of the Peridotite Peak area, where phacoidal serpentinite is often present as metre-scale outcrops.

Cache Creek Gabbro to Quartz Diorite

Intrusive rocks underlie much of the map area, and range in composition from gabbro to quartz diorite. In the eastern part of the map area, they are found exclusively as isolated knobs within the ultramafic rocks or as metre-scale, north-striking and steeply dipping diabase dikes. The texture and modal mineralogy of these diabase dikes are identical to those in the Menatatuline massif at hand-sample scale. In contrast, in the central and western parts of the mapping area, the intrusive rocks are more voluminous and the ultramafic-intrusive contacts closely follow topographic contours. Similar contacts were observed on the northern side of Peridotite Peak, suggesting that the gabbro to quartz diorite may form a shallowly northeast-dipping intrusive sheet underlying the ultramafic rocks, which are exposed only at higher elevations. Alternatively, the ultramafic rocks may be structurally emplaced upon the gabbro intrusions by a shallowly northeast-dipping thrust fault.

The gabbroic rocks are grey weathering, very fine to medium grained, and are locally varitextured on a scale of tens of metres. Fresh surfaces are medium blue to greenish grey, and mafic minerals are variably chloritized. Where the composition is more dioritic, the texture is generally coarser grained than in the gabbro (i.e., mostly medium grained). Modal proportions for the gabbroic rocks are generally 60% plagioclase and 40% pyroxene. Quartz diorite proportions of plagioclase to pyroxene and/or amphibole are similar, although with the addition of 1–5% quartz and local biotite.

Nakina Formation

Mafic volcanic rocks, previously mapped as part of the Triassic Nakina Formation (Mihalynuk et al., 1996; English et al., 2002; Mihalynuk et al., 2002), are observed in faulted contact against the Hardluck massif to the north and south of Peridotite Peak. To the north of the ultramafic body, pyroxene-phyric amygdaloidal basalt underlies a sedimentary package. This green-grey weathering porphyritic basalt contains approximately 8% pyroxene phenocrysts, ranging in size from 1 to 3 mm, and up to 20% calcite-filled amygdules that are typically 2 mm in diameter. Sparsely plagioclase-phyric basalt occurs as isolated sheets within a gabbro-dominated drainage south of Peridotite Peak. The basalt is grey to green-grey weathering, variably chloritized, locally foliated, and is commonly crosscut by thin quartz veins. Both the pyroxene-phyric amygdaloidal basalt and the sparsely plagioclase-phyric basalt include centimetre-scale, irregular-shaped inclusions of grey limestone (Figure 8).

South of the Hardluck massif, mafic volcanic rocks are in faulted contact along a portion of the Nahlin fault separating the Cache Creek terrane from the Jurassic Laberge Group. At this locality, the volcanic rocks comprise aphanitic massive basalt with sparse amygdules and twinned, needle-like pyroxene phenocrysts.

Kedahda Formation

North of the ultramafic body, clastic sedimentary rocks previously mapped as the Kedahda Formation (Mihalynuk et al., 1996; Mihalynuk et al., 2002) include chert, cherty siltstone and fine sandstone. Dark grey chert occurs along portions of the northern contact with the ultramafic rocks, and typically contains abundant crosscutting quartz and/or calcite veins. The Kedahda Formation chert locally preserves radiolarians that yield Late Carboniferous to pre-

Figure 8: Irregular-shaped inclusions of grey, fine-grained limestone in highly amygdaloidal pyroxene-phyric basalt near the contact between mantle and supracrustal rocks in the northern part of the Peridotite Peak area.

dominantly Middle Triassic ages (Mihalynuk et al., 2002). Sedimentary rocks overlying a sliver of pyroxene-phyric amygdaloidal basalt to the north of the Hardluck massif ultramafic rocks include cherty siltstone to fine sandstone in thin, west-striking, steeply dipping beds. Outcrops of these fine-grained sedimentary rocks are fissile and rusty orange weathering, although fresh surfaces are dark grey. No graded bedding or other way-up indicators were observed in these rock units.

Laberge Group

A west-striking sedimentary package of siltstone, mudstone, fine to very coarse lithic sandstone, and lithic-rich biotite-bearing granule conglomerate is exposed along drainage channels to the south of the Hardluck massif. These have been previously mapped as part of the Jurassic Laberge Group (Mihalynuk et al., 1996; Mihalynuk et al., 2003). Graded bedding, flame structures, rip-up clasts and channels indicate upright stratigraphy (S_0 ~270°/60°), in which interbedded mudstone and siltstone overlying fissile mudstone are incised and overlain by interbedded fine to very coarse lithic sandstone (Figure 9). Interbedded siltstone and mudstone overlie the lithic sandstone, and are in turn overlain by lithic granule conglomerate.

The interbedded grey to black siltstone and mudstone is finely laminated on a millimetre scale and locally contains veins of pyrite. Fine to very coarse sandstone comprises quartz, feldspar, mafic minerals, including biotite, and clasts of dark grey to black fine-grained siltstone to mudstone. Sandstone beds vary in thickness from subcentimetre scale to ~20 cm. The coarsest grained rock unit is a lithic-rich and biotite-bearing granule conglomerate, which is clast supported and crudely bedded. The locally red-stained outcrop is crosscut by abundant thin, rusty

veins, which contain pyrite and chalcopyrite along broken surfaces.

Sloko Group

Hypabyssal felsic rocks, previously mapped as part of the Eocene Sloko Group (Mihalynuk, 1999), were observed to the north of Yeth Creek. Sparsely quartz-phyric, flow-banded rhyolite is pale grey to chalky white and fissile weathering, and is locally clay altered, with disseminated pyrite. Rhyolite locally hosts metre-scale, matrix-supported breccia zones, which contain angular to subrounded 3 mm to 3 cm clasts of dark siltstone, chert and rhyolite in a dark grey, fine-grained matrix. The genesis of this breccia and its relation to the host rhyolite are still unclear, although it may represent a hydrothermal breccia zone or a volcaniclastic deposit. Field observations of the Sloko Group suggest that it crosscuts the Laberge Group sedimentary rocks and that this contact represents an unconformity (Figure 10).

Structure

Certain primary features are preserved throughout both map areas, including bedding and way-up indicators in sedimentary rocks, pillow structures, crosscutting relationships, and mantle tectonite fabrics. The diabase dikes show primary crosscutting relationships with straight boundaries, suggesting that they have been essentially unstrained. The variably developed layering and orthopyroxene-defined fabric (S_1) in the harzburgite tectonites are interpreted as primary features related to high-temperature ductile flow in the mantle (Dick and Sinton, 1979; Nicolas and Violette, 1982; Nicolas, 1995). Some pyroxenite dikes in the harzburgite bodies define locally isoclinal metre-scale folds that are also suggestive of shearing and ductile flow, which would have occurred shortly after the hot lithosphere

Figure 9: Rip-up clasts of dark grey mudstone at the base of a coarse sandstone bed, and graded bedding (white arrow indicating direction of fining) indicating that bedding is right way up (S_0 ~270°/60°) in the Laberge Group sedimentary rocks south of the Hardluck massif, in the Peridotite Peak area.

Figure 10: White-weathering Eocene Sloko Group hypabyssal felsic rocks intruding rusty orange-weathering, Jurassic Laberge Group sedimentary rocks in the southern part of the Peridotite Peak area. Dashed line traces intrusive contact.

was formed. In the Menatatuline Range area, orientations of pyroxenite dikes in the Hardluck massif indicate the possible presence of a large-scale, west-trending antiformal fold, likely of similar origin.

The harzburgite bodies in both map areas are structurally juxtaposed with the mafic volcanic rocks, and carbonate and siliciclastic sedimentary rocks. The most conspicuous structure affecting the Peridotite Peak–Menatatuline Range area is the Nahlin fault (Figure 3), a southwest-vergent thrust fault separating the Cache Creek terrane from the Laberge Group sediments to the south (Monger, 1975; Terry, 1977; Mihalynuk et al., 2003; English et al., 2010).

Menatatuline Range Area

The Menatatuline Range area is transected by several northwest-trending faults. The Hardluck massif ultramafic rocks and gabbro are thrust over the Triassic (?) Yeth Creek volcanic rocks (informal; Mihalynuk et al., 2004; English et al., 2010) and Jurassic Laberge Group sedimentary rocks along the Nahlin fault (see fault labelled in Figure 1; Monger, 1975; Terry, 1977; Mihalynuk et al., 2003). The Nahlin fault (see Figure 1) appears to be a brittle structure that corresponds to regions of low topography. Evidence of deformation along the Nahlin fault is marked by the development of a moderately intense foliation in the Yeth Creek volcanic rocks, and by the formation of scaly serpentinite shear zones in the Hardluck massif (Figure 2).

The Hardluck massif is in fault contact (fault 1 on Figure 2) with the Kedahda Formation and Horsefeed Formation limestone to the north. Although the contact dips steeply to the northeast, reliable kinematic indicators were not observed. It is possible that this fault is related to the similarly-oriented southwest-directed Nahlin fault, in which case it has thrust supracrustal rocks over the mantle, and presumably represents a second or later generation thrust. Sedimentary rocks of the Kedahda and Horsefeed formations are internally folded and are likely imbricated. Complex internal structure is apparent in outcrops, where fine-scale, commonly chaotic folding is present in chert units, and in map view, where the Horsefeed Formation limestone drastically thins to the southeast and Triassic Kedahda (?) limestone is repeated.

The southern belt of the Nakina Formation is fault bounded. The southern boundary is a moderately to steeply dipping fault similarly oriented to the Nahlin fault, and may represent a southwest-directed thrust, placing Nakina Formation basalt over the Kedahda Formation (fault 2 on Figure 2). The northern boundary is a late, brittle, northwest-striking fault separating the Nakina volcanic rocks from the Menatatuline massif ultramafic rocks to the north (fault 3 on Figure 2). The dip magnitude and direction of this fault

were not observed, although based on its interaction with topography, it is interpreted to be steeply dipping.

The Menatatuline massif ultramafic rocks are thrust to the northeast over the northern belt of the Nakina Formation mafic volcanic rocks (fault 4 on Figure 2). This fault is moderately southwest dipping, and a zone of phacoidal serpentinite separates the hanging wall harzburgite from the footwall volcanic rocks (Figure 11a). A late normal fault (fault 5 on Figure 2) is suspected, based on map-pattern offsets, to run along the major south-southwest-trending drainage channel separating the Menatatuline Range on the hanging wall from Nahlin Mountain.

Peridotite Peak Area

South of Peridotite Peak, ultramafic, intrusive and volcanic rocks of the Cache Creek terrane are thrust over the Laberge Group sedimentary rocks along the Nahlin fault (fault 1 on Figure 3; Monger, 1975; Terry, 1977; Mihalynuk et al., 2003). A sliver of mafic volcanic rocks is also thrust over the Laberge Group (fault 2 on Figure 3), and is truncated by the Nahlin fault. The ultramafic rocks are interpreted to be either intruded by a subhorizontal sheet of the lower crustal intrusions, or structurally emplaced over the gabbro to quartz diorite intrusive rocks by a shallowly dipping thrust fault (Figure 11b).

North of Peridotite Peak, a sharp contact juxtaposes Nakina Formation mafic volcanic rocks and Kedahda Formation sedimentary rocks against the harzburgites of the Hardluck massif. This contact crosses topography at a high angle, suggesting a steeply dipping faulted contact (fault 3 on Figure 3). The nature of the displacement along this approximately west-trending fault is unresolved, although, as with the similar contact between the Hardluck massif ultramafic rocks and overlying Kedahda Formation in the Menatatuline Range area, it may be related to the southwest-vergent Nahlin fault and may represent a later generation thrust fault.

Economic Potential

There are several rock units within the Cache Creek terrane that are potential hosts of awaruite, gold and other base metals. The highly serpentinized ultramafic rocks throughout the Nahlin ultramafic body are prospective hosts for awaruite, a naturally occurring nickel-iron alloy. These same ultramafic rocks are the target of several ongoing projects by First Point Minerals Corporation in central and northwestern BC and southern Yukon (e.g., Rabb and Britten, 2012; Britten et al., 2014). Listwaenite, observed near diabase dikes in the harzburgite bodies throughout the Nahlin ultramafic body, has been associated with lode gold occurrences (Ash et al., 1992; Hansen et al., 2004), which have historically played a major role in the economy of the Atlin–Cassiar region. Near Peridotite Peak, the contact
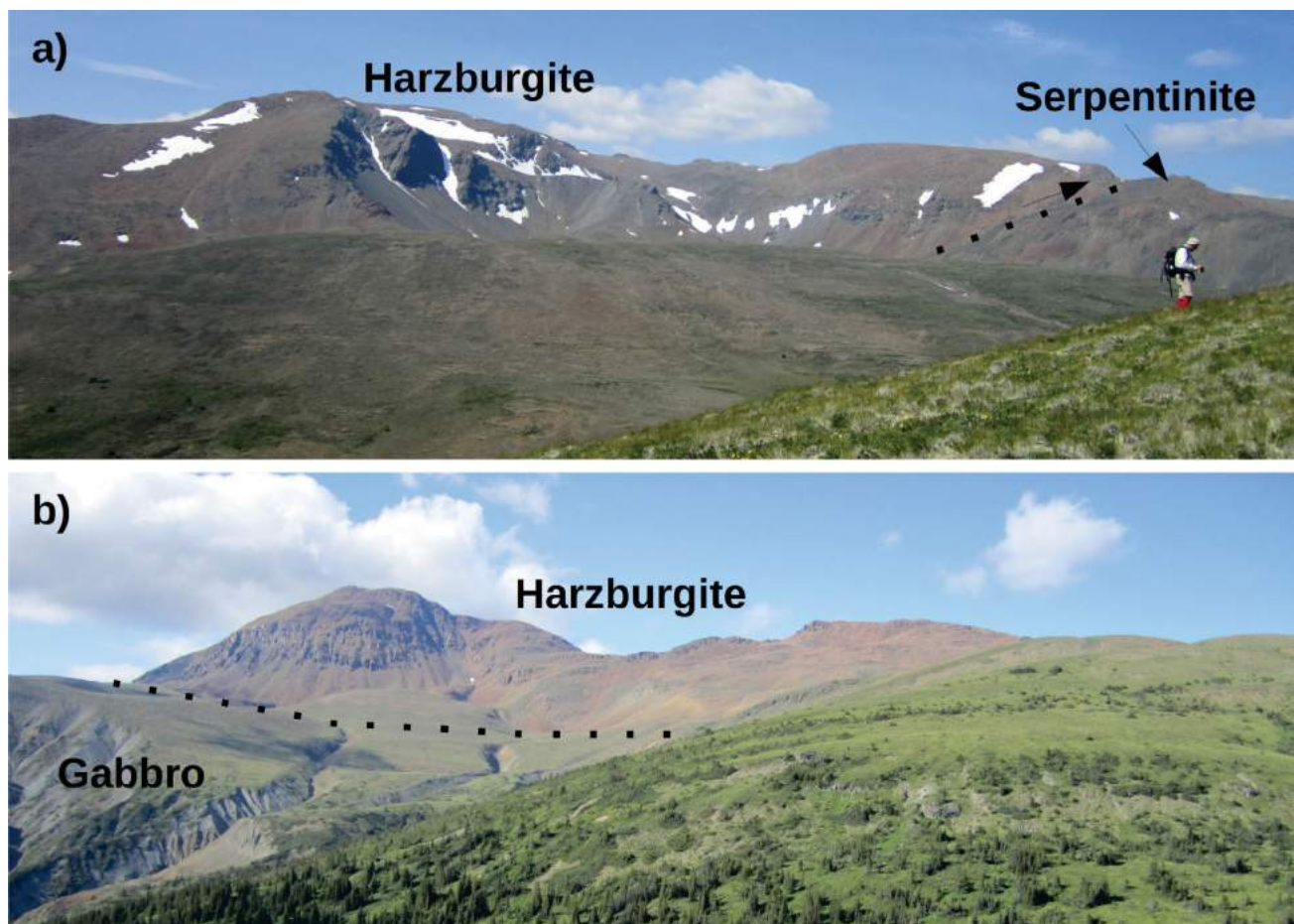
Figure 11: a) Ultramafic rocks of the Menatatuline massif thrust to the northeast over the Nakina Formation mafic volcanic rocks in the northern part of the Menatatuline Range area (fault 4 on Figure 2). View looking west-southwest. **b)** Shallow contact between ultramafic rocks on Peridotite Peak and underlying gabbroic intrusion exposed at lower elevations and along a drainage channel. The exact nature of this contact relationship is unresolved at present. View looking northwest toward Peridotite Peak.

area between the Hardluck massif and Kedahda Formation, the southern Laberge Group sedimentary rocks, and the crosscutting Sloko Group felsic volcanic rocks have been examined as potential hosts of base metals. Samples from this area yielded elevated, but not significant, concentrations of Au, Ag, Pb, Zn and Cu (Brown and Shannon, 1982; Mawer, 1988; Dynes, 1989; Mann and Newton, 2006).

Summary and Future Work

The Nahlin ultramafic body in the northern section of the Cache Creek terrane appears to conspicuously lack components of the classic Penrose-model ophiolite (Anonymous, 1972), most notably the sheeted-dike complex and significant lower crustal cumulates. However, the mantle, lower crustal and hypabyssal intrusions, and volcano-sedimentary sequences are all present, albeit structurally disrupted, within the Cache Creek terrane. The features of the Nahlin ultramafic body, including the absent sheeted-dike complex and significant supracrustal sequences, are similar to other Tethyan ophiolites that are now interpreted as oceanic-core complexes exhumed along low-angle detachments

on the ocean floor (e.g., Lagabrielle et al., 2015). Future work on this project will aim to determine if this interpretation can be applied to the Nahlin ultramafic body.

Preliminary interpretations from the 2015 fieldwork indicate that although some primary contact relations may be obscured by faulting, it is still possible to work toward constraining the tectonostratigraphy of the Cache Creek terrane in this area. For example, existing biostratigraphic data can constrain ages in some chert units within the Kedahda Formation and within various carbonate units in the Cache Creek terrane (Cordey et al., 1991; Orchard et al., 2001). Radiolarian chert and fossiliferous carbonate samples collected during 2015 will provide further constraints on the ages and distribution of these units, and may elucidate the nature of some faults throughout the map areas. Results from planned geochemical analyses will provide the data necessary to test the homogeneity of the various mantle, intrusive and volcanic rocks. The geochemical relations between these, or lack thereof, will be used to re-evaluate the existing maps and interpreted tectonostratigraphy. Geochemical data will also be used in inversion modelling to

yield compositions of melts in the mantle, which will be compared to compositional data from Cache Creek volcanic rocks. Uranium-lead geochronology of pegmatitic and coarse-grained gabbro and diorite samples will constrain the timing of magmatism. Additionally, mineral chemistry and the application of several geothermometers to the ultramafic rocks will aim to quantify the thermal history of the ophiolite, and interpret this in light of a possible oceanic-core complex hypothesis.

Acknowledgments

References

Aitken, J.D. (1959): Atlin map-area, British Columbia; Geological Survey of Canada, Memoir 307, 89 p.

Anonymous (1972): Penrose field conference on ophiolites; Geotimes, v. 17, no. 12, p. 22–24.

Ash, C.H. (1994): Origin and tectonic setting of ophiolitic ultramafic and related rocks in the Atlin area, British Columbia (NTS 104N); BC Ministry of Energy and Mines, BC Geological Survey, Bulletin 94, 48 p.

Ash, C.H., MacDonald, R.W.J. and Arksey, R.L. (1992): Towards a deposit model for ophiolite related mesothermal gold in British Columbia; in Geological Fieldwork 1991, BC Ministry of Energy and Mines, BC Geological Survey, Paper 1992-1, p. 253–260.

Bickerton, L., Colpron, M. and Gibson, D. (2013): Cache Creek terrane, Stikinia, and overlap assemblages of eastern Whitehorse (NTS 105D) and western Teslin (NTS 105C) map areas; in: Yukon Exploration and Geology 2012, K.E. MacFarlane, M.G. Nordling and P.J. Sack (ed.), Yukon Geological Survey, p. 1–17.

Bloodgood, M.A. and Bellefontaine, K.A. (1990): The geology of the Atlin area (Dixie Lake and Teresa Island) (104N/ 6 and parts of 104N/ 5 and 12); in Geological Fieldwork, 1989, BC Ministry of Energy and Mines, BC Geological Survey, Paper 1990-1, p. 205–215.

Britten, R., Rabb, T., Gagnon, M. and Carr, I.J.A. (2014): Geology, geochemistry and geophysics on the Wale, Polar and Orca properties, northern BC; BC Ministry of Energy and Mines, Assessment Report 34556, 135 p.

Brown, D. and Shannon, K. (1982): Assessment report on the Goat Claims; BC Ministry of Energy and Mines, Assessment Report 10701, 19 p.

Childe, F.C. and Thompson, J.F.H. (1997): Geological setting, U-Pb geochronology, and radiogenic isotopic characteristics of the Permo-Triassic Kutcho Assemblage, north-central British Columbia; Canadian Journal of Earth Sciences, v. 34, no. 10, p. 1310–1324.

Colpron, M. and Nelson, J.L. (2011): A Digital Atlas of Terranes for the Northern Cordillera; accessed online from Yukon Geological Survey, URL <http://www.geology.gov.yk.ca> [September 2015].

Cordey, F., Gordey, S.P and Orchard, M.J. (1991): New biostratigraphic data from the northern Cache Creek terrane, Teslin map area, southern Yukon; in Current Research, Part E; Geological Survey of Canada, Paper 91-1E, p. 67–76.

Dick, H.J.B. and Sinton, J.M. (1979): Compositional layering in Alpine peridotites: Evidence for pressure solution creep in the mantle; Journal of Geology, v. 87, p. 403–416.

Dynes, W.J. (1989): Assessment report on the Yeth Property; BC Ministry of Energy and Mines, Assessment Report 19376, 33 p.

English, J.M. and Johnston, S.T. (2005): Collisional orogenesis in the northern Canadian Cordillera: Implications for Cordilleran crustal structure, ophiolite emplacement, continental growth, and the terrane hypothesis; Earth and Planetary Science Letters, v. 232, p. 333–344.

English, J.M., Mihalynuk, M.G., Johnston, S.T. and Devine, F.A. (2002): Atlin TGI Part III: Geology and petrochemistry of mafic rocks within the northern Cache Creek terrane and tectonic implications; in BC Geological Fieldwork 2001, BC Ministry of Energy and Mines, BC Geological Survey, Paper 2002-1, p. 19–30.

English, J.M., Mihalynuk, M.G. and Johnston, S.T. (2010). Geochemistry of the northern Cache Creek Terrane and implications for accretionary processes in the Canadian Cordillera; Canadian Journal of Earth Sciences, v. 47, no. 1, p. 13–34.

Gabrielse, H. (1991): Late Paleozoic and Mesozoic terrane interactions in north-central British Columbia; Canadian Journal of Earth Sciences, v. 28, p. 947–957.

Gordey, S. P., McNicoll, V.J. and Mortensen, J.K. (1998): New U-Pb ages from the Teslin area, southern Yukon, and their bearing on terrane evolution in the northern Cordillera; in Current Research; Geological Survey of Canada, Paper 1998-F, p. 129–148.

Hansen, L.D., Anderson, R.G., Dipple, G.M. and Nakano, K. (2004): Geological setting of listwanite (carbonated serpentinite) at Atlin, British Columbia: implications for CO_2 sequestration and lode-gold mineralization; in Current Research 2004-A5, Geological Survey of Canada, 12 p.

Johnston, S.T. and Borel, G.D. (2007): The odyssey of the Cache Creek terrane, Canadian Cordillera: implications for accretionary orogens, tectonic setting of Panthalassa, the Pacific superwell, and break-up of Pangea; Earth and Planetary Science Letters, v. 253, p. 415–428.

Kelemen, P.B. and Dick, H.J.B. (1995): Focused melt flow and localized deformation in the upper mantle: Juxtaposition of replacive dunite and ductile shear zones in the Josephine peridotite, SW Oregon; Journal of Geophysical Research, v. 100, p. 423–438.

Lagabrielle, Y., Brovarone, A.V. and Ildefonse, B. (2015): Fossil oceanic core complexes recognized in the blueschist metaophiolites of Western Alps and Corsica; Earth-Science Reviews, v. 141, p. 1–26.

Mann, R.K. and Newton, A.C. (2006): Assessment report on the Fall Property; BC Ministry of Energy and Mines, Assessment Report 28090, 61 p.

Mawer, A.B. (1988): Assessment report on the Per Group Claims; BC Ministry of Energy and Mines, Assessment Report 18040, 20 p.

Mihalynuk, M.G. (1999): Geology and mineral resources of the Tagish Lake area, northwestern British Columbia; BC Ministry of Energy and Mines, Bulletin 105, 201 p.

Mihalynuk, M.G., Smith, M.T., Gabites, J.E., Runkle, D. and Lefebure, D. (1992): Age of emplacement and basement character of the Cache Creek terrane as constrained by new isotopic and geochemical data; Canadian Journal of Earth Sciences, v. 29, p. 2463–2477.

Mihalynuk, M.G., Nelson, J. and Diakow, L.J. (1994): Cache Creek terrane entrapment: Oroclinal paradox within the Canadian Cordillera; Tectonics, v. 13, p. 575–595.

Mihalynuk, M.G., Bellefontaine, K.A., Brown, D.A., Logan, J.M., Nelson, J.L., Legun, A.S. and Diakow, L.J. (1996): Geological compilation, northwest British Columbia (NTS 94E, L, M; 104F, G, H, I, J, K, L, M, N, O, P; 114J, O, P); BC Ministry of Energy and Mines, Open File, 1996-11.

Mihalynuk, M.G., Erdmer, P., Ghent, E.D., Archibald, D.A., Friedman, R.M., Cordey, F., Johannson, G.G. and Beanish, J. (1999): Age constraints for emplacement of the northern Cache Creek Terrane and implications of blueschist metamorphism; BC Ministry of Energy and Mines, Paper 1999-1, p. 127–142.

Mihalynuk, M.G., Johnston, S.T., Lowe, C., Cordey, F., English, J.M., Devine, F.A.M., Larson, K. and Merran, Y. (2002): Atlin TGI Part II: preliminary results from the Atlin Targeted Geoscience Initiative, Nakina area, northwest British Columbia; in BC Geological Fieldwork 2001, BC Ministry of Energy and Mines, Paper 2002-1, p. 5–18.

Mihalynuk, M.G., Johnston, S.T., English, J.M., Cordey, F., Villeneuve, M.E., Rui, L. and Orchard, M.J. (2003): Atlin TGI, Part II: regional geology and mineralization of the Nakina area (NTS 104N/2W and 3); in Geological Fieldwork 2002, BC Ministry of Energy and Mines, Paper 2003-1, p. 9–37.

Mihalynuk, M.G., Fiererra, L., Robertson, S., Devine, F.A.M. and Cordey, F. (2004): Geology and new mineralization in the Joss'alun belt, Atlin area; in BC Geological Fieldwork 2003, BC Ministry of Energy and Mines, Paper 2004-1, p. 61–82.

Monger, J.W.H. (1975): Upper Paleozoic rocks of the Atlin Terrane, northwestern British Columbia and south-central Yukon; Geological Survey of Canada, Paper 74-47, 63 p.

Monger, J.W.H. and Ross, C.A. (1971): Distribution of fusulinaceans in the western Canadian Cordillera; Canadian Journal of Earth Sciences, v. 8, p. 259–278.

Natural Resources Canada (1990a): Teditua Creek NTS 104K/16; Natural Resources Canada, National Topographic System map sheet, 104K/16, scale 1:50 000, raster image.

Natural Resources Canada (1990b): Yeth Creek NTS 104K/15; Natural Resources Canada, National Topographic System map sheet, 104K/15, scale 1:50 000, raster image.

Nicolas, A. (1995): The Mid-Oceanic Ridges: Mountains Below Sea Level; Springer Verlag, Heidelberg, Germany, 200 p.

Nicolas, A. and Violette, J.F. (1982): Mantle flow at oceanic spreading centers: models derived from ophiolites; Tectonophysics, v. 81, p. 319–339.

Orchard, M.J., Struik, L.C., Rui, L., Bamber, E.W., Mamet, B., Sano, H. and Taylor, H. (2001): Palaeontological and biogeographical constraints on the Carboniferous to Jurassic Cache Creek terrane in central British Columbia; Canadian Journal of Earth Sciences, v. 38, no. 4, p. 551–578.

Rabb, T. and Britten, R. (2012): Klow property, BC: Geology and geochemistry (NTS 093N/3 and 4); BC Ministry of Energy and Mines, Assessment Report 33056, 53 p.

Schiarizza, P. (2012): Geology of the Kutcho Assemblage between Kehlechoa and Tucho Rivers, northern British Columbia (NTS 104I/01, 02); in Geological Fieldwork 2011, BC Ministry of Energy and Mines, Paper 2012-1, p. 99–118.

Souther, J.G. (1971): Geology and mineral deposits of Tulsequah map-area, British Columbia; Geological Survey of Canada, Memoir 362, 84 p.

Terry, J. (1977): Geology of the Nahlin ultramafic body, Atlin and Tulsequah map-areas, northwestern British Columbia; in Current Research Part A, Geological Survey of Canada, Paper 77-1A, p. 263–266.

Preliminary Report: Biogenic Controls on Reservoir Properties in the Lower Triassic Montney Formation, Dawson Creek Area, Northeastern British Columbia and Northwestern Alberta

D.T. Prenoslo, University of Alberta, Edmonton, AB, dprenosl@ualberta.ca

A.E. Gegolick, University of Alberta, Edmonton, AB

M.K. Gingras, University of Alberta, Edmonton, AB

J.-P. Zonneveld, University of Alberta, Edmonton, AB

Introduction

Over the past decade, the Montney Formation has evolved into western Canada's premier unconventional exploration play, containing an estimated 449 trillion cubic feet of marketable natural gas in addition to natural gas liquids and condensate (Faraj et al., 2002; National Energy Board et al., 2013). Historically, Montney Formation exploration has focused on conventional reservoir intervals, such as the turbidite interval and clastic and bioclastic shoreface intervals (Davies et al., 1997; Zonneveld et al., 2010). Although low porosity and low permeability siltstone intervals make up the largest portion of the Montney Formation, they have until recently been overlooked. With the advent of horizontal drilling and multistage hydraulic fracturing, these intervals have become highly prospective (National Energy Board et al., 2013).

Considering the economic importance of the Montney Formation, detailed geological analyses focusing on the sedimentology of the unconventional reservoir portions of the Montney Formation remain limited. Interpretations of depositional environments within the Montney Formation are constrained to petroleum fields along the eastern subcrop edge as well as those along the turbidite trend (Davies et al., 1997; Moslow, 2000; Zonneveld et al., 2010). Montney Formation successions in the western part of the Western Canada Sedimentary Basin have been referred to as distal, offshore or basin-centred due primarily to the restricted grain sizes observed in core and outcrop (Gibson and Edwards, 1990; Dixon, 2000). Preliminary core analysis suggests that this is not the case and a more complicated depositional scenario exists.

Keywords: *Montney Formation, ichnology, sedimentology, stratigraphy, unconventional resources*

This publication is also available, free of charge, as colour digital files in Adobe Acrobat® PDF format from the Geoscience BC website: http://www.geosciencebc.com/s/DataReleases.asp.

Despite minimal variation in grain size between facies, it has become apparent that primary depositional characteristics play a seminal role in preserved reservoir attributes. In particular, the presence and nature of bioturbation is increasingly recognized as a key element in resource distribution. Bioturbation has long been recognized as a potentially significant control on porosity and permeability in both conventional and unconventional reservoir units (Pemberton and Gingras, 2005; Baniak et al., 2015). The subtle nature of Montney Formation bioturbation makes trace fossils difficult to observe in hand sample. As a result, in published literature there has been minimal focus on the potential effects of bioturbation on reservoir properties of the Montney Formation. Recent studies have focused on the relationship between bioturbation and water saturation in Montney Formation siltstone (Wood, 2012). However, bioturbation and its relationship to porosity and permeability in the Montney Formation remains to be investigated.

Research Objectives

The goal of this research is to 1) investigate the influence of bioturbation on reservoir quality in the Montney Formation; 2) characterize the depositional setting and develop a stratigraphic framework for the Montney Formation in the Pouce Coupe–Dawson Creek area; 3) refine stratigraphic and sedimentological models used for defining reservoir units, reservoir correlations and properties important to reservoir quality; and 4) develop predictive models to help decrease exploration risk.
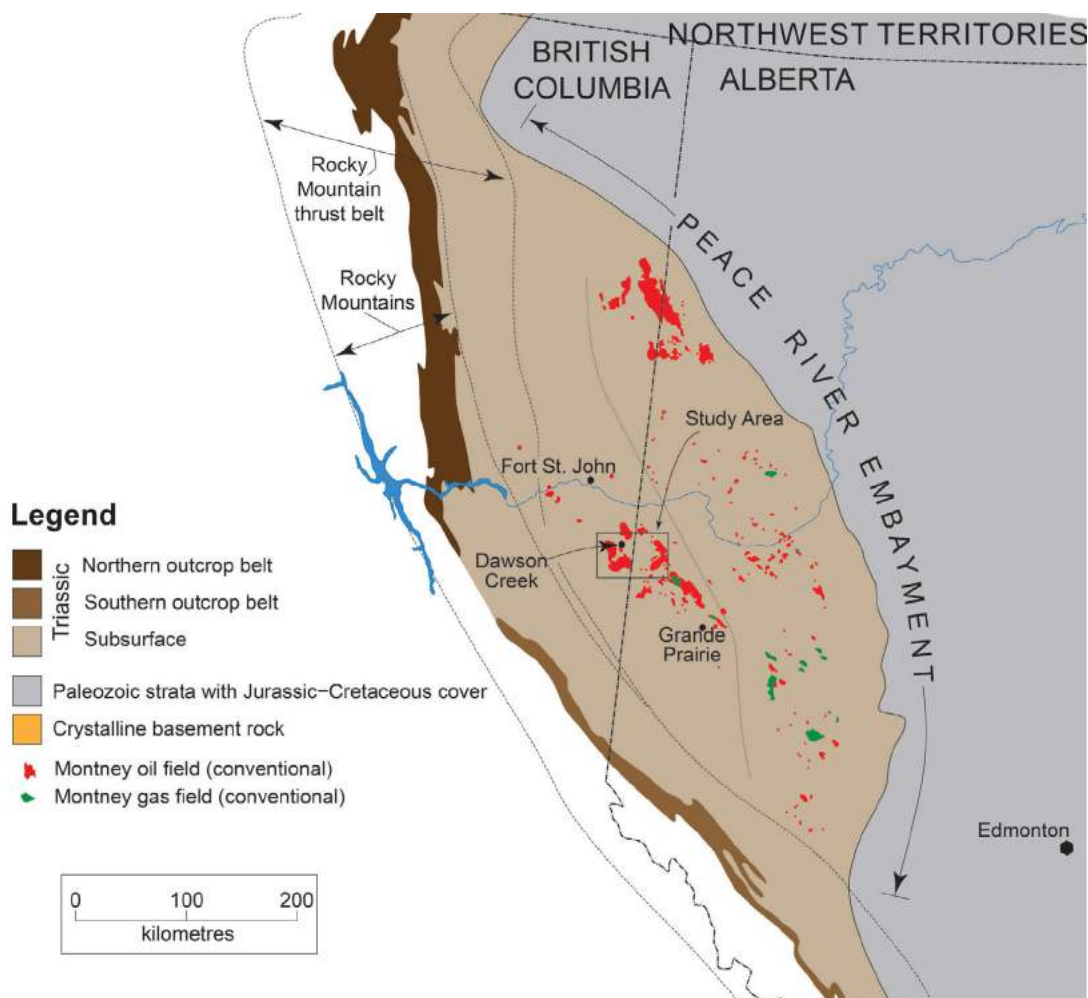
Study Area

The study area is located on either side of the Alberta–British Columbia border near the town of Dawson Creek, approximately 75 km south-southeast of Fort St. John (Figure 1). This area overlaps the Montney Formation turbidite trend, which was a prolific oil play during the 1990s. With advances in technology allowing the exploitation of the

Figure 1. Distribution of Triassic strata in the Western Canada Sedimentary Basin (after Zonneveld et al., 2011). Location of study area outlined in black.

tight siltstone intervals, this area is once again an active exploration target. The studied interval directly overlies the Montney Formation turbidite and although stratigraphically equivalent successions are dry in surrounding areas, this area is characterized by liquid-rich natural gas. In the study area there are 2753 wells that penetrate the Montney Formation, of which 247 are cored.

Geological Framework

The Montney Formation is a complex accumulation dominated by siltstone and sandstone with shale and bioclastic packstone/grainstone occurring in some areas (Zonneveld et al., 2011). Deposition took place along the northwestern coast of Pangaea with the thickest accumulations occurring near the collapsed Peace River arch (Davies et al., 1997). An extensional tectonic regime combined with underlying Devonian reef complexes exerted a strong influence on the regional and local structure during the early Triassic (Moslow, 2000). During this time, the northwestern coast of Pangaea was situated in a midlatitudinal setting and was

characterized by arid conditions with dominant northeast trade winds (Davies et al., 1997). The aridity of the region combined with exceptionally long sediment transport distances resulted in dominantly fine-grained clastic deposition throughout all environments; consequently, Montney Formation depositional environments are not easily segregated on the basis of grain size alone (Zonneveld et al., 2011).

In the study area, cores from 50 wells (Figure 2) were logged to assess the ichnological and sedimentological character of constituent lithofacies. Sedimentological analysis focused on bedding thickness, bedding contacts, grain size, penecontemporaneous deformation structures, primary physical sedimentary structures and sorting. Ichnological observations included ichnogenera identification, relative ichnogenera abundance, assemblage diversity and intensity of bioturbation. Thin section analyses were used to determine framework grain and cement compositions, as well as to observe subtle bioturbated fabrics. Permeability measurements were obtained using a Core Labo-
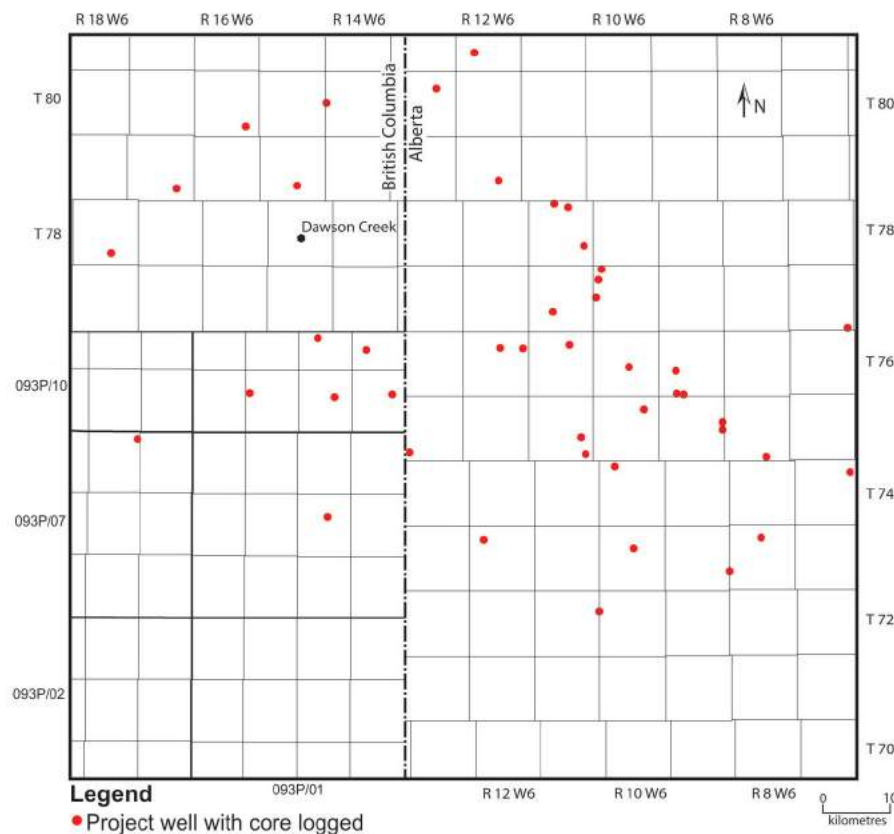
Figure 2. Location of 50 wells from which cores were analyzed in the study area, northeastern British Columbia and northwestern Alberta.

ratories pressure-decay profile permeameter located at the University of Alberta.

Preliminary Results and Future Work

In the studied core, the most common ichnofabric observed is cryptic bioturbation, which has been recognized throughout the interval and has altered much of the rock fabric. Bioturbation modifies the relationship between vertical permeability and horizontal permeability (i.e., it decreases permeability anisotropy), and preliminary porosimetry work indicates that the bioturbation has had an affect on resource storativity and deliverability. The trace fossils are also useful for subdividing the interval into facies. These facies will be mapped and together with observed facies-associated permeability trends will enable the development of a predictive framework for the delineation of areas with superior reservoir quality.

Acknowledgments

References

Baniak, G.M., Gingras, M.K., Burns, B.A. and Pemberton, S.G. (2015): Petrophysical characterization of bioturbated sandstone reservoir facies in the Upper Jurassic Ula Formation, Norwegian North Sea, Europe; Journal of Sedimentary Research, v. 85, no. 1, p. 62–81.

Davies, G.R., Moslow, T.F. and Sherwin, M.D. (1997): The lower Triassic Montney Formation, west-central Alberta; *in* Triassic of the Western Canada Sedimentary Basin, T.F. Moslow and J. Wittenberg (ed.), Bulletin of Canadian Petroleum Geology, v. 45, p. 474–505.

Dixon, J. (2000): Regional lithostratigraphic units in the Triassic Montney Formation of Western Canada; Bulletin of Canadian Petroleum Geology, v. 48, p. 80–83.

Faraj, B., Harold, W., Addison, G., McKinstry, B., Donaleshen, R., Sloan, G., Lee, J., Anderson, T., Leal, R., Anderson, C., Lafleur, C. and Ahlstrom, A. (2002): Shale gas potential of selected Upper Cretaceous, Jurassic, Triassic and Devonian shale formations in the WCSB of Western Canada: implications for shale gas production; Gas Technology Institute, Des Plaines, Illinois, 103 p.

Gibson, D.W. and Edwards, D.E. (1990): An overview of Triassic stratigraphy and depositional environments in the Rocky Mountain foothills and western interior plains, Peace River arch area, northeastern British Columbia; Bulletin of Canadian Petroleum Geology, v. 38, no. 1, p. 146–158.

Moslow, T.F. (2000): Reservoir architecture of a fine-grained turbidite system: Lower Triassic Montney Formation, West-

ern Canada Sedimentary Basin; *in* Deep-Water Reservoirs of the World, P. Weimer, R.M. Slatt, J. Coleman, N.C. Rosen, H. Nelson, A.H. Bouma, M.J. Styzen, and D.T. Lawrence (ed.), Society of Economic Paleontologists and Mineralogists, Gulf Coast Section, Conference Proceedings, December 3–6, 2000, Houston, Texas, p. 686–713.

National Energy Board, BC Oil and Gas Commission, Alberta Energy Regulator and BC Ministry of Natural Gas Development (2013): Energy briefing note: the ultimate potential for unconventional petroleum from the Montney Formation of British Columbia and Alberta; National Energy Board, BC Oil and Gas Commission, Alberta Energy Regulator and BC Ministry of Natural Gas Development, 17 p.

Pemberton, S.G. and Gingras, M.K. (2005): Classification and characterizations of biogenically enhanced permeability; American Association of Petroleum Geologists, AAPG Bulletin, v. 89, no. 11, p. 1493–1517.

Wood, J.M. (2012): Water distribution in the Montney tight gas play of the Western Canadian Sedimentary Basin: significance for resource evaluation; SPE Reservoir Evaluation & Engineering, v. 16, no. 3, p. 290–302.

Zonneveld, J.-P., Golding, M., Moslow, T.F., Orchard, M.J., Playter, T. and Wilson, N. (2011): Depositional framework of the Lower Triassic Montney Formation, west-central Alberta and northeastern British Columbia; *in* recovery – 2011 CSPG CSEG CWLS Convention, p. 1–4.

Zonneveld, J.-P., MacNaughton, R.B., Utting, J., Beatty, T.W., Pemberton, S.G. and Henderson, C.M. (2010): Ichnology and sedimentology of the lower Montney Formation (Lower Triassic), Kahntah River and Ring Border gas fields, Alberta and British Columbia; *in* Applications of Ichnology to Petroleum Exploration, J-P. Zonneveld, M.K. Gingras and J.A. MacEachern (ed.), Bulletin of Canadian Petroleum Geology, v. 58, p. 115–140.

Geochemical Mapping of the Deerhorn Copper-Gold Porphyry Deposit and Associated Alteration through Transported Cover, Central British Columbia (NTS 093A/03)

S.D. Rich, Mineral Deposit Research Unit, University of British Columbia, Vancouver, BC, srich@eos.ubc.ca

P.A. Winterburn, Mineral Deposit Research Unit, University of British Columbia, Vancouver, BC

Introduction

Central British Columbia comprises at least three volcanic arc terranes that are considered important hosts of porphyry copper deposits (McMillan and Panteleyev, 1995; Logan and Mihalynuk, 2014). These deposits are significant contributors to the economy of BC; however, discoveries of new economic deposits, which are mostly discovered from outcrop, have declined in the past 20 years. Deposits may be overlain by young (<9000 years) glacial overburden, making their discovery challenging. Anomalous geochemical responses have been reported in several independent initiatives targeting sulphide deposits buried by younger glacial cover (Hamilton et al., 2004; Bissig et al., 2013; Eppinger et al., 2013); however, the transfer of these results into practical exploration tools has been inhibited by a lack of understanding surrounding the genesis of the anomalies. Innovative research into geochemical technology, surface materials and surface processes will lead to the development of novel exploration tools, increasing the likelihood of new discoveries.

The Deerhorn Cu-Au porphyry deposit (MINFILE 093A 269; BC Geological Survey, 2015), located 70 km northeast of Williams Lake (Figure 1), is one of at least five undeveloped porphyry systems that form the Woodjam area, which is currently being explored by Consolidated Woodjam Copper (and previously by Gold Fields Canada Exploration). The deposit and its immediate surroundings are covered by 10 to 150 m of glacial sediment <9000 years old with little or no evidence of extensive surface disturbance other than logging activities and exploration drilling. Mining has not been initiated. The subglacial paleosurface of the Deerhorn Cu-Au porphyry has been mapped from

drill core (Figure 1; Sherlock et al., 2013; del Real Contreras, 2015). Bissig et al. (2013) indicated the presence of anomalous geochemistry over the porphyry. This study significantly expands on that previous work, extending the survey an additional three sampling lines to produce a surficial geochemistry map. This study also adds new exploration methods, including metal isotopes (Cu, Mo and Pb), a self-potential geophysical survey and an organic geochemical application assessment. Chemical and physical parameters of the surface environment (e.g., geomorphology, soil types, pH, moisture content, oxidation reduction potential [ORP] and organic carbon content) will be integrated with the data to differentiate the response of mineralization from background responses and potential false positives.

Background

The Deerhorn Cu-Au porphyry is a high-K, calcalkaline intrusive complex discovered in 2009 by Consolidated Woodjam Copper and Gold Fields Canada Exploration. Between 2009 and 2011, 37 drillholes defined the underlying geology and current mineral resource estimate of 38.2 Mt grading 0.22% Cu and 0.49 g/t Au (Sherlock et al., 2013). Volcanic and sedimentary rocks are intruded by three distinct monzonite intrusions. Mineralization, which consists of disseminated and vein-hosted Cu and Au, is preferentially hosted in the monzonitic intrusions in comparison with the local country rocks, which consist of thickly bedded, volcanic-derived sandstone that is overlain by andesite flow breccia (R. Sherlock, pers. comm., 2015). The mineralized resource is defined by a zone approximately 500 m in diameter occurring at the bedrock-till interface.

Late Wisconsinan glaciation (Dyke and Prest, 1987) may have unroofed the deposit as it is currently exposed in subcrop. Glaciofluvial, glacial and glaciolacustrine sediments overlie the mineralization and surrounding country rocks. These till deposits are now densely vegetated by mixed conifer forest, which is being selectively logged.
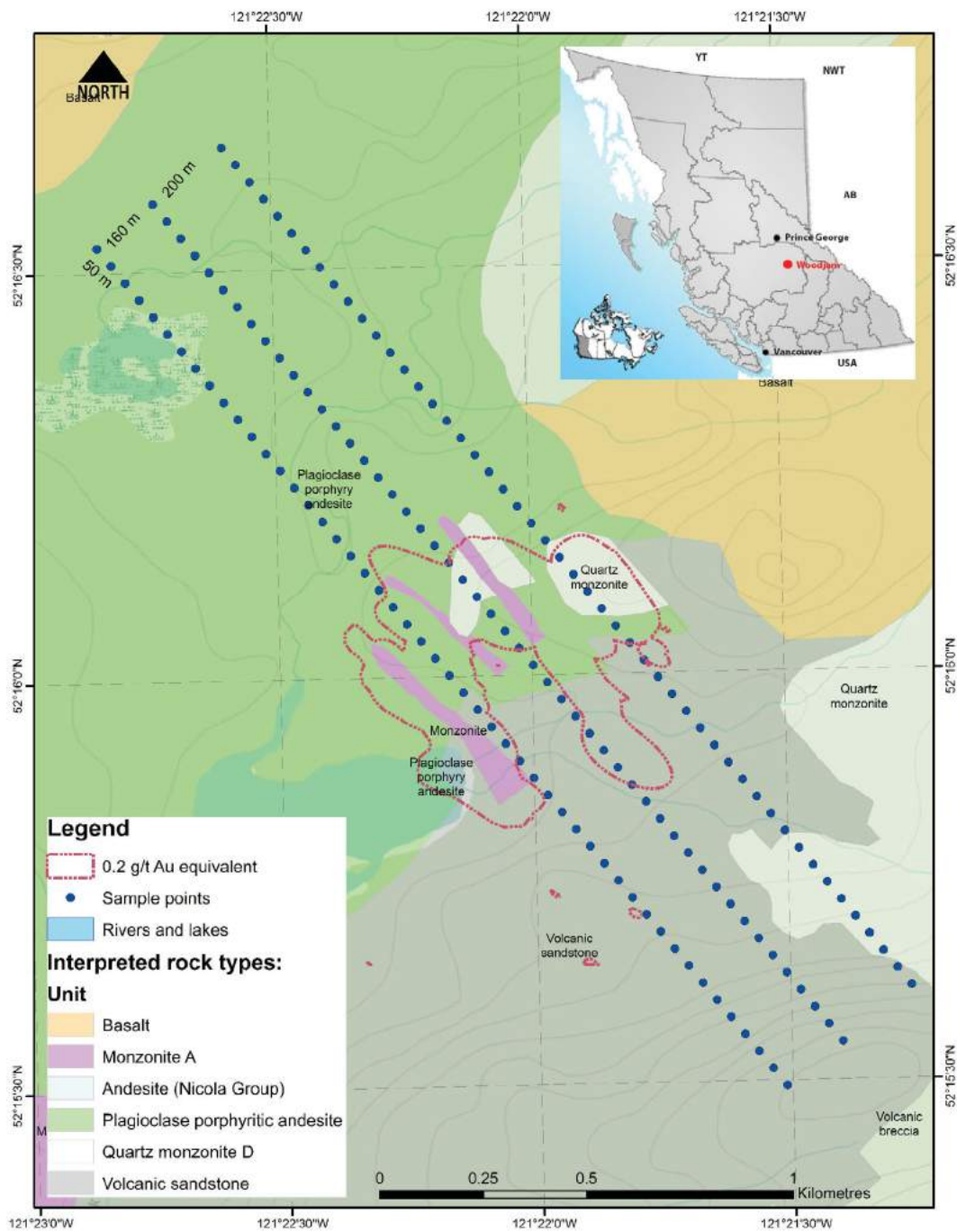
Figure 1. Bedrock geology of the Woodjam project area (Quaternary overburden removed), showing the location of the mineralized zone and the three sample lines completed as part of this study. The three transect lines show the area of detailed regolith mapping shown in Figure 2. The location of study area is identified in the inset. Geological map shapefile courtesy of Gold Fields Canada Exploration and Consolidated Woodjam Copper.

During the 2015 summer field season, 24 days were spent traversing the project area to construct a surface regolith map. A total of 157 soil samples was collected for chemical analysis. Hydrocarbon collectors were placed in the ground at each sample site for 63 days and a self-potential geophysical survey was conducted over the mineralized zone. Detailed field data were collected at each sample location.

Regolith Mapping

In May 2015, an area 2.5 by 0.6 km that encompassed the sampling and geophysical survey slocations underwent regolith mapping . Geomorphological units, anthropogenic activities and potential contamination, vegetation types and topographic variations were noted during the mapping
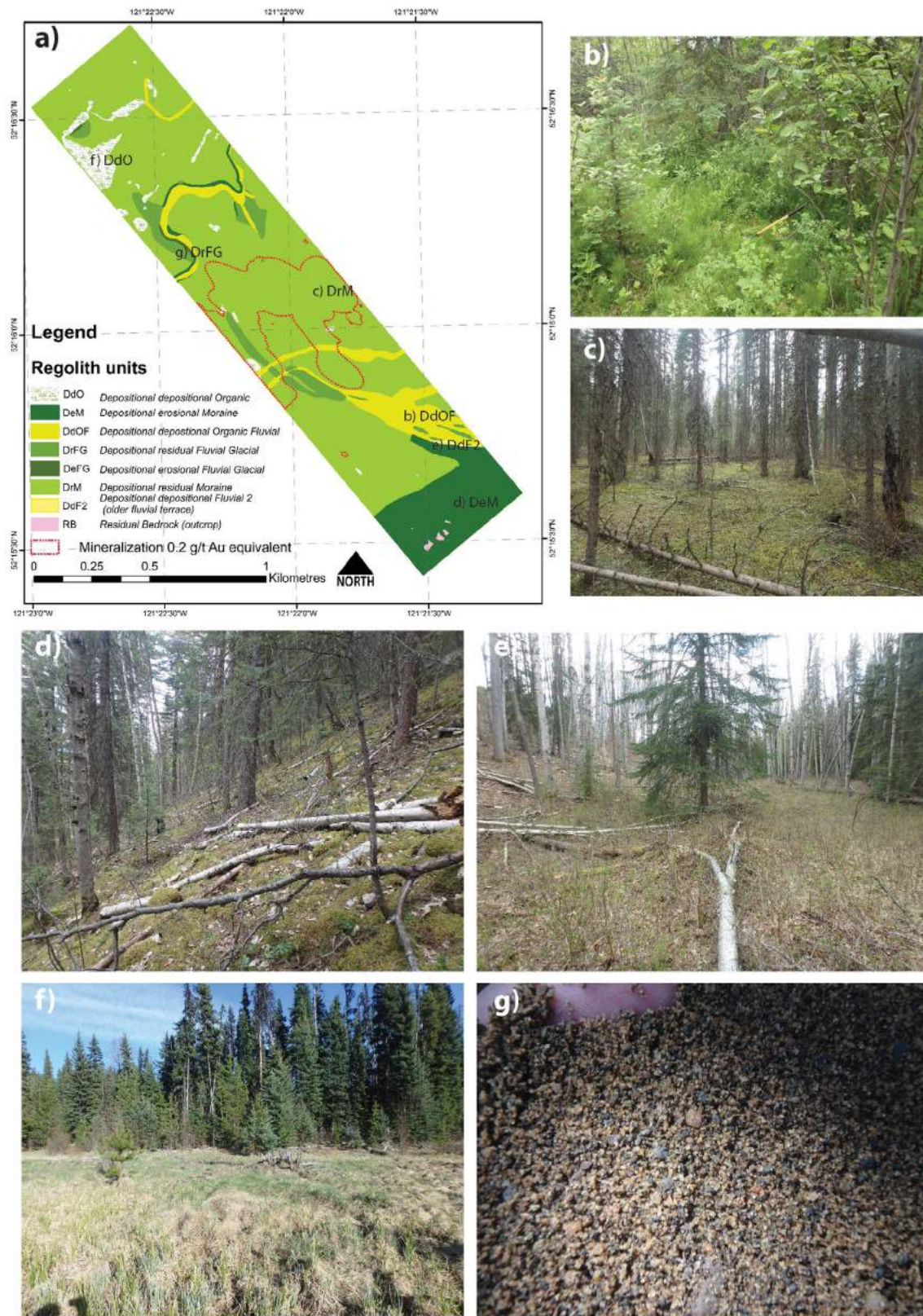
Figure 2. a) Regolith (surficial geology) of the study area (as shown in Figure 1); mapping is classified under the RED (residual, erosional and depositional) mapping scheme introduced by the Cooperative Research Centre for Landscape Environments and Mineral Exploration (Pain, 2008); geomorphological modifiers (to the right-hand side of an RED classification) are classified under the terrain classification system for British Columbia (Howes and Kenk, 1997); **b–g)** photographs of example locations of the residual, erosional and depositional (RED) environments; location of each photo indicated in Figure 2a.

(Figure 2). Regolith mapping over the deposit, combined with inorganic and organic chemistry assays, confirmed geochemical relationships that are dependent on the geomorphological environment. Awareness of these relationships can assist in identifying and deprioritizing potential false anomalies, while characterizing the background noise for removal by data filtering. This approach can strengthen subtle anomalies that may be related to buried mineralization.

Soil Sampling

A total of 157 soil samples (including seven duplicates) were collected from the upper B soil horizon (immediately below the Ae horizon, where present) on a predetermined set of three lines at 200 m spacing with 50 m spaced samples crossing mineralization and extending into background on either side of the deposit. The lines were oriented to minimize variability in the subcrop geology, take into account two stages of ice movement and avoid the lake to the southwest. Extensive metadata were collected at each location, including

- descriptions of all soil horizons present in the profile, their depths, colour, in situ pH, conductivity and moisture content (Figure 3);
- the ratio of soil to de-ionized water slurry (1:1) measurements including pH, acidified pH (following the method of Smee [2009]) and ORP;
- vegetation types, canopy and under-canopy height;
- slope and aspect measurements; and
- photographic documentation of the sample environment and soil profile.

All samples were submitted to ALS Laboratories (Vancouver, BC) for aqua-regia digestion, de-ionized water extrac-

tions, inductively coupled plasma–mass spectrometry (ICP-MS) multi-element analysis and C_{org} measurement.

Reducing the Impact of Major Components in Soils on Trace-Element Variability

Organic matter (analyzed using ALS assay C-IRO6a), along with clay, quartz and mineral and rock fragments, can be a significant component in soil. Organic acids, created during the breakdown of plant material, have a significant capacity to sequester and retain cations from the ambient environment. Organic material tends to accumulate in depressions, such as in swamps or drainage channels, resulting in the generation of potential false anomalies (Figure 4). Accounting for the variation in organic carbon, for example by simple normalization, can reduce the significance of organic enhanced trace-metal responses.

Self-Potential Survey

Electrochemistry has shown potential for identifying buried sulphide ore deposits due to the reduced nature of regolith increasing the conductivity above oxidizing sulphide ore (Smee, 1983; Hamilton et al., 2004). A self-potential (SP; also known as spontaneous potential) survey was conducted along each sample line at the end of July 2015 to image the electrical response at the surface (Figure 5). At the Deerhorn Cu-Au porphyry deposit, measurements using Cu-CuSO$_4$ electrodes were recorded at 50 m intervals, using the same locations as the soil samples collected along the soil survey transects. Evaluation of the Deerhorn SP data is ongoing, in particular taking into account the surface variability recorded during the regolith mapping and soil sampling. Soil moisture at each SP station requires integration with the SP data. This is important given the observations of Burr (1981) and Corry et al.
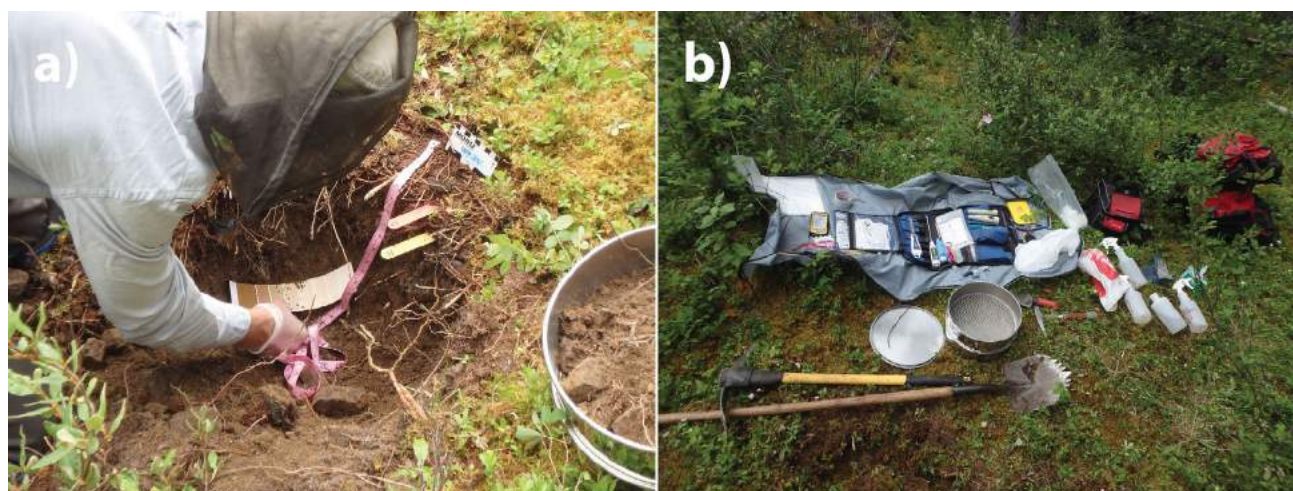
Figure 3. a) Soil profile measurement undertaken at each location; b) equipment used to conduct soil survey.
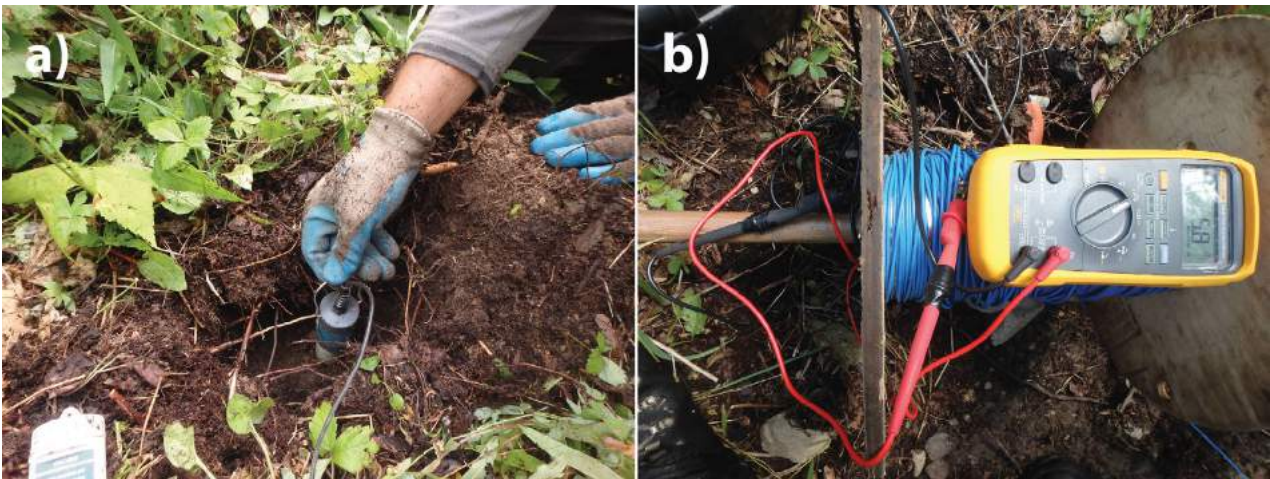
**Figure 4. a)** Insertion of copper–copper sulphate electrode used during the self-potential survey; **b)** copper wire and voltmeter used for the self-potential survey connected to copper-copper electrode.
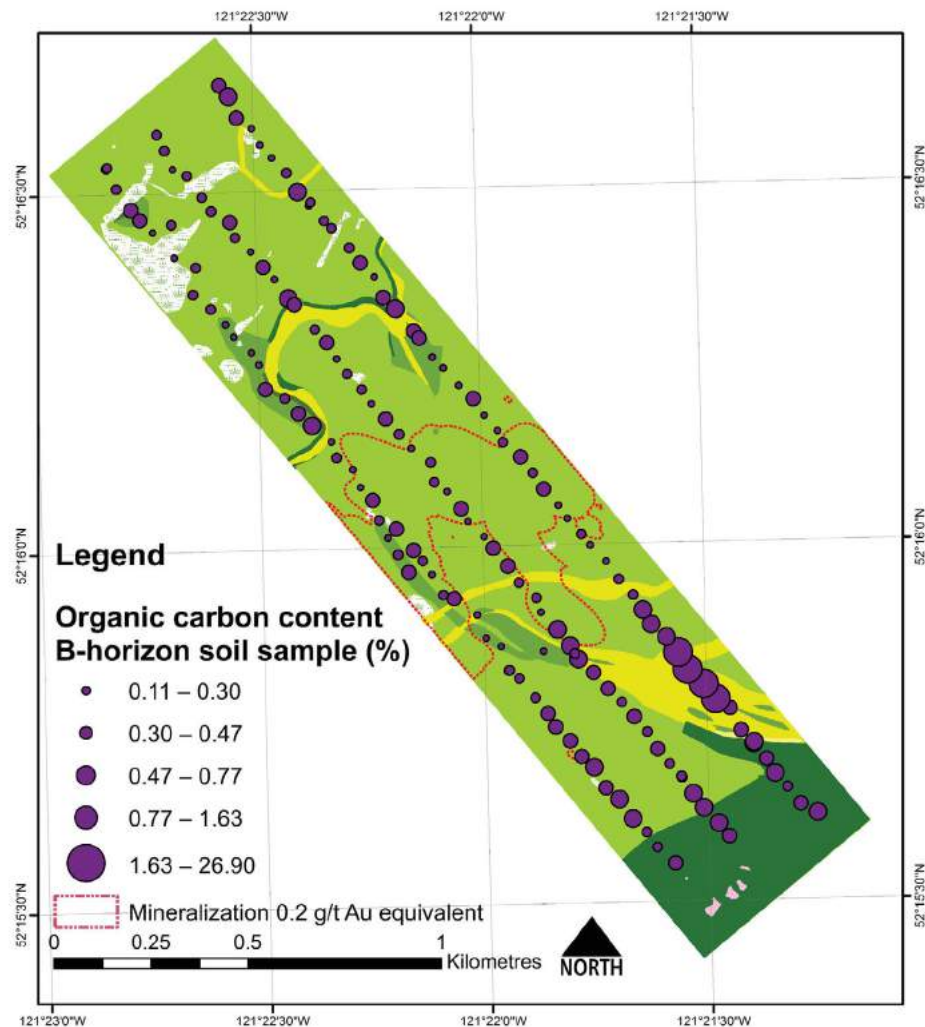
Figure 5. Spatial attribute map for organic chemistry results (C_{org}) over the Deerhorn Cu-Au porphyry deposit. Organic-rich swamps and organic fluvial areas mapped as Depositional depositional Organic Fluvial (DdOF) and Depositional depositional Organic (DdO) in Figure 2 correlate with higher concentrations of C_{org}. The locations of results displayed represent the 150 predetermined locations (including seven field duplicates) for the soil profile analyses and soil sampling survey, as well as the subsequent hydrocarbon collection and self-potential survey locations. Legend as in Figure 2.
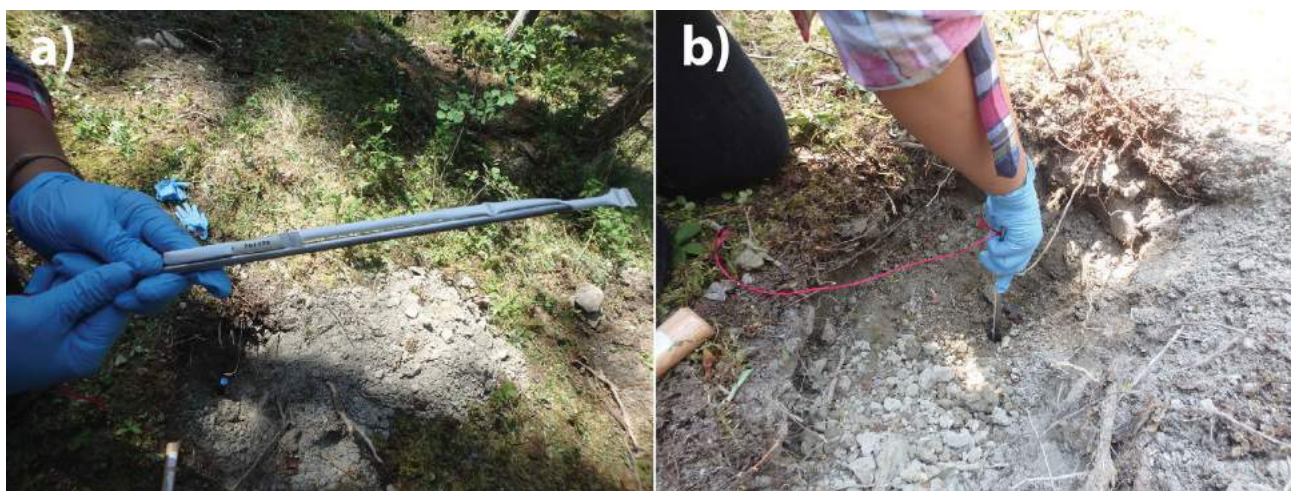
Figure 6. a) Gore-Tex® membrane hydrocarbon collector supplied by AGI Laboratories; **b)** insertion of hydrocarbon collector 45–60 cm below the surface.

(1983) that variable moisture content can induce a strong interference in voltage measurements.

Hydrocarbon Collection

In total, 157 hydrocarbon collectors (including seven duplicates) consisting of water-impermeable–gas-permeable Gore-Tex® membranes housing activated carbon were buried at a depth of 45–60 cm and left for 63 days at each sample location (Figure 6). The hydrocarbons in the collectors will be analyzed by thermal desorption followed by high-resolution gas chromatography–mass spectroscopy at Amplified Geochemical Imaging (Delaware, United States; Anderson, 2006). These data will be integrated with the inorganic and regolith data to determine if a viable response in the hydrocarbons can be detected and correlated with mineralization.

Summary

Extensive geomorphological and surface mapping was undertaken at the Deerhorn Cu-Au porphyry deposit and is being integrated with the organic, inorganic and physicochemical results from 150 sample sites in the till that overlies the deposit and the surrounding area to differentiate true anomalous response from background noise and false anomalies. A critical component that is often overlooked in the interpretation of geochemical surveys is quantifying the history of the horizon being sampled. The integration of the surface, environment, relative age and composition information will allow for a filtering of the surface noise and will enable the identification of subtle geochemical anomalies related to mineralization.

Acknowledgments

References

Anderson, H. (2006): Amplified geochemical imaging: an enhanced view to optimize outcomes; First Break, v. 24, no. 8, p. 77–81.

BC Geological Survey (2015): MINFILE BC mineral deposits database; BC Ministry of Energy and Mines, BC Geological Survey, URL <http://minfile.ca/> [November 2015].

Bissig, T., Heberlein, D. and Dunn, C. (2013): Geochemical techniques for detection of Blind porphyry copper-gold mineralization under basalt cover, Woodjam property, south-central British Columbia, NTS 093A/03, /06; Geoscience BC, Report 2013-17, 97 p., URL <http://www.geosciencebc.com/i/project_data/GBCReport2013-17/GBCReport2013-17_Report.pdf> [November 2015].

Burr, S.V. (1981): A guide to prospecting by the self-potential method; Ontario Geological Survey, Miscellaneous Paper 99, 15 p. URL <http://www.geologyontario.mndmf.gov.on.ca/mndmfiles/pub/data/imaging/MP099/MP099.pdf> [November 2015].

Corry, C.E., DeMoully, G.T. and Gerety, M.T. (1983): Field procedure manual for self-potential surveys; unpublished company field manual, Zonge Engineering Tucson, Arizona, 63 p., URL <http://corry.ws/PDF/SP_field_manual.pdf>

del Real Contreras, I. (2015): Geology, alteration, mineralization and magmatic evolution of the Southeast Zone (Cu-Mo) and Deerhorn (Cu-Au) porphyry deposits, Woodjam, central British Columbia, Canada; M.Sc. thesis, University of British Columbia, 330 p.

Dyke, A.S. and Prest, V.K. (1987): Late Wisconsinan and Holocene history of the Laurentide Ice Sheet; Géographie physique et Quaternaire, v. 41, no. 2, p. 237–263.

Eppinger, R.G., Fey, D.L., Giles, S.A., Grunsky, E.C., Kelley, K.D., Minsley, B.J., Munk, L. and Smith, S.M. (2013): Summary of exploration geochemical and mineralogical studies at the Giant Pebble porphyry Cu-Au-Mo deposit, Alaska: implications for exploration under cover; Economic Geology, v. 108, no. 3, p. 495–527.

Hamilton, S.M., Cameron, E.M., McClenaghan, M.B. and Hall, G.E.M. (2004): Redox, pH and SP variation over mineralization in thick glacial overburden. Part II: Field investigation at Cross Lake VMS property*; Geochemistry: Exploration, Environment, Analysis, v. 4, no. 1, p. 45–58.

Howes, D.E. and Kenk, E., editors (1997): Terrain classification system for British Columbia, v. 2; BC Ministry of Forests, Lands and Natural Resource Operations, 144 p., URL <https://www.for.gov.bc.ca/hts/risc/pubs/teecolo/terclass/terclass_system_1997.pdf> [November 2015]

Logan, J.M. and Mihalynuk, M.G. (2014): Tectonic controls on early Mesozoic paired alkaline porphyry deposit belts (Cu–Au±Ag–Pt–Pd–Mo) within the Canadian Cordillera; Economic Geology, v. 109, no. 4, p. 827–58.

McMillan, W.J. and Panteleyev, A. (1995): Porphyry copper deposits of the Canadian Cordillera; Arizona Geological Society Digest, v. 20, p. 203–218.

Pain, C.F. (2008): Field Guide for Describing Regolith and Landforms; Cooperative Research Centre for Landscape Environments and Mineral Exploration, 108 p., URL <http://crcleme.org.au/Pubs/guides/regolith_description_methods.pdf> [November 2015].

Sherlock, R., Blackwell, J. and Skinner, T. (2013): NI 43-101 technical report for 2012 activities on the Woodjam North property; prepared for Gold Fields Horsefly Exploration Corp. and Consolidated Woodjam Copper Corporation, 285 p., URL <http://www.infomine.com/index/pr/PB/33/17/PB331766.PDF> [November 2015]

Smee, B.W. (1983): Laboratory and field evidence in support of the electrogeochemically enhanced migration of ions through glaciolacustrine sediment; Journal of Geochemical Exploration, v. 19, no. 1–3, p. 277–304.

Smee, B.W. (2009): Soil micro-layer, airborne particles, and pH: the Govett Connection; in Proceedings of the 24th International Applied Geochemistry Symposium, v. 1, p. 91–95.

Hydrothermal Alteration and Mineralization at the Kerr and Deep Kerr Copper-Gold Porphyry Deposits, Northwestern British Columbia (Parts of NTS 104B/08)

S. Rosset, Mineral Deposit Research Unit, University of British Columbia, Vancouver, BC, srosset@eos.ubc.ca

C.J.R. Hart, Mineral Deposit Research Unit, University of British Columbia, Vancouver, BC

Introduction

Porphyry copper±gold and molybdenum deposits are well represented in British Columbia, traditionally contributing the largest copper reserves and significant resources of molybdenum, and hosting nearly 50% of gold reserves in the province (Panteleyev, 1995). The Quesnel and Stikine terranes of BC host belts of calcalkalic and alkalic porphyry deposits, related to Late Triassic to Middle Jurassic volcanic arcs that accreted to the western margin of North America (Figure 1). Related porphyry copper±gold and molybdenum deposits are largely restricted to a 15 m.y. epoch from the Late Triassic to the Early Jurassic, and are a result of slab subduction (Logan and Mihalynuk, 2014).

These Mesozoic deposits are difficult exploration targets, with complex alteration and metal-zoning patterns. Post-emplacement deformation further complicates improved understanding of these deposits and subsequent exploration decision making. The character, distribution and intensity of hydrothermal-alteration–mineral assemblages in porphyry deposits reflect the nature and distribution of economic metals. Research into the complexity of alteration-mineral assemblages and their zoning can better define the deposit and the relationships between alteration and mineralization. This is particularly important since hostrocks are highly altered and can be difficult to identify. Characterization of the chemical composition of hydrothermal-alteration assemblages, and isotopic composition of sulphides and sulphates, provide data on hydrothermal fluids, such as pH, temperature and oxidation state, that can provide exploration vectors toward mineralization (Wilson et al., 2007; Jimenez, 2011; Cohen; 2012; Dilles, 2012).

The Kerr and Deep Kerr deposits are part of the Kerr-Sulphurets-Mitchell (KSM) property, which represents one of the largest undeveloped porphyry systems in the world.

Keywords: Stikine terrane, Stuhini Group, Hazelton Group, Texas Creek Plutonic Suite, porphyry, copper, gold, molybdenum, hydrothermal alteration, KSM property, Kerr, Deep Kerr

This publication is also available, free of charge, as colour digital files in Adobe Acrobat® PDF format from the Geoscience BC website: http://www.geosciencebc.com/s/DataReleases.asp.

A research project jointly initiated by the Mineral Deposit Research Unit at the University of British Columbia and Seabridge Gold Inc., with support from Geoscience BC, will focus on the characterization and evolution of hydrothermal-alteration assemblages and mineralization to provide a
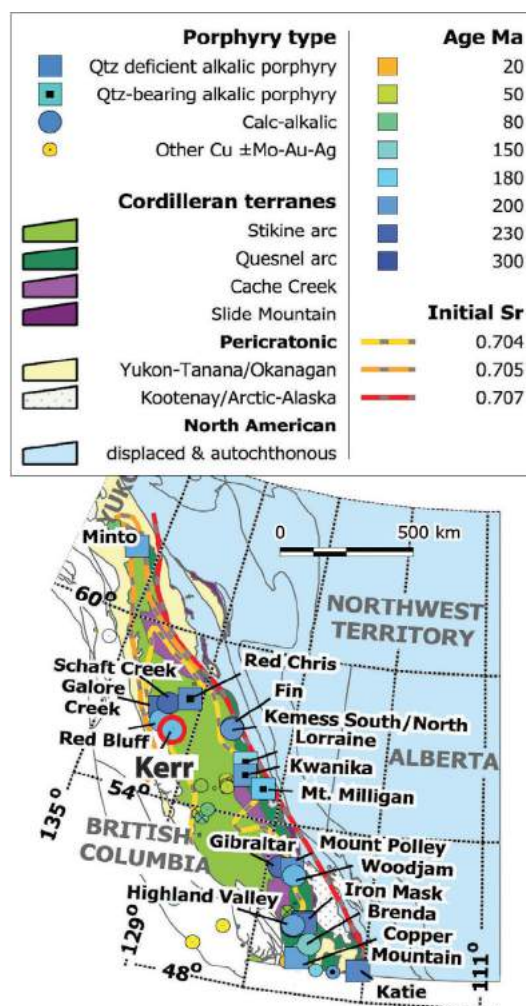
Figure 1. Porphyry deposits within the Canadian Cordillera, and location of the Kerr deposit in northwestern British Columbia (modified from Logan and Mihalynuk, 2014). Deposits are colour coded according to age, with Late Triassic to Early Jurassic porphyry deposits in blue; initial Sr isopleths are those of Mesozoic plutons (Logan and Mihalynuk, 2014).

better understanding of their correlation. This will be achieved through 1) detailed petrographic analysis and macroscopic observations; 2) shortwave infrared spectroscopy (SWIR); 3) major- and minor-element geochemistry and verification of SWIR results through scanning electron microscopy (SEM), X-ray powder diffraction (XRD), and electron probe micro-analysis (EPMA); and 4) sulphur-isotope analysis of sulphide and sulphate minerals to identify variability with respect to mineralization and alteration-mineral assemblages. This research project aims to contribute to the improvement of exploration tools and geometallurgical decision making, thereby increasing exploration and economic success in British Columbia and similar environments globally.

Fieldwork during 2015 focused on a 2.5 km southeast-trending cross-section across the north-central Kerr and Deep Kerr deposits. Nine drillholes were logged and sampled for a total of over 7000 m, with emphasis on detailed alteration logging and documentation of crosscutting relationships to establish vein paragenesis. More than 1100 chip samples for SWIR analysis were collected, with an additional 152 samples for whole-rock geochemical, petrographic and sulphur-isotope analysis. These observations will form the basis for ongoing petrographic, SWIR, SEM, XRD, EPMA and sulphur-isotope analyses in order to characterize the spatial distribution and evolution of hydrothermal alteration and mineralization.

Tectonic Setting

British Columbia is composed largely of terranes of exotic crustal fragments that accreted to the ancient North American margin during the Mesozoic era. The Intermontane Belt comprises much of the accreted material along the Canadian Cordillera in British Columbia and is predominantly composed of the Stikine terrane, the Quesnel terrane and the intervening Cache Creek terrane. Porphyry deposits are concentrated within the Stikine and Quesnel terranes, which feature nearly equivalent stratigraphy and Devonian to Early Jurassic evolution (Logan and Mihalynuk, 2014). The KSM property is hosted within the western margin of northern Stikinia, in the Sulphurets district. Porphyry mineralization in this district has been dated between 197 and 190 Ma (Bridge, 1993; Margolis, 1993; Kirkham and Margolis, 1995; Febbo et al., 2015).

Regional Geology

The Stikine terrane in northwestern British Columbia is composed of island-arc volcano-sedimentary successions that include the Stikine assemblage (Paleozoic), Stuhini Group (Late Triassic) and Hazelton Group (Early Jurassic). These successions are overlain by sedimentary rocks of the Middle Jurassic to Tertiary Bowser Lake and Sustut groups and the Late Cretaceous to Tertiary Sloko Group, and Ter-

tiary[1] Edziza and Spectrum volcanic rocks (Logan et al., 2000). A regional-scale unconformity between the volcano-sedimentary Stuhini Group and overlying volcanic and sedimentary Hazelton Group varies from a sharp angular unconformity to a near disconformity (Kyba, 2014; Nelson and Kyba, 2014). The Early Jurassic Texas Creek Plutonic Suite is comagmatic and coeval with the Lower Hazelton Group, and comprises I-type, calcalkaline intrusive rocks that are cospatial with Hazelton volcanic rocks (Logan et al., 2000). The Mitchell intrusions of the Sulphurets district are considered a subset of the Texas Creek plutons (Kirkham, 1963; Alldrick and Britton, 1991).

KSM Property Overview and Geology

The KSM property is in northwestern British Columbia, 65 km north of the town of Stewart (Figure 2), and is one of the largest undeveloped gold projects in the world. The claims are 100% owned by Seabridge Gold Inc. The KSM property comprises the Kerr, Deep Kerr, Sulphurets, Mitchell, Iron Cap and Lower Iron Cap deposits, and has an estimated total proven and probable reserve of 38.2 million ounces gold and 9.9 billion pounds copper (Seabridge Gold Inc., 2015a). The Kerr deposit contains an estimated probable reserve of 242 million tonnes grading 0.45% copper and 0.24 g/t gold (containing 2.4 billion lb. copper and 1.9 million oz. gold; Seabridge Gold Inc., 2015a). The Deep Kerr deposit, discovered in 2013, had an initial inferred resource estimate in 2014 and an updated inferred estimate in 2015 of 782 million tonnes grading 0.54% copper and 0.33 g/t gold (containing 9.3 billion lb. copper and 8.2 million oz. gold; Seabridge Gold Inc., 2015b).

The KSM deposits are hosted in volcanic arc–related Triassic to Jurassic volcanic and sedimentary assemblages that were intruded by Early Jurassic diorite, monzonite and quartz syenite intrusions. Volcanic and sedimentary rocks of the Stuhini and Hazelton groups are cut by feldspar porphyry intrusive rocks. These Premier and Sulphurets intrusive rocks are suites within the Mitchell intrusions, and therefore part of the Texas Creek Plutonic Suite. Geochronology and crosscutting relationships suggest that the Sulphurets suite magmatism postdates, and potentially overlaps with Premier suite magmatism (Febbo et al., 2015). The Sulphurets suite fine- to medium-grained diorite to monzonite porphyry hosts porphyry mineralization in the district (Febbo et al., 2015). At the KSM deposits, shallow vein systems and skarns transition to sedimentary- and volcanic-hosted porphyry mineralization in the transitional

---

[1] *'Tertiary' is an historical term. The International Commission on Stratigraphy recommends using 'Paleogene' (comprising the Paleocene to Oligocene epochs) and 'Neogene' (comprising the Miocene and Pliocene epochs). The author used the term 'Tertiary' because it was used in the source material for this paper.*
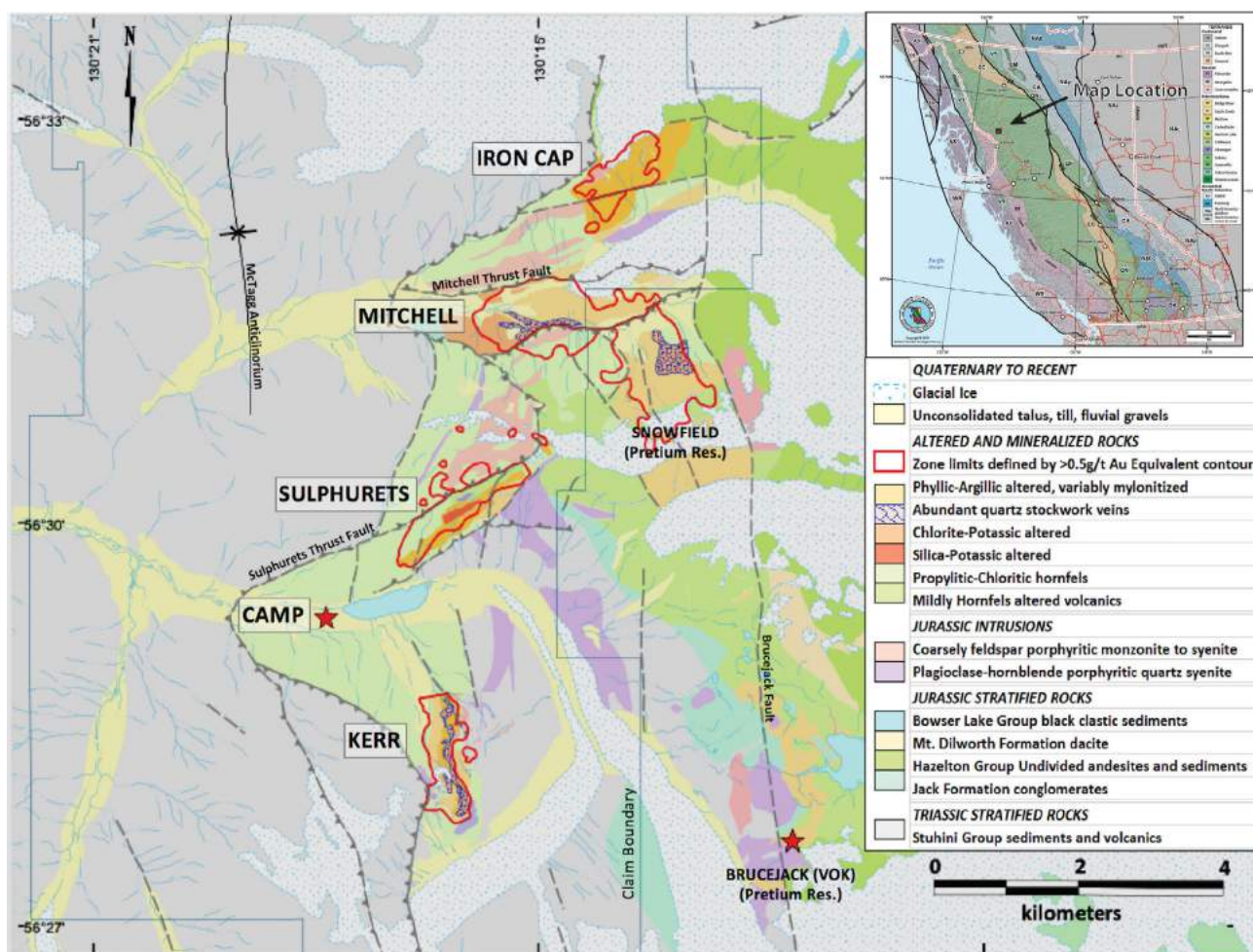
Figure 2. KSM property geology with deposit locations (Seabridge Gold Inc., pers. comm., 2015).

environment, and to intrusion-hosted porphyry mineralization at depth (M. Savell, pers. comm., 2015).
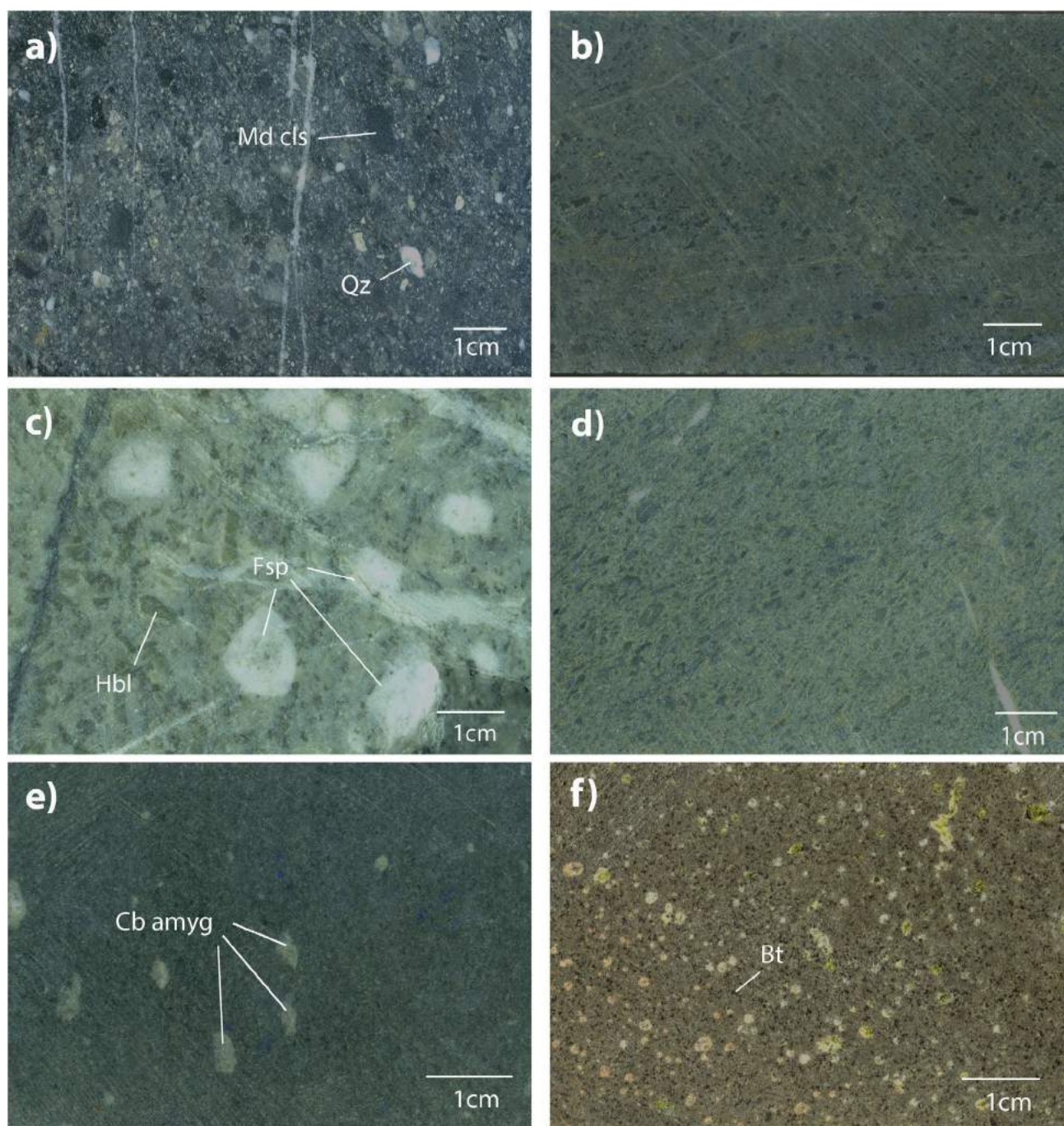
Kerr and Deep Kerr Deposits

Deposit Structure and Lithology

The Kerr and Deep Kerr deposits strike north and dip steeply to the west, with the shallower portion of the deposit (upper ~500 m) defined as the Kerr deposit and the newly discovered Deep Kerr deposit underlying the Kerr deposit and open at depth. The steeply dipping 'F2' reverse fault bounds the western margin of the deposit (Febbo et al., 2014). This structure was previously identified as the Sulphurets thrust fault (Bridge, 1993), which has subsequently been mapped to the west as a moderately west-dipping reverse fault (Lewis, 2001; Febbo et al., 2014). Footwall assemblages are represented by sedimentary and volcaniclastic rocks of the Stuhini and Hazelton groups. The F2 fault thrusts Triassic Stuhini Group to Jurassic Hazelton Group basinal-fill rocks over younger Hazelton Group rocks in the footwall (Seabridge Gold, pers. comm., 2015). The Kerr deposit is strongly deformed, as pre-existing structures and intense alteration led to the development of a low-competency zone where Cretaceous compression was focused (Ditson et al., 1995).

The Kerr deposit is largely hosted by assemblages of the Stuhini and Hazelton groups, whereas the Deep Kerr deposit is largely intrusion-hosted. Late Triassic Stuhini Group hostrocks are predominantly siltstone, graphitic shale and mudstone, while Early Jurassic Hazelton Group volcanic and sedimentary hostrocks are represented by sandstone, conglomerate (e.g., Jack Formation; Figure 3a) and lesser volcanic rocks. Synmineralization composite intrusions of porphyritic hornblende–plagioclase±K-feldspar–biotite are the most abundant intrusions at the Kerr and Deep Kerr deposits, and constitute the bulk of the Deep Kerr (Figure 3b). These intrusions crosscut each other, with multiple overprinting intrusive phases, and are highly altered within the deposit, making recognition of primary phases difficult. Early Jurassic K-feldspar–megacrystic porphyry dikes (Figure 3c) are late mineralization and overprinted by epithermal gold-silver mineralization (Bridge, 1993). Postmineralization dikes include Early Ju-

Figure 3. Key rock types of the Kerr and Deep Kerr deposits (sample number, drillhole number, depth in metres): **a)** Jack Formation conglomerate, featuring mudstone intraclasts and quartz pebbles (2015-062, K-14-37, 388.95 m); **b)** porphyritic andesite with chlorite/sericite pseudomorphs after hornblende and feldspar (2014-014, K-13-34, 532.6 m); **c)** postmineralization porphyritic diorite dike with chlorite/sericite pseudomorphs after hornblende and feldspar (2015-091, K-13-31, 517.8 m); **d)** K-feldspar–megacrystic porphyry (2015-003, K-12-20, 149.4 m); **e)** aphanitic diorite dike with carbonate amygdules (2014-016, K-13-34, 568.13 m); **f)** postmineralization biotite porphyry dike with feldspar (2015-039, K-13-30, 617.3 m). Abbreviations: Bt, biotite; Cb amyg, carbonate amygdules; Fsp, feldspar; Hbl, hornblende; Md cls, mudstone clasts; Qz, quartz.
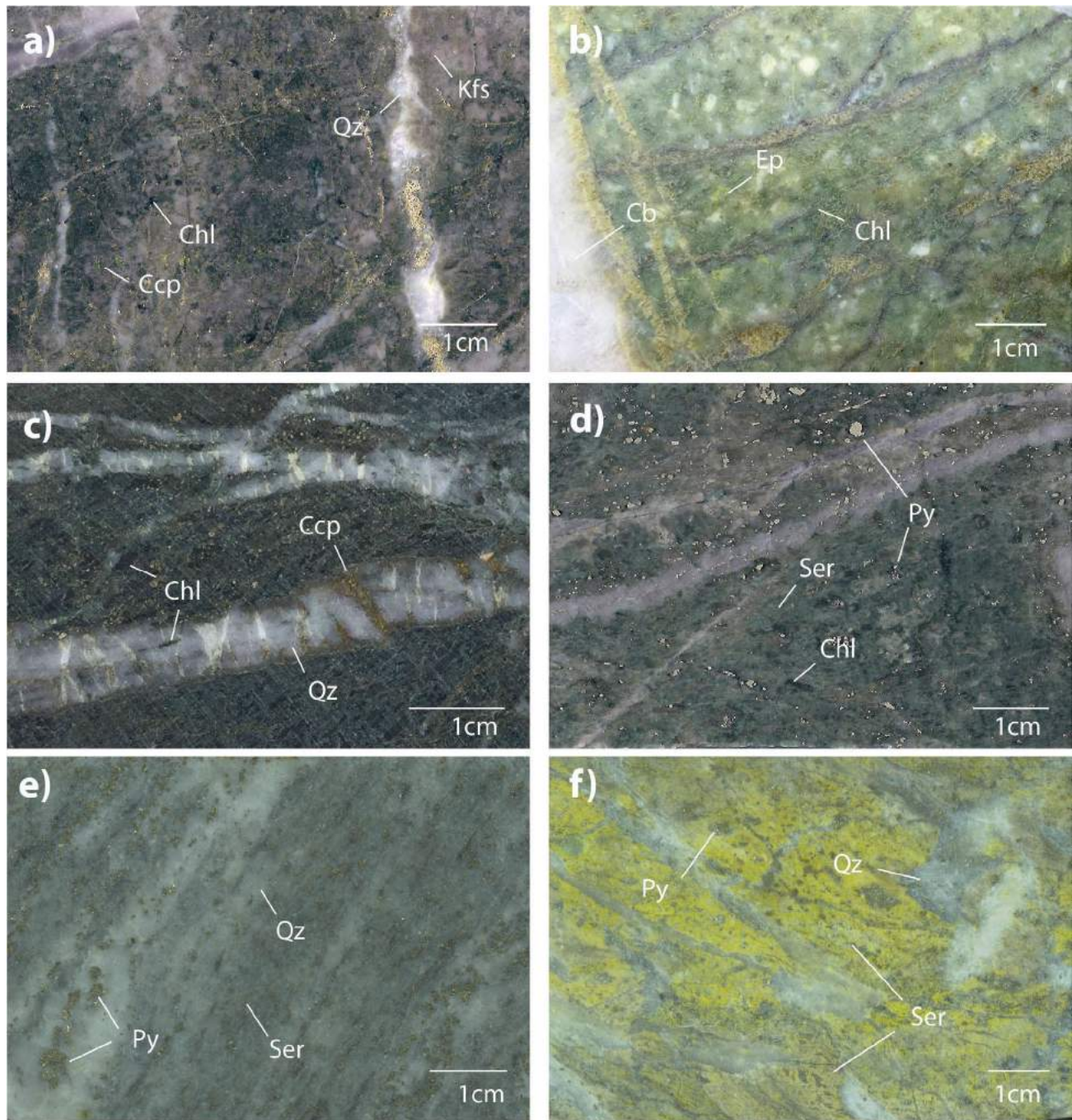
Figure 4. Key alteration assemblages of the Kerr and Deep Kerr deposits (sample number, drillhole number, depth in metres): **a)** K-feldspar–chlorite–magnetite alteration with fine-grained chalcopyrite in hornblende-phyric intrusion cut by quartz vein (K-15-49, 1476.6 m); **b)** epidote-chlorite-carbonate alteration within a feldspar-phyric intrusive (K-14-37, 978.4 m); **c)** pervasive chlorite alteration within a hornblende- and feldspar-phyric intrusion, and associated quartz-chalcopyrite-chlorite veining (K-13-31, 594.4 m); **d)** pervasive chlorite-sericite and disseminated pyrite alteration within a hornblende-phyric intrusion (K-14-39, 952.2 m); **e)** pervasive, intense quartz-sericite-pyrite alteration of unknown protolith (2014-023, K-13-31, 1110.9 m); **f)** intense yellow-sericite alteration of a sedimentary protolith (2015-094, K-31-34, 447.7 m). Abbreviations: Cb, carbonate; Ccp, chalcopyrite; Chl, chlorite; Ep, epidote; Kfs, K-feldspar; Py, pyrite; Qz, quartz; Ser, sericite.
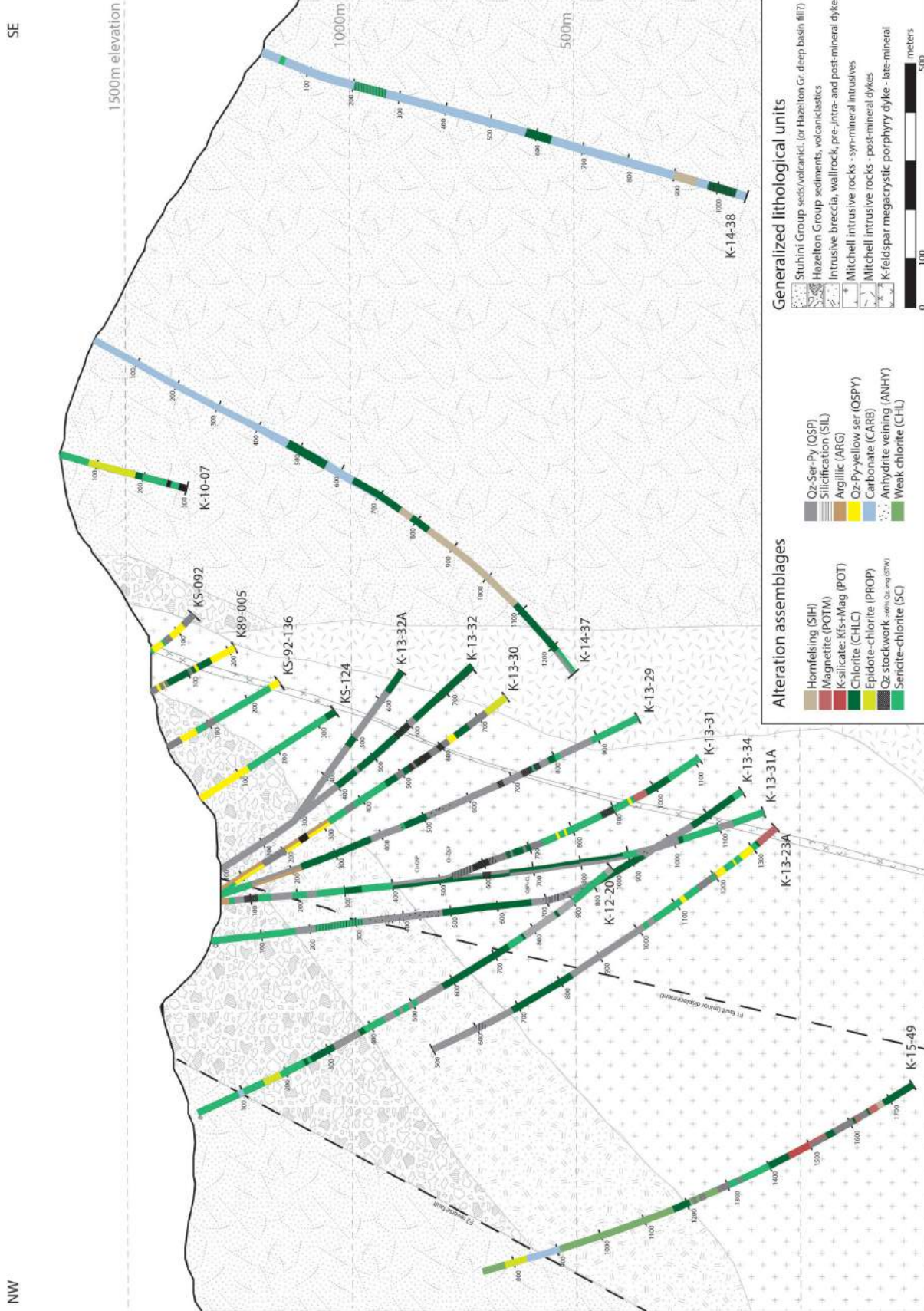
Figure 5. Cross-section, striking ~295° and measuring 2.5 km, across the northern Kerr and Deep Kerr deposits, centred on ~421261E, 6259537N, with a section envelope of 100 m. Data obtained from geochemical analysis, petrography, sulphur-isotope analysis and shortwave infrared spectroscopy (SWIR) will be integrated with macroscopic observations obtained during fieldwork to complete the alteration cross-section. Geology is highly generalized (Seabridge Gold., pers. comm., 2015).

rassic porphyritic diorite dikes (Figure 3d) and aphanitic diorite dikes (Figure 3e), and Eocene biotite porphyry kersantitic lamprophyre dikes (Figure 3f; Bridge, 1993).

Alteration

Alteration at the Kerr deposit is the result of a long-lived, relatively shallow hydrothermal system produced by intrusion of monzonite (Ditson et al., 1995). Alteration at both the Kerr and Deep Kerr deposits (Figures 4, 5) affects sedimentary and volcanic hostrocks, as well as pre- to synmineralization intrusions, with weaker alteration of postmineralization intrusive rocks and very weak alteration of late postmineralization intrusive rocks. Supergene alteration is noted in the shallower Kerr deposit to consist of leached hematite/jarosite, minor native copper and chalcocite/covellite, with extensive hydration of anhydrite to gypsum (Bridge, 1993). This hydration has caused an extensive 'rubble' zone in the near-surface environment at Kerr.

Early K-feldspar–chlorite–magnetite alteration (Table 1, Figure 4a) is minor, and preservation is limited to remnant 'rafts' in the core of the deposit and at depth in drillhole K-15-49 (Figure 5). Early epidote-chlorite±carbonate alteration (Figure 4b) is minor, and visible at the eastern and western margins of the deposit. K-feldspar–chlorite–magnetite alteration appears to have been largely overprinted by dark green, pervasive chlorite alteration (Figure 4c) with minor remnant magnetite. K-feldspar, chlorite and magnetite alteration are associated with chalcopyrite±bornite mineralization. Pale green, pervasive chlorite-phengite± illite alteration (Figure 4d) occurs within the deposit and is abundant peripheral to the deposit on the west and east, and in shallow hostrocks. This alteration assemblage, as well as the dark chlorite core alteration, are typically overprinted by a widespread quartz-sericite-pyrite assemblage (Figure 4e), which has an extensive distribution overprinting the core and margins of the deposit. Yellow sericite–pyrite±quartz alteration (Figure 4f) is typically intense and pervasive within minor sedimentary rafts at depth in the deposit (K-13-23A), and in shallow sedimentary hostrocks within the deposit. This alteration was noted by previous workers to be a selective alteration of sedimentary rocks and, due to its peripheral distribution, to contain the lowest metal grades among the alteration assemblages (Ditson et al., 1995).

Vein Paragenesis

Early magnetite veins (Table 2, Figure 6a) have a limited distribution within the core and at depth at the Kerr and Deep Kerr deposits, and are associated with K-feldspar–chlorite±magnetite alteration. Alteration of magnetite to pyrite may obscure the original extent of these veins. Quartz-chalcopyrite-pyrite veining (Figure 6b, c) is extensive and intimately associated with copper and gold mineralization, forming dense stockworks within the core of the deposit. Extensive quartz-pyrite veining (Figure 6d) overprints earlier veining and is associated with chlorite-sericite and quartz-sericite-pyrite alteration assemblages. These veins are typically planar, with 2–20 mm sericite haloes indicating disequilibrium with surrounding pervasive alteration. Late, white quartz–chalcopyrite–carbonate± chlorite veins (Figure 6e) are distributed throughout the deposit, with higher chalcopyrite contents in higher grade areas suggesting local remobilization. A high-sulphidation overprint is visible as bornite, tennantite/enargite and dickite/pyrophyllite overprinting core stockwork zones (Figure 6f). Anhydrite veining is dominated by late, white to grey veins that overprint quartz-stockwork zones and

Table 1. Overview of alteration assemblages at the Kerr and Deep Kerr deposits; vein-type analogues are derived from Sillitoe (2010), modified after Gustafson and Hunt (1975).

Alteration assemblage	Sulphide assemblage	Vein types and analogues[1]	Distribution	Alteration assemblage analogue
K-feldspar–chlorite–magnetite±biotite	Pyrite-chalcopyrite±bornite	Quartz-sulphides (A and B types), magnetite	Limited distribution; occurs at depth (DDH K-15-49), with only remnant rafts within deposit, where magnetite±K-feldspar alteration has been largely overprinted	K-silicate
Epidote–chlorite±carbonate	Pyrite	Quartz-pyrite-epidote	Limited peripheral distribution; occurs at eastern and western margins of deposit	Propylitic
Chlorite±magnetite	Chalcopyrite-pyrite	Quartz-sulphides (A and B types), magnetite associated	Throughout the deposit, with the most intense chlorite alteration within the core of the deposit; potential artifact of K-feldspar–magnetite±biotite alteration	Chlorite
Chlorite–phengite±illite	Pyrite	Quartz-pyrite (D type)	Throughout the deposit, abundant peripheral to core, and overprinting earlier chlorite alteration	Sericite-chlorite
Quartz–sericite	Pyrite	Quartz-pyrite (D type)	Abundant throughout the deposit, commonly overprinting chlorite alteration in the core, and peripheral sericite-chlorite alteration	Phyllic
Yellow sericite±quartz	Pyrite	Quartz-pyrite (D type)	Limited distribution; occurs extensively within sedimentary units peripheral to deposit, and within sedimentary rafts	-

Table 2. Overview of vein types at the Kerr and Deep Kerr deposits; vein-type analogues derived from Sillitoe (2010), modified after Gustafson and Hunt (1975). Abbreviation: PCD, porphyry copper deposits.

Mineral-sulphde assemblage	Vein selvage	Description	Alteration assemblage	Distribution	PCD vein-type analogue[1]
Magnetite±pyrite-quartz	None	3–30 mm; sharp, sinuous margins; alter to pyrite	K-feldspar–chlorite–magnetite and chlorite-magnetite	At depth (K-15-49), with minor remnant magnetite within chloritic alteration in the core of the deposit	M type
Quartz-chalcopyrite ±pyrite-bornite-molybdenite	Typically none; Kfs locally (B veins)	Granular to translucent; white to gray/pink; 5–40 mm; A veins sinuous, B veins more planar and may contain sulphide centreline	K-feldspar–chlorite–magnetite and chlorite–magnetite	Common in deposit core, associated with grade and quartz-stockwork veining	A & B types
Quartz–pyrite± sphalerite–galena	Sericite±quartz± pyrite	2–10 mm; parallel margins; wide selvages	Sericite-chlorite and quartz-sericite-pyrite	Throughout the deposit, with sphalerite/galena common on margins of deposit into wallrock	D type
Anhydrite	None	Grey, white or pink; 1 mm to >1 m; recessively weathered, alter to gypsum	Anhydrite	Late stage, overprinting quartz-stockwork zones in core of deposit, and above core to surface, where they are mainly altered to gypsum	-
Quartz–bornite-tennantite/enargite	Quartz–pyropyllite/ dickite	5–40 mm; crackle sulphides within quartz veins	High sulphidation	Overprinting quartz-stockwork zones in centre of deposit	-

[1] Sillitoe (2010), modified from Gustafson & Hunt (1975)

shallower areas of the deposit, where they alter to gypsum (Table 2).

Mineralization

Mineralization at the Kerr and Deep Kerr deposits is present as disseminations and within veins as fine-grained hypogene chalcopyrite, bornite, molybdenite and pyrite, with the occurrence of gold and silver intimately associated with sulphide mineralization (M. Savell, pers. comm., 2015). Mineralization is controlled by permeability, and is therefore more homogeneous within deeper, intrusion-hosted portions of the system and more erratic in shallower, mixed sedimentary, volcanic, and intrusion-hosted portions of the deposit. Mineralization is associated with early K-feldspar, chlorite and magnetite alteration, although later mineralization, such as evidenced by the high-sulphidation overprint of earlier stockworks, may have locally enriched metal grades.

Discussion

To characterize the spatial and temporal distribution of alteration and mineralization, and their relation to hostrock lithology, fieldwork focused on relogging more than 7000 m of core on a cross-section across northern Kerr/ Deep Kerr. Crosscutting relationships were utilized to develop a vein paragenesis, and will be corroborated with results from sulphur-isotope and petrographic analyses. Sulphur-isotope analyses will also substantiate correlation of

alteration assemblages with vein types and validate timing, such as the high-sulphidation overprint of quartz-stockwork zones. Field observations, such as the link between sedimentary rocks and yellow sericite alteration, and remnant K-feldspar–magnetite–chlorite alteration, will be characterized by whole-rock geochemistry, petrography and SWIR analysis. Samples collected for whole-rock geochemistry and petrographic analysis will be utilized for characterization of hosting rock types and alteration assemblages, which will aid in identification of altered hostrocks within the deposit. The more than 1100 chip samples collected will be utilized for SWIR analysis, which will be used in conjunction with geochemistry, petrography and field observations to produce a cross-sectional alteration model. The SWIR analysis will be verified through in-depth analyses by SEM, XRD and EPMA to provide confidence in this method as a rapid and reliable exploration tool.

The combination of these methods will enable the development of a hydrothermal-alteration cross-sectional model for the Kerr and Deep Kerr deposits that encompasses the spatial and temporal evolution of the ore system. It is anticipated that the results will provide a foundation for a better understanding of the complex hydrothermal alteration associated with porphyry deposits and lead to improved exploration success and geometallurgical decision making, both in British Columbia and in other porphyry districts.
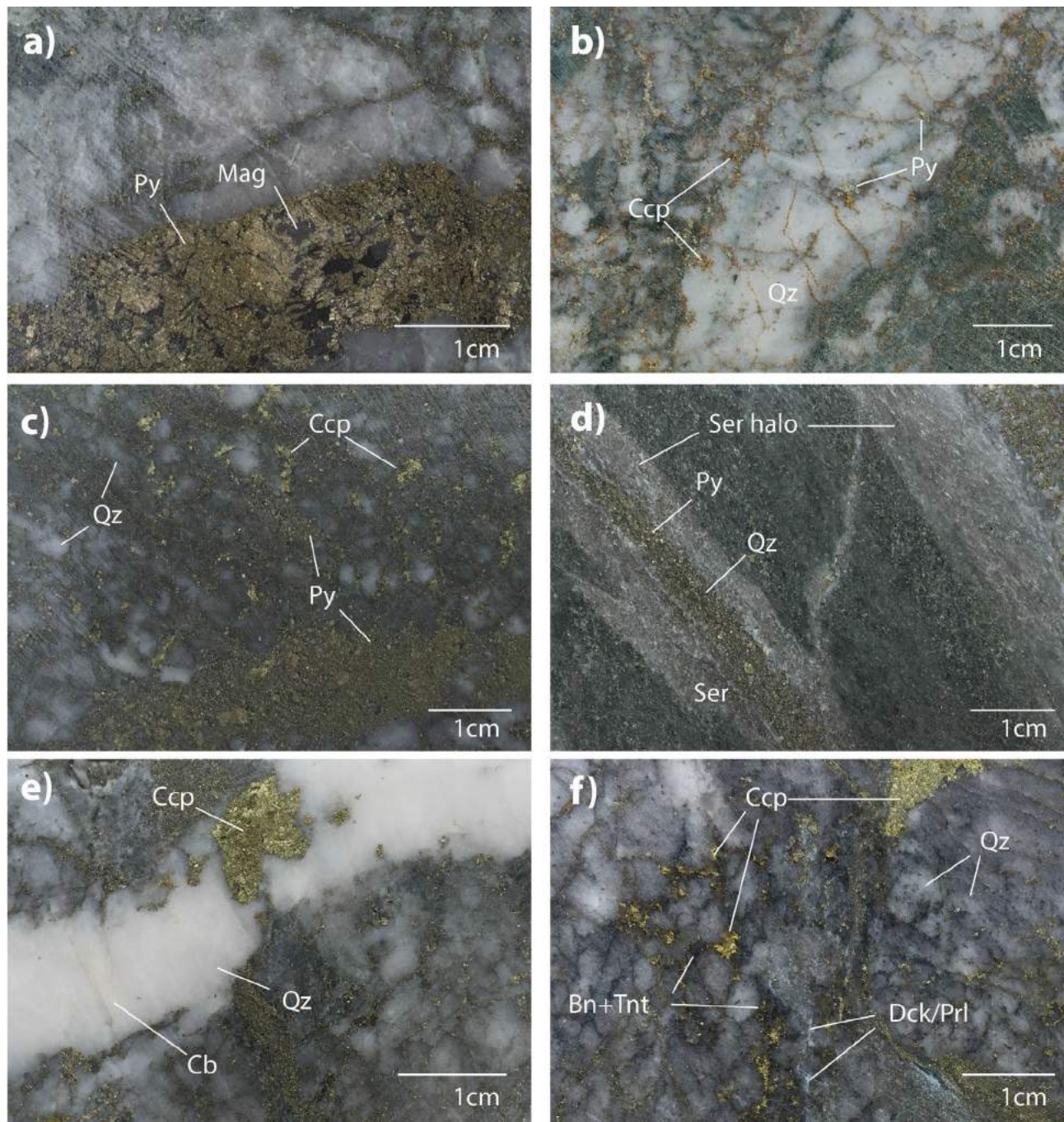
Figure 6. Overview of vein types at the Kerr and Deep Kerr deposits (drillhole number, depth in metres): **a)** magnetite-pyrite vein with alteration of magnetite to pyrite (K-13-32, 635 m); **b)** early granular milky quartz–chalcopyrite–pyrite A-type vein (K-13-34, 483.4 m); **c)** quartz-chalcopyrite-pyrite stockwork veining in core of deposit (K-13-31, 590 m); **d)** quartz-pyrite vein with wide sericite halo overprinting chlorite-sericite alteration (K-13-30, 749.6 m); **e)** late white quartz–chalcopyrite–carbonate vein (K-13-30, 598.6 m); **f)** high-sulphidation bornite–tennantite±dickite/pyrophyllite overprint of quartz stockwork with chalcopyrite in core of deposit (K-13-30, 567.2 m). Abbreviations: Bn, bornite; Cb, carbonate; Ccp, chalcopyrite; Chl, chlorite; Dck, dickite; Mag, magnetite; Prl, pyrophyllite; Py, pyrite; Qz, quartz; Ser, sericite; Tnt, tennantite.

References

Alldrick, D.J. and Britton, J.M. (1991): Sulphurets area geology; BC Ministry of Energy and Mines, BC Geological Survey, Open File 1991-21, scale 1:20 000.

Bridge, D.J. (1993): The deformed Early Jurassic Kerr copper-gold porphyry deposit, Sulphurets gold camp, northwestern British Columbia; M.Sc. thesis, University of British Columbia, 319 p.

Cohen, J.F. (2012): Compositional variation in hydrothermal white mica and chlorite from wall-rock alteration at the Ann-Mason porphyry copper deposit, Nevada; M.Sc. thesis, Oregon State University, 138 p.

Dilles, J.H. (2012): Footprints of porphyry Cu deposits vectors to the hydrothermal center using mineral mapping and lithogeochemistry; final technical report for USGS MRERP Grant Award G10AP00052, Oregon State University, 599 p., URL <http://minerals.er.usgs.gov/mrerp/reports/Dilles-G10AP00052.pdf> [November 2015].

Ditson, G.M., Wells, R.C. and Bridge, D.J. (1995): Kerr: the geology and evolution of a deformed porphyry copper-gold deposit, northwestern British Columbia; *in* Porphyry Deposits of the Northwestern Cordillera of North America, T.G. Schroeter (ed.), Canadian Institute of Mining, Metallurgy and Petroleum, Special Volume 46, p. 509–523.

Febbo, G.E., Kennedy, L.A., Savell, M., Creaser, R.A. and Friedman, R.M. (2015): Geology of the Mitchell Au-Cu-Ag-Mo porphyry deposit, northwestern British Columbia, Canada; *in* Geological Fieldwork 2014, BC Ministry of Energy and Mines, BC Geological Survey, Paper 2015-1, p. 59–86, URL <http://www.empr.gov.bc.ca/Mining/Geoscience/PublicationsCatalogue/Fieldwork/Documents/2014/04_Febbo_etal.pdf> [October 2015].

Febbo, G.F., Freeman, J., Kraft, T. and Kennedy, L.A. (2014): Geology of the KSM property: waste rock characterization; in-house geology map for Seabridge Gold Inc.

Gustafson, L.B. and Hunt, J.P. (1975): The porphyry copper deposit at El Salvador, Chile; Economic Geology, v. 90, p. 2–16.

Jimenez, T.R.A. (2011): Variation in hydrothermal muscovite and chlorite composition in the Highland Valley porphyry Cu-Mo district, British Columbia, Canada; M.Sc. thesis, University of British Columbia, 249 p.

Kirkham, R.V. (1963): The geology and mineral deposits in the vicinity of the Mitchell and Sulphurets glaciers, northwest British Columbia; M.Sc. thesis, University of British Columbia, 142 p.

Kirkham, R.V. and Margolis, J. (1995): Overview of the Sulphurets area, northwestern British Columbia; *in* Porphyry Deposits of the Northwestern Cordillera of North America, T.G. Schroeter (ed.), Canadian Institute of Mining, Metallurgy and Petroleum, Special Volume 46, p. 473–483.

Kyba, J. (2014): The Stuhini-Hazelton unconformity of Stikinia: investigations at KSM-Brucejack, Snip–Johnny Mountain and Red Chris areas (abstract); 2014 Geological Society of America Annual Meeting, Vancouver, BC, October 19–22, 2014, Abstracts with Programs, v. 46, no. 6, p. 589, URL <https://gsa.confex.com/gsa/2014AM/webprogram/Paper248935.html> [October 2015].

Lewis, P.D. (2001): Geological maps of the Iskut River area; *in* Metallogenesis of the Iskut River Area, Northwestern British Columbia, P.D. Lewis, A. Toma and R.M. Tosdal (ed.), University of British Columbia, Mineral Deposit Research Unit, Special Publication 1, p. 77–83.

Logan, J.M. and Mihalynuk, M.G. (2014): Tectonic controls on Early Mesozoic paired alkaline porphyry deposit belts (Cu-Au±Ag-Pt-Pd-Mo) within the Canadian Cordillera; Economic Geology, v. 109, p. 827–858.

Logan, J.M., Drobe, J.R. and McClelland, W.C (2000): Geology of the Forrest Kerr–Mess Creek area, northwest British Columbia (NTS 104B/10, 15 and 104/G2, 7W); BC Ministry of Energy and Mines, BC Geological Survey, Bulletin 104, 163 p., URL <http://www.empr.gov.bc.ca/mining/geoscience/publicationscatalogue/bulletininformation/bulletinsafter1940/Pages/Bulletin104.aspx> [October 2015].

Margolis, J. (1993): Geology and intrusion-related copper-gold mineralization, Sulphurets, British Columbia; Ph.D. thesis, University of Oregon, 289 p.

Nelson, J. and Kyba, J. (2014): Structural and stratigraphic control of porphyry and related mineralization in the Treaty Glacier–KSM–Brucejack–Stewart trend of western Stikinia; *in* Geological Fieldwork 2013, BC Ministry of Energy and Mines, BC Geological Survey, Paper 2014-1, p. 111–140, URL <http://www.empr.gov.bc.ca/Mining/Geoscience/PublicationsCatalogue/Fieldwork/Documents/2013/07_Nelson_Kyba.pdf> [October 2015].

Panteleyev, A. (1995): Porphyry Cu±Mo±Au; *in* Selected British Columbia Mineral Deposit Profiles, D.V. Lefebure and G.E. Ray (ed.), BC Ministry of Energy and Mines, BC Geological Survey, Open File 1995-20, p. 87–92, URL <http://www.empr.gov.bc.ca/mining/geoscience/mineraldepositprofiles/listbydepositgroup/pages/lporphyry.aspx#l04> [September 2015].

Seabridge Gold Inc. (2015a): Mineral reserves and resources (updated March 26, 2015); Seabridge Gold Inc., URL <http://seabridgegold.net/resources.php> [December 2015].

Seabridge Gold Inc. (2015b): Seabridge Gold reports 52% resource expansion for KSM's Deep Kerr deposit; Seabridge Gold Inc., press release, March 23, 2015, URL <http://seabridgegold.net/News/Article/516/seabridge-gold-reports-52%25-resource-expansion-for-ksm-s-deep-kerr-deposit-estimated-782-million-tonne-inferred-resource-averages-0.54%25-copper-and-0.33-g-t-gold.-deposit-now-contains-estimated-8.2-million-ounces-gold> [December 2015]

Sillitoe, R.H. (2010): Porphyry copper systems; Economic Geology, v. 105, p. 3–41.

Wilson, A.J., Cooke, D.R., Harper, B.J. and Deyell, C.L. (2007): Sulfur isotopic zonation in the Cadia district, southeastern Australia: exploration significance and implications for the genesis of alkalic porphyry gold-copper deposits; Mineralium Deposita, v. 42, p. 465–487.

Geoscience BC

VISION

Earth science for everyone

MISSION

We are a trusted partner providing earth science to
encourage investment that benefits all British Columbians